The role of tumor-derived lactic acid in immunomodulation

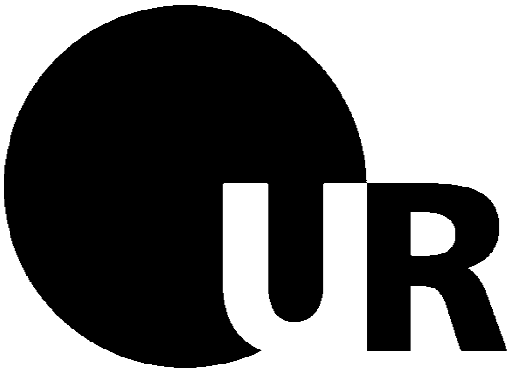

DISSERTATION ZUR ERLANGUNG DES
DOKTORGRADES DER NATURWISSENSCHAFTEN (DR. RER. NAT.)
DER FAKULTÄT FÜR BIOLOGIE UND VORKLINISCHE MEDIZIN
DER UNIVERSITÄT REGENSBURG

vorgelegt von
Almut Brand
aus Immenstadt i. Allgäu
im Jahr 2016

The present work was carried out from July 2011 to April 2016 at the Clinic and Polyclinic of Internal Medicine III at the University Hospital Regensburg.

Die vorliegende Arbeit entstand im Zeitraum von Juli 2011 bis April 2016 an der Klinik und Poliklinik für Innere Medizin III des Universitätsklinikums Regensburg.

Das Promotionsgesuch wurde eingereicht am:
25. April 2016

Die Arbeit wurde angeleitet von:
Prof. Dr. Marina Kreutz

Prüfungsausschuss:

Vorsitzender:	Prof. Dr. Wolfram Gronwald
Erstgutachter:	Prof. Dr. Marina Kreutz
Zweitgutachter:	Prof. Dr. Wolfgang Müller-Klieser
Drittprüfer:	Prof. Dr. Herbert Tschochner
Ersatzprüfer:	Prof. Dr. Armin Kurtz

Unterschrift:

_____

Table of Contents

List of Figures

List of Tables

List of Abbreviations

^{18}F-FDG	^{18}F-fluorodeoxyglucose
Acetyl-CoA	Acetyl coenzyme A
AKT	v-akt murine thymoma viral oncogene homolog 1
APC	Allophycocyanin
APS	Ammonium persulfate
ARD1	Arrest-defective 1
ARG	Arginase
ATM	Ataxia telangiectasia mutated
ATP	Adenosin triphosphate
BAK	BCL2 antagonist/killer
BAP1	BRCA1-associated protein 1
BAX	BCL2-associated X protein
BCL2	B-cell CLL/lymphoma 2
BRAF	v-raf murine sarcoma viral oncogene homolog B1
BRCA	Breast cancer
BV	Brilliant Violet
CAR	Chimeric antigen receptor
CCL2	Chemokine (C-C motif) ligand 2
CCR2	Chemokine (C-C motif) receptor 2
CD	Cluster of differentiation
cDNA	Copy DNA
CO_2	Carbon dioxide
COX	Cyclooxygenase
CRISPR/Cas9	Clustered, regularly interspaced, short palindromic repeats/Caspase 9
CSF	Colony-stimulating factor
CTLA-4	Cytotoxic T lymphocyte-associated protein 4
CXCL2	Chemokine (C-X-C motif) ligand 2
Cy7	Cyanin 7
DAPI	4',6-diamidino-2-phenylindole
DCs	Dendritic cells
DMSO	Dimethyl sulfoxide
DNA	Deoxyribonucleic acid
dNTPs	2'-deoxyribonucleosid-5'-triphosphates
dsDNA	double-stranded DNA
ECL	Enhanced chemiluminescence
ECM	Extracellular matrix
EDTA	Ethylene diamine tetraacetate
EGFR	Epidermal growth factor receptor
ELISA	Enzyme-linked immunosorbent assay
FASL	Fas ligand
FCS	Fetal calf serum
FH	Fumarate hydratase
FITC	Fluorescein isothiocyanate

Fox	Forkhead box
FSC	Forward scatter
GLUT	Glucose transporter
GM-CSF	Granulocyte-macrophage colony-stimulating factor
H_2O_2	Hydrogen peroxide
H_2O_{bidest}	Double-distilled water
H_2O_{USB}	Diethylpyrocarbonate treated RNAse-free water (USB Corporation)
HBSS	Hank's balanced salt solution
HCl	Hydrochloric acid
HIF	Hypoxia-inducible factor
HK	Hexokinase
HRAS	v-Ha-ras Harvey rat sarcoma viral oncogene homolog
HRP	Horse raddish peroxidase
IDH	Isocitrate dehydrogenase
IDO	Indoleamine 2,3-dioxygenase
IFN	Interferon
Ig	Immunoglobulin
IGF	Insulin-like growth factor
IL	Interleukin
ImBI	Induced metabolic bioluminescence imaging
IRF-1	Interferon regulatory factor 1
JNK	c-Jun N-terminal kinase
KRAS	v-Ki-ras2 Kirsten rat sarcoma viral oncogene homolog
LA	*L*-Lactic acid
LDH	Lactate dehydrogenase
LPS	Lipopolysaccharide
MCT	Monocarboxylate transporter
MDSCs	Myeloid-derived suppressor cells
MHC	Major histocompatibility complex
miR	Micro RNA
MLH1	mutL homolog 1
M-MLV	Murine moloney leukemia virus
mRNA	Messenger RNA
MSH	mutS homolg
mTOR	Mammalian target of rapamycin
MYC	v-myc avian myelocytomatosis viral oncogene homolog
NAD	Nicotinamide adenine dinucleotide
NaL	Sodium *L*-lactate
NFAT	Nuclear factor of activated T cells
NF-κB	Nuclear factor κB
NK	Natural killer
NKG2D	Natural-killer group 2, member D
NO	Nitric oxide
NOS	Nitric oxide synthase
NRAS	Neuroblastoma RAS viral oncogene homolog
OXPHOS	Oxidative phosphorylation
PB	Pacific blue

PBS	Phosphate buffered saline
PCR	Polymerase chain reaction
PD-1	Programmed cell death 1
PDH	Pyruvate dehydrogenase
PDK1	Pyruvate dehydrogenase kinase 1
PD-L1	Programmed cell death ligand 1
PE	Phycoerythrin
PerCP	Peridinin chlorophyll protein
PET	Positron emission tomography
PHDs	Prolyl hydroxylases
PI3K	Phosphoinositide 3-kinase
PMA	Phorbol 12-myristate 13-acetate
PPI	Proton pump inhibitors
PPP	Pentose-phophate pathway
PTEN	Phosphatase and tensin homolog
PVDF	Polyvinylidene difluoride
qRT-PCR	Quantitative real-time PCR
RNA	Ribonucleic acid
ROS	Reactive oxygen species
s.e.m.	Standard error of the mean
SCID	Severely combined immunodeficient
SDH	Succinate dehydrogenase
SDS-PAGE	Sodium dodecylsulfate polyacrylamide gel electrophoresis
shRNA	Short hairpin RNA
siRNA	Small interfering RNA
SOC	Super optimal broth
SSC	Side scatter
STAG2	Stromal antigen 2
STAT3	Signal transducer and activator of transcription 3
TAMs	Tumor-associated macrophages
TB	Terrific Broth
TBS	Tris buffered saline
TBST	TBS buffer + Tween 20
TCA	Tricarboxylic acid
TCR	T cell receptor
TEMED	N,N,N’,N’-tetramethylethylenediamine
TET2	Tet oncogene family member 2
TGF	Transforming growth factor
Th	T helper
TIGAR	TP53-induced glycolysis and apoptosis regulator
TNF	Tumor necrosis factor
TP53	Tumor protein p53
TRAIL	Tumor necrosis factor-related apoptosis-inducing ligand
Tregs	Regulatory T cells
UV	Ultraviolet
VEGF	Vascular endothelial growth factor
VHL	Von Hippel-Lindau

1 Introduction

1.1 The hallmarks of cancer - Functional capabilities of tumor cells

Cancer, as a leading cause of death worldwide, is a global health problem and its occurrence is increasing due to demographic changes and unhealthy lifestyle behaviors[1].

The multistep process of tumor formation and progression is accompanied by the acquirement of several functional features, known as hallmarks of cancer (Figure 1-1), which ensure survival, proliferation and dissemination of tumor cells[2].

Figure 1-1. The hallmarks of cancer
Scheme of the functional capabilities of tumors acquired during tumorigenesis. (Modified from Hanahan and Weinberg, Cell 2011[2])

Genome instability and mutation is causal for tumorigenesis. While the accumulation of spontaneous mutations during cell replication is very low, due to high efficiency and accuracy of deoxyribonucleic acid (DNA) repair mechanisms in normal cells, cancerous cells develop numerous mutations. This results from a compromised DNA repair system by inactivating mutations and/or epigenetic repression via DNA methylation and histone modifications[2]. Loss of function of the genes *ATM* (*ataxia telangiectasia mutated*), *BRCA1* (*breast cancer 1*), *BRCA2*, *BAP1* (*BRCA1-associated protein 1*), *MLH1* (*mutL homolog 1*), *MSH2* (*mutS homolog 2*), *MSH6* and *STAG2* (*stromal antigen 2*), which are involved in DNA damage control, were demonstrated in several tumors and thereby behave as tumor suppressor genes[3].

The accumulation of mutations is further accelerated by impaired surveillance systems that normally safeguard genomic integrity. Loss of tumor suppressor *TP53* (*tumor protein p53*), known as the guardian of the genome, is the most prominent example. It plays a crucial role in triggering cell death as a response to DNA damage[3] and is said to be the most frequently mutated gene in human tumors[4]. Other tumor suppressor genes involved in cell survival or fate, which show a loss of function in several types of cancer, are *PTEN* (*phosphatase and tensin homolog*), *TET2* (*tet oncogene family member 2*) and *VHL* (*von Hippel-Lindau*). Besides, several oncogenes implied in cell survival or fate are activated in tumors, including *AKT* (*v-akt murine thymoma viral oncogene homolog 1*), *BCL2* (*B cell CLL/lymphoma 2*), *BRAF* (*v-raf murine sarcoma viral oncogene homolog B1*), *EGFR* (*epidermal growth factor receptor*), *HRAS* (*v-Ha-ras Harvey rat sarcoma viral oncogene homolog*), *KRAS* (*v-Ki-ras2 Kirsten rat sarcoma viral oncogene homolog*), *NRAS* (*neuroblastoma RAS viral oncogene homolog*), *IDH1* (*isocitrate dehydrogenase 1*), *IDH2* and *MYC* (*v-myc avian myelocytomatosis viral oncogene homolog*)[3]. Additionally, in premalignant lesions, decreased telomerase expression leads to the loss of telomers and successive chromosomal aberrations. Resulting amplification or deletion of chromosomal segments also favors tumor-promoting mutations[2].

The most essential characteristic and thereby important hallmark of cancer is **sustained proliferative signaling**. In normal tissues, cell growth and cell division are elaborately regulated by the production and release of growth factors in order to maintain cell homeostasis and normal tissue function. In cancer, this signaling is deregulated. The production of growth factor ligands by tumor cells themselves or by stroma cells after stimulation with tumor-derived signals leads to tumor cell proliferation. Upregulation of growth factor receptors on tumor cells renders them hyperresponsive and allows proliferation, also in the presence of otherwise insufficient amounts of growth factor ligands. Alterations in the structure of growth factor receptors of tumor cells even permit ligand-independent activation and thereby growth factor independence. Furthermore, also independent of ligand-receptor interactions is a constitutive activation of downstream signaling pathways[2]. Structural changes of the BRAF protein by activating mutations, which were observed in a multitude of melanoma patients, for instance, result in constitutive signaling of the RAF to mitogen-activated protein (MAP)-kinase pathway[5]. Similarly, a wide range of tumors exhibit mutations in phosphoinositide 3-kinase (PI3K) isoforms, which leads to the hyperactivation of the AKT signal transducer. The loss of negative feedback mechanisms further supports constant proliferation of tumor cells. Prominent examples are the compromised RAS GTPase activity due to oncogenic mutations in *RAS* genes and loss-of-function mutations in the tumor suppressor *PTEN*, which counteracts PI3K in non-malignant cells, leading to amplified PI3K signaling in tumor cells[6,7].

In support of sustained proliferative signaling is the **evasion of growth suppressors**. This cancer hallmark implies the circumvention of mechanisms that negatively regulate cell proliferation. Thereby tumor suppressor genes play critical roles. The RB (retinoblastoma-associated) and TP53 proteins are potent inhibitors of proliferation. In case of stress or abnormality signals, TP53 can arrest cell-cycle progression until normalization or trigger apoptosis in the event of irreparable damage. Thus, the inactivation of these tumor suppressor genes results in ablation of cell-cycle

control. Additionally, the orchestration of contact inhibition, meaning the suppression of cell growth upon cell-to-cell contact in dense populations, serves to overcome proliferative barriers[2].

Another hallmark of cancer is the **resistance to cell death**. Apoptosis, which is programmed cell death, has been recognized as a protective mechanism for cancer development. Hereby, extracellular death-inducing signals, involving, e.g., Fas receptor/Fas ligand (FAS/FASL) interactions, or intracellular signals result in the activation of caspase 8 or 9, initiating proteolysis by effector caspases and the subsequent disassembling and phagocytosis of the cell. Important pro-apoptotic triggering proteins are BAX (BCL2-associated X protein) and BAK (BCL2 antagonist/killer) which are inhibited by anti-apoptotic proteins like BCL2. Tumors developed a multiplicity of apopotosis-evasion strategies, including the loss of TP53 as a damage-sensing and apoptosis-inducing factor, the upregulation of anti-apoptotic regulators like BCL2, along with the downregulation of pro-apoptotic factors like BAX and the avoiding of extrinsic ligand-induced death pathways[2].

Replicative immortality, which enables tumor cells to generate macroscopic tumors, is also regarded as a hallmark of cancer. Telomeres, which are responsible for the protection of chromosome ends and which shorten during cell replication, are thought to be centrally involved in the trait of unlimited proliferation of tumor cells. The upregulation of telomerase expression and subsequent maintenance of telomeric DNA, thus, secures integrity of chromosome ends and allows tumor outgrowth[2].

In a later stage of tumor formation, a trait that was thought to be important was the generation of neovasculature by the process of **angiogenesis**. The fact that recent data revealed a critical role of angiogenesis also in premalignant neoplastic growth cemented its status as an integral hallmark of cancer. Vasculature, which is in charge of nutrient- and oxygen-supply for tissues as well as the elimination of metabolic waste products and carbon dioxide, develops during embryogenesis and becomes largely quiescent in adults. Contrarily, in tumor cells, established vasculature grows new vessels (angiogenesis). This process is mostly controlled by the upregulation of vascular endothelial growth factor A (VEGF-A) in areas of inadequate oxygen supply (hypoxia) or via oncogenic signaling[2].

Another hallmark of cancer is **tumor-promoting inflammation**[2]. This is described by the expression that tumors are wounds that never heal[8]. Practically every tumor is infiltrated by immune cells, which secrete growth factors, survival factors and pro-angiogenic factors, and thereby contribute to tumor growth and metastasis. By the supply of mentioned bioactive molecules, tumor-promoting inflammation can, therefore, contribute to multiple hallmark capabilities[2].

Activating invasion and metastasis is the last step in tumor progression for many types of cancer. This hallmark implies the dissemination of primary tumor cells to distant sites. A key molecule involved in metastasis is the cell-to-cell adhesion protein E-cadherin, whose downregulation and inactivation was frequently observed in human cancer[2].

The eight hallmarks mentioned above have been shown to be fundamental acquired capabilities in most types of tumors, elucidating, in part, the complex biology of cancer. Yet, two other striking

traits of tumors came into focus during the past years: **deregulated energy metabolism** and **evasion of immune destruction**[2].
In the following chapters, these two novel aspects will be further highlighted.

1.2 Tumor metabolism

Tumors show alterations in their metabolism to fulfill the demands of hyperproliferation. Besides orchestrated glutamine pathways, the most prominent changes occur in glucose metabolism, which is mainly responsible for energy production, but also important for the generation of building blocks for cell proliferation[9]. Alterations in glucose metabolism, as well as alterations regarding amino acid and lipid metabolism, will be described in detail in the following chapters.

1.2.1 Glucose metabolism

In the presence of oxygen, non-malignant cells take up glucose via glucose transporter 1 (GLUT1) and convert it to pyruvate, which is then transported into the mitochondria to fuel oxidative phosphorylation (OXPHOS) and maximize energy yield in form of adenosine triphosphate (ATP) production. Contrarily, in most cancer cells, pyruvate is metabolized to lactate by lactate dehydrogenase 5 (LDH-5), even in the presence of oxygen. Lactate is exported from the cell via monocarboxylate transporters (MCTs) to allow constant glycolytic activity. This process is known as aerobic glycolysis or “Warburg effect” after its discoverer, Nobel prize laureate Otto Warburg (Figure 1-2)[10].

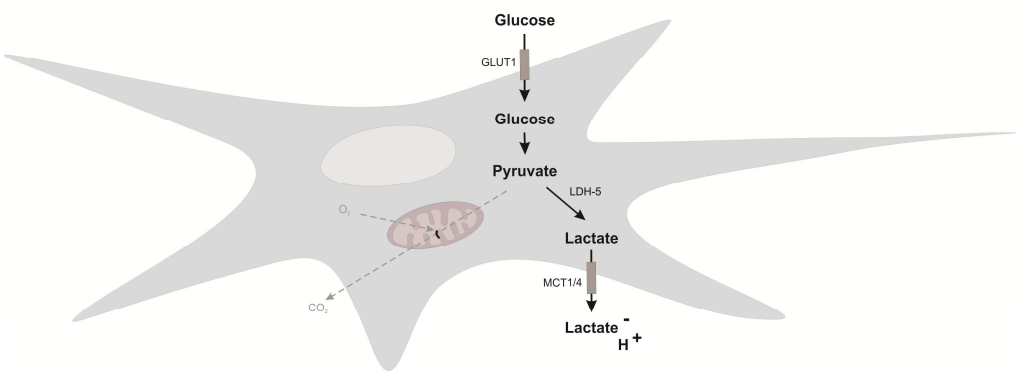

Figure 1-2. Tumors are characterized by accelerated aerobic glycolysis (Warburg phenotype)
Glucose transporter 1 (GLUT1) enables glucose uptake into the cell which is followed by the conversion to pyruvate. In tumor cells, instead of introducing glucose-derived pyruvate into the mitochondria for efficient energy generation, pyruvate is metabolized to lactate by means of lactate dehydrogenase 5 (LDH-5), regardless of the presence of oxygen (O_2), and exported from the cell via monocarboxylate transporters 1 and 4 (MCT1/4).

The considerable lower ATP yield of glycolysis compared to OXPHOS in cancer cells is counterbalanced by an upregulation of GLUT1, leading to increased glucose uptake and an increased flux rate to fulfill the tumor's energy demand[11-13].

Glucose uptake serves as a potent tool for tumor diagnosis and staging: positron emission tomography (PET) measures the uptake and accumulation of the non-metabolizable glucose analog ^{18}F-fluorodeoxyglucose (^{18}F-FDG) by tumor cells. Nowadays, the availability of a wide range of radiotracers also facilitates the investigation of various other aspects of aberrant tumor metabolism, like amino acid uptake, fatty acid and nucleotide synthesis[14].

At first sight, it seems contradictory that cancer cells prefer the inefficient aerobic glycolysis to generate ATP. However, ATP levels in highly proliferating cells relying on aerobic glycolysis seem to be sufficient[12,15].

Otto Warburg attributed the accelerated glycolysis to a disturbed mitochondrial function in tumor cells[10], which today is disproved by several groups, showing that glycolysis is also performed by tumor cell lines with unimpaired mitochondrial capacity[16]. Furthermore, it has been shown recently that some tumor cells even depend on mitochondrial activity[17].

Another hypothesis was that aerobic glycolysis provides a selection advantage in hypoxic areas of tumors, where oxygen supply is insufficient[18]. However, studies by Vander Heiden and colleagues demonstrated that the accelerated glycolysis is not only important for energy production but also needed for the generation of building blocks. Glycolytic intermediates fuel the synthesis of non-essential amino acids and lipids, and serve for the generation of nucleotides via the pentose phosphate pathway (PPP), thereby providing increasing biomass to support rapid cell division (Figure 1-3)[9].

1.2.1.1 Molecular mechanisms of metabolic reprogramming

70% of all human tumors display overexpression of glycolysis-related genes[19]. The glycolytic switch and increased flux of glucose and also glutamine by cancer cells is regulated by hypoxia-inducible factor (HIF), oncogenes and tumor suppressor genes, in order to maximize the synthesis of substrates for membranes, nucleic acids and proteins required for cell growth and division[20].

The HIF family comprises three transcription factors, HIF-1, HIF-2 and HIF-3, which are heterodimers consisting of a stable β-subunit and an unstable α-subunit. Under normoxic conditions, the α-subunit is degraded by oxygen-dependent prolyl hydroxylases (PHDs) and by the von Hippel-Lindau (VHL) ubiquitin ligase. In hypoxia, which frequently occurs in advanced tumors[21], the α-unit is stabilized and assembles with the β-unit[22]. Activation of HIF-1 leads to its binding to hypoxia response elements in the nucleus and to the transcription of several glycolysis-associated genes like *GLUT1*, *HK1* (*hexokinase 1*), *HK2*, *LDHA* and *MCT4*[23,24]. Additionally, pyruvate dehydrogenase kinase 1 (PDK1) is activated and reduces the conversion of pyruvate to acetyl coenzyme A (acetyl-CoA) by inhibiting pyruvate dehydrogenase (PDH)[25]. Together, these alterations compromise OXPHOS, accelerate glycolysis and drive tumor cells into a Warburg phenotype.

Moreover, oncogenes and tumor suppressor genes regulate tumor metabolism and HIF activation independently of oxygen supply. The loss of the tumor suppressor gene *PTEN* augments nutrient- and mitogen-sensing PI3K/AKT and mTOR (mammalian target of rapamycin) activity, which in turn activate HIF[20]. Impairment of PHD activity through accumulation of tricarboxylic acid (TCA) cycle intermediates like succinate due to mutations of genes coding for the TCA cycle proteins succinate dehydrogenase (SDH) and fumarate hydratase (FH) represent another oxygen-independent pathway of HIF stabilization and activation[26].

HIF-1α stabilization is associated with poor prognosis in gastric cancer and linked to decreased chemo- and radiosensitivity[27,28]. HIF is not only upregulated in cancer cells but also in cells of the tumor stroma. In myeloid-derived suppressor cells (MDSCs), which accumulate in many tumor types, HIF-1 was found to regulate their function and differentiation[29].

Furthermore, HIF interacts with other transcription factors like MYC[30]. Oncogenic MYC activates transcription of more than 1,000 genes involved in proliferation and metabolism, like glutaminase-1, which converts glutamine to glutamate. MYC is also responsible for the transcription of genes for ribosomal RNA and proteins assuring protein synthesis and increase in biomass[20]. Another MYC-responsive gene is *LDHA*, which is highlighted in Chapter 1.2.1.2[31]. The tumor suppressor *TP53* represents the most frequently mutated gene in human tumors[4]. It positively regulates OXPHOS via upregulation of the synthesis of the *cytochrome C oxidase 2* gene. Accordingly, loss or mutation of *TP53* accelerates glycolysis[32]. Furthermore, Bensaad et al. identified a TP53-inducible gene named *TIGAR* (*TP53-induced glycolysis and apoptosis regulator*), which directly inhibits glycolysis and redirects glucose to the PPP[33]. Activated TP53 also induces the transcription of *PTEN*, which negatively modulates the AKT-mTOR pathway, resulting in the arrest of cell growth and division[34]. Likewise, TP53-directed apoptosis and activation of autophagy can occur, e.g., in case of DNA damage[35].

In summary, a network of transcription factors, upregulated oncogenes, like *MYC*, and loss of tumor suppressors, like *TP53* or *PTEN* lead to cancer-associated modifications in glucose metabolism resulting in a Warburg phenotype accompanied by alterations in amino acid metabolism (Figure 1-3)[23].

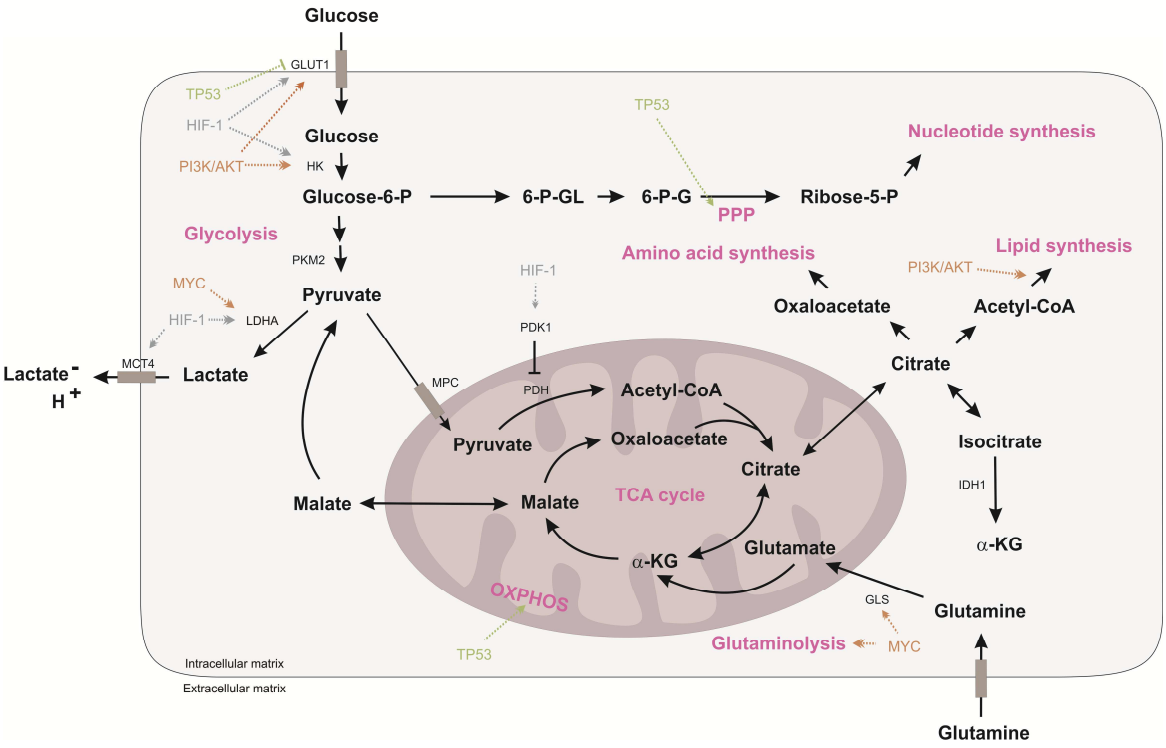

Figure 1-3. Energy metabolism of cancer cells is controlled by alterations in oncogenes and tumor suppressor genes
Scheme depicting the interconnections of glycolysis, oxidative phosphorylation (OXPHOS), glutaminolysis and the pentose phosphate pathway (PPP). Metabolites generated during glycolysis and the tricarboxylic acid (TCA) cycle fuel the synthesis of nucleotides, amino acids and lipids. The influence of HIF-1 (grey), tumor suppressor TP53 (green) and oncogenes MYC and PI3K/AKT (orange) on a variety of enzymes and transporters of metabolic pathways is illustrated. Dotted arrows represent positive and bars represent negative impacts. Glucose-6-P, glucose-6-phosphate; 6-P-GL, 6-phosphogluconolactone; 6-P-G, 6-phosphogluconate; Ribose-5-P, ribose-5-phosphate; GLUT1, glucose transporter 1; HK, hexokinase; PKM2, pyruvate kinase M2; LDH-5, lactate dehydrogenase 5; MCT1/4, monocarboxylate transporter 1 and 4; MPC, mitochondrial pyruvate carrier; PDH, pyruvate dehydrogenase; PDK1, pyruvate dehydrogenase kinase 1; α-KG, α-ketoglutarate; GLS, glutaminase; IDH1, isocitrate dehydrogenase 1. (Adapted from Vander Heiden et al., Science 2009[9])

1.2.1.2 Lactate dehydrogenase

LDH is a major enzyme involved in the Warburg effect. It is a tetramer and composed of two different protein subunits, LDHA (LDH-M, muscle) and LDHB (LDH-H, heart), encoded by the *LDHA* gene and *LDHB* gene, respectively. Subunit A and B can form five possible tetramers/isoenzymes: LDH-1 (B4), LDH-2 (B3A1), LDH-3 (B2A2), LDH-4 (B1A3) and LDH-5 (A4). LDHs catalyze the interconversion of pyruvate and lactate, dependent on the composition of the protein subunits. The LDH-1 enzyme, which is present in oxygenated tissues, e.g., the heart muscles, predominantly catalyzes the conversion of lactate to pyruvate. Conversely, the LDH-5 enzyme, mainly found in the skeletal muscle, catalyzes the conversion of pyruvate to lactate, coupled with the restoration of NAD^+ (nicotinamide adenine dinucleotide), which in turn fuels glycolysis[36].

Early analyses of various human tumors revealed a higher prevalence of LDH-M subunits compared to adjacent non-malignant tissue[37]. In renal cell carcinoma and gastric cancer, overexpression of LDHA correlates to the clinical disease stage and is linked with aggressiveness

and poor prognosis, suggesting that LDHA holds promise as a prognostic marker[38,39]. In melanoma patients, where serum LDH levels are predictive of prognosis and response to treatment, overexpression of LDH-5 in tumor tissues is related to reduced overall survival[40].

Moreover, LDH-5 is a direct target of HIF-1 and the proto-oncogene MYC (Figure 1-4)[41,42]. In pancreatic tumor cells, increased expression of forkhead box protein M1 (FOXM1) led to an upregulation of *LDHA* via direct binding to the promoter region[43]. In contrast, *LDHA* was repressed by miR-34a (microRNA 34a)[44]. MicroRNAs, a group of small endogenous, non-coding RNAs, bind to the 3' untranslated region of mRNAs, promote mRNA degradation and/or inhibit translation. Thereby they regulate gene expression, which makes them important players in tumorigenesis[45]. Besides transcriptional and post-transcriptional regulation, LDHA is controlled by post-translational modifications. Tyrosine phosphorylation and lysine acetylation of LDHA were shown to control LDH-5 activity and thereby seem to be involved in the Warburg effect[46-48].

Fantin et al. demonstrated that downregulation of LDHA by means of shRNA (short hairpin RNA) resulted in an increase in OXPHOS in tumor cells and under hypoxia, tumor proliferation was diminished[49]. Accordingly, downregulation of LDHA by siRNA (small interfering RNA) or a small molecule inhibitor FX11 reduced ATP levels, elevated oxygen consumption and reactive oxygen species (ROS), and finally led to cancer cell death[50]. Consistently, after *LDHA* disruption in human renal cancer cells, non-small cell lung cancer cells or mouse breast cancer cells and subsequent inoculation into mice, tumors showed reduced growth and delayed metastatic spread[51-53]. In line with these findings in mouse models, Wang et al. described a positive correlation between LDHA expression and tumor size in human breast cancer specimen[54].

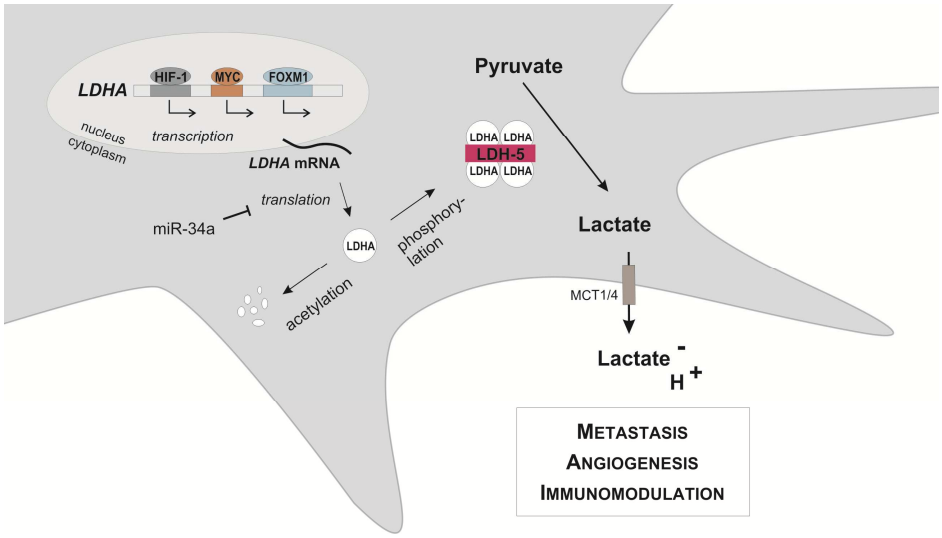

Figure 1-4. Mechanisms and impact of *LDHA* regulation
HIF-1, MYC and FOXM1 are transcription factors for the *LDHA* gene leading to *LDHA* mRNA expression after binding to the *LDHA* promoter region. *LDHA* mRNA is translated to LDHA proteins, which form the homotetrameric enzyme LDH-5. LDHA is post-transcriptionally regulated by the repressor miR-34a and post-translationally by acetylation and subsequent proteolysis. In contrast, phosphorylation enhances LDH-5 tetramer formation. LDH-5 catalyzes the conversion of pyruvate to lactate, and lactate export via MCT1 and 4 (MCT1/4) leads to accumulation of lactic acid ($Lactate^- H^+$), which in turn facilitates metastasis, angiogenesis and immunomodulation. (Adapted from Augoff et al., Cancer Letters 2015[55])

1.2.1.3 Lactate and lactic acid

The Warburg phenotype of tumors is characterized by aerobic glycolysis which leads to the excessive generation of lactate[10]. Several publications demonstrate that the production of lactate is favorable for the tumor (Figure 1-4). Walenta et al. described a positive correlation of high lactate levels in primary human tumors (up to 40 µmol/g) and the incidence of distant metastases[56,57]. In addition, tumor-derived lactate has been shown to fuel OXPHOS in oxygenated tumor cells in heterogeneous tumors[58]. It increases cancer stemness and metastases[59] as well as migration of tumor cells, while inhibiting monocyte motility[60]. Consistently, downregulation of lactate production by *LDHA* siRNA abrogated the migration of glioma cells and attenuated TGF-β2 (transforming growth factor β2) secretion, which is important for extracellular matrix (ECM) remodeling[61]. Lactate also promoted the migration of endothelial cells by increasing their production of VEGF[62]. VEGF, in turn, is an important factor implicated in angiogenesis. Furthermore, lactate induced the upregulation of hyaluronan, a component of the ECM which enables cell movement, and its receptor CD44 (cluster of differentiation molecule 44) on melanoma cells, resulting in an aggressive phenotype[63]. Hyaluronan and CD44 expression was also fostered on fibroblasts when they were cultured with lactate[64]. Tumor-associated fibroblasts are known to take up lactate which leads to lactate "recycling", as they convert it to pyruvate and use it for the TCA cycle and OXPHOS. So it seems that tumor and stroma cells complement each other, recycle products of glycolysis and thereby buffer the tumor environment[65].

In tumor xenografts of head and neck squamous cell carcinoma, lactate levels positively correlated with radioresistance[66]. These results underline the importance of glycolysis and subsequent lactate production for tumor progression and metastasis.

Lactate is exported from the tumor cell in co-transport with protons via MCT1 and MCT4[67], where it accumulates as lactic acid and leads to a subsequent acidification of the tumor environment[68]. While the extracellular pH value in normal tissues is around pH 7.5, the tumor microenvironment can exhibit values between pH 6.5 and pH 6.0[69-71]. This tumor acidosis leads to enhanced degradation of the ECM, thereby increasing the invasiveness of tumors[18]. Thus, normalizing the pH by means of buffering or proton pump inhibitors (PPI) counters spontaneous metastasis and tumor growth[71-73]. Moreover, acidification upregulates the expression of VEGF in brain tumors[74]. Importantly, lactic acid suppresses the anti-tumor immune response in the tumor microenvironment, which is described in detail in Chapter 1.4.

1.2.2 Amino acid metabolism

Besides glucose, glutamine, as the most abundant amino acid in the body, is a crucial nutrient for cell proliferation. In fast growing tumor cells, the uptake of glutamine is increased, followed by the conversion to glutamate or lactate, a process called glutaminolysis (Figure 1-3)[75]. Increased glutamine metabolism is linked to MYC expression[76] and upregulation of glutaminase in cancer patients[77]. The resulting increase in glutamate levels has been shown to inhibit T cell activity[78].

Other amino acids that play important roles in tumor metabolism are tryptophan and arginine, which will be discussed more in detail in the following chapters.

1.2.2.1 Tryptophan metabolism

Tumors often show a deregulation in tryptophan metabolism in order to evade immune control[79]. Mechanisms and outcomes for the tumor will be explained in the following chapter.

Tryptophan is converted to kynurenine by indoleamine 2,3-dioxygenase (IDO). IDO overexpression, of both the classic form IDO1 as well as a novel form IDO2, has been described in several types of cancer[80,81]. Decreased serum tryptophan levels are linked to poor prognosis in melanoma[82]. In colorectal cancer, increased malignancy was related to overexpression of IDO and subsequent diminution of tumor infiltrating lymphocytes. As T cell activation depends on tryptophan uptake, the depletion of tryptophan by excessive IDO activity of cancer cells, leads to an unresponsiveness of T cells[83]. However, T cell function is not only impaired due to overexpression of IDO by tumor cells but also by IDO expression of macrophages and dendritic cells[84]. Besides the immunosuppressive properties of tryptophan depletion, kynurenine, the primary product of tryptophan metabolism by IDO, exerts negative effects on T cell activity. Opitz et al. further discovered that tryptophan 2,3-dioxygenase, a liver enzyme which was not yet reported to be involved in cancer biology, is overexpressed in glioma cells and leads to tryptophan degradation in brain tumors[85]. Treatment with IDO inhibitors and IDO silencing by siRNA improved T cell responses and anti-tumor immunity, diminished tumor formation and augmented responses to chemotherapy[86-89].

1.2.2.2 Arginine metabolism

Arginine is important for polyamine synthesis, which is essential for cell growth and differentiation. It is metabolized by arginase (ARG) to ornithine and urea. Ornithine is a precursor of polyamine synthesis and also serves as precursor for proline synthesis, which is involved in collagen production. In mammals, two different genes code for the two arginase isoforms ARG1 and ARG2[90]. ARG1 is found in the cytosol of hepatocytes, where it plays an important role in the urea cycle and is also expressed in granulocytes[91], while ARG2 is constitutively expressed in mitochondria of different cell types like, e.g., renal cells, neurons, macrophages and enterocytes[90]. In various types of cancer, an increased ARG activity was observed[92]. Therefore, the availability of ARG and the expression of ARG1 and ARG2 seem to be of crucial importance for tumors due to the supply with polyamines and negative effects on T cell function[93], as described in Chapter 1.3.2.1.1.

Alternatively, nitric oxide synthase (NOS) converts arginine to citrulline and nitric oxide (NO). NOS comprises a family of enzymes: NOS1 (nNOS) is expressed mainly in neuronal tissue, NOS2 (iNOS) is inducible in various immune cells and NOS3 (eNOS) is present primarily in endothelial cells. After full activation via assembly with calmodulin and several co-factors, NOS converts arginine to NO[93]. NO production by activated macrophages is known to inhibit tumor growth and

to induce tumor cell death[94]. Elevated levels of NO were detected in various human tumors, yet, the role of NOS expression in the tumor environment is still not clear[95,96].

1.2.3 Lipid metabolism

Here, exclusively the metabolism of arachidonic acid involving cyclooxygenases 1 and 2 (COX1, COX2), resulting in the synthesis of prostanoids, which function as mediators of inflammation, will be outlined. While COX1 is constitutively expressed in almost every kind of tissue, COX2 expression is induced by inflammation and oncogenes, like the proto-oncogene *RAS*, and is primarily found in tumors[97]. Overexpression of COX2 is associated with poor prognosis in breast carcinoma[98] and seems to be linked to HIF expression, resulting in augmented survival of colorectal cancer cells[99]. Consistently, inhibition of COX2 mitigated tumor growth by preventing the infiltration of tumor-promoting MDSCs and impairing their ARG expression[100-104].

1.3 Tumor immunology

The first observation that neoplastic tissues are infiltrated by leukocytes was made by Rudolf Virchow in 1863 and led him to the conclusion that cancer is linked to inflammation[105]. In 1986, Harold F. Dvorak compared tumors to wounds that do not heal, highlighting the contribution of stroma cells to tumor growth[8]. Nowadays, tumor-promoting inflammation is recognized as a hallmark of cancer and immune escape mechanisms, utilized by tumors to prevent elimination by immune cells, represent a newly discovered trait of human malignancies[2]. In the following chapters, both the role of inflammation in cancer and the interactions between tumor and immune cells will be discussed in detail.

1.3.1 Inflammation and cancer

Inflammation plays an essential role in all stages of tumorigenesis and is recognized as a hallmark of cancer, as described in Chapter 1.1[2]. Only a minority of tumors is caused by germline mutations, whereas about 90% of tumors develop due to somatic mutations and environmental factors. Among the latter, chronic infections account for almost 20% of tumors. For instance, infections with *Helicobacter pylori* are a common cause for gastric cancer and chronic infections with hepatitis B virus or hepatitis C virus increase the risk for hepatocellular carcinoma. Accordingly, patients suffering from inflammatory bowel disease have a higher risk to develop colorectal cancer[106].

Other contributing environmental factors are tobacco smoking, inhaled pollutants and an unbalanced diet. Exposure to noxae as well as obesity can in turn trigger inflammation. Cigarette smoking, for instance, provokes chronic bronchitis which can lead to lung cancer[107].
Inflammation, which is characterized by heat (calor), pain (dolor), redness (rubor) and swelling (tumor), occurs in two manifestations: acute inflammation is the physiological and timely limited response of the immune system to infections; in contrast, chronic inflammations persist for a long time[107]. However, not all chronic inflammatory diseases increase cancer risk. Psoriasis for instance seems to exert the opposite effect[108]. This suggests that cancer-associated chronic inflammation differs from normal chronic inflammation, meaning that solid tumors trigger intrinsic inflammation to favor a pro-tumorigenic microenvironment. Cancer-associated inflammation is characterized by the overexpression of oncogenes like *MYC* and *RAS*, which, besides the initiation of hyperproliferation and angiogenesis, induce the production of pro-tumoral cytokines and chemokines and thereby facilitate the recruitment of immune cells of myelomonocytic origin, like MDSCs[109].

1.3.2 Immune cells in the tumor microenvironment

The tumor stroma consists of fibroblasts, endothelial cells, pericytes, mesenchymal cells and cells of the innate and adaptive immune system. Innate immune cells like macrophages, neutrophils, eosinophils, basophils, mast cells, dendritic cells (DCs) and natural killer (NK) cells represent the first line of defense against invading pathogens. Tissue-resident macrophages, mast cells and DCs diligently police their environment for distress signals and release mediators like cytokines, chemokines, histamine, matrix remodeling proteases and ROS to attract the infiltration of leukocytes to the site of damage, leading to inflammation. The activation of vascular and fibroblast responses by macrophages and mast cells contributes to wound healing. DCs as mediators between innate and adaptive immunity, take up foreign antigen, move to the lymphoid organs and present their antigens to T cells in a major histocompatibility complex (MHC)-dependent manner. NK cells interact with DCs to regulate their maturation and in turn become activated by mature DCs[110].
Contrary to the rapid rather unspecific first-line defense by the innate immune system, the adaptive immunity is directed against a specific antigen and characterized by a memory function. The cells of the adaptive immune system, B and T lymphocytes, undergo clonal expansion upon recognition of foreign antigens presented by DCs and, therefore, constitute a much more sophisticated but time-consuming immune response[110].
Immune cells present in the tumor microenvironment represent a double-edged sword as they can promote or inhibit tumor growth. The balance between these extremes is regulated by tumor-derived factors which control abundance and activity of different types of immune cells in the tumor microenvironment[111]. The interaction between tumor cells and immune cells, the so-called “cancer immunoediting”, can be categorized in three states: elimination, equilibrium and escape (Figure 1-5)[112]. In the elimination phase, the immune system functions as a tumor suppressor and

kills tumor cells. This immunosurveillance is lost in immunocompromised mice reflected by the increased incidence of tumors. Similar observations show elevated tumor development in immunosuppressed patients after organ transplantation or in case of HIV[113]. If tumor cells survive the attack of immune cells, proliferation can still be controlled by immunological mechanisms, which leads to a state of equilibrium[114]. Tumor immune evasion means that tumors overcome anti-tumor immunity and become clinically apparent[115].

Several mechanisms leading to tumor immune evasion have been identified. Tumors can evade immune recognition via downregulation of MHC class I molecules leading to compromised activation of cytotoxic T cells ($CD8^+$ T cells). Furthermore, tumors create an immunosuppressive microenvironment by producing factors like TGF-β, interleukin 10 (IL-10) and VEGF, which in turn lead to the accumulation of immunosuppressive cells like regulatory T cells (Tregs) and MDSCs. Immunosuppression is also achieved via induction of inhibitory receptors like CTLA-4 (cytotoxic T lymphocyte-associated protein 4) and PD-1 (programmed cell death 1) on immune effector cells and PD-L1 (programmed cell death ligand 1) on tumor cells[115]. The interplay between tumor cells and specific immune cell populations present in the tumor microenvironment will be highlighted in the following chapter.

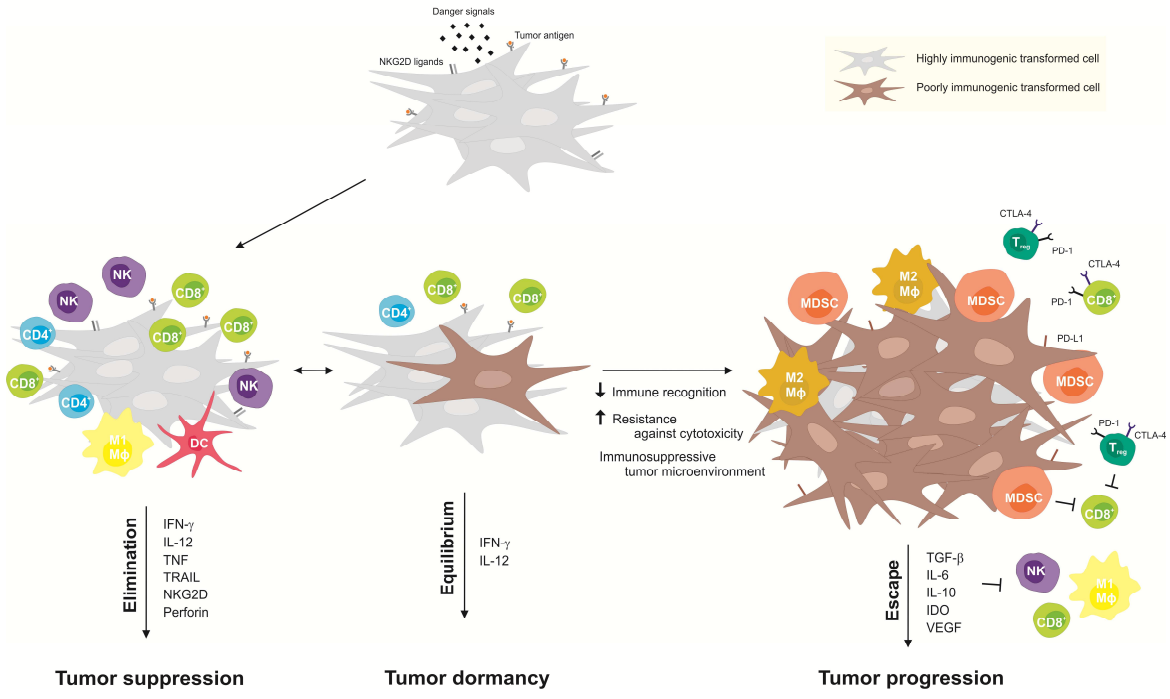

Figure 1-5. Cross-talk of immune and cancer cells: Immunoediting
Malignant transformed cells are recognized and eliminated by cytotoxic T cells ($CD8^+$), NK cells and innate immune cells. Tumor cells, that survive elimination, enter an equilibrium phase, where tumor outgrowth is inhibited by cells of the adaptive immune system. Due to constant selection pressure, tumor cell variants can emerge, which display reduced immune recognition or suppress immune cell function, leading to tumor progression. NKG2D, NK group 2, member D; NK, natural killer cell; MΦ, macrophage; DC, dendritic cell; IFN, interferon; IL, interleukin; TNF, tumor necrosis factor; TRAIL, tumor necrosis factor-related apoptosis-inducing ligand; MDSC, myeloid-derived suppressor cell; T_{reg}, regulatory T cell; CTLA-4, cytotoxic T lymphocyte-associated protein-4; PD-1, programmed cell death 1; PD-L1, programmed cell death ligand 1; TGF-β, transforming growth factor β; IDO, indoleamine 2,3-deoxygenase; VEGF, vascular endothelial growth factor. (Adapted from Schreiber et al., Science 2011[116])

1.3.2.1 Myeloid cells

1.3.2.1.1 Macrophages and myeloid-derived suppressor cells

The most abundant immune cells found in tumors are tumor-associated macrophages (TAMs). They originate from circulating monocytes or tissue-resident macrophages and are recruited into the tumor microenvironment, e.g., via the chemokine CCL2 (chemokine (C-C motif) ligand 2)[117], CSF1 (colony-stimulating factor 1) and VEGF[118]. TAMs are present during all stages of tumorigenesis[112] and are involved in angiogenesis, invasion and metastasis[119]. Consistently, high numbers of infiltrating TAMs correlate with poor prognosis[120]. Macrophages can be subdivided in M1 macrophages, found during inflammation, and anti-inflammatory M2 macrophages, preferentially accumulating in the tumor microenvironment. M1 macrophages develop upon stimulation with IFN-γ (interferon γ) and microbial factors (classical activation), and display a pro-inflammatory phenotype with high expression of TNF-α (tumor necrosis factor α), IL-1, IL-6, IL-12, IL-23, MHC molecules and iNOS, thereby promoting an anti-tumor response. In contrast, M2 macrophages, which differentiate after stimulation with IL-4, IL-10 and IL-13 (alternative activation), produce anti-inflammatory cytokines like IL-10, show downregulation of MHC class II expression, and express scavenger receptor A and ARG[121]. However, a strict separation of M1 and M2 macrophages is not possible as both “types” represent only the extremes of these highly plastic myeloid cells, which can rapidly adapt their phenotype to the microenvironment. This variable polarization could possibly explain the observation that a high grade of infiltration with TAMs can also be related to a favorable prognosis in a minority of human tumors[122].

Another myeloid cell type sharing some characteristics with M2-like TAMs is the so-called MDSC. This population mainly consists of immature myeloid cells co-expressing the classical myeloid lineage marker CD11b and the granulocytic marker Gr-1 in mice[123,124]. MDSCs are potent inhibitors of T cells via arginine deprivation in the tumor microenvironment due to high ARG1 expression[125]. Furthermore, they cause nitration of the T cell receptor (TCR) via excessive ROS and peroxynitrite production during direct cell-cell contact[126]. MDSCs also induce Treg activation and expansion. At present, MDSCs can be divided into two main subsets: the more prevalent granulocytic MDSCs and the monocytic MDSCs, which are characterized by CCR2 (chemokine (C-C motif) receptor 2) expression and show higher immunosuppressive capacity[127]. Their expansion is promoted by granulocyte-macrophage colony-stimulating factor (GM-CSF=CSF2, colony-stimulating factor 2)[128].

1.3.2.1.2 Dendritic cells

DCs are important inducers of an anti-tumor immune response as they cross-present antigens to T cells. This task can only be performed by fully mature DCs. Various factors like VEGF and IL-10, which are released by tumor cells and TAMs can lead to an immature or tolerogenic DC phenotype[129]. Tolerogenic DCs are characterized by IL-10, TGF-β and IDO production, resulting in a compromised ability to activate T cells[130]. The production of angiogenic factors by immature DCs directly promotes tumor growth[131]. Moreover, these cancer-associated DCs augment the

expansion of Tregs and cause T cell anergy. Altogether, tumor cells are capable to elicit a reprogramming of DCs towards an immunosuppressive and pro-angiogenic phenotype that promotes tumor growth[132].

DCs also play a role in NK cell activation, thereby promoting a potent immune response against tumors. In addition, direct cytotoxic effects of DCs against tumor cells were observed. However, until now, no clear correlation of DC infiltration and prognosis can be demonstrated in human tumors[133].

1.3.2.2 Lymphoid cells

1.3.2.2.1 Natural killer cells

NK cells, as potent players in cancer immunosurveillance, are not only capable of targeting tumors indirectly via the secretion of IFN-γ and activation of M1 and T helper 1 (Th1) anti-tumor immune responses[134]; they can also directly lyse tumor cells irrespective of prior activation and without MHC restriction. This process occurs through the release of perforin and granzyme from cytolytic granules[135] and is controlled by NK cell surface receptors, such as NKG2D (natural-killer group 2, member D) which recognizes stress-induced NKG2D ligands on target cells[136]. NK cells also lyse tumor cells that lost MHC class I molecules[135] and thereby escaped from the immunologic control by cytotoxic T cells[137]. Thus, high numbers of infiltrating NK cells correlate with a favorable prognosis in patients with lung, gastric, colorectal and head and neck cancer[138,139]. However, in melanoma, renal, breast and liver carcinoma, NK cell infiltration is impaired[140-143] and isolated NK cells from tumor lesions are inactive. These findings suggest that NK cell effector functions are inhibited by tumor cells[137]. Several immune escape mechanisms have been identified that help tumor cells to evade NK cell cytotoxicity, e.g., repression of NK cell infiltration and effector function, and tumor editing towards a poorly immunogenic tumor phenotype[130]. Tumor cells prevent NK cell attraction via downregulation of chemokines like CXCL2 (chemokine (C-X-C motif) ligand 2)[134,135] and generate an immunosuppressive tumor microenvironment by means of TGF-β production[137]. Additionally, hypoxia in the tumor microenvironment impairs the expression of activating receptors on NK cells, such as NKG2D, and thereby limits their ability to kill tumor cells[144]. Tumor cells' editing towards a poorly immunogenic phenotype involves downregulation of NKG2D ligand expression on tumor cells and thereby impedes the recognition by NK cells[130,145]. Upregulation of MHC class I molecules on tumors, a phenomenon observed for instance in melanoma lesions[142], also contributes to the evasion of tumor cells[145]. The reprogramming of NK cells towards a tumor-promoting phenotype, displaying compromised cytolytic functions and pro-angiogenic properties, was observed in lung, colorectal and breast cancer[135]. In this context, findings linking high NK cell infiltration to poor outcome in metastatic ovarian carcinoma and invasive ductal breast cancer are not surprising[146,147].

1.3.2.2.2 T lymphocytes

Similar to NK cells, cytotoxic T cells possess potent anti-cancer properties, which are based on the recognition of tumor-specific antigens or tumor-associated antigens expressed by cancer cells, and the consequent induction of a cytotoxic T cell response[112]. $CD8^+$ effector T cells secrete IFN-γ and TNF-α and directly kill tumor cells via the release of perforin or granzyme from lytic granules[148]. Consistently, high numbers of infiltrating $CD8^+$ T cells predict a favorable outcome in ovarian cancer, melanoma, colorectal cancer and breast cancer[149-152].

Hence, efforts are made to identify tumor-specific mutations, which implies extensive genome sequencing[153]. The accumulation of mutational epitopes in tumors correlated with increased patient survival and was linked to elevated infiltration of cytotoxic T cells[154]. However, targeting tumor-specific antigens by adoptively transferred T cells had only limited success in melanoma, lung and bladder cancer[155].

Unlike tumor-specific antigens, tumor-associated antigens are not exclusively expressed on cancer cells but also on normal cells[112]. Recognition of tumor-associated antigens can, therefore, lead to mechanisms of self-tolerance, resulting in an inefficient anti-tumor immune response[156].

Tregs are a specific subpopulation of T helper cells ($CD4^+$ T cells) and are characterized by the expression of CD4, CD25 and FOXP3 (forkhead box P3). Under physiological conditions, Tregs protect against autoimmune diseases via suppression of self-reactive T cells. In the tumor microenvironment, Tregs suppress anti-tumor immunity by secreting immunosuppressive factors like IL-10 and TGF-β. TGF-β production by tumor cells or Tregs can convert conventional T cells into Tregs which then inhibit effector functions of lymphocytes. Furthermore, Tregs compete with other lymphocytes for IL-2 and thereby limit T cell proliferation and activation[157]. However, in humans, no clear association has been described regarding Treg infiltration and prognosis, and the outcome seems to depend on the type of cancer[112].

The heterogeneous population of $CD4^+$ T cells further consists of Th1 cells and Th2 cells, which arise upon stimulation with IL-12 and IL-4, respectively, as well as Th17 cells which are induced by IL-6 and TGF-β. Th1 cells secrete IFN-γ and TNF-α, and thereby promote a cytotoxic T cell response, whereas the production of IL-4, IL-5 and IL-13 by Th2 cells leads to tumor promotion. Th17 cells secrete IL-17, IL-21 and IL-22 and play an ambiguous role in cancerogenesis, facilitating either tumor rejection or tumor progression, depending on the type of cancer[158].

1.3.2.2.3 Regulation of the T cell response by checkpoint molecules

Effector functions of T cells are regulated by the balance of co-stimulatory and co-inhibitory signals. T cells recognize (tumor-)antigens presented on MHC molecules of antigen-presenting cells, like DCs, via the TCR. Apart from this signal, T cells require additional stimulation by antigen-independent co-stimulatory receptors, such as CD28, in order to become fully activated. In contrast, the stimulation of an inhibitory co-receptor on T cells, e.g., PD-1 or CTLA-4, leads to T cell inhibition. These immune checkpoint molecules limit the extent and duration of the immune response. PD-1 is upregulated on a variety of activated immune cells, including T and B cells, NK cells, monocytes and DCs, and represents a negative feedback loop to control T cell activation,

since T cell cytokines like IFN-γ or IL-4 upregulate PD-1 ligands. PD-L1 is expressed by a variety of solid and hematological human tumors and helps tumor cells to evade anti-tumor T cell effector functions. Consistently, a link between PD-L1 expression and poor outcome in various types of cancer has been demonstrated, which might also partially explain their resistance to adoptive T cell therapies[112].

1.3.3 Cytokines in the tumor microenvironment

The communication of cells in the tumor microenvironment occurs either directly via cell-cell-contact or via soluble factors such as cytokines and chemokines, which can act in an autocrine and paracrine manner[111].

The cytokine and chemokine profile in the tumor microenvironment regulates immune cell function and can either promote or inhibit tumor growth[111]. While anti-tumor immunity is achieved by cytokines like IL-12 and IFN-γ as well as by TRAIL (tumor necrosis factor-related apoptosis-inducing ligand), tumor promotion is mediated through cytokines like IL-1, IL-6, IL-17, IL-23 and TNF. Transcription factors involved in cytokine/chemokine production, which are activated in the majority of tumors and act as non-classical oncogenes are NF-κB (nuclear factor κB) and STAT3 (signal transducer and activator of transcription)[159]. Despite the heterogeneity of human cancer, common cytokine patterns could be identified which lead to immunostimulation or are accompanied by a cancer-protective immunosuppression[160]. Some critical components of the cytokine profile in the tumor microenvironment of human cancer are presented below (Figure 1-6).

1.3.3.1 Immunostimulatory cytokines

Typical immunostimulatory cytokines are IL-2, IL-12, IFN-γ, TNF-α and IL-6.

IL-2 functions as a growth factor for stimulated T cells, necessary for clonal expansion after antigen contact, and is mainly secreted by activated $CD4^+$ T cells but also by naïve $CD8^+$ T cells and DCs[161]. Moreover, IL-2 stimulates the activation of NK cells[162] and plays a crucial role in the development and expansion of Tregs[161].

IL-12 is critical for the connection between innate and adaptive immune responses[163]. It is mainly produced by DCs and stimulates Th1 cells, which in turn activate $CD8^+$ T cells[160]. IL-12 induces IFN-γ production of T and NK cells[163].

The major cytokine for macrophage activation, IFN-γ, upregulates MHC class I and II expression, which is required for antigen recognition by $CD8^+$ and $CD4^+$ T cells, respectively[160]. IFN-γ is mainly produced by cytotoxic T cells, Th1 cells and NK cells, and inhibits the production of the immunosuppressive factor TGF-β[164].

TNF-α - as an acute-phase response cytokine like IL-1 - is produced by macrophages as a rapid response to inflammatory stimuli. It activates neutrophils and monocytes and recruits them to the site of inflammation via regulation of adhesion molecules on endothelial cells. The potent

immunostimulatory characteristics of TNF-α contribute to a pro-inflammatory tumor microenvironment in established tumors[160].

TNF-α induces the production of IL-6, another pro-inflammatory cytokine, by monocytes and macrophages[165]. IL-6 is also responsible for the recruitment of leukocytes to the site of inflammation[166]. Furthermore, it facilitates T cell differentiation and activation, mediates the conversion of B cells into antibody-generating plasma cells and activates fibroblasts to produce matrix metalloproteases for ECM degradation[160]. It blocks Treg development and together with TGF-β induces the polarization of Th17 cells[167].

In many types of human cancer, the concentrations of immunostimulatory cytokines like IL-2, IL-12 and IFN-γ are low, which is often linked to poor prognosis. On the contrary, serum concentrations of immunostimulatory cytokines TNF-α and IL-6 are frequently elevated and correlate with disease progression or worse prognosis[160].

1.3.3.2 Immunosuppressive cytokines

Besides immunostimulatory cytokines, immunosuppressive cytokines are present in the tumor microenvironment, among which TGF-β and IL-10 play major roles.

TGF-β, which is produced, e.g., by tumor cells, is known to suppress a range of pro-inflammatory cytokines like IL-12, IL-2 and IFN-γ, and thereby limits the function of antigen-presenting cells, T cell proliferation and activity of T and NK cells. Besides, B cell proliferation and differentiation is impeded. In contrast, TGF-β supports Th17 and Treg differentiation. Thus, TGF-β, as a potent immunosuppressive factor exerting various effects on other cytokines and immune cells, is a major inducer of local tolerance in the tumor microenvironment[160].

Furthermore, TGF-β upregulates the highly immunosuppressive cytokine IL-10, which in turn leads to increased TGF-β production as a positive feedback mechanism[168].

IL-10 is secreted by a wide range of cells, predominantly by Th2 cells, subsets of Tregs, Th1, Th17 cells, monocytes, macrophages and subsets of DCs but can also be produced by tumor cells. It inhibits the production of the key pro-inflammatory cytokines IL-1, IL-6, IL-12 and TNF-α[169], as well as the production of IL-2 and IFN-γ by Th1 cells. In addition, antigen-presentation of DCs is impaired by IL-10, as MHC class II expression and upregulation of co-stimulatory molecules CD80 and CD86 are compromised[168].

Elevated serum levels of both TGF-β and IL-10 are detected in patients with various cancer types and are correlated with advanced cancer stages, poor outcome or metastases[160].

In summary, the balance between immunoinhibitory and immunostimulatory factors present in human cancer seems to determine the activity of immune cells, and thereby patient outcome (Figure 1-6)[160].

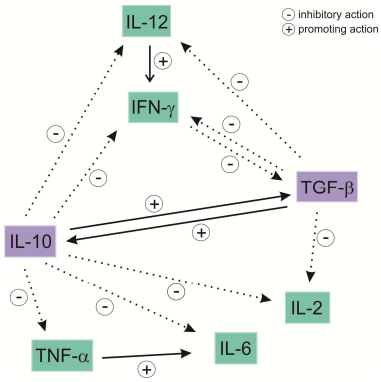

Figure 1-6. Cytokine network in the tumor microenvironment
Simplified scheme of interactions between immunostimulatory (green) and immunosuppressive (purple) cytokines present in the tumor microenvironment. Decreased concentrations of IL-2, IL-12 and IFN-γ and elevated concentrations of TNF-α, IL-6, TGF-β and IL-10 are often linked to poor prognosis in human cancer.

1.4 Impact of tumor metabolism on the immune system

The metabolism of tumors is adapted to provide favorable conditions for tumor growth. This phenomenon does not only influence tumor cells themselves but also exerts effects on stroma cells like immune cells. Accelerated glucose metabolism for instance was found to be correlated with low $CD8^+$ T cell infiltration in renal cell carcinoma[170]. This is in line with the finding that tumor cells deprive the microenvironment of glucose which restricts T cell glycolysis and effector function[171,172]. Several metabolites accumulating in the tumor microenvironment, due to the alterations in tumor metabolism, exhibit immunosuppressive properties. Besides glutamate, kynurenin and methylthioadenosin, lactate represents a potent immunomodulator[173] and is, therefore, highlighted in the following.

In addition to its tumor promoting attributes like the induction of angiogenesis and metastasis[59,62] (Chapter 1.2.1.3), lactate and especially its protonated form lactic acid has been demonstrated to exert inhibitory effects on a range of immune cells. In dendritic cells, differentiation and activation was impeded by lactic acid[174,175], while in human monocytes, TNF secretion was inhibited upon lactic acid exposure[176]. Human T cells showed an impaired proliferation and cytokine production upon treatment with lactic acid[177]. Tumor lactic acidosis further resulted in a compromised function of cytotoxic T lymphocytes via inhibition of P38 and JNK (c-Jun N-terminal kinase)/c-Jun activation[178]. In line with this finding, restoration of the physiological pH by buffering or PPI overrides T cell dysfunction[70,73]. In human monocytes and macrophages, lactic acid was shown to induce the production of IL-23 and thereby facilitate secretion of IL-17, which is a pro-inflammatory cytokine involved in Th17 immune responses[179]. In mice with LDHA-depleted tumors, decreased numbers of MDSCs were found in spleens and NK cell function was inhibited[180]. Moreover, it was demonstrated that lactic acid polarizes TAMs towards an M2 phenotype via the induction of HIF-1α[181].

These findings strongly suggest that lactic acid is a potent immunomodulator. However, little is known about the impact of lactic acid on immune cells *in vivo*.

2 Research Objectives

Metabolic reprogramming of tumor cells is the basis for their excessive proliferation. Changes in the glucose pathway remain the most prominent feature of tumor cells and are known as the Warburg effect. The increased uptake of glucose, subsequent conversion of pyruvate to lactate and the export of the latter in co-transport with protons occurs in the majority of malignant neoplasia. Lactate and lactic acid have been shown to exert a range of direct tumor-promoting functions and there is evidence that lactic acid compromises various types of immune cells.

The aim of this dissertation was to clarify the immunomodulatory role of tumor-derived lactic acid and its impact on tumor growth. In preliminary studies, *Ldha* expression was downregulated in mouse melanoma cells by means of shRNA technology, which resulted in low-lactate producing melanoma tumor cell clones. Tumor growth, immune cell infiltration and activation should be analyzed in respective tumors grown from these cells in immunocompetent and immunodeficient mice. In parallel, *in vitro* analyses should be performed to compare *in vitro* and *in vivo* effects of lactic acid on different types of immune cells.

Finally, biopsies of melanoma patients should be analyzed regarding lactate production and the impact of the latter on immune cell infiltration.

3 Material

3.1 Equipment

ADVIA 1650	Bayer, Tarrytown, USA
Autoclave	Technomara, Fernwald, Germany
Balance LP1200S	Sartorius, Göttingen, Germany
Bioanalyzer 2100	Agilent Technologies, Santa Clara, CA, USA
Biofuge fresco	Heraeus, Hanau, Germany
BioPhotometer	Eppendorf, Hamburg, Germany
Bug Box Hypoxic Work Station	Ruskinn, Bridgend, UK
CASY Cell Counter	Innovatis/Roche, Basel, Switzerland
Centrifuge Megafuge 3.0R	Heraeus, Hanau, Germany
Centrifuge Sigma 2	Sartorius, Göttingen, Germany
Cryo 1 ℃ Freezing Container	Thermo Fisher Scientif ic, Waltham, MA, USA
Electrophoresis equipment	Biometra, Göttingen, Germany
Electrophoresis equipment (PFGE)	Biostep, Jahnsdorf, Germany
ELISA plate reader	MWG Biotech, Ebersberg, Germany
EVOS Cell Imaging System	Life Technologies, Carlsbad, CA, USA
FACS Calibur flow cytometer	BD Biosciences, Franklin Lakes, NJ, USA
Forceps	Aesculap, Tuttlingen, Germany
Heat sealer	Eppendorf, Hamburg, Germany
Incubator Shaker I26	New Brunswick Scientific, Edison, NJ, USA
Incubators	Heraeus, Hanau, Germany
Laminar Flow Cabinet Clean Air	Telstar, Woerden, The Netherlands
LSR II flow cytometer	BD Biosciences, Franklin Lakes, NJ, USA
Microscopes	Zeiss, Jena, Germany
Microtiter plates washer	Thermo Electron Corporation, Waltham, MA, USA
Multifuge 3S-R	Heraeus, Hanau, Germany
Multipipettor Multipette plus	Eppendorf, Hamburg, Germany
NanoDrop 1000	PeqLab, Erlangen, Germany
Oxygraph-2k	Oroborus Instruments, Innsbruck, Austria
PCR Thermocycler PTC-200	MJ-Research/Bio-Rad, Munich, Germany
pH Meter	Knick, Berlin, Germany
pH Meter, portable	Hanna Instruments, Kehl am Rhein, Germany
Picofuge	Heraeus, Hanau, Germany
Pipetboy	Integra Biosciences, Fernwald, Germany
Pipettes	Gilson, Milddleton, WI, USA
Pipettes	Eppendorf, Hamburg, Germany
Power supplies	Biometra, Göttingen, Germany
Pulsed field electrophoresis equipment	GE Healthcare, Chalfont St Giles, UK

Pulsed field gel electrophoresis equipment	Biostep, Jahnsdorf, Germany
Realplex Mastercycler epGradient S	Eppendorf, Hamburg, Germany
Rocking plattform HS250	IKA Labortechnik, Staufen, Germany
Rotilabo mini centrifuge	Carl Roth, Karlsruhe, Germany
Sonorex Ultrasonic Bath	Bandelin, Berlin, Germany
Speed Vac	Christ, Osterode, Germany
Test tube shaker IKA	Sigma-Aldrich, St. Louis, MO, USA
Thermomixer	Eppendorf, Hamburg, Germany
TissueLyser	Qiagen, Hilden, Germany
Vortexer	Scientific Industries Ink., Bohemia, NY, USA
Wallac Betaplate Counter	PerkinElmer, Rodgau, Germany
Wallac Harvester	PerkinElmer, Rodgau, Germany
Water purification system	Merck Millipore, Billerica, MA, USA
Waterbath	Julabo, Seelstadt, Germany
Western blot chamber	Biometra, Göttingen, Germany

3.2 Consumables

Cell culture dishes	BD, Franklin Lakes, NJ, USA
Cell culture flasks	Costar, Cambridge, MA, USA
Cell scrapers	Sarstedt, Nümbrecht, Germany
Cell strainer (70 µm, 100 µm)	Falcon, Heidelberg, Germany
Combitips for Eppendorf multipette	Eppendorf, Hamburg, Germany
Cryo tubes	Corning, Corning, NY, USA
Ep dualfilter T.I.P.S	Eppendorf, Hamburg, Germany
Heat sealing film	Eppendorf, Hamburg, Germany
Hyperfilm ECL	Amersham/GE Healthcare, Chalfont St Giles, UK
Immobilon-P PVDF membrane	Merck Millipore, Billerica, MA, USA
Micro test tubes (0.5 ml, 1.5 ml, 2 ml)	Eppendorf, Hamburg, Germany
Micropore filters	Sartorius, Göttingen, Germany
Microtiter plates (6, 12, 24, 96 wells)	Costar, Cambridge, MA, USA
PCR plate Twin.tec 96 well	Eppendorf, Hamburg, Germany
Petri dishes	Falcon, Heidelberg, Germany
Pipette tips	Eppendorf, Hamburg, Germany
Plastic pipettes	Costar, Cambridge, MA, USA
Polystyrene test tubes	Falcon, Heidelberg, Germany
Polystyrene test tubes with cell strainer cap	Corning, Corning, NY, USA
Scalpels (No. 10), disposable	Feather, Osaka, Japan
Syringe Filters, sterile	Sartorius, Göttingen, Germany
Syringes and needles	BD, Franklin Lakes, NJ, USA
Tubes (5 ml, 15 ml, 50 ml, 225 ml)	Falcon, Heidelberg, Germany
UniFilter plates	PerkinElmer, Rodgau, Germany
Whatman Chromatography Paper	Sigma-Aldrich, St. Louis, MO, USA

3.3 Media, buffers and solutions

2-Mercaptoethanol	Gibco/Life Technologies, Carlsbad, CA, USA
Acrylamide	Carl Roth, Karlsruhe, Germany
APS	Merck Millipore, Billerica, MA, USA
Aqua	B. Braun Melsungen, Melsungen, Germany
Biocoll Separating Solution	Biochrom/Merck Millipore, Billerica, MA, USA
Bovine serum albumine	Sigma-Aldrich, St. Louis, MO, USA
CasyTON	Roche, Basel, Switzerland
DMSO	Sigma-Aldrich, St. Louis, MO, USA
FACS clean	BD Biosciences, Franklin Lakes, NJ, USA
FACS flow	BD Biosciences, Franklin Lakes, NJ, USA
FACS rinse	BD Biosciences, Franklin Lakes, NJ, USA
Fetal calf serum	PAA/GE Healthcare, Chalfont St Giles, UK
Glycerin	Merck Millipore, Billerica, MA, USA
Glycine	Merck, Darmstadt, Germany
H_2O_2	Merck, Darmstadt, Germany
H_2O_{USB}	USB/Affymetrix, Santa Clara, CA, USA
HBSS	Sigma-Aldrich, St. Louis, MO, USA
HCl	Carl Roth, Karlsruhe, Germany
Isopropanol	B. Braun Melsungen, Melsungen, Germany
L-Alanyl-*L*-Glutamine	Biochrom/Merck Millipore, Billerica, MA, USA
MEM Non-Essential Amino Acid Solution	Sigma-Aldrich, St. Louis, MO, USA
MEM Sodium Pyruvate	Sigma-Aldrich, St. Louis, MO, USA
MEM Vitamin Solution	Sigma-Aldrich, St. Louis, MO, USA
Methanol	Thermo Fisher Scientific, Waltham, MA, USA
NaCl	VWR, Radnor, PA, USA
Nuclease-free water	Gibco/Life Technologies, Carlsbad, CA, USA
PBS	Sigma-Aldrich, St. Louis, MO, USA
RIPA buffer	Sigma-Aldrich, St. Louis, MO, USA
RPMI 1640	Gibco/Life Technologies, Carlsbad, CA, USA
SOC medium	Invitrogen, Camarillo, CA, USA
TB medium	Interchim, Wörgl, Austria
TEMED	Sigma-Aldrich, St. Louis, MO, USA
Tris	USB/Affymetrix, Santa Clara, CA, USA
Triton X100	Sigma-Aldrich, St. Louis, MO, USA
Tween 20	Sigma-Aldrich, St. Louis, MO, USA
Typsin-EDTA	PAN Biotech, Aidenbach, Germany

3.4 Enzymes, kits and reagents

^{3}H-thymidine	Hartmann Analytic, Braunschweig, Germany
Agilent RNA 6000 Nano Kit	Agilent Technologies, Santa Clara, CA, USA
Amersham ECL Prime Western Blotting Detection Reagent	Amersham/GE Healthcare, Chalfont St Giles, UK
BD Comp Beads	BD Biosciences, Franklin Lakes, NJ, USA
BD GolgiPlug	BD Biosciences, Franklin Lakes, NJ, USA
Bio-Rad DC protein assay	Bio-Rad, Munich, Germany
Bromophenol blue	Sigma-Aldrich, St. Louis, MO, USA
Caproic acid	Sigma-Aldrich, St. Louis, MO, USA
Carboxy SNARF-1 AM acetate	Life Technologies, Carlsbad, CA, USA
CD8α^{+} T cell Isolation Kit	Miltenyi Biotec, Bergisch Gladbach, Germany
Collagenase IV	Worthington, Lakewood, NJ, USA
Collagenase Type IA	Sigma-Aldrich, St. Louis, MO, USA
Cyclosporin A (Sandimmun®)	Novartis, Basel, Switzerland
DAPI	Sigma-Aldrich, St. Louis, MO, USA
DNase I	Sigma-Aldrich, St. Louis, MO, USA
dNTPs	GE Healthcare, Chalfont St Giles, UK
DuoSet ELISA mouse TGF-β1	R&D Systems, Minneapolis, MN, USA
EDTA	Sigma-Aldrich, St. Louis, MO, USA
FcR-Blocking reagent mouse	Miltenyi Biotec, Bergisch Gladbach, Germany
FoxP3 transciption factor staining buffer set	eBioscience, San Diego, CA, USA
IL-2 (Proleukin)	Novartis, Basel, Switzerland
Intracellular pH Calibration Kit	Life Technologies, Carlsbad, CA, USA
Ionomycin	Enzo Life Sciences, Farmingdale, NY, USA
JetPrime Transfection Reagent	Polyplus-transfection, Illkirch, France
$KHCO_3$	Fluka, Buchs, Switzerland
L-Lactic acid	Sigma-Aldrich, St. Louis, MO, USA
LPS	Enzo Life Sciences, Farmingdale, NY, USA
Luminol	Sigma-Aldrich, St. Louis, MO, USA
MitoTracker Green	Thermo Fisher Scientific, Waltham, MA, USA
M-MLV Reverse Transcriptase	Promega, Madison, WI, USA
MycoAlert Mycoplasma Detection Kit	Cambrex, Rockland, ME, USA
Myxothiazol	Sigma-Aldrich, St. Louis, MO, USA
$NaHCO_3$	Merck, Darmstadt, Germany
NH_4Cl	Merck, Darmstadt, Germany
NK cell Isolation Kit II	Miltenyi Biotec, Bergisch Gladbach, Germany
p-Coumaric acid	Sigma-Aldrich, St. Louis, MO, USA
Plasmid Maxi Kit	Qiagen, Hilden, Germany
PMA	Calbiochem, San Diego, CA, USA
Propidium iodide	Invitrogen, Camarillo, CA, USA
QIAshredder™	Qiagen, Hilden, Germany
QuantiFast SYBR® green PCR Kit	Qiagen, Hilden, Germany
Random Decamers	Ambion/Life Technologies, Carlsbad, CA, USA
RNA*later*™	Qiagen, Hilden, Germany

RNase-free DNase Set	Qiagen, Hilden, Germany
RNeasy Mini Kit	Qiagen, Hilden, Germany
Rotenone	Sigma-Aldrich, St. Louis, MO, USA
SDS	Sigma-Aldrich, St. Louis, MO, USA
Sodium citrate	Merck, Darmstadt, Germany
Sodium *L*-lactate	Sigma-Aldrich, St. Louis, MO, USA

3.5 Antibiotics

Ampicillin	Calbiochem, San Diego, CA, USA
Blasticidin	Invitrogen, Camarillo, CA, USA
G418	Sigma-Aldrich, St. Louis, MO, USA
Penicillin/streptomycin	Gibco/Life Technologies, Carlsbad, CA, USA

3.6 Molecular weight standards

Kaleidoscope Prestained Standard from Bio-Rad (Munich, Germany) was used as a molecular weight standard for proteins.

3.7 Oligonucleotides for quantitative real-time PCR

Unmodified HPLC-purified oligonucleotides were designed as described in Chapter 4.2.2.2 and purchased from Eurofins MWG Operon (Ebersberg, Germany). *Nos2* was provided in the TaqMan® Gene Expression Assay (Life Technologies, Carlsbad, CA, USA). Small letters indicate mouse genes, capital letters indicate human genes.

Gene	**Primer Sequence (sense and antisense)**
Arg1	5'-GACTCCCTGCATATCTGCCAAAGAC-3'
	5'-GTCTCTTCCATCACCTTGCCAATCC-3'
Arg2	5'-TGCATTTGACCCTAAACTGGCTCC-3'
	5'-ATTGACTTCAACAAGATCCAGAGCTGAC-3'
Cd4	5'-ACTCTGACTCTGGACAAAGGGACAC-3'
	5'-GAGTCCATCTTGACCTTATCACCTTCAC-3'
Cd8a	5'-AACGAAGGCTACTATTTCTGCTCAGTC-3'
	5'-TGTAAATATCACAGGCGAAGTCCAATCC-3'
Cox1	5'-CGCCTACAGCCCTTCAATGAATACC-3'
	5'-CCAACTCAGCAGCCATCTCCTTCTC-3'

Gene	Primer Sequence (sense and antisense)
Cox2	5'-CAATGAGTACCGCAAACGCTTCTCC-3'
	5'-TGTCACTGTAGAGGGCTTTCAATTCTG-3'
Csf2	5'-GCCATCAAAGAAGCCCTGAACCT-3'
	5'-CTGCTCGAATATCTTCAGGCGGGTC-3'
Foxp3	5'-CCCATCCCCAGGAGTCTTGC-3'
	5'-ACCATGACTAGGGGCACTGTA-3'
Glut1	5'-CGTCCTGCTGCTATTGCTGTG-3'
	5'-GGTGAAGATGAAGAAGAGCACGAGG-3'
Hk1	5'-GACGACATCAGAACAGACTTCGAC-3'
	5'-CAATCAGGATGTTACGGACGATCTC-3'
Hk2	5'-GTGGACTGGACAACCTCAAAGTGAC-3'
	5'-GAAGGACACGTCACATTTCGGAG-3'
Ido1	5'-TCTCTATTGGTGGAAATCGCAGCTTCTC-3'
	5'-TCCAATGCTTTCAGGTCTTGACGCTC-3'
Ido2	5'-TGCTGCCAAGATCTCTTGCCATTCC-3'
	5'-ACTGCTGCCTTCTCCACCAAGAC-3'
Ifng	5'-TCAAGTGGCATAGATGTGGAAGAA-3'
	5'-TGGCTCTGCAGGATTTTCATG-3'
Il10	5'-GGTTGCCAAGCCTTATCGGA-3'
	5'-ACCTGCTCCACTGCCTTGCT-3'
Il17a	5'-GCTCCAGAAGGCCCTCAGA-3'
	5'-AGCTTTCCCTCCGCATTGA-3'
Il6	5'-GAGGATACCACTCCCAACAGACC-3'
	5'-AAGTGCATCATCGTTGTTCATACA-3'
Ldha	5'-TATCTTAATGAAGGACTTGGCGGATGAG-3'
	5'-GGAGTTCGCAGTTACACAGTAGTC-3'
LDHA	5'-GGTTGGTGCTGTTGGCATGG-3'
	5'-TGCCCCAGCCGTGATAATGA-3'
Ldhb	5'-TTGTGGCCGATAAAGATTACTCTGTGAC-3'
	5'-AGGAATGATGAACTTGAACACGTTGAC-3'
Rn18s (18S)	5'-ACCGATTGGATGGTTTAGTGAG-3'
	5'-CCTACGGAAACCTTGTTACGAC-3'
Tgfb1	5'-CACCGGAGAGCCCTGGATA-3'
	5'-TGTACAGCTGCCGCACACA-3'
Tnf	5'-CATCTTCTCAAAATTCGAGTGACAA-3'
	5'-TGGGAGTAGACAAGGTACAACCC-3'
Vegfa	5'-CTGGAGTGTGTGCCCACTGA-3'
	5'-TCCTATGTGCTGGCCTTGGT-3'

3.8 Antibodies

3.8.1 Antibodies for western blotting

Specificity	Source	Species cross-reactivity	Molecular Weight	Dilution	Manufacturer
α-Actin	Rabbit	Human, animal	42 kDa	1:2,000	Sigma-Aldrich, St. Louis, MO, USA
α-ARD1	Rabbit	Human, mouse	31 kDa	1:30,000	Provided by Jacques Pouysségur (Institute of Research on Cancer and Ageing (IRCAN), University of Nice-Sophia Antipolis-CNRS-Inserm, Centre A. Lacassagne, Nice, France)
α-LDHA	Rabbit	Human, mouse, rat, monkey	37 kDa	1:1,000	Cell Signaling Technology, Danvers, MA, USA
α-LDHA (for $Ldha^{-/-}$ clones)	Rabbit	Human, mouse, rat, monkey	36 kDa	1:1,000	Abcam, Cambridge, UK
α-LDHB (431.1)	Mouse	Human	35 kDa	1:1,000	Santa Cruz Biotechnology, Dallas, TX, USA
α-Mouse HRP	Goat	-	-	1:2,500	Dako, Glostrup, Denmark
α-Phospho-LDHA	Rabbit	Human, mouse, rat	37 kDa	1:1,000	Cell Signaling Technology, Danvers, MA, USA
α-Rabbit HRP	Goat	-	-	1:2,500	Dako, Glostrup, Denmark

3.8.2 Antibodies for flow cytometry

3.8.2.1 Anti-mouse antibodies

Specificity	Isotype	Conjugation	Clone	Manufacturer
α-CD11b	Rat IgG2b	FITC	M1/70	eBioscience, San Diego, CA, USA
α-CD11c	Armenian Hamster IgG1	PE	HL3	BD Biosciences, Franklin Lakes, NJ, USA
α-CD19	Rat IgG2a	PE-Cy7	eBio1D3	eBioscience, San Diego, CA, USA
α-CD25	Rat IgG1	APC	PC61.5	eBioscience, San Diego, CA, USA
α-CD3ε	Armenian Hamster IgG	FITC	145-2C11	eBioscience, San Diego, CA, USA
α-CD3ε	Armenian Hamster IgG1	PerCP	145-2C11	BD Biosciences, Franklin Lakes, NJ, USA
α-CD3ε	Armenian Hamster IgG1	APC-Cy7	145-2C11	BD Biosciences, Franklin Lakes, NJ, USA
α-CD4	Rat IgG2a	eFluor450	RMA4-5	eBioscience, San Diego, CA, USA
α-CD45	Rat IgG2b	PE	30-F11	BD Biosciences, Franklin Lakes, NJ, USA

Specificity	Isotype	Conjugation	Clone	Manufacturer
α-CD45	Rat IgG2b	PerCP	30-F11	BD Biosciences, Franklin Lakes, NJ, USA
α-CD45	Rat IgG2b	V500	30-F11	BD Biosciences, Franklin Lakes, NJ, USA
α-CD8α	Rat IgG2a	PerCP	53-6.7	BD Biosciences, Franklin Lakes, NJ, USA
α-CD8α	Rat IgG2a	FITC	53-6.7	BD Biosciences, Franklin Lakes, NJ, USA
α-Gr-1	Rat IgG2b	PB	RB6-8C5	BioLegend, San Diego, CA, USA
α-Granzyme B	Rat IgG2a	PE	NGZB	eBioscience, San Diego, CA, USA
α-I-Ab	Mouse IgG2a	APC	AF6-120.1	BioLegend, San Diego, CA, USA
α-IFN-γ	Rat IgG1	APC	XMG1.2	BD Biosciences, Franklin Lakes, NJ, USA
α-IL-17	Rat IgG2a	PE	eBio17B7	eBioscience, San Diego, CA, USA
α-IL-2	Rat IgG2b	PE	JES6-5H4	BD Biosciences, Franklin Lakes, NJ, USA
α-IL-6	Rat IgG1	PE	MP5-20F3	eBioscience, San Diego, CA, USA
α-NFATc1	Mouse IgG1	PE	7A6	BioLegend, San Diego, CA, USA
α-NK1.1	Mouse IgG2a	APC	PK136	eBioscience, San Diego, CA, USA
α-NK1.1	Mouse IgG2a	eFluor450	PK136	eBioscience, San Diego, CA, USA
α-NK1.1	Mouse IgG2a	BV421	PK136	BioLegend, San Diego, CA, USA
α-NKp46	Rat IgG2a	V450	29A1.4	BD Biosciences, Franklin Lakes, NJ, USA
α-PD-L1	Rat IgG2b	BV421	10F.9G2	BioLegend, San Diego, CA, USA

3.8.2.2 Anti-human antibodies

Specificity	Isotype	Conjugation	Clone	Manufacturer
α-CD25	Mouse IgG1	APC	2A3	BD Biosciences, Franklin Lakes, NJ, USA
α-CD3ε	Mouse IgG1	APC	SK7	eBioscience, San Diego, CA, USA
α-CD3ε	Mouse IgG1	BV510	SK7	BioLegend, San Diego, CA, USA
α-CD3ε	Mouse IgG2a	FITC	HIT3a	BD Biosciences, Franklin Lakes, NJ, USA
α-CD45	Mouse IgG1	PE	HI30	Invitrogen, Camarillo, CA, USA
α-CD8α	Mouse IgG1	PE-Cy7	SK1	BioLegend, San Diego, CA, USA
α-CD8α	Mouse IgG1	PerCP	SK1	BioLegend, San Diego, CA, USA

3.8.3 Antibodies for the depletion of specific cell populations

Specificity	Isotype	Manufacturer
α-CCR2 (MC-21)	IgG2b (MC-67)	Provided by Matthias Mack (Department of Internal Medicine II, University Hospital Regensburg, Germany)
α-CD8α (Clone 2.43)	Rat IgG2b	Bio X Cell, West Lebanon, NH, USA
α-CD4 (Clone GK1.5)	Rat IgG2b	Bio X Cell, West Lebanon, NH, USA

3.9 Bacteria

E. coli	Provided by Jacques Pouysségur (Institute of Research on Cancer and Ageing (IRCAN), University of Nice-Sophia Antipolis-CNRS-Inserm, Centre A. Lacassagne, Nice, France)

3.10 Cell lines

For animal experiments the mouse melanoma cell line B16.SIY E12 was used. This cell line was created by removal of GFP from the SIY-pLeGFP vector (present in B16.SIY E12 cells, containing the SIY antigen which is recognized by *2C/RAG2*$^{-/-}$ CD8^{+} T cells[182]) and subsequently transfected into B16.F10 cells by the group of Christian Blank (Division of Immunology, The Netherlands Cancer Institute, Antoni van Leeuwenhoek Hospital, Amsterdam, The Netherlands).

Additionally, B16.SIY E12 cells were transfected with a pGeneClip hMGFP plasmid containing shRNA sequences against *Ldha* to generate cells with low *Ldha* levels (Ldha^{low} cells), a scrambled shRNA sequence for control cells, as well as GFP and an ampicillin resistance gene. As parental B16.SIY E12 cells already contained an ampicillin resistance gene against G418 on the SIY-pLeGFP vector, a pGene/V5-His vector containing a blasticidin-resistence gene was used as a second plasmid, allowing cultivation of Ldha^{low} cells under antibiotic selection. The generation of Ldha^{low} cells from B16.SIY E12 was performed by Michael Kastenberger[183].

In another approach to decrease LDHA levels, performed at the Institute of Research on Cancer and Ageing (IRCAN) of the University of Nice-Sophia Antipolis-CNRS-Inserm, Centre A. Lacassagne in Nice, France, under the supervision of Jacques Pouysségur, CRISPR/Cas9, targeting *Ldha* in B16.SIY E12 was used to generate *Ldha*$^{-/-}$ clones (Chapter 4.7).

The P815.B71 mastocytoma cell line for priming of *2C/RAG2*$^{-/-}$ CD8^{+} T cells (Chapter 4.4.3.1) was provided by Christian Blank (Division of Immunology, The Netherlands Cancer Institute, Antoni van Leeuwenhoek Hospital, Amsterdam, The Netherlands).

3.11 Mice

2C/Rag2$^{-/-}$	Provided by Christian Blank (Division of Immunology, The Netherlands Cancer Institute, Antoni van Leeuwenhoek Hospital, Amsterdam, The Netherlands)
C57BL/6J	Charles River, Wilmington, MA, USA
C57BL/6N	Taconic, Hudson, NY, USA
Ccr2$^{-/-}$	Provided by Uwe Ritter (Institute of Immunology, University of Regensburg, Germany)
Cd8$^{-/-}$	The Jackson Laboratory, Bar Harbor, ME, USA
Ifngr1$^{-/-}$	The Jackson Laboratory, Bar Harbor, ME, USA
Ifng$^{-/-}$	The Jackson Laboratory, Bar Harbor, ME, USA

Pfp$^{-/-}$	Provided by Petra Hoffmann (Department of Internal Medicine III, University Hospital Regensburg, Germany)
Rag2$^{-/-}$	Taconic, Hudson, NY, USA
Rag2$^{-/-}\gamma c^{-/-}$	Taconic, Hudson, NY, USA

3.12 Patient material

After informed consent, biopsies of primary melanoma, melanoma in situ, cutaneous metastases of melanoma and adjacent healthy skin or nevi of respective patients, who had undergone surgery for skin tumors at the Department of Dermatology at the University Hospital of Regensburg, Germany, were obtained. The study was approved by the institutional ethics committee (approval number 13-101-0127), designed and conducted in accordance with the Declaration of Helsinki and performed in cooperation with Elisabeth Kohl and Sebastian Haferkamp (Department of Dermatology, University Hospital Regensburg, Germany).

3.13 Databases and software

The following databases and software tools were used to design experiments and process data.

CorelDraw X4	Corel, Ottawa, Ontario, Canada
EndNote X7	Thomson Reuters, New York, NY, USA
FlowJo v9.5.3	FlowJo,LLC, Ashland, OR, USA
GeneRunner version 3.05	http://www.generunner.com
GraphPad Prism 5.02	GraphPad Software, La Jolla, CA, USA
ImageLab v4.0	Bio-Rad, Munich, Germany
Microsoft Excel 2003/2007/2010	Microsoft Deutschland GmbH
PerlPrimer version 1.1.14	http://perlprimer.sourceforge.net/
PubMed	http://www.ncbi.nlm.nih.gov/entrez
UCSC Genome Browser	http://www.genome.ucsc.edu

4 Methods

4.1 Cell culture methods

All cells were handled under a laminar flow cabinet with sterile consumables. If not otherwise stated, all media used were supplemented with 10% heat-inactivated fetal calf serum (FCS), 1% *L*-glutamine and 0.5% penicillin/streptomycin, cells were incubated at 37 °C/5% CO_2/95% relative humidity and centrifugation was performed at 345 g for 7 minutes at 4 °C.

4.1.1 Cell passaging

The CRISPR *Ldha*$^{-/-}$ clones were cultured without selection antibiotics. The *Ldha* shRNA transfected and untransfected B16.SIY E12 mouse melanoma cells were cultured in medium with selection antibiotics G418 and blasticidin. Cells were passaged every 3-4 days and, therefore, rinsed with PBS and trypsinized for 3-5 minutes with 0.05% Trypsin/0.02% EDTA at 37 °C. To inactivate trypsin, medium was added in a 10:1 ratio and cells were centrifuged. After cells were resuspended in 1-5 ml of medium, depending on the pellet size, cells were counted with the CASY cell counter and 0.5-1 x 10^6 cells were seeded in fresh medium.
P815.B71 mastocytoma cells were passaged every 2-3 days by transferring some cells into fresh medium (subcultivation ratio of 1:10).

4.1.2 Freezing and thawing

For freezing, the volume of 0.5-5 x 10^6 cells was mixed with freezing medium (FCS 20%, dimethyl sulphoxide, DMSO 80%) in cryo tubes in a 1:2 ratio and slow-frozen in cryo freezing containers for short-term storage at 80 °C or long-term storage in liquid nitrogen.
Frozen cells were thawed at room temperature and immediately added to warm medium. After centrifugation cells were seeded in fresh medium.

4.1.3 Cell counting

Cell numbers and viability were determined by means of electronic pulse area analysis using a CASY cell counter. This method obtains signals when a cell passes in a low-voltage field through the system's high-precision measuring pore.

4.1.4 Mycoplasma test

All cell lines were routinely tested for mycoplasma with the MycoAlert mycoplasma detection kit according to the manufacturer's recommendations.

4.1.5 ^{3}H-thymidine incorporation assay

To measure proliferation of cell lines, the incorporation of the radioactive nucleoside ^{3}H-thymidine into new strands of chromosomal DNA during mitotic cell division was assessed. Therefore, 2.5 x 10^{4} cells per well were seeded into flat-bottom 96-well microtiter plates, incubated for 2 hours until cells were fully adherent, and 0.5 µCi (=0.00185 MBq) [methyl-^{3}H]-thymidine was added. After 20-22 hours cells were transferred to UniFilter plates with a Wallac Harvester and incorporated ^{3}H-thymidine was measured with a Wallac Betaplate counter.

4.1.6 Enzymatic determination of lactate

To determine lactate concentrations in supernatants, 2.5 x 10^{4} cells were seeded into flat-bottom 96-well microtiter plates and incubated for 24 hours. Supernatants were analyzed with a routine procedure using an ADVIA 1650 analyzer at the Department of Clinical Chemistry (University Hospital Regensburg, Germany). By means of an enzymatic assay the hydrogen peroxide, which emerges from the oxidation of lactate by lactate oxidase, reacts with a chromogen in presence of a peroxidase. The amount of resulting dye is proportional to the lactate concentration and can be measured by spectrophotometry.

4.1.7 Cell cycle analysis

For cell cycle analysis, 5 x 10^{5} cells were rinsed with ice-cold PBS, resuspended in 300 µl propidium iodide buffer (0.1% Triton X100, 0.1% sodium citrate, 50 µg/ml propidium iodide in distilled water), vortexed thoroughly and incubated for 24 hours at 4 ℃. Cells were then measured by flow cytometry at the BD LSR II and cell cycle was analyzed according to "Dean/Jett/Fox" using FlowJo software.

4.1.8 High-resolution respirometry and analysis of mitochondria

Respiration of cells was determined by high-resolution respirometry using the oxygraph O2-k. 0.5-1 x 10^6 cells were analyzed in cell culture medium for routine respiration during 20 minutes. Values were corrected for residual oxygen consumption being not related to the respiratory system, which was determined after addition of rotenone (0.5 µM) and myxothiazol (2.5 µM).
To analyze mitochondrial content, 5 x 10^5 cells were seeded in a 75 cm^2 flask. After 72 hours cells were drained of medium and medium without additives containing green-fluorescent mitochondrial stain MitoTracker Green (25 nM) and cyclosporin A (16 nM), serving as export inhibitor of the dye from the mitochondria, was added. After 2 hours incubation at 37 ℃, the cells were trypsinized (Chapter 4.1.1), centrifuged twice with 1 ml flow cytometry buffer (PBS containing 2% FCS), resuspended in 400 µl flow cytometry buffer and measured at the flow cytometer. Unstained cells were used to determine autofluorescence.

4.2 Molecular biology techniques

4.2.1 Preparation of ribonucleic acids

To obtain total ribonucleic acids (RNA) of cell lines, 1 x 10^6 cells/well were incubated in 6-well microtiter plates for 24 hours, rinsed with PBS, lysed using the RNeasy Mini Kit, detached with cell scrapers and sheared 10 times using a 1 ml syringe. Procedures were performed on ice and RNA lysates were frozen at -80 ℃ for storage.
To obtain total RNA of tissues, dissected mouse or human tumors were homogenized using TissueLyser (3 min, 20 Hz) and QIAshredder columns according to the manufacturer's instructions.
Subsequent isolation of total cellular RNA and additional on-column DNA digestion with the RNase-free DNase Set against potential DNA contamination was performed according to the manufacturer's instructions using the RNeasy Mini Kit. RNA concentration was determined with the NanoDrop 1000 spectrophotometer. RNA quantification and integrity was measured on RNA Nano LabChips using the 2100 Bioanalyzer.

4.2.2 Polymerase chain reaction

Polymerase chain reaction (PCR) is a method to *in vitro*-amplify specific DNA fragments with the help of a DNA template, a thermoresistant DNA polymerase and sequence-specific oligonucleotide primers which flank the DNA fragment of interest. The quantitative real-time PCR

(qRT-PCR) used here, serves to quantify the expression level of specific genes. Therefore, total cellular RNA had to be converted into DNA (=copy DNA, cDNA) by means of reverse transcription.

4.2.2.1 Reverse transcription

In order to determine gene expression levels, isolated total RNA was transcribed into cDNA using a reverse transcriptase derived from the murine moloney leukemia virus (M-MLV), random decamer primers and 2'-deoxyribonucleosid-5'-triphosphates (dNTPs). The reaction was performed in a PCR thermocycler according to the following protocol (Table 4-1) with a reaction volume of 20 µl.

Table 4-1. Protocol for reverse transcription

(1) Mix and incubate at 65 ℃ for 5 min	
Total RNA	0.5 µg
Random decamer primers (10 µM)	1 µl
dNTPs (10 µM)	1 µl
H_20_{USB}	ad 15 µl
(2) Add and incubate at 42 ℃ for 2 min	
M-MLV buffer (5X)	4 µl
(3) Add and incubate at 42 ℃ for 50 min, then at 70 ℃ for 15 min	
M-MLV reverse transcriptase	1 µl

4.2.2.2 Primer design

For qRT-PCR, oligonucleotide primers with specificity towards the genes of interest (Chapter 3.7) were constructed with the help of the 'PerlPrimer' software and the UCSC genome browser, following the criteria below (Table 4-2). Primers generated in this way were verified by means of 'Blat' and '*in silico*' PCR (UCSC genome browser) and secondary structure analysis was performed with the help of the GeneRunner software.

Table 4-2. Criteria for primer design

GC content	40-60%
Melting temperature (T_m)	65-68 ℃
Length primer	20-28 bp
Length amplicon	70-250 bp
Position	On 2 different exons spanning an intron

4.2.2.3 Quantitative real-time PCR

In order to quantify gene expression levels, qRT-PCR makes use of a dye which intercalates double-stranded DNA and becomes fluorescent in its bound form. The amount of fluorescence is proportional to the amount of amplified DNA. Quantification of PCR products takes place in the early exponential phase of the PCR reaction, determining the PCR cycle when the fluorescence of the sample exceeds the background fluorescence for the first time as cycle threshold (ct)-value. By amplification of known amounts of cDNA (positive control) and corresponding ct-values, a standard curve can be generated and from measured ct-values of samples the amounts of amplified cDNA can be determined.

With the exception of *iNos*, which was quantified by the group of Christian Bogdan (Microbiology Institute-Clinical Microbiology, Immunology and Hygiene, Erlangen, Germany) using the *Nos2* TaqMan Gene Expression Assay, here the QuantiFast SYBR Green Kit was used for qRT-PCR. Reactions were prepared in 96-well PCR microtiter plates at a volume of 10 µl/well with a reaction mix depicted in Table 4-3. Samples were pipetted in triplicates and a positive control for generation of a standard curve was pipetted in duplicates.

Table 4-3. Reaction mix for qRT-PCR

Reagent	Volume
QuantiFast SYBR Green-mix	5 µl
cDNA (1:10 in H_20_{USB})	1 µl
Sense primer (10 µM)	0.5 µl
Antisense primer (10 µM)	0.5 µl
H_20_{USB}	3 µl

After sealing the microtiter plate with heat-sealing film and quick centrifugation, qRT-PCR was carried out by Realplex Mastercycler EpGradient S according to the following program (Table 4-4).

Table 4-4. Program for qRT-PCR

Process	Temperature	Duration	
Initial denaturation	95 °C	5 min	
Denaturation	95 °C	8 s	45 cycles
Annealing/elongation	60 °C	20 s	
Melting curve	95 °C	15 s	
	65 °C	15 s	
	65-95 °C	10 min	

Specific amplification of the expected PCR product was controlled by the pattern of the melting curve. By means of the slope of the standard curve and the y-axis intercept, the amount of cDNA was calculated by the Realplex software. The amount of messenger RNA (mRNA) which corresponds to the calculated amount of cDNA was finally normalized to that of *18S* rRNA.

4.3 Biochemical methods

All samples were treated as described in the following, except samples generated in the laboratory of Jacques Pouysségur (Institute of Research on Cancer and Ageing (IRCAN), University of Nice-Sophia Antipolis-CNRS-Inserm, Centre A. Lacassagne, Nice, France), which are described in Chapter 4.7.

4.3.1 Preparation of proteins

In order to obtain total protein, 1 x 10^6 cells were incubated in 6-well microtiter plates for 24 hours. Afterwards, cells were rinsed twice with 1 ml PBS and 100 µl RIPA buffer, containing additional protease inhibitor, were added. Adherent cells were then detached with cell scrapers and vortexed thoroughly for 1 minute. All procedures were performed on ice and protein lysates were stored at -80 °C.

For determining protein concentrations, samples were centrifuged at 13,000 g for 15 minutes at 4 °C and supernatants were subjected to the Bio-Rad D C Protein Assay according to the manufacturer's instructions. Known concentrations of bovine serum albumin (BSA) were used as internal standards to calculate protein content.

For further procedure, equal volumes of 10 µg protein lysate diluted with the same volume of SDS sample buffer (2X) (Table 4-5) were prepared.

Table 4-5. Composition of SDS sample buffer

Working reagent	Components		
SDS sample buffer (2X)	20%	(10 ml)	Glycerin
	125 mM	(5 ml)	Tris/HCl (pH 6.8, 1.25 M)
	4%	(2 g)	SDS
	10%	(5 ml)	2-Mercaptoethanol
	0.02%	(10 mg)	Bromophenol blue
	ad 50 ml		H_2O_{bidest}

4.3.2 SDS polyacrylamide gel electrophoresis

Sodium dodecylsulfate polyacrylamide gel electrophoresis (SDS-PAGE) is a technique developed by U.K. Laemmli to electrophoretically separate proteins according to their molecular weight using the denaturation properties of SDS as an anionic detergent and its feature to coat proteins with uniform negative charge.

As running gel served a 12% acrylamide gel (ideal for 20-60 kDa proteins), as stacking gel a 5% acrylamide gel, which were prepared with ammonium persulfate (APS) as oxidizing agent and N,N,N',N'-tetramethylethylenediamine (TEMED) as reaction catalyst. Running gel was mixed

according to Table 4-6, Table 4-7 and Table 4-8, immediately filled in the casting frames and left coated with isopropanol for 30 minutes. Then stacking gel was mixed according to Table 4-6, Table 4-7 and Table 4-8, filled on top of running gel and a well-forming comb was placed. The gel was led to polymerize at room temperature.

To perform electrophoresis, the SDS gel was placed in the electrophoresis chamber and bathed in electrode buffer (1X). After carefully removing the comb, wells were rinsed with electrode buffer and loaded with equal volumes of 10 µg protein lysates (Chapter 4.3.1) which were first heated at 95 ℃ for 10 minutes and second cooled on ice. Additionally, one well was loaded with 5 µl Kaleidoscope Prestained Standard as molecular weight standard.

Samples were run at voltages of 80-100 V and as soon as they reached the running gel, voltage was increased to 120-130 V. Electrophoresis was stopped at the time point when the lowest sign of the protein marker reached the lower bottom of the gel.

Table 4-6. Composition of SDS polyacrylamide gels

Components	12% running gel	5% stacking gel
Running gel solution	18 ml	-
Stacking gel solution	-	10 ml
TEMED	18 µl	10 µl
APS (10%)	90 µl	80 µl

Table 4-7. Composition of SDS polyacrylamide gel solutions

Components	Running gel solution (12%)	Stacking gel solution (5%)
Running gel buffer	25 ml	-
Stacking gel buffer	-	25 ml
SDS (10%)	1 ml	1 ml
Acrylamide (30%)	40 ml	16.65 ml
H_2O_{bidest}	ad 100 ml	ad 100 ml

Table 4-8. Working solutions for SDS-PAGE

Working solutions	Components		
Running gel buffer	1.5 M	(90.83 g)	Tris/HCl (pH 8.8)
	ad 500 ml		H_2O_{bidest}
Stacking gel buffer	0.5 M	(30 g)	Tris/HCl (pH 8.8)
	ad 500 ml		H_2O_{bidest}
SDS (10%)	10%	(10 g)	SDS
	ad 100 ml		H_2O_{bidest}
Acrylamide (30%)	30%	(30 ml)	Acrylamide
	ad 100 ml		H_2O_{bidest}
APS (10%)	10%	(100 mg)	APS
	ad 1 ml		H_2O_{bidest}
	Freshly prepared for each usage.		
Electrode buffer (5X)	40 mM	(15 g)	Tris
	0.95 M	(216 g)	Glycine
	0.5%	(15 g)	SDS
	ad 3,000 ml		H_2O_{bidest}

4.3.3 Western blotting

The western blotting method was applied to detect specific proteins within the range of separated proteins by SDS-PAGE.

In a first step, proteins from the SDS gel were transferred to a polyvinylidene difluoride (PVDF)-membrane in a semi-dry electro-blotting system. Therefore, the PVDF membrane was cut to a size similar to the SDS gel, hydrophilized in methanol for 2 minutes and equilibrated in buffer B (buffers used are described in Table 4-9). The SDS gel was removed from the glass plates and also placed in buffer B. Meanwhile, three layers of filter paper soaked with buffer A were placed on the bottom part of a semi-dry transfer cell (anode), followed by three layers of filter paper soaked in buffer B. The wet membrane was put on the filter paper and then the SDS gel was put on top of the membrane and it was covered with three layers of filter paper soaked in buffer C. It was made sure that the construction was air bubble-free. The system was closed with the upper part of the semi-dry transfer cell (cathode) and transfer of the proteins onto the PVDF membrane was carried out at 0.8 mA/cm^2 gel surface for 30-45 minutes.

In a second step, the proteins on the membrane were subjected to immunostaining. Each step was performed with shaking for maximum accessibility of reagents. To minimize non-specific binding, the membrane was incubated in blocking buffer over night at 4 ℃. Subsequently, the membrane was swirled in a dilution of primary antibody in blocking buffer (Chapter 3.8.1) for 1.5 hours at room temperature. Then, the membrane was washed three times in Tris-buffered saline (TBS) and Tween 20 (TBST) buffer for 10 minutes, each, before incubation with a dilution of a secondary antibody in blocking buffer (Chapter 3.8.1), specific to the isotype of the primary antibody for 1 hour at room temperature. The membrane was washed again three times in TBST

buffer for 10 minutes, each, and proteins were visualized on an imaging film using luminol-based enhanced chemiluminescence (ECL) solutions (Table 4-10). Hereby, the horseradish peroxidase (HRP) conjugated to the secondary antibody catalyzed the oxidation of luminol, inducing chemiluminescence. This emitted light was then captured by the image film and resulting protein bands could be qualified by the molecular weight standard and quantified by the protein expression of the housekeeping gene Actin.

Table 4-9. Buffers for western blotting

Buffers	Components		
Buffer A	0.3 M	(36.3 g)	Tris/HCl (pH 10.4)
	20%	(200 ml)	Methanol
	ad 1,000 ml		H_2O_{bidest}
Buffer B	25 mM	(3.03 g)	Tris/HCl (pH 10.4)
	20%	(200 ml)	Methanol
	ad 1,000 ml		H_2O_{bidest}
Buffer C	4 mM	(5.2 g)	Caproic acid (pH 7.6)
	20%	(200 ml)	Methanol
	ad 1,000 ml		H_2O_{bidest}
TBS buffer (2X)	20 mM	(9.16 g)	Tris/HCl (pH 7.4)
	150 mM	(35.1 g)	NaCl
	ad 2,000 ml		H_2O_{bidest}
TBST buffer	1X	(500 ml)	TBS (2X)
	0.1%	(1 ml)	Tween 20
	ad 1,000 ml		H_2O_{bidest}
Blocking buffer	5%	(5 g)	Non-fat dry milk
	ad 100 ml		TBST buffer

Table 4-10. Composition of ECL solutions

Solutions	Components		
ECL solution A	250 mM	(100 mg)	Luminol
	ad 2 ml		H_2O_{bidest}
ECL solution B	90 mM	(14.8 mg)	*p*-Coumaric acid
	ad 1 ml		DMSO
ECL mix	2 ml		ECL solution A
	0.89 ml		ECL solution B
	20 ml		Tris/HCl (pH 8.5, 1 M)
	ad 200 ml		H_2O_{bidest}
	Stored away from sunlight.		
ECL working solution	5 ml		ECL mix
	1.5 µl		30% H_2O_2

4.4 Mouse experiments

All mouse experiments were conducted according to the regulations of the government of Upper Palatinate, Regensburg, Germany, and in cooperation with Gudrun Koehl (Department of Surgery, University Hospital Regensburg, Germany).
As differences in tumor growth and immune cell infiltration were observed, depending on sex, age and housing temperature of the mice (Figure 4-1), unless otherwise indicated, all experiments were performed with male age- and housing temperature-matched animals.

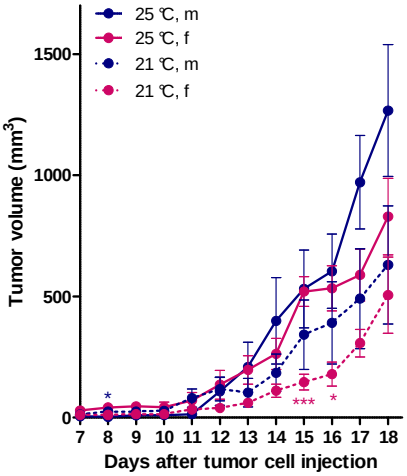

Figure 4-1. Tumor growth depends on sex and housing temperature of mice
Tumor growth after subcutaneous injection of 1 x 10^5 B16.SIY E12 cells transfected with a scrambled shRNA sequence in male (m) and female (f) C57BL/6 mice, housed at 25 ℃ and 21 ℃, respectively (*n* = 5-8 mice). In statistical analyses, tumor growth of mice housed at 25 ℃ and 21 ℃ was compared in female mice (p ink asterisks) and male mice (blue asterisk). Data are presented as the mean tumor volume and s.e.m. * P < 0.05 and *** P < 0.001 (unpaired Student's *t*-test).

4.4.1 Tumor inoculation

To generate tumors in mice, 1 x 10^4, 1 x 10^5 or 1 x 10^6 B16.SIY E12 Ldha^{low} cells, control and wild type cells were injected subcutaneously in the dorsal region of mice. Tumor volumes were estimated by measurements of the short (a) and long (b) axis of the mass and the following formula: $V = \pi/6 \times 0.5 \times a^2 \times b$, starting on the first day when tumors became visible to the naked eye (earliest on day 7). Animals were monitored on a daily basis for tumor size and their general condition. When the tumor diameter reached 1 cm, mice were killed and blood, spleens, and tumors of mice bearing tumors, grown from 1 x 10^5 B16.SIY E12 cells were prepared for analysis. To exclude size effects only tumors with a max. size of 1,000 mm^3 were included in analyses.

4.4.2 Depletion of specific cell populations using monoclonal antibodies

4.4.2.1 Depletion of monocytes

Monocytes were depleted by using an α-CCR2 antibody. Therefore, after injection of tumor cells into mice (Chapter 4.4.1), 30 or 50 µg of an α-CCR2 monoclonal antibody and the respective isotype (Chapter 3.8.3) were administered intraperitoneally into mice, starting treatment from day 3 until day 7 or 8. Retrobulbar blood was analyzed on days 0, 4, 7 and 10 to confirm depletion of monocytes as described in Chapters 4.4.3.4 and 4.6.2.

4.4.2.2 Depletion of T cells

$CD4^+$ or $CD8^+$ T cells were depleted using α-CD4 or α-CD8 antibodies. Therefore, 2 and/or 4 days prior to injection of tumor cells into mice (Chapter 4.4.1), intraperitoneal injection of 250 µg of α-CD4 or α-CD8 monoclonal antibodies and respective isotypes (Chapter 3.8.3) was performed. In some experiments, the treatment with the depleting antibodies was continued on days 3, 8, and 13 after tumor cell injection. Analyses of retrobulbar blood (Chapters 4.4.3.4 and 4.6.2) throughout the experiments served to confirm depletion of $CD4^+$ and $CD8^+$ T cells.

4.4.3 Sample preparation for flow cytometry

4.4.3.1 Isolation and expansion of $CD8^+$ T cells and NK cells

$CD8^+$ T cells and NK cells were isolated from spleens of *2C/Rag2*$^{-/-}$ and C57BL/6 mice, respectively by magnetic bead separation using the $CD8\alpha^+$ T cell isolation kit or the NK cell isolation kit II according to the manufacturer's instructions.

1×10^5 purified $CD8^+$ T cells were stimulated twice with 5×10^5 irradiated (20 Gy) P815.B71 mastocytoma cells and cultured in 24-well microtiter plates with media containing 10% FCS, 1% *L*-glutamine, 0.5% penicillin/streptomycin, 0.4% vitamins, 1% non-essential amino acids, 1% sodium pyruvate, 0.1% 2-mercaptoethanol and 10 U/ml IL-2. Stimulated $CD8^+$ T cells were collected and purified by gradient centrifugation.

NK cells were expanded for 5 days in media as described above, containing 100-1000 U/ml IL-2.

4.4.3.2 Preparation of tissue samples

For flow cytometry analyses, tissues of mice had to be processed to single-cell suspensions. For maintaining cell viability, tissues dissected from mice were collected in ice-cold PBS and tissue preparation was performed on ice.

Tumors were injected with 3 ml medium supplemented with 0.5% Collagenase Type IA (10 mg/ml) and 0.4% DNase I (10 mg/ml) and incubated for 1 hour in 6-well microtiter plates, being minced with a scalpel after 30 minutes. Tumors were then passed through a 70 µm cell strainer and centrifuged.

Spleens were processed to single-cell suspensions by scratching out cells with curved forceps in a petri dish containing medium. Afterwards, they were filtered via 100 µm cell strainers and centrifuged.

Erythrocytes in single-cell suspensions of tumors and spleens were lysed with 2 ml ACK lysis buffer (0.155 M NH_4Cl, 0.1 M $KHCO_3$ and 0.1 mM EDTA, diluted 1:6 with H_2O) for 3 minutes at room temperature. The reaction was stopped by adding 10 ml medium and cells were centrifuged. Pelleted cells were resuspended in 1-50 ml medium (volume dependent on pellet size) and filtered via 100 µm cell strainers. After counting the cells with the CASY cell counter, 0.5-3 x 10^6 cells were used for flow cytometry staining.

4.4.3.3 Preparation of single cells for intracellular staining

In order to analyze cytokines in tumors of C57BL/6 mice, 3 x 10^6 single cells obtained under a laminar air flow cabinet by the procedure described in Chapter 4.4.3.2 were incubated for 3 hours in 6 ml medium in 6-well microtiter plates with Golgi Plug as protein transport inhibitor.

For assessing cytokines in splenocytes of healthy mice, single cells were incubated as described above with addition of phorbol 12-myristate 13-acetate (PMA, final concentration 50 ng/ml) and ionomycin (final concentration 750 ng/ml) as stimuli, and in the presence or absence of 10 and 20 mM *L*-lactic acid. 20 mM sodium *L*-lactate and acidification by hydrochloric acid (HCl) corresponding to the pH at 20 mM lactic acid (~pH 5.8) were used as controls.

To analyze the transcription factor nuclear factor of activated T cells (NFAT), 0.5 x 10^5 $CD8^+$ T cells and 1 x 10^5 NK cells were cultured in U-bottom 96-well microtiter plates in the presence or absence of 15 mM *L*-lactic acid, hydrochloric acid (HCl) corresponding to the pH of 15 mM *L*-lactic acid (~pH 6.4) and 15 mM sodium *L*-lactate for 24 hours. 30 minutes before harvesting, cells were stimulated with PMA (final concentration 20 ng/ml) and ionomycin (final concentration 750 ng/ml).

4.4.3.4 Preparation of blood samples

Blood of mice was collected from the vena cava in heparin tubes. 2-3 drops of blood were lysed with 1 ml ACK lysis buffer (Chapter 4.4.3.2) for 5 minutes at room temperature. The reaction was stopped by adding 2 ml flow cytometry buffer (PBS containing 2% FCS). After centrifugation, supernatants were carefully aspired, leaving ~50 µl to avoid disturbing the pellet and ACK lysis was repeated until the pellet was colorless. At last, the pellet was resuspended in 1 ml of flow cytometry buffer for subsequent flow cytometry analysis.

4.4.4 Sample preparation for RNA isolation

Tissues were dissected from mice and immediately stored in RNAlater according to the manufacturer's instructions. In this way RNA was stabilized and the gene expression profile was preserved. RNA isolation was performed as described in Chapter 4.2.1.

4.4.5 Analysis of growth factors in tumor supernatants

Single-cell suspensions of tumors were obtained as described in Chapter 4.4.3.2. 5 x 10^5 cells were incubated in 12-well microtiter plates and stimulated with LPS (lipopolysaccharide, 1 µg/ml) for 24 hours. Supernatants were analyzed regarding TGF-β concentrations by means of sandwich ELISA (enzyme-linked immunosorbent assay) according to the manufacturer's recommendations. Here, the antigen of interest binds to an antibody which is attached to the bottom of a microtiter plate and is detected by a specific detection antibody. This detection antibody is coupled to an enzyme which induces a color reaction proportional to bound antigen and thereby indicates the amount of antigen present in the respective sample.

4.4.6 Sample preparation for bioluminescence imaging

For bioluminescence imaging tissues were immediately snap-frozen upon dissection to preserve the metabolic profile.

4.5 Induced metabolic bioluminescence imaging

To determine intracellular lactate levels of tumors *ex vivo*, induced metabolic bioluminescence imaging (imBI) was performed by the group of Wolfgang Mueller-Klieser (Institute of Pathophysiology, University Medical Center of the Johannes Gutenberg University Mainz, Germany). Lactate concentrations were measured in serial tumor cryosections by the imBI method[184]. Briefly, reaction solutions containing specific enzymes linking the metabolite of interest to the luciferase of *Photobacterium fischeri* or *Photinus pyralis* were used. Light emission was induced in a temperature stabilized reaction chamber positioned on the stage of a microscope (Axiophot; Zeiss) connected to a 16-bit electron-multiplying charge-coupled device camera with an imaging photon counting system (iXonEM + DU-888; Andor Technology PLC). Images of the spation distribution of light intensities were calibrated by using appropriate standards. Metabolite concentrations were acquired exclusively from histologically viable tissue by interactive optical microdissection. The concentrations were calculated in micromoles per gram of tumor tissue and were displayed in color-coded images. Three sections per metabolite were analyzed for each

tumor, and the mean value was used as a parameter for the metabolite concentration of a tumor. Further methodological details and representative calibration curves have been reported elsewhere[57,185].

4.6 Flow cytometry

Flow cytometry is the gold standard technique for cell analysis, as it allows counting, examining and sorting of individual cells. With the help of monoclonal antibodies which are conjugated to fluorochromes, labeling and detection of specific cell populations is possible.
Therefore, cells separately pass a laser beam, generating scatter light and fluorescence. Scatter light indicates size (forward scatter, FSC) and granularity (side scatter, SSC) of the cells; fluorescence gives information about a specific cell type.
Various fluorochrome-conjugated antibodies against components of the immune system were used in 6-color measurements (Chapter 3.8.2) performed at the BD LSR II, equipped with a red, blue, violet and UV laser. Staining procedures were performed on ice to preserve cell viability. Dead cells were excluded by 4',6-diamidino-2-phenylindole (DAPI), which is a blue fluorescent dye that binds to double-stranded DNA (dsDNA) after entering cells with damaged membranes. Analysis of flow cytometry data was performed the with FlowJo software.

4.6.1 Compensation

Compensation is an essential element of adequate experimental set-up for multicolor flow-cytometry assays. It is based on the overlap of fluorescence emission wavelengths, which can occur when two different fluorochrome-conjugated antibodies bind to one cell. This spillover is calculated with the help of single-stained controls as so called compensation values by means of which fluorescence emission values are properly corrected.
In this case, compensation values were established using CompBeads, a compensation-particles set, according to the manufacturer's instructions. Unstained cells were used to correct autofluorescence.

4.6.2 Surface staining

For staining of surface antigens, 0.5-3 x 10^6 cells were resuspended in 1 ml flow cytometry buffer and centrifuged at 523 g for 4 minutes at 4 ℃. For mouse cells, 1 µl FcR blocking reagent was added and cells were incubated for 15 minutes at 4 ℃. Then, cells were incubated with fluorochrome-conjugated antibodies (Chapter 3.8.2.1 and 3.8.2.2, amounts according to the manufacturer's recommendations) for 15-20 minutes at 4 ℃ in the dark. After addition of 1 ml flow

cytometry buffer, cells were centrifuged at 523 g for 4 minutes at 4 °C and the pellet was resuspended in 300 µl flow cytometry buffer. Measurement took place on the same day after passing cells through a 35 µm cell strainer cap (only for tissues) and adding 10% DAPI for life-dead staining. For blood and spleens 5,000-200,000 cells were recorded and for tumors the maximum possible number of cells was recorded.

4.6.3 Intracellular staining

After incubation, adherent cells were detached with cell scrapers and centrifuged at 523 g for 4 minutes at 4 °C with 1 ml flow cytometry buffer. Subsequent staining with antibodies against surface markers was performed (Chapters 4.6.2 and 3.8.2.1, amount of antibodies used according to the manufacturer's recommendations) for 15 minutes at 4 °C in the dark. Then, cells were centrifuged at 523 g for 4 minutes at 4 °C with 1 ml flow cytometry buffer and intracellular staining was performed with a Foxp3 staining buffer set. Therefore, 0.5 ml of Fix/Perm Mix (1:4 ratio of Fix/Perm concentrate and Fix/Perm diluent) was added to the cells, vortexed thoroughly and incubated for 15 minutes at 4 °C in the dark. Cells were centrifuged twice with 1 ml permeabilization buffer (1:10 dilution in H_2O) at 523 g for 4 minutes at 4 °C and staining with antibodies against cytokines and/or transcription factor NFAT (Chapter 3.8.2.1) was conducted followed by 20 minutes incubation at 4 °C in the dark. After centrifugation at 523 g for 4 minutes at 4 °C with 1 ml permeabilization buffer and then 1 ml flow cytometry buffer, cells were resuspended in 250 µl flow cytometry buffer, filtered through 35 µm cell strainer caps and subjected to measurement.

4.6.4 Quantification of intracellular pH

0.5 x 10^6 $CD8^+$ T cells isolated from *2C/Rag2*$^{-/-}$ mice (Chapter 4.4.3.1) were centrifuged at 345 g for 7 minutes at 4 °C and resuspended in 1 ml Hank's balanced salt solution (HBSS, containing 2 g/l $NaHCO_3$). After adding 10 µM Carboxy SNARF-1 AM acetate, cells were incubated for 30 minutes in the incubator. Then centrifugation was performed with 1 ml HBSS at 345 g for 7 minutes at 4 °C. Afterwards, cells were resuspended in 1 ml HBSS containing different amounts of *L*-lactic acid (0, 10, 15 and 20 mM) or HCl corresponding to the pH of 15 mM lactic acid (~pH 6.4) and were incubated at 37 °C for 30 minutes and 7 hours, respectively. For *in situ* pH calibration, instead of being treated with lactic acid, cells were incubated with a mix of pH-controlled buffers and valinomycin/nigericin according to the manufacturer's recommendations. Samples were then subjected to measurement at the FACS Calibur flow cytometer. For analyses, ratios of emission wavelength λ_1, transmitted by a 585/42BP filter and wavelength λ_2, transmitted by a 670LP filter, were calculated.

4.7 Generation of *Ldha*$^{-/-}$ clones with CRISPR/Cas9

Clustered, regularly interspaced, short palindromic repeats (CRISPR)/Caspase 9 (Cas9) systems, originally found in bacteria as defense mechanisms against invading viruses, nowadays serve as potent novel tools for genome engineering[186]. By means of a single guide RNA (gRNA), the Cas9 endonuclease can be directed to a specific locus in the genome and perform a double-strand break at the desired site. This is mis-repaired by error-prone non-homologous end-joining, resulting in a gene deletion. To exclude possible off-target activity by the Cas9 endonuclease parallel targeting of different sites of the desired gene is recommended.

For the knockout of *Ldha* by means of CRISPR/Cas9, two different loci on exon 4 of the *Ldha* gene in B16.SIY E12 cells were targeted by means of two different gRNAs (Plasmid generation by Jérôme Durivault, group of Jacques Pouysségur, Centre Scientifique de Monaco, Département de Biologie Médicale, Monaco). Successful knockout was determined by LDHA immunoblotting of whole-cell lysates from cells cultivated in 1% O_2 hypoxia for 24 hours, as described by Marchiq et al.[187], using 11% SDS polyacrylamide gels and an α-LDHA antibody (Chapter 3.8.1).

These experiments were performed in the laboratory of Jacques Pouysségur (Institute of Research on Cancer and Ageing (IRCAN), University of Nice-Sophia Antipolis-CNRS-Inserm, Centre A. Lacassagne, Nice, France).

4.7.1 Plasmid amplification and isolation

The CRISPR/Cas9 system was provided by Jérôme Durivault (group of Jacques Pouysségur, Centre Scientifique de Monaco, Département de Biologie Médicale, Monaco) as an all-in-one plasmid (Figure 10-1) and transformed into *E. coli*. Therefore, 200 ng of CRISPR/Cas9 plasmid were added to *E. coli* in pre-cooled tubes and incubated for 30 minutes on ice followed by incubation at 42 °C in the waterbath for 45 seconds. After 2 minutes incubation on ice, 100 µl SOC medium were added and incubated for 15 minutes at 37 °C on a heatblock. Bacteria were plated out on ampicillin agar plates and incubated for ~16 hours. One colony was picked and incubated in TB medium with ampicillin in the incubator shaker at a 45 ° ankle at 37 °C for 24 hours. Then, the bacteria were transferred in an Erlenmeyer flask with TB medium containing ampicillin and incubated for another 24 h in the incubator shaker. Plasmid DNA was obtained using the Qiagen Plasmid Maxi Kit according to the manufacturer's instructions.

4.7.2 Transfection and cloning of *Ldha*$^{-/-}$ cells

For transfection, 2 x 10^6 B16 SIY.E12 cells were seeded in small cell culture dishes and incubated for 24 hours. After incubation the cells were transfected with 10 µg plasmid DNA using the

jetPRIME DNA transfection kit according to the manufacturer's instructions. Transfection efficiency of over 90 % could be achieved.
Cells were seeded in a low density of 1,000 cells/10 cm cell culture dish and as soon as visible colonies formed, clones were picked.

4.8 Analysis of human biopsies

4.8.1 Sample preparation for flow cytometry analysis

In order to obtain single-cell suspensions from human tissue, biopsies were minced with a scalpel and incubated in 1 ml medium containing 100 µl Collagenase IV (2100 U) and 45 µl DNase I (10 mg/ml) in 12-well microtiter plates for 2 hours. Medium with minced tissue was then passed through 70 µm cell strainers, and microtiter plates were rinsed with 20 ml medium to collect all cells. After centrifugation at 345 g for 7 minutes at 4 ℃, cells were resuspended in 1 ml medium and subjected to cell counting. If the pellet contained erythrocytes, ACK lysis was performed before cell counting with 3 ml ACK lysis buffer (Chapter 4.4.3.2) for 2 minutes at room temperature, stopped by addition of 10 ml medium and subsequent centrifugation. Samples were then subjected to surface staining (Chapter 4.6.2).

4.8.2 Sample preparation for RNA isolation and bioluminescence imaging

Freshly dissected human tissues were immediately snap-frozen to preserve the metabolic profile. RNA isolation was performed as described in Chapter 4.2.1. Bioluminescence imaging was performed according to Chapter 4.5.

4.9 Statistical analyses

Results represent the mean and standard error of the mean (s.e.m.). Comparison between groups was performed using paired or unpaired Student's *t*-test. Correlations were calculated by the Pearson test. *P*-values of < 0.05 were considered statistically significant. All calculations were performed using GraphPad Prism software.

5 Results

5.1 Immunomodulatory role of lactic acid *in vitro*

Tumor cells are characterized by a highly glycolytic phenotype in order to sustain hyperproliferation, which leads to the excessive production of lactate and in turn to the accumulation of lactic acid in the tumor microenvironment. As data on the impact of lactic acid on mouse immune cells are scarce, here, lymphoid and myeloid cell populations were analyzed after exposure to lactic acid.

5.1.1 Effects on lymphoid cells

To assess the impact of lactic acid on lymphoid cells, splenocytes from C57BL/6 mice were stimulated with PMA/ionomycin and incubated in the absence or presence of pathophysiological concentrations of lactic acid[57] for 3 hours. In parallel, the effects of sodium lactate and pH changes similar to that of 20 mM lactic acid (~pH 5.8) were studied to distinguish between the impact of lactate itself and acidification, which is coupled to lactate export. After 3 hours, the activity of lymphoid cells was determined by measuring cytokine production using flow cytometry.
Initially, IFN-γ, as an important cytokine for T and NK cell anti-tumor immunity was analyzed. Among $CD4^+$ T cells only 6% IFN-γ producing cells were found (Figure 5-1 A), whereas 25% of $CD8^+$ T cells and nearly 40% of NK cells were identified as IFN-γ-producing cells (Figure 5-1 B,C). Regarding the impact of lactic acid on IFN-γ, a severe reduction was observed in all three cell populations with increasing concentrations of lactic acid. In contrast, incubation with sodium lactate showed no effect on IFN-γ production, whereas acidification (~pH 5.8) resulted in a decrease of IFN-γ production comparable to that of 20 mM lactic acid. Comparing the inhibitory effect of lactic acid on IFN-γ production between T cells and NK cells, $CD8^+$ T cells were found to be the most susceptible cell type. Upon treatment with 20 mM lactic acid, IFN-γ production in $CD8^+$ T was almost completely abolished, while $CD4^+$ T cells and NK cells were able to maintain a residual IFN-γ production.

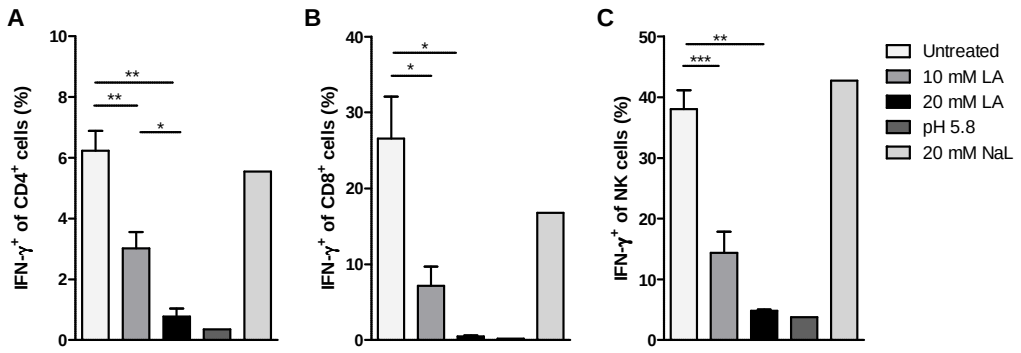

Figure 5-1. Lactic acid suppresses IFN-γ production of T and NK cells
(**A-C**) Quantification of IFN-γ^+ cells among $CD4^+$ T cells (**A**), $CD8^+$ T cells (**B**) and NK cells (**C**) from stimulated splenocytes of healthy C57BL/6 mice after incubation in the absence (untreated) or presence of lactic acid (10 and 20 mM LA), acidified medium corresponding to the pH of 20 mM LA (~pH 5.8) as well as 20 mM sodium lactate (NaL) for 3 hours, by flow cytometry (n = 3, mean and s.e.m., n = 1 for pH 5.8 and 20 mM NaL). * $P < 0.05$, ** $P < 0.01$, and *** $P < 0.001$ (paired Student's t-test).

As the anti-tumor activity of lymphoid cells is not only based on IFN-γ but also implicates granzyme B, which is important for cytolytic effector functions of T cells and NK cells, the latter was studied as well. Flow cytometry analyses revealed that the number of granzyme B^+ cells was almost three times higher in NK cells than in $CD8^+$ T cells and the expression did not differ significantly after treatment with lactic acid, acidification or sodium lactate (Figure 5-2 A,B), suggesting that granzyme B production, unlike IFN-γ production, seems to be lactic acid insensitive.

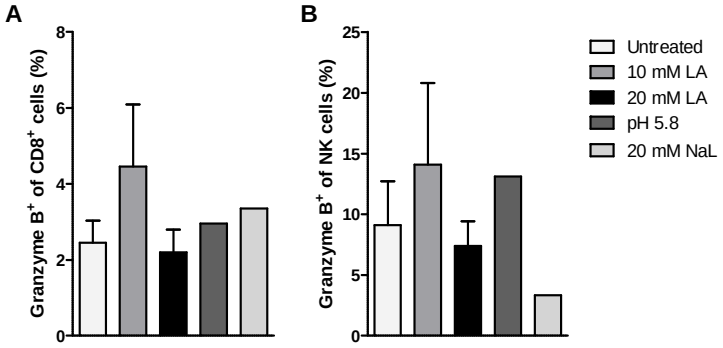

Figure 5-2. Granzyme B production of $CD8^+$ T cells and NK cells is not impaired by lactic acid
(**A,B**) Quantification of granzyme B^+ cells among $CD8^+$ T cells (**A**) and NK cells (**B**) from stimulated splenocytes of healthy C57BL/6 mice after incubation in the absence (untreated) or presence of lactic acid (10 and 20 mM LA), acidified medium corresponding to the pH of 20 mM LA (~pH 5.8) as well as 20 mM sodium lactate (NaL) for 3 hours by flow cytometry (n = 3, mean and s.e.m., n = 1 for pH and 20 mM NaL).

5.1.2 Effects on myeloid cells

In addition to lymphoid cells, myeloid cells were analyzed regarding their sensitivity towards lactic acid by measuring cytokine production as described in Chapter 5.1.1.

A prominent cytokine produced by myeloid cells is IL-6. Its expression is upregulated in many types of cancer and associated with tumor progression and poor prognosis[160]. Splenocytes were

stimulated with PMA/ionomycin and incubated in the absence or presence of pathophysiological concentrations of lactic acid[57], corresponding acidification and sodium lactate for 3 hours. As depicted in Figure 5-3, the number of IL-6$^+$ CD11b$^+$ cells showed no differences in the non-treated versus lactic acid-treated cells, i.e. IL-6 production by myeloid cells is not affected by lactic acid.

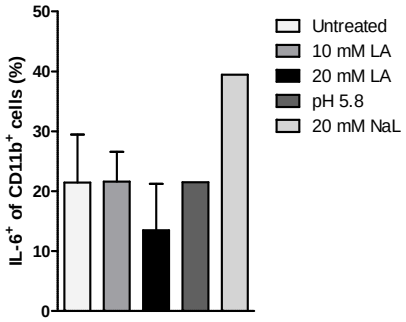

Figure 5-3. IL-6 production of myeloid cells is not affected by lactic acid
Quantification of IL-6$^+$ cells among CD11b$^+$ cells from stimulated splenocytes of healthy C57BL/6 mice after incubation in the absence (untreated) or presence of lactic acid (10 and 20 mM LA), acidified medium corresponding to the pH of 20 mM LA (~pH 5.8) as well as 20 mM sodium lactate (NaL) for 3 hours, by flow cytometry (*n* = 3, mean and s.e.m., *n* = 1 for pH and 20 mM NaL).

5.2 Immunomodulatory role of lactic acid *in vivo*

The previous experiments proved that lactic acid has a negative impact on the IFN-γ production of T and NK cells from spleens of healthy C57BL/6 mice. Together with similar findings on human T cells[177,178,188,189] and human myeloid cells[174-176], these data strongly suggest a modulatory role of lactic acid on immune cells also *in vivo*. To investigate this hypothesis, tumor cell lines producing different levels of lactic acid were used to generate tumors in immunocompetent and immunodeficient mice, which were then analyzed regarding immune cell infiltration and activation, and the impact on tumor growth.

5.2.1 Characterization of B16.SIY E12 Ldha^{low} cells for *in vivo* experiments

In order to investigate the role of lactic acid on immune cells *in vivo,* B16.SIY E12 mouse melanoma cells, producing high amounts of lactate, were transfected with *Ldha* shRNA plasmids to generate clones with reduced *Ldha* expression (Ldha^{low}) and in this way to decrease lactate production of the cells[183]. Untransfected cells (WT) and cells transfected with a scrambled shRNA (Ctrl) served as controls.
The following chapters describe the characterization of the Ldha^{low} clones.

5.2.1.1 Enzymes and transporters involved in glucose metabolism

To confirm the knockdown by shRNA technology, *Ldha* mRNA levels were analyzed in B16.SIY E12 cells in comparison to mRNA expression of other enzymes or transporters linked to glycolysis which could possibly be influenced by the downregulation of *Ldha*.

Wild type cells (WT), cells transfected with a scrambled shRNA sequence (Ctrl) and Ldha^{low} clones (Ldha^{low1} and Ldha^{low2}) were cultured for 24 hours at a cell density of 1 x 10^6 cells in 6-well microtiter plates, total RNA was isolated using the RNeasy Mini Kit and reverse transcription was performed. qRT-PCR with primers for *Ldha*, *Ldhb*, *Glut1*, *Hk1* and *Hk2* was performed and normalized to the mRNA expression of *18S* rRNA.

Results revealed that *Ldha* mRNA expression levels in Ldha^{low} clones were reduced by almost 50% compared to controls, suggesting the efficient knockdown of *Ldha (*Figure 5-4 A). This was accompanied by an upregulation of *Ldhb* in Ldha^{low} clones (Figure 5-4 B), which could catalyze the inverse reaction, i.e. transforming lactate into pyruvate. The expression of *Glut1* was not affected by the knockdown (Figure 5-4 C), whereas *Hk1* mRNA expression was elevated in Ldha^{low} clones compared to control cells, and *Hk2* mRNA expression was decreased compared to wild type cells (Figure 5-4 D,E).

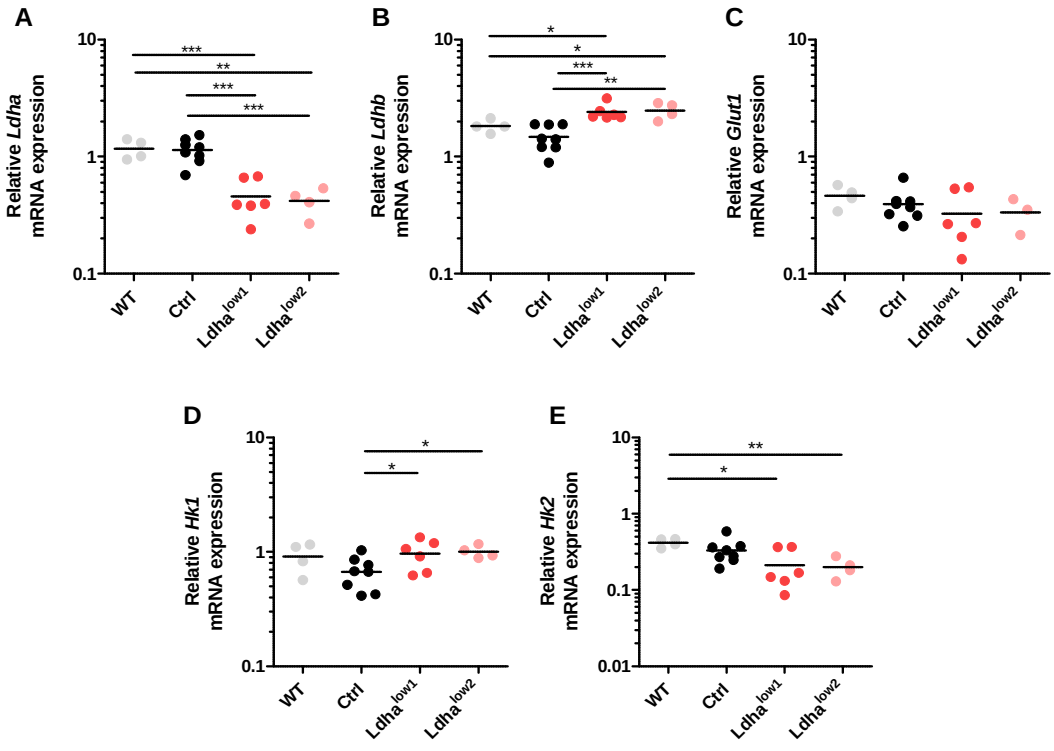

Figure 5-4. Ldha^{low} clones show downregulation of *Ldha* mRNA and upregulation of *Ldhb*
(**A-E**) qRT-PCR analysis of *Ldha* (**A**), *Ldhb* (**B**), *Glut1* (**C**), *Hk1* (**D**) and *Hk2* (**E**) in untransfected cells (WT), cells transfected with a scrambled shRNA sequence (Ctrl), and cells transfected with shRNA for *Ldha* (Ldha^{low}). The results are presented relative to the level of *18S* rRNA. Each dot represents an individual experiment and horizontal lines indicate the mean. * $P < 0.05$, ** $P < 0.01$, and *** $P < 0.001$ (unpaired Student's *t*-test).

As mRNA levels do not always correspond to protein levels, protein expression of LDHA and LDHB was analyzed to investigate changes in the abundance of the enzymes after knockdown by *Ldha* shRNA. Actin served as loading control.

Results from western blotting revealed that, on protein level, LDHA and its phosphorylated form were strongly reduced in Ldha^{low} clones (Figure 5-5 A), matching the results on mRNA level (Figure 5-4 A). In contrast, no change in LDHB protein expression was observed in Ldha^{low} clones compared to controls (Figure 5-5 B).

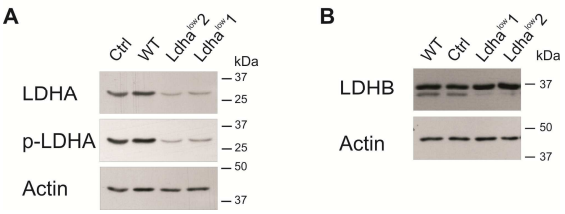

Figure 5-5. LDHA protein levels are diminished in Ldha^{low} clones compared to control cells
(**A,B**) Western blot analysis of LDHA and its phosphorylated form (p-LDHA) (**A**) and LDHB (**B**) in whole-cell lysates of cells transfected with a scrambled shRNA sequence (Ctrl), untransfected cells (WT) and cells transfected with shRNA for *Ldha* (Ldha^{low}). Actin served as loading control. One representative experiment of three is shown.

5.2.1.2 Lactate production

The efficient knockdown of *Ldha* on mRNA and protein level, as shown above, does not allow conclusions regarding the activity of the LDH-5 enzyme.

In order to examine the functional consequences of the *Ldha* knockdown by shRNA, cells were cultured at a density of 2.5 x 10^4 cells in 96-well microtiter plates and lactate levels were assessed in cell culture supernatants after 24 hours by an enzymatic assay. Analyses, performed by the Department of Clinical Chemistry (University Hospital Regensburg, Germany), revealed that lactate production in Ldha^{low} cells was reduced by ~50% compared to controls (Figure 5-6). This result shows that the *Ldha* shRNA knockdown was successful and the Ldha^{low} clones represent a suitable tool to study the role of lactic acid in immunomodulation.

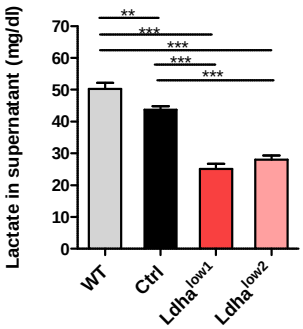

Figure 5-6. Ldha^{low} clones produce lower amounts of lactate than controls
Lactate concentrations in the supernatant of 2.5 x 10^4 untransfected cells (WT), control cells (Ctrl), Ldha^{low1} and Ldha^{low2} cells, cultured for 24 h ($n \geq 21$ per group, mean and s.e.m.). ** $P < 0.01$, and *** $P < 0.001$ (unpaired Student's *t*-test).

5.2.1.3 Proliferation

To ensure that the decrease in lactate production of Ldha^{low} clones was not due to reduced cell growth, proliferation was assessed by a ^{3}H-thymidine incorporation assay.

After 24 hours incubation, Ldha^{low} cells did not show an impairment regarding proliferation compared to control cells (Figure 5-7). On the contrary, Ldha^{low1} cells proliferated even more than the control cells and Ldha^{low2} cells. Thus, the reduced lactate production of Ldha^{low} cells was independent of cell proliferation.

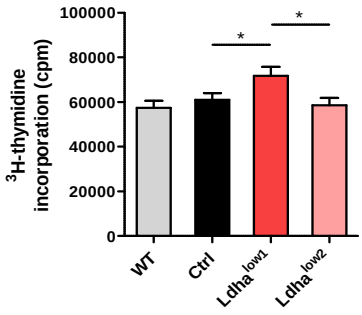

Figure 5-7. Ldha^{low} clones proliferate similarly to controls
Proliferation of 2.5 x 10^{4} untransfected cells (WT), control (Ctrl), Ldha^{low1} and Ldha^{low2} cells, based on ^{3}H-thymidine incorporation, after 24 h ($n \geq 3$ per group, mean and s.e.m.). * $P < 0.05$ (unpaired Student's *t*-test).

5.2.1.4 Cell cycle

Ldha^{low} cells were not only analyzed regarding proliferation but also regarding their cell cycle distribution, as cell cycle regulation is interconnected with cellular metabolism, crucial for cell survival and proliferation[190] and, therefore, important for the stability of the Ldha^{low} clones.

In all cell lines analyzed, the majority of cells (~70%) resided in the resting phase (G0/G1), while a smaller amount of ~20%, each, resided in the synthesis phase (S) and pre-mitosis phase (G2), respectively (Figure 5-8). No differences were observed in the distribution of cells in the cell cycle states between Ldha^{low}, control and wild type cells. Therefore, neither the stability of the Ldha^{low} clones nor the replication properties were affected by the knockdown.

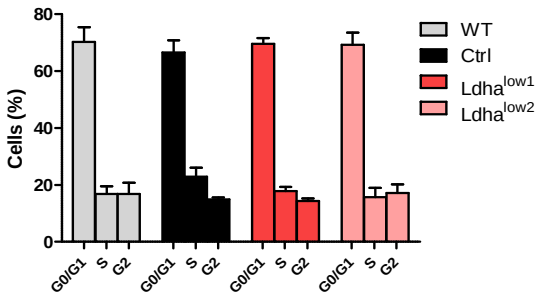

Figure 5-8. Cell cycle properties do not differ between Ldha^{low} clones and controls
Cell cycle analysis of wild type (WT), control (Ctrl) or Ldha^{low1} and Ldha^{low2} cells after seeding of 5 x 10^{5} cells for 24 h and staining with propidium iodide buffer (n = 3-5, mean and s.e.m.).

5.2.1.5 Respiration

The knockdown of *Ldha*, which is crucial for glycolysis, could possibly impair the energy yield of the cell. Thus, it is conceivable that the cell attempts to compensate this energy loss by upregulating OXPHOS, in order to maintain energy levels.

To clarify, whether this hypothesis proves true, cells were analyzed by high-resolution respirometry, and the results show that Ldha^{low} clones exhibit a higher basal respiration compared to control cells (Figure 5-9 A). Analysis of mitochondria with the green-fluorescent mitochondrial dye MitoTracker Green demonstrated that the higher respiration of Ldha^{low} clones compared to control cells was due to an increased quantity of mitochondria (Figure 5-9 B,C). This allows the conclusion that Ldha^{low} cells compensate their impaired glycolysis by upregulating their mitochondrial content and thereby increasing respiratory capacity, whereas control cells, showing lower mitochondrial content and lower respiration, seem to rely mainly on glycolysis.

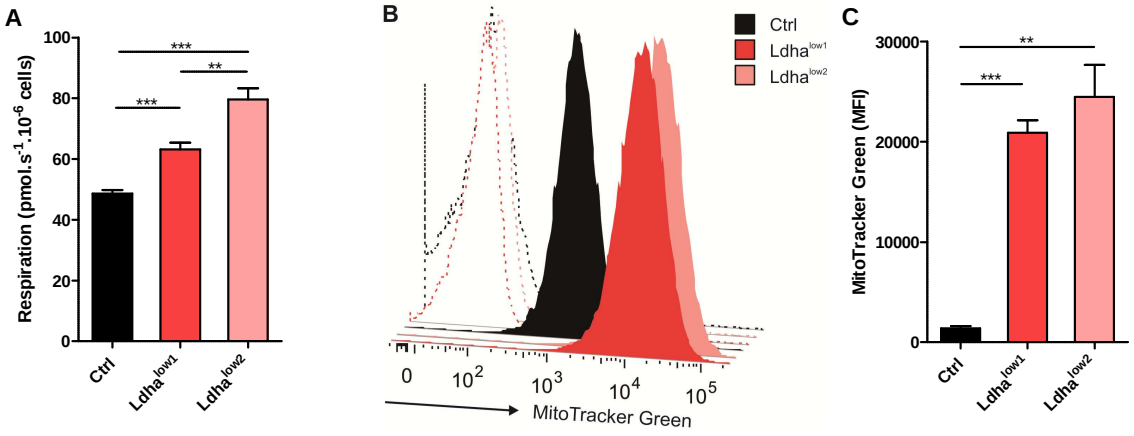

Figure 5-9. Ldha^{low} clones show increased respiratory capacities compared to control cells
(**A**) Basal respiration of control (Ctrl), Ldha^{low1} and Ldha^{low2} cells (n = 5-6, mean and s.e.m.) measured by high-resolution respirometry. Values were corrected for residual oxygen consumption. (**B**) Histogram of MitoTracker Green staining by flow cytometry of cells described in **A**. Dashed peaks show unstained cells. One representative experiment of three is displayed. (**C**) Mean fluorescence intensity (MFI) of MitoTracker Green staining normalized to unstained cells as measured in **B** (n = 3, mean and s.e.m.). ** $P < 0.01$ and *** $P < 0.001$ (unpaired Student's t-test).

5.2.2 Analysis of Ldha^{low} tumors in immunocompetent C57BL/6 mice

The most common way to study human tumors is a tumor xenograft model. In this approach, human tumor cells are transplanted subcutaneously or in organs of interest into immunocompromised mice like athymic nude mice or severe combined immunodeficient (SCID) mice. Thereby, tumor rejection by immune cells is prevented and growing tumors can be analyzed regarding invasiveness, metastasis, survival, response to therapeutics and many more parameters.

Although the xenograft model reflects many characteristics of human tumors, the role of the immune system is totally neglected. As the complex mutual interactions between the immune

system and tumors are important for immunosurveillance or immune escape, we decided to use a syngeneic mouse model in order to study the role of tumor-derived lactic acid on immune cells in the tumor microenvironment. Here, transplanted cancer cells and the host are MHC matched, which prevents transplant rejection. This allows the investigation of a “real-life” situation in the tumor microenvironment.

To generate tumors in immunocompetent C57BL/6 mice, 1 x 10^5 B16 tumor cells transfected with a scrambled shRNA sequence (Ctrl) or Ldha^{low} clones (Ldha^{low1}, Ldha^{low2}) were injected subcutaneously into the dorsal region of the mice. Between day 13 and 21, tumors were dissected and subjected to various analyses.

5.2.2.1 Metabolic characteristics of tumors

Dissected tumors were immediately stored in RNAlater reagent according to the manufacturer’s instructions and isolation of total RNA as well as reverse transcription were performed. qRT-PCR was conducted with primers targeting genes of glucose metabolism, amino acid and prostaglandin metabolism to analyze the impact of the *Ldha* knockdown on other pathways *in vivo*. The results obtained were normalized to *18S* rRNA expression.

5.2.2.1.1 Glucose metabolism

To see whether the successful knockdown *in vitro* (Figure 5-4 A) remained stable under *in vivo* conditions, the expression of *Ldha* was examined in control and Ldha^{low} tumors. Results from qRT-PCR demonstrated significantly decreased *Ldha* mRNA levels of Ldha^{low} tumors compared to control tumors (Figure 5-10 A). This finding proved that Ldha^{low} cells maintain reduced *Ldha* mRNA levels not only *in vitro* but also *in vivo*.

Ldha, the target of the shRNA in Ldha^{low} clones, codes for an important enzyme of the glucose metabolism. It is possible, that by its knockdown, other “players” of the glucose metabolism are altered due to the tumor microenvironment *in vivo*.

Expression levels of *Ldhb,* as well as *Glut1*, being responsible for glucose uptake into the cells and *Hk1* and *Hk2,* which are the rate-limiting enzymes in glucose metabolism, were analyzed in control and Ldha^{low} tumors. *Ldhb* was found to be downregulated in Ldha^{low2} tumors but not in Ldha^{low1} tumors compared to control tumors (Figure 5-10 B). The *in vitro* results showed an upregulation of *Ldhb* in both Ldha^{low} cells (Figure 5-4 B). No differences were found in the expression levels of *Glut1* mRNA in control and Ldha^{low} tumors (Figure 5-10 C), which matches the results *in vitro* (Figure 5-4 C). *Hk1* mRNA levels *in vivo* were only increased in Ldha^{low1} and not in Ldha^{low2} tumors compared to control tumors (Figure 5-10 D), whereas *in vitro* both Ldha^{low} clones showed increased *Hk1* mRNA expression levels (Figure 5-4 D). Regarding *Hk2* mRNA expression, in line with the *in vitro* results (Figure 5-4 E), no differences between control and Ldha^{low} tumors were observed *in vivo* (Figure 5-10 E).

These results suggest that the tumor microenvironment can influence certain “players” of the glucose metabolism, resulting in changes of mRNA expression levels. However, in our model, *Ldha* mRNA expression remained stable under *in vivo* conditions.

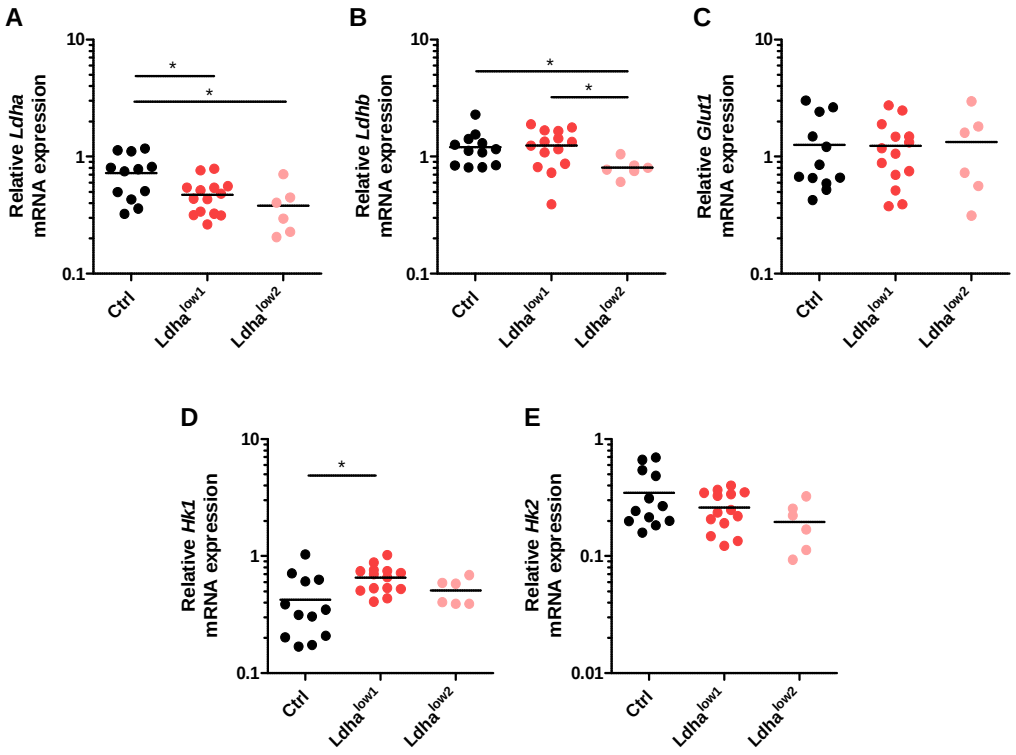

Figure 5-10. *Ldha* shRNA knockdown remains stable *in vivo*
(**A-E**) qRT-PCR analysis of *Ldha* (**A**), *Ldhb* (**B**) *Glut1* (**C**), *Hk1* (**D**) and *Hk2* (**E**) mRNA in tumors of C57BL/6 mice after subcutaneous injection of 1 x 10^5 control (Ctrl), $Ldha^{low1}$ or $Ldha^{low2}$ cells. The results are presented relative to the level of *18S* rRNA. Each dot represents an individual mouse and horizontal lines indicate the mean. * $P < 0.05$ (unpaired Student's *t*-test).

Gene expression could also be linked to differences in tumor size, as large tumors lead to hypoxia, which in turn regulates the transcription of a variety of genes. Even though endeavors were made to obtain tumors with comparable sizes, this is often not possible due to time- and experimental limitations. Hence, in statistical analyses, tumor volumes were correlated to the amount of mRNA expression. Results revealed that the mRNA expression of *Ldha*, *Ldhb*, *Glut1*, *Hk1* and *Hk2* was not dependent on tumor volume (data not shown). This suggests that the differences between control and $Ldha^{low}$ clones are predominantly due to the downregulation of *Ldha*.

5.2.2.1.2 Amino acid and prostaglandin metabolism

Fast proliferating tumor cells do not only show metabolic alterations in glucose metabolism but also exhibit a deregulated tryptophan and arginine metabolism, and changes in prostaglandin metabolism.

Overexpression of the tryptophan-converting enzyme IDO is found in several types of cancer[80,81] and leads to T cell unresponsiveness[83]. Accordingly, decreased serum tryptophan levels are linked to poor prognosis in melanoma[82]. Similarly, elevated expression of ARG1 and ARG2 leads to arginine depletion and subsequent impairment of T cell function[93]. Alternatively, arginine is metabolized by NOS which was detected in various human tumors[95,96].

While COX1 is constitutively expressed in all cells, COX2 expression is mainly found at sites of inflammation and is overexpressed in tumors[97]. It causes release of prostaglandins, especially prostaglandin E2, which is further stimulating inflammation and inducing angiogenesis, and thereby promotes tumor growth[191].

Regarding mRNA expression of *Ido1*, *Ido2*, *Arg1*, *Arg2*, *iNos*, *Cox1* and *Cox2* no significant differences were observed in Ldha^{low} tumors compared to control tumors (Figure 5-11 A-G). This indicates that the downregulation of *Ldha* has no impact on other important tumor-promoting factors.

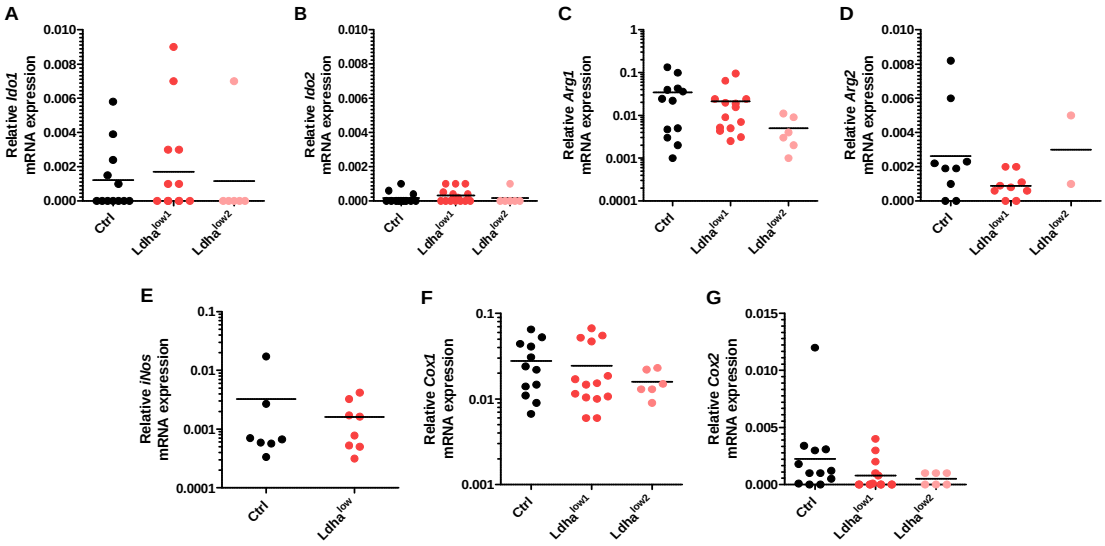

Figure 5-11. Ldha^{low} tumors show no alterations in the expression of other tumor-promoting enzymes
(**A-G**) qRT-PCR analysis of *Ido1* (**A**), *Ido2* (**B**), *Arg1* (**C**), *Arg2* (**D**), *iNos* (**E**), *Cox1* (**F**) and *Cox2* (**G**) mRNA in tumors of C57BL/6 mice after subcutaneous injection of 1 x 10^5 control (Ctrl), Ldha^{low1} or Ldha^{low2} cells. The results are presented relative to the level of *18S* rRNA. Each dot represents an individual mouse and horizontal lines indicate the mean.

5.2.2.2 Intratumoral lactate levels

In vitro, Ldha^{low} cells were shown to have a decreased *Ldha* expression both on mRNA and on protein level (Figure 5-4 A and Figure 5-5 A) and diminished lactate concentrations in the supernatant (Figure 5-6). Reduction of *Ldha* mRNA levels in Ldha^{low} clones remained stable *in vivo* (Figure 5-10 A). To analyze whether the enzyme activity of LDH-5 is still compromised in tumors grown in mice, intratumoral lactate levels were determined. Therefore, tumors were immediately snap-frozen upon dissection and induced metabolic bioluminescence imaging was performed by the group of Wolfgang Mueller-Klieser (Institute of Pathophysiology, University Medical Center of the Johannes Gutenberg University Mainz, Germany). Analyses revealed that Ldha^{low} tumors exhibited two-fold lower intratumoral lactate levels compared to control tumors (Figure 5-12 A,B), implying that the *Ldha* knockdown in Ldha^{low} clones is stable *in vitro* and *in vivo*.

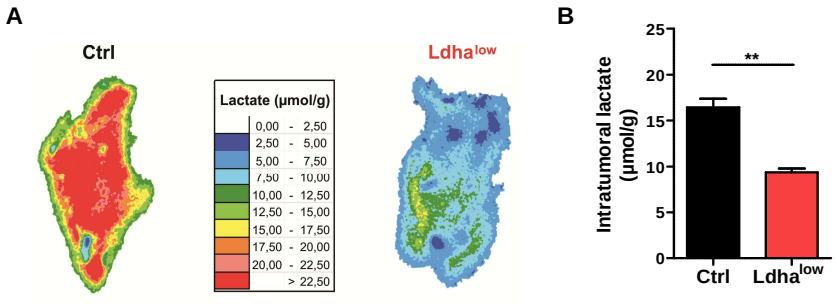

Figure 5-12. Ldha^{low} tumors exhibit lower intratumoral lactate levels than control tumors
(**A**) Induced metabolic bioluminescence imaging of intratumoral lactate levels in sections of tumors grown after injection of 1 x 10^5 control or Ldha^{low} cells in C57BL/6 mice. Two representative images are shown. (**B**) Quantification of intratumoral lactate levels identified as in **A** (*n* = 3-5 mice per group, mean and s.e.m., multiple tumor areas per sample analyzed). ** $P < 0.01$ (unpaired Student's *t*-test).

5.2.2.3 Lactate levels upon recultivation of cells after tumor excision

In addition to the induced metabolic bioluminescence imaging technique, lactate levels of tumors grown in mice were analyzed by another approach. After excision of tumors, single-cell suspensions were generated and cultivated for 7 days in cell culture medium in the absence or presence of selection antibiotics. After this period, due to the lack of stimulation and/or survival factors for stroma cells, only tumor cells were present. Lactate production of 2.5 x 10^4 cells cultivated for 24 hours was measured in the supernatants by the Department of Clinical Chemistry (University Hospital Regensburg, Germany) using an enzymatic assay. Analyses revealed that Ldha^{low} tumor cells showed significantly decreased amounts of lactate compared to control tumor cells (Figure 5-13), with values similar to those measured *in vitro* (Figure 5-6). These results were independent of the addition of selection antibiotics, suggesting that the enzymatic activity of LDH-5 remained unchanged *in vivo*.

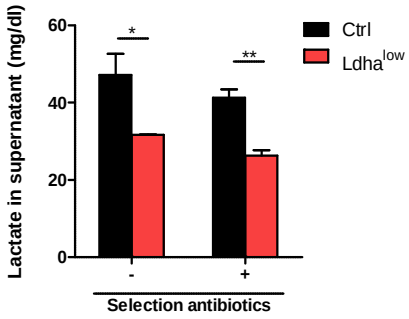

Figure 5-13. Cells from Ldha^{low} tumors produce less lactate than cells from control tumors
Lactate production of 24 h-single-cell suspension cultures containing 2.5 x 10^4 cells generated from excised tumors grown in C57BL/6 mice after subcutaneous injection of 1 x 10^5 control (Ctrl) and Ldha^{low} cells, following cultivation for 7 days in the absence or presence of selection antibiotics (*n* = 3 tumors per group, mean and s.e.m.). * $P < 0.05$ and ** $P < 0.01$ (unpaired Student's *t*-test).

5.2.2.4 Growth factors

One major hallmark of cancer is the sustained proliferation of tumor cells, which is in part based on the upregulation of growth factor expression including TGF-β, VEGF and CSF2 in the tumor environment. These factors are produced by tumor cells or stroma cells. TGF-β is a potent immunosuppressive cytokine[160] and VEGF is a key regulator of angiogenesis. Both factors can be induced by lactate[61,62]. CSF2 is responsible for the expansion of pro-tumoral MDSCs[128].

Several studies proved that the accelerated glycolysis and lactate production of tumors are favorable for cancer progression. To analyze the impact of compromised glycolysis on growth factor expression, mRNA levels of *Tgfb1*, *Vegfa* and *Csf2* from Ldha^{low} tumors grown in C57BL/6 mice were determined by qRT-PCR. While Ldha^{low} tumors exhibited significantly decreased levels of *Tgfb1* compared to controls (Figure 5-14 A), *Vegfa* and *Csf2* mRNA expression were similar in Ldha^{low} tumors and control tumors (Figure 5-14 B,C). *Tgfb* expression, therefore, seems to be compromised in a tumor microenvironment with low lactate levels. However, only minor amounts of TGF-β protein were detectable in the supernatants of control tumors (mean value 125 pg/ml, range 0-430 pg/ml) and Ldha^{low} tumors (mean value 150 pg/ml, range 0-318 pg/ml) and values did not differ significantly.

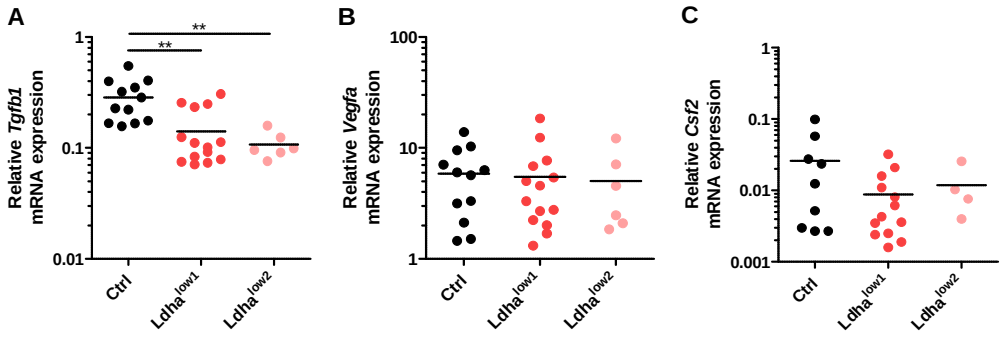

Figure 5-14. Ldha^{low} tumors are characterized by lower levels of *Tgfb1* mRNA
(**A-C**) qRT-PCR analysis of mRNA for *Tgfb1* (**A**), *Vegfa* (**B**) and *Csf2* (**C**) in tumors of C57BL/6 mice after subcutaneous injection of 1 x 10^5 control (Ctrl), Ldha^{low1} or Ldha^{low2} cells. The results are presented relative to the level of *18S* rRNA. Each dot represents an individual mouse and horizontal lines indicate the mean. ** $P < 0.01$ (unpaired Student's *t*-test).

5.2.2.5 Chemokine and cytokine profile

Besides growth factors, being responsible for tumor cell proliferation and angiogenesis, the cytokine pattern in the tumor microenvironment is pivotal for tumor outcome. Tumor promotion is mediated for instance by TNF, IL-6, IL-10 and IL-17, while anti-tumor immunity is achieved by cytokines such as IFN-γ. In order to establish the role of tumor-derived lactate on cytokine expression *in vivo*, mentioned cytokines were analyzed in tumors from C57BL/6 mice by means of qRT-PCR. Results revealed that mRNA expression of *Tnf*, *Il6*, *Il10* and *Il17a* was similar in Ldha^{low} tumors and control tumors (Figure 5-15 A-D). In contrast, *Ifng* mRNA expression was significantly elevated in Ldha^{low1} tumors compared to control tumors (Figure 5-15 E). This is suggestive of an

immunosuppressive role of lactate on IFN-γ and in line with the finding of a diminished IFN-γ production in lymphocytes upon exposure of lactic acid *in vitro* (Figure 5-1*)*.

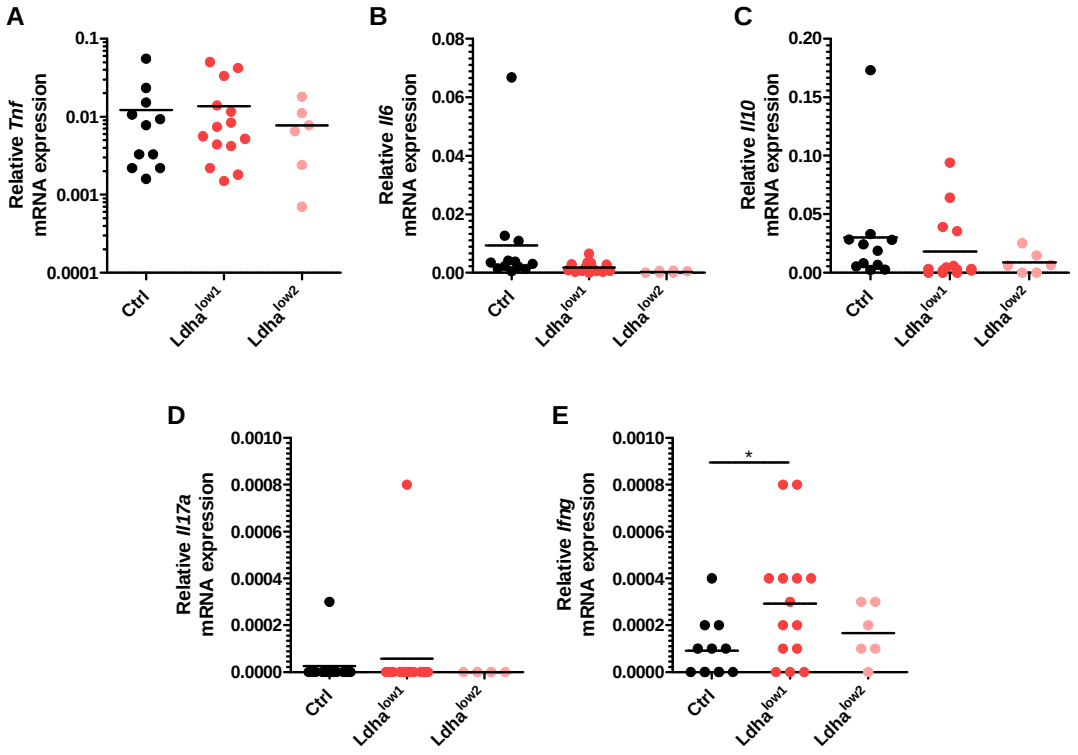

Figure 5-15. Ldha^{low} tumors express higher *Ifng* mRNA levels compared to control tumors
(**A-E**) qRT-PCR analysis of mRNA for *Tnf* (**A**), *Il6* (**B**), *Il10* (**C**), *Il17a* (**D**) and *Ifng* (**E**) in tumors of C57BL/6 mice after subcutaneous injection of 1 x 10^5 control (Ctrl), Ldha^{low1} or Ldha^{low2} cells. The results are presented relative to the level of *18S* rRNA. Each dot represents an individual mouse and horizontal lines indicate the mean. * $P < 0.05$ (unpaired Student's *t*-test).

5.2.2.6 Tumor growth

In order to analyze whether *Ldha* knockdown by means of shRNA technique influences the growth of tumors *in vivo* and to understand the impact of lactate on the immune system, tumor growth in immunocompetent C57BL/6 mice was measured. Therefore, 1 x 10^4, 1 x 10^5 or 1 x 10^6 wild type (WT) cells, cells transfected with a scrambled shRNA (Ctrl) and Ldha^{low} tumor cells, each, were injected subcutaneously into the dorsal region of C57BL/6 mice.

After subcutaneous injection of 1 x 10^4 tumor cells, on day 17, WT and Ctrl tumors reached a mean volume between 100 and 200 mm^3, whereas no tumors of Ldha^{low1} and Ldha^{low2} cells were detected (Figure 5-16 A). On day 21, 90% of the mice in the Ldha^{low1} group, 80% of the mice in the Ldha^{low2} group, but only 30% of the mice in the WT and Ctrl group were tumor-free (Figure 5-16 B). This finding suggested that tumor growth control is possible in the *Ldha* knockdown tumors. Since the tumors should be analyzed, the number of injected tumor cells was augmented. Results from the injection of 1 x 10^5 tumor cells in male and female mice revealed that on day 18, control tumors reached a mean volume of about 1,400 mm^3 (Figure 5-16 C). In contrast, Ldha^{low} tumors only reached a mean volume of about 400 mm^3. Although tumor growth was not entirely

inhibited, the significant difference in tumor growth between Ctrl and Ldha^{low} tumors remained, irrespective of the gender. In a further experiment, 1 x 10^6 tumor cells were injected in mice. Here, a loss of the growth difference between control and Ldha^{low} tumors was observed (Figure 5-16 D) suggesting that tumor control was not possible with an unphysiologically high tumor load.

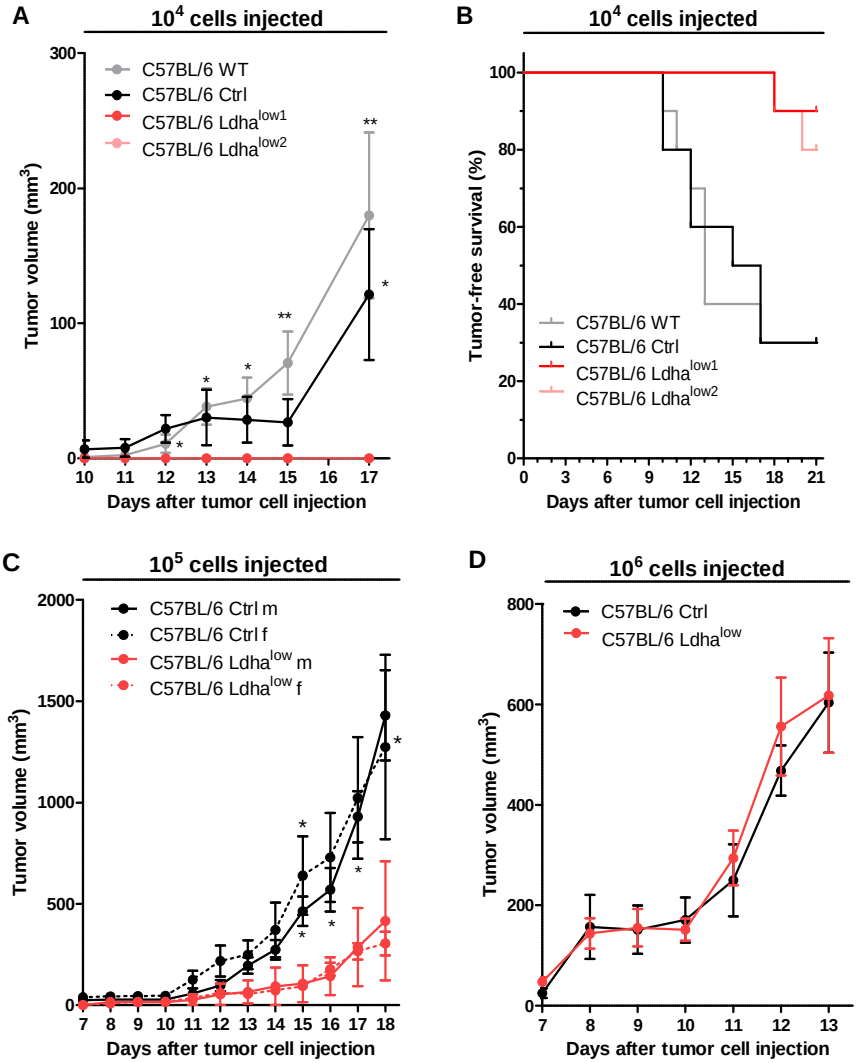

Figure 5-16. Growth of Ldha^{low} tumors is suppressed in C57BL/6 mice with low tumor burden
(**A**) Tumor growth after subcutaneous injection of 1 x 10^4 untransfected cells (WT), control cells (Ctrl) or Ldha^{low} cells (Ldha^{low1}, Ldha^{low2}) in C57BL/6 mice (*n* = 10). In statistical analyses WT or Ctrl tumors were compared to Ldha^{low} tumors. (**B**) Tumor-free survival of mice described in **A**. (**C**) Tumor growth after subcutaneous injection of 1 x 10^5 control (Ctrl) or Ldha^{low} cells in male (m) and female (f) C57BL/6 mice (*n* = 4-5). In statistical analyses, growth of tumors was compared between control cells and Ldha^{low} cells among mice of the same sex. (**D**) Tumor growth after subcutaneous injection of 1 x 10^6 control (Ctrl) or Ldha^{low} cells into C57BL/6 mice (*n* = 4-5). Data are presented as the mean tumor volume or mean tumor-free survival and s.e.m. * $P < 0.05$ and ** $P < 0.01$ (unpaired Student's *t*-test).

5.2.2.7 Immune cell infiltration

The observation of diminished growth of Ldha^{low} tumors compared to Ctrl tumors after injection of low numbers of tumor cells in C57BL/6 mice led to the conclusion that tumor immunosurveillance was possible in tumors with low lactate levels but not in the presence of higher lactate levels. To examine the effect of lactate on the immune cell infiltrate, excised tumors were analyzed by qRT-PCR and by flow cytometry.

5.2.2.7.1 T cell marker expression

As differences in the *Ifng* expression were observed between Ldha^{low} and control tumors, T cells as major producers of *Ifng* were analyzed on mRNA level. For this purpose, several T cell marker genes like *Cd4* for T helper cells, *Foxp3* for Tregs and *Cd8* for cytotoxic T cells were analyzed. Results from qRT-PCR analyses did not show any significant differences between control and Ldha^{low} tumors regarding *Cd4*, *Foxp3* and *Cd8a* expression levels (Figure 5-17 A-C).

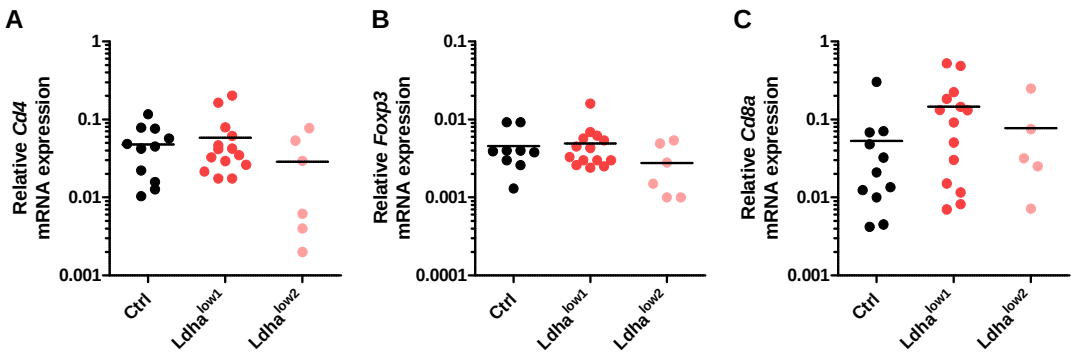

Figure 5-17. T cell marker gene expression is similar in Ldha^{low} and control tumors
(**A-C**) qRT-PCR analysis of mRNA for *Cd4* (**A**), *Foxp3* (**B**) and *Cd8a* (**C**) in tumors of C57BL/6 mice after subcutaneous injection of 1 x 10^5 control (Ctrl), Ldha^{low1} or Ldha^{low2} cells. The results are presented relative to the level of *18S* rRNA. Each dot represents an individual mouse and horizontal lines indicate the mean.

5.2.2.7.2 Immune cell infiltrate and tumor size

Analyses from qRT-PCR regarding T cell markers did not reveal any differences in control and Ldha^{low} tumors. However, as mRNA expression does not always correspond to protein levels and as T cells are not the only “players” in the tumor microenvironment, tumors were dissociated to single-cell suspensions, stained with fluorochrome-conjugated antibodies against various immune cell populations and subjected to flow cytometry.

Antibodies against the following common immune cell markers were used: CD45 as pan-leukocyte marker, CD11b as myeloid marker, Gr-1 as a marker for MDSCs and NK1.1 as NK cell marker. To stain B cells, α-CD19, and for T cells, antibodies against CD3 were used. T cell subpopulations were characterized by α-CD4 antibodies for T helper cells and α-CD8 antibodies for cytotoxic T cells. Analyses of aforementioned immune cell markers were performed after the exclusion of dead cells (DAPI^{+}) and doublets (FSC-W^{high}), using the gating strategy illustrated in Figure 5-18 (B cells not shown).

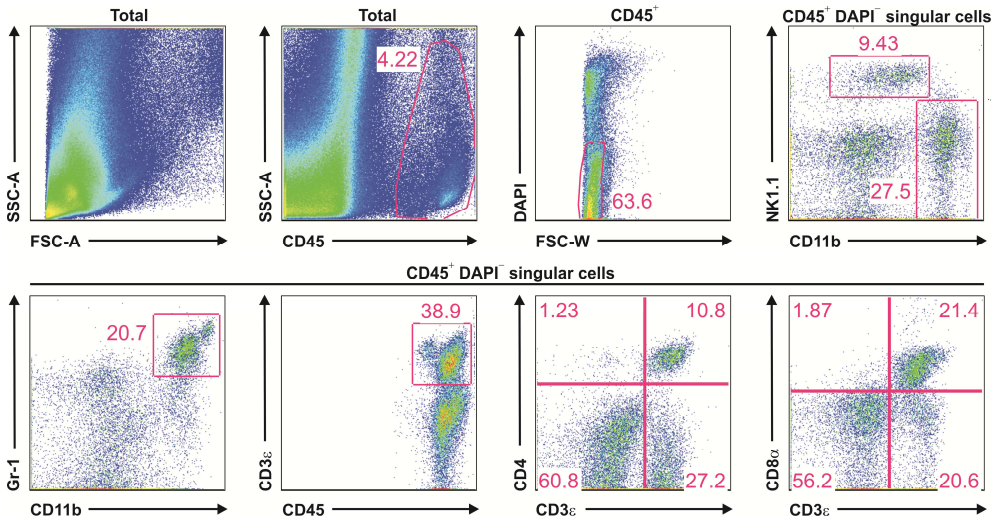

Figure 5-18. Gating strategy to detect immune cells in the tumor microenvironment
Gating strategy for leukocytes ($CD45^+$) among total cells in the tumor, living singular cells ($DAPI^-FSC\text{-}W^{low}$) among $CD45^+$ cells and myeloid cells ($CD11b^+$), NK cells ($NK1.1^+$), MDSCs ($CD11b^+Gr\text{-}1^+$), T cells ($CD3\varepsilon^+$), $CD4^+$ T cells ($CD3\varepsilon^+CD4^+$) and $CD8^+$ T cells ($CD3^+CD8\alpha^+$) among $CD45^+DAPI^-$ singular cells in tumors of C57BL/6 mice after subcutaneous injection of 1 x 10^5 control (Ctrl) or $Ldha^{low}$ cells. Numbers in graphs indicate the percentage of cells. Plots of data from one representative $Ldha^{low}$ tumor are shown.

As it was not possible to obtain tumors with exactly the same size, and to exclude possible effects of tumor size on immune cell infiltration, correlations of specific immune cell populations with tumor volumes were calculated. Results demonstrated that, up to a tumor size of 1,000 mm^3, tumor volume did not correlate with any of the analyzed immune cell populations. Overall leukocyte infiltration (Figure 5-19 A), infiltration with myeloid cells (Figure 5-19 B), MDSCs (Figure 5-19 C), B cells (Figure 5-19 D), T cells (Figure 5-19 E) and NK cells (Figure 5-19 F) were independent of tumor volume. In contrast, when bigger tumors with volumes up to 2,000 mm^3 were included in the calculations, tumor volumes strongly correlated with numbers of infiltrating B cells (data not shown), indicating that the immune cell pattern in the tumor microenvironment is changed after tumors reach a certain size.

For this reason, all tumors analyzed did not exceed a tumor volume of 1,000 mm^3, guaranteeing the results to be size-independent.

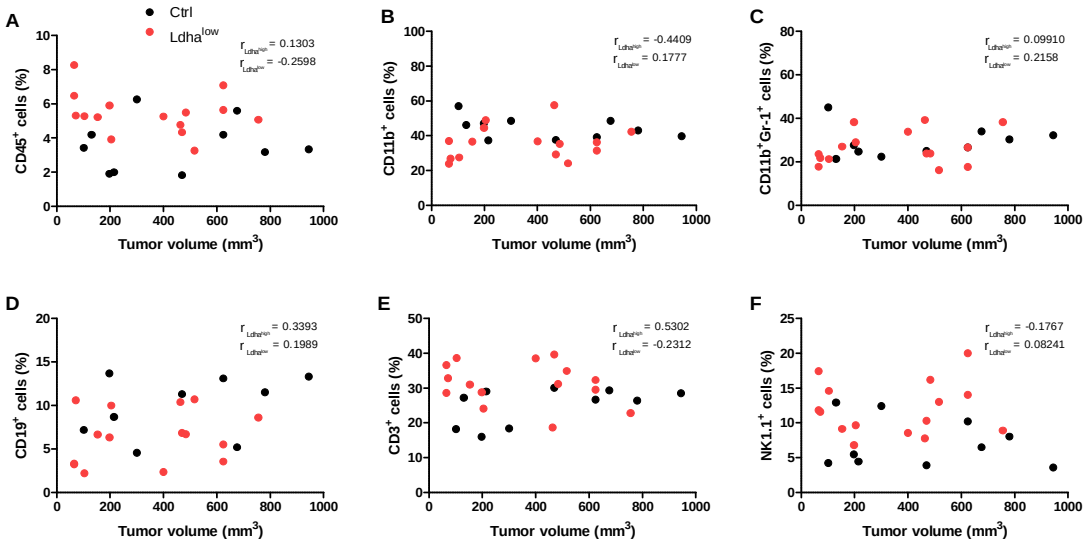

Figure 5-19. Immune cell infiltrate in tumors does not correlate with tumor size
(**A-F**) Correlations of immune cells with tumor volume: $CD45^+$ cells among all cells (**A**) derived from tumors grown after injection of $1x10^5$ control (Ctrl) or $Ldha^{low}$ cells in C57BL/6 mice and myeloid cells (**B**), MDSCs (**C**), B cells (**D**), T cells (**E**) and NK cells (**F**) among living $CD45^+$ leukocytes in those tumors, determined by flow cytometry. Each symbol represents an individual mouse. Correlations were calculated using a Pearson test.

5.2.2.7.3 Composition of the immune cell infiltrate

Figure 5-20 depicts the immune cell composition in tumors with maximum sizes of 1,000 mm^3, grown from 1 x 10^5 and 1 x 10^6 control and $Ldha^{low}$ cells, respectively, analyzed as illustrated in Figure 5-18. Tumor sizes of tumors analyzed were equally distributed in control and $Ldha^{low}$ groups of tumors grown from 1 x 10^5 and 1 x 10^6 cells, respectively (Figure 5-20 A). Both after injection of low tumor cell numbers as well as of high tumor cell numbers, the overall leukocyte infiltration was elevated in $Ldha^{low}$ tumors compared to control tumors (Figure 5-20 B). This indicates that reduced lactate levels in the tumor facilitate the immigration or survival of immune cells. Interestingly, the numbers of intratumoral $CD11b^+$ cells in $Ldha^{low}$ tumors were significantly decreased compared to control tumors only when 1 x 10^5 tumors cells were injected but not after injection of 1 x 10^6 cells (Figure 5-20 C). Thus, only in tumors grown from lower amounts of cells, a low-lactate environment seems to prevent enrichment of $CD11b^+$ in the tumor stroma resulting in decreased tumor growth. No differences in cell numbers between control and $Ldha^{low}$ tumors were observed regarding $CD11b^+Gr\text{-}1^+$ cells, the so-called MDSCs (Figure 5-20 D). Similar to $CD11b^+$ cells, lower numbers of B cells were detected in the $Ldha^{low}$ tumors grown from 1 x 10^5 cells but not from 1 x 10^6 cells (Figure 5-20 E), indicative of a tumor-promoting role of B cells. Analyses of NK cells and T cells revealed significantly increased levels of both populations in $Ldha^{low}$ tumors after injection of 1 x 10^5 cells (Figure 5-20 F,G). This phenomenon was not observed for tumors after injection of 1 x 10^6 cells, suggesting that infiltration of NK cells as well as T cells is linked to the decreased tumor growth. Subsets of T cells were analyzed subsequently. $CD8^+$ T cell numbers, but not $CD4^+$ T cell numbers, were significantly increased in $Ldha^{low}$ tumors compared to controls after injection of 1 x 10^5 cells (Figure 5-20 H,I). In contrast, tumors derived from 1 x 10^6 cells showed no significant difference in $CD4^+$ and $CD8^+$ T cell

infiltration. Comparing the percentage of immune cells between tumors grown from 1 x 10^5 and 1 x 10^6 cells, it is striking that the infiltration of myeloid cells was decreased in tumors grown from 1 x 10^6 (Figure 5-20 C) and T cell infiltration was increased (Figure 5-20 G). However, as tumor growth was not different in Ldha^{low} and control tumors grown from 1 x 10^6 cells (Figure 5-16 D), even a high number of infiltrating effector T cells is seemingly not able to control tumor growth when the tumor load exceeds a certain level.

In contrast, 1 x 10^5 tumor cells allow tumor control in Ldha^{low} tumors compared to control tumors and these tumors show an immune cell infiltration profile characterized by increased numbers of cytotoxic effector cells like NK cells and T cells, and decreased numbers of myeloid cells and B cells, which corresponds to the significantly reduced tumor growth of Ldha^{low} tumors.

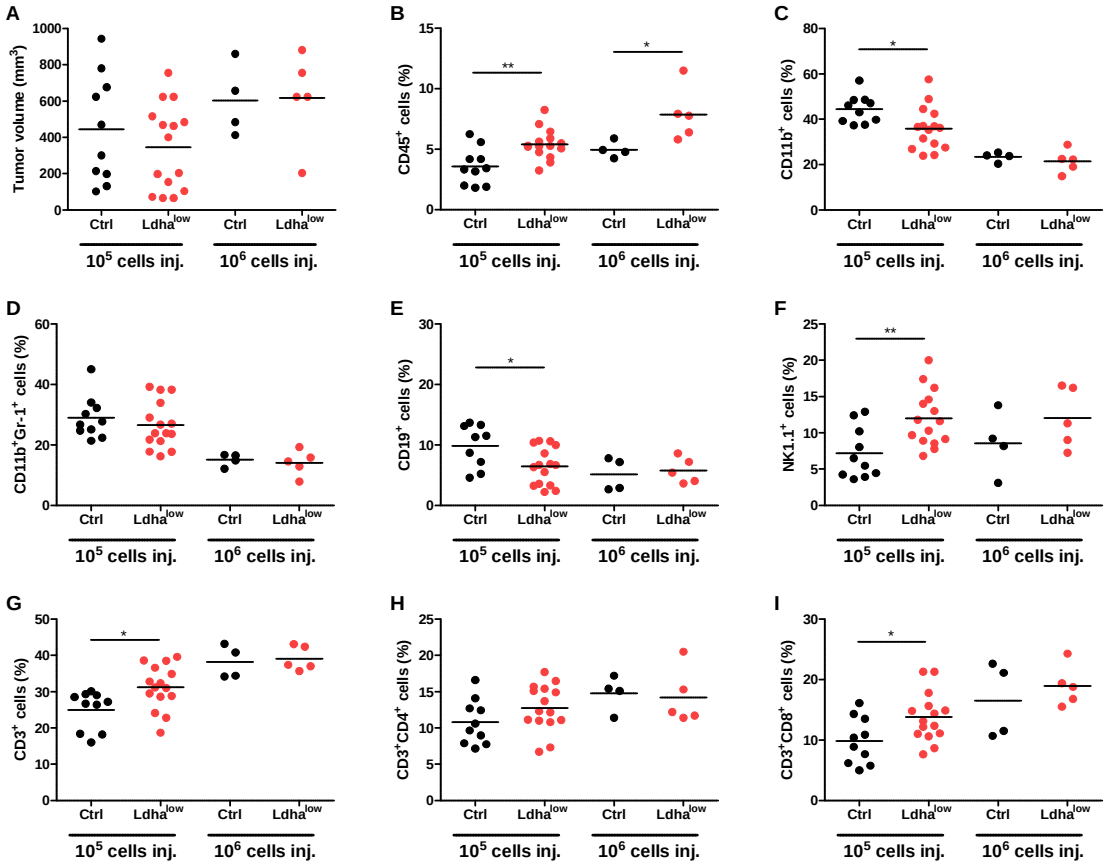

Figure 5-20. Ldha^{low} tumors contain higher numbers of anti-tumor effector cells than control tumors in C57BL/6 mice with low tumor burden

(**A**) Tumor volume of tumors grown after injection of 1 x 10^5 or 1 x 10^6 control (Ctrl) or Ldha^{low} cells in C57BL/6 mice at day of excision. (**B-I**) Percentage of CD45$^+$ leukocytes among all cells (**B**) derived from tumors described in **A** and percentage of immune cell populations among living singular CD45$^+$ leukocytes: myeloid cells (**C**), MDSCs (**D**), B cells (**E**), NK cells (**F**), T cells (**G**), CD4$^+$ T cells (**H**) and CD8$^+$ T cells (**I**), determined by flow cytometry. In statistical analyses, control tumors were compared to Ldha^{low} tumors in the respective groups. Each symbol represents an individual mouse; small horizontal lines indicate the mean. * $P < 0.05$ and ** $P < 0.01$ (unpaired Student's *t*-test).

5.2.2.7.4 Immune cells in the periphery

To investigate whether the knockdown of *Ldha*, besides causing changes in the tumor immune cell infiltration, also influences the immune cell composition in the periphery, blood and spleens of tumor-bearing mice were examined by flow cytometry as illustrated in Figure 5-18. In the blood of mice bearing control and Ldha^{low} tumor cells, no differences in numbers of immune cells were observed regarding myeloid cells, MDSCs, NK cells and T cells in the two groups (Figure 5-21 A-D). Though, comparison between immune cell composition of healthy mice and tumor-bearing mice revealed significant differences. Numbers of myeloid cells, MDSCs and NK cells were elevated in the blood of tumor-bearing mice (Figure 5-21 A-C). In contrast, numbers of T cells were severely reduced in the blood of tumor-bearing mice (Figure 5-21 D). In the spleen, similar to the blood, immune cell infiltration in mice bearing control cells and Ldha^{low} cells showed no differences for myeloid cells, MDSCs, NK cells and T cells (Figure 5-21 E-H). Alterations in tumor-bearing mice compared to healthy mice were only observed for NK cells, which were present at higher numbers in spleens of tumor-bearing mice (Figure 5-21 G), and for T cells, which were diminished in spleens of Ldha^{low} tumor-bearing mice (Figure 5-21 H). It seems that NK cells as well as T cells play a major role in tumor development as their numbers are altered in the periphery of tumor-bearing mice, irrespective of the LDHA profile of the tumor.

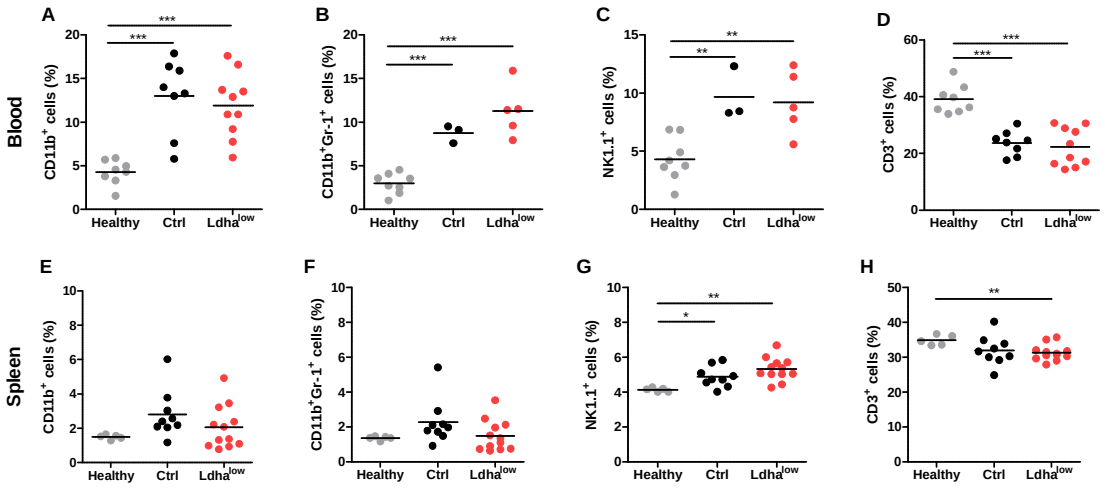

Figure 5-21. Tumor burden leads to systemic changes in the immune cell composition regardless of the LDHA profile of B16 tumor cells
(**A-D**) Quantification of myeloid cells (**A**), MDSCs (**B**), NK cells (**C**) and T cells (**D**) among living mononuclear cells in the blood of healthy C57BL/6 and C57BL/6 mice after subcutaneous injection of 1 x 10^5 control (Ctrl) or Ldha^{low} cells by flow cytometry. (**E-H**) Quantification of myeloid cells (**E**), MDSCs (**F**), NK cells (**G**) and T cells (**H**) among living leukocytes in spleens as described in **A-D**. Each symbol represents an individual mouse; small horizontal lines indicate the mean. * $P < 0.05$, ** $P < 0.01$, and *** $P < 0.001$ (unpaired Student's *t*-test).

5.2.2.7.5 Activity of immune cells in the tumor microenvironment

Absolute numbers of immune cells present in the tumor microenvironment do not fully explain tumor growth control in this model (Figure 5-20 C,G). Therefore, the activity of immune cells was analyzed by determining cytokines.

As T cells and NK cells are known to exert anti-tumor effector functions via the production of IFN-γ and granzyme B, both factors were analyzed by flow cytometry. For this purpose, tumors were dissociated to single-cell suspensions and incubated with an inhibitor of the Golgi apparatus to restrain proteins within the cell. Intracellular levels of IFN-γ and granzyme B were analyzed by intracellular staining with fluorochrome-conjugated antibodies. Results revealed that in Ldha^{low} tumors compared to control tumors, higher numbers of IFN-γ^{+} CD8^{+} T cells and NK cells were present (Figure 5-22 A,B). Regarding CD4^{+} T cells, no differences were observed between control and Ldha^{low} tumors (Figure 5-22 C). Additionally, granzyme B^{+} CD8^{+} T cells were elevated in Ldha^{low} tumors compared to control tumors (Figure 5-22 D). In contrast, no significant difference was observed in granzyme B^{+} NK cells between control and Ldha^{low} tumors (Figure 5-22 E). IL-17, a cytokine mainly produced by Th17 cells, exerting regulatory functions, was equally produced in CD4^{+} T cells of control and Ldha^{low} tumors (Figure 5-22 F). These results suggest that, apart from higher numbers of CD8^{+} T cells and NK cells in Ldha^{low} tumors, these immune cell populations exhibit higher functional activity in tumor microenvironments with lower lactate levels.

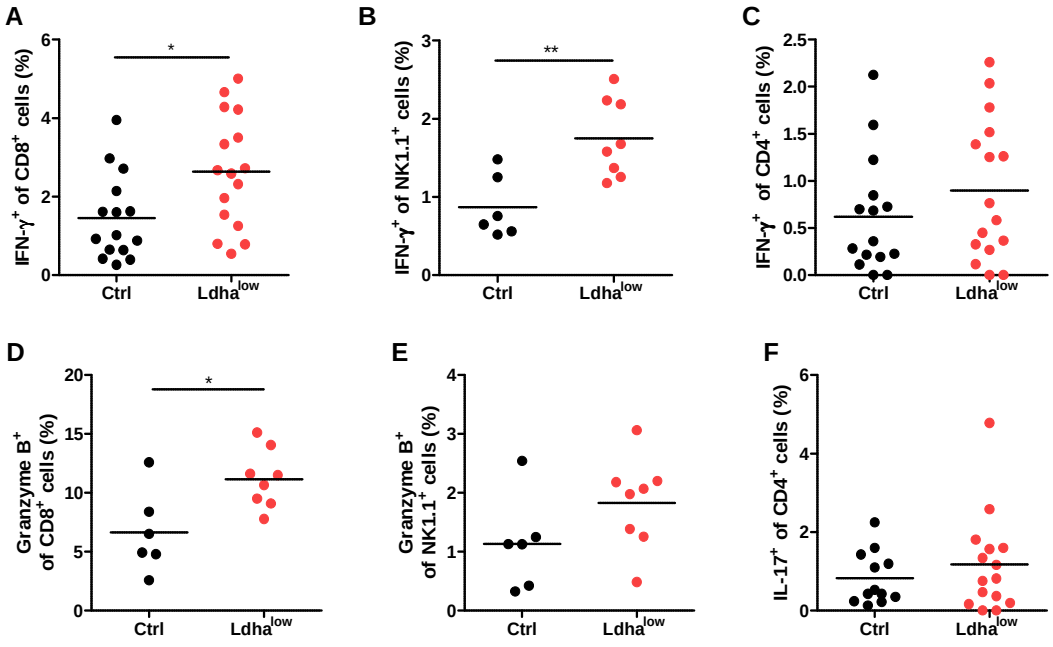

Figure 5-22. Ldha^{low} tumors contain higher numbers of activated CD8^{+} T cells and NK cells
(**A-C**) Numbers of IFN-γ^{+} cells among CD8^{+} T cells (**A**), NK1.1^{+} cells (**B**) and CD4^{+} T cells (**C**) in tumors grown from 1 x 10^{5} control (Ctrl) and Ldha^{low} cells in C57BL/6 mice, determined by flow cytometry. (**D-F**) Numbers of granzyme B^{+} cells among CD8^{+} T cells (**D**) and NK cells (**E**), and IL-17^{+} cells among CD4^{+} T cells (**F**) from tumors as described in **A-C**. Each symbol represents an individual mouse; small horizontal lines indicate the mean. * $P < 0.05$ and ** $P < 0.01$ (unpaired Student's *t*-test).

Analyses of the myeloid compartment in the tumor microenvironment demonstrated that Ldha^{low} tumors contained less IL-6^{+} cells than control tumors (Figure 5-23). This is consistent with the finding of lower numbers of CD11b^{+} cells (Figure 5-20 C) and reduced tumor growth of Ldha^{low} tumors (Figure 5-16 C), as IL-6 has been shown to be a tumor-promoting cytokine[159].

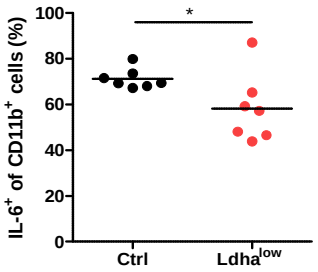

Figure 5-23. Ldha^{low} tumors contain less IL-6^{+} myeloid cells than control tumors
Numbers of IL-6^{+} cells among myeloid cells (CD11b^{+}) in tumors grown from 1 x 10^{5} control (Ctrl) and Ldha^{low} cells in C57BL/6 mice, determined by flow cytometry. Each symbol represents an individual mouse; small horizontal lines indicate the mean. * $P < 0.05$ (unpaired Student's *t*-test).

5.2.3 Analysis of Ldha^{low} tumors in CCR2-deficient mice

Results from flow cytometry analyses in immunocompetent C57BL/6 mice demonstrated a higher infiltration with myeloid cells, accompanied by an increased IL-6 production in control tumors compared to Ldha^{low} tumors (Figure 5-20 C and Figure 5-23). These tumors proliferated faster, which suggests a link between myeloid cells and tumor growth. To further examine the role of myeloid cells in tumor development, CCR2-depletion experiments were performed. CCR2 is a chemokine receptor which is mainly expressed on monocytic MDSCs (CD11b^{+}Gr-1^{+}). CD4^{+} and CD8^{+} T cells, B cells, NK cells and tumor cells, *in vitro* and *in vivo,* were CCR2 negative (data not shown). A monoclonal antibody against CCR2 and the corresponding isotype (kindly provided by Matthias Mack, Department of Internal Medicine II, University Hospital Regensburg, Germany) were administered intraperitoneally into C57BL/6 mice, starting on day 3 after injection of 1 x 10^{5} tumor cells. Antibodies were injected daily for 5 to 6 days. On days 0, 4, 7 and 10, retrobulbar blood from mice was analyzed by flow cytometry to confirm the depletion of monocytes. Therefore, blood was stained with α-CD11b and α-Gr-1, or α-Ly6C (expressed on monocytes) and α-Ly6G (expressed on granulocytes). After administration of the monoclonal antibodies, a severe decrease in the CD11b^{+}Gr-1^{+} and Ly6C^{+}Ly6G^{-} population was observed in the blood of the α-CCR2-treated group compared to the isotype control group on day 4 and day 7 (data not shown). These results proved the efficient depletion of monocytes by the α-CCR2 monoclonal antibody in the blood of the mice. To analyze the impact of CCR2^{+} monocyte depletion on tumor growth, tumor volume was measured. A slight reduction of tumor growth was observed in the α-CCR2-treated group compared to the control group without antibody injection (Figure 5-24). However, tumor growth was also slightly reduced in the mice injected with an isotype control antibody, suggesting a CCR2-independent effect of the antibody application on tumor growth and

immune cell activation. Therefore, no clear conclusions regarding the impact of monocytes on tumor growth can be drawn from these results.

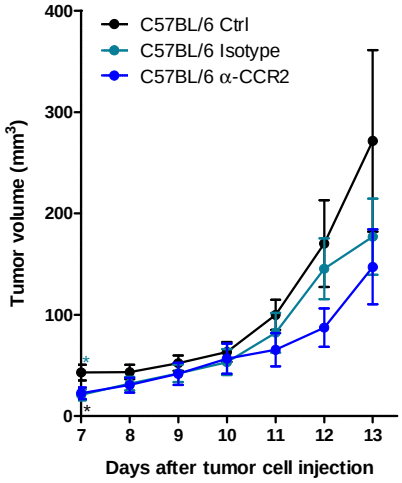

Figure 5-24. CCR2-independent effects of antibody application on tumor growth
Tumor growth after subcutaneous injection of 1 x 10^5 control cells into C57BL/6 mice and treatment with an α-CCR2 monoclonal antibody or the corresponding isotype compared to untreated tumors (Ctrl) (*n* = 10-15). Data are presented as mean tumor volume and s.e.m. In statistical analyses, growth of control tumors was compared to isotype-treated tumors (blue asterisk) and α-CCR2-treated tumors, respectively (black asterisk). * $P < 0.05$ (unpaired Student's *t*-test).

In order to circumvent effects of antibody application on tumor growth, *Ccr2*$^{-/-}$ mice, lacking CCR2$^+$ cells, were used to further analyze the role of monocytes in tumor development. Therefore, 1 x 10^5 control tumor cells were injected subcutaneously into the dorsal region of *Ccr2*$^{-/-}$ and C57BL/6 mice and tumor volumes were determined. Until day 14, tumor growth was similar between tumors in *Ccr2*$^{-/-}$ mice and C57BL/6 mice (Figure 5-25). Subsequently, tumors in C57BL/6 mice began to grow exponentially, resulting in tumors with an average size of 1,000 mm^3 on day 20. In contrast, tumors in *Ccr2*$^{-/-}$ mice only reached a mean tumor volume of less than 500 mm^3 on day 20. These findings indicate a tumor-promoting role of CCR2$^+$ monocytes and suggest that the balance between both growth-promoting and growth-inhibitory immune cells determines tumor growth.

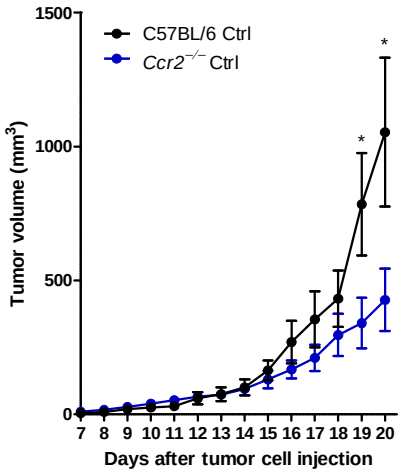

Figure 5-25. Tumor growth is impaired in the absence of CCR2$^+$ cells
Tumor growth after subcutaneous injection of 1 x 10^5 control cells (Ctrl) into C57BL/6 and *Ccr2*$^{-/-}$ mice (n = 9-10). Data are presented as mean tumor volume and s.e.m. * $P < 0.05$ (unpaired Student's t-test).

5.2.4 Analysis of Ldha^{low} tumors in immunodeficient *Rag2*$^{-/-}$ and *Rag2*$^{-/-}\gamma c^{-/-}$ mice

The experiments with *Ccr2*$^{-/-}$ mice demonstrated that a lack of pro-tumoral monocytes resulted in decreased tumor growth compared to that in C57BL/6 mice, but was not sufficient to abolish tumor growth. Other additional "players" of the immune system seem to be involved in tumor growth control, among which anti-tumor effector cells like T cells and NK cells are promising candidates.

To investigate the role of T cells, *Rag2*$^{-/-}$ mice, lacking B and T cells were used. *Rag2*$^{-/-}\gamma c^{-/-}$ mice, which additionally lack NK cells, were used to examine the role of NK cells. Therefore, 1 x 10^5 control cells or Ldha^{low} cells were injected subcutaneously in immunocompetent C57BL/6 mice, and immunodeficient *Rag2*$^{-/-}$ and *Rag2*$^{-/-}\gamma c^{-/-}$ mice. First, tumor growth was determined and second, tumors were excised, dissociated to single-cell suspensions, stained with fluorochrome-conjugated antibodies and measured by flow cytometry in order to investigate tumor-infiltrating immune cells.

5.2.4.1 Tumor growth

Results from measurements of the tumor volume demonstrated that control tumors grew similarly in C57BL/6, *Rag2*$^{-/-}$ and *Rag2*$^{-/-}\gamma c^{-/-}$ mice (Figure 5-26 A). In contrast, Ldha^{low} tumors showed a different growth in the three mouse strains (Figure 5-26 B). Ldha^{low} tumors in C57BL/6 exhibited the slowest proliferation with a mean tumor volume of 200 mm^3 on day 18, followed by tumors in *Rag2*$^{-/-}$ mice with a mean tumor volume of 400 mm^3 and tumors in *Rag2*$^{-/-}\gamma c^{-/-}$ mice, which reached a mean tumor volume of 700 mm^3. Thus, T cells alone and in combination with NK cells, can partially control tumor growth of Ldha^{low} tumors, whereas in their absence, Ldha^{low} tumors

grow similarly as control tumors. In contrast, the growth of control tumors was not influenced by the absence of T and/or NK cells.

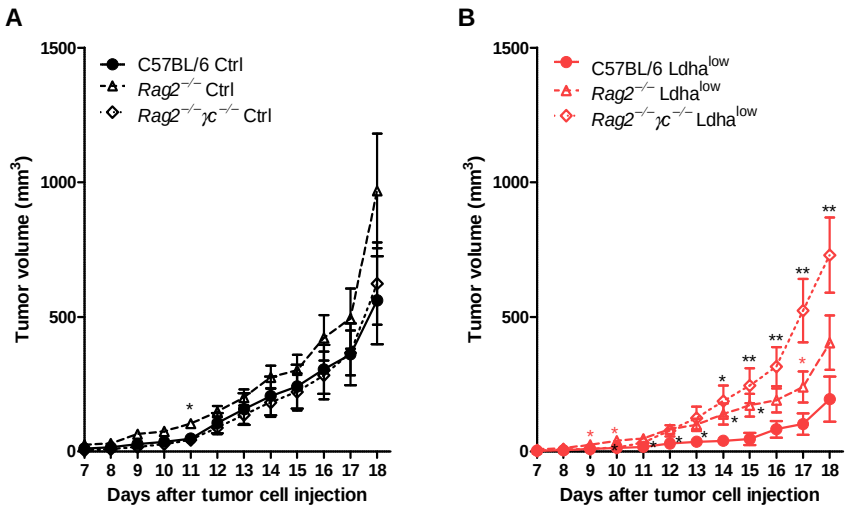

Figure 5-26. Growth control of Ldha^{low} tumors is lost in *Rag2*$^{-/-}$ and *Rag2*$^{-/-}\gamma c^{-/-}$ mice
(**A,B**) Tumor growth after subcutaneous injection of 1 x 10^5 control (Ctrl) cells (**A**) or Ldha^{low} cells (**B**) into C57BL/6 mice, and immunodeficient *Rag2*$^{-/-}$ and *Rag2*$^{-/-}\gamma c^{-/-}$ mice (n = 8-10). Data are presented as mean tumor volume and s.e.m. In statistical analyses, the growth of tumors in C57BL/6 mice was compared to *Rag2*$^{-/-}$ and *Rag2*$^{-/-}\gamma c^{-/-}$ mice, respectively (black asterisks), and the growth of Ldha^{low} tumors in *Rag2*$^{-/-}$ mice was compared to the growth of Ldha^{low} tumors in *Rag2*$^{-/-}\gamma c^{-/-}$ mice (red asterisks). * $P < 0.05$ and ** $P < 0.01$ (unpaired Student's t-test).

5.2.4.2 Immune cell infiltration

By means of flow cytometry, immune cell infiltration of tumors from C57BL/6 mice, *Rag2*$^{-/-}$ and *Rag2*$^{-/-}\gamma c^{-/-}$ mice was analyzed regarding the following surface molecules: CD45 as pan-leukocyte marker, CD11b for the detection of myeloid cells, PD-L1 as immune inhibitory protein, CD11c and I-Ab as marker for dendritic cells, and NK1.1 as a marker for NK cells. Importantly, as *Rag2*$^{-/-}$ and *Rag2*$^{-/-}\gamma c^{-/-}$ mice have a C57BL/6N background, the latter were used as control mice here, whereas all other experiments described were performed with C57BL/6J mice. Analyses demonstrated elevated numbers of infiltrating leukocytes in Ldha^{low} tumors compared to control tumors but this difference was only significant in C57BL/6 mice (Figure 5-27 A). As expected, the percentage of myeloid cells increased in *Rag2*$^{-/-}$ mice and in *Rag2*$^{-/-}\gamma c^{-/-}$ mice, due to the lack of T and NK cells. Myeloid CD11b$^+$ and CD11b$^+$PD-L1$^+$ cells were decreased in Ldha^{low} tumors of C57BL/6 mice but not in immunodeficient mice (Figure 5-27 B,C). Regarding dendritic cells, slightly increased numbers were found in Ldha^{low} tumors of C57BL/6 and *Rag2*$^{-/-}$ mice but not *Rag2*$^{-/-}\gamma c^{-/-}$ mice (Figure 5-27 D). In C57BL/6 mice, infiltration of NK cells was increased in Ldha^{low} tumors compared to control tumors, although not significantly, whereas the amount of NK cells did not differ between control and Ldha^{low} tumors in *Rag2*$^{-/-}$ mice (Figure 5-27 F). In *Rag2*$^{-/-}\gamma c^{-/-}$ mice, immune cell infiltrates were similar in control and Ldha^{low} tumors, in line with a similar tumor growth in these mice. In contrast, immune cell infiltration in C57BL/6 and *Rag2*$^{-/-}$ mice was different in Ldha^{low} and control tumors, accompanied by a different tumor growth.

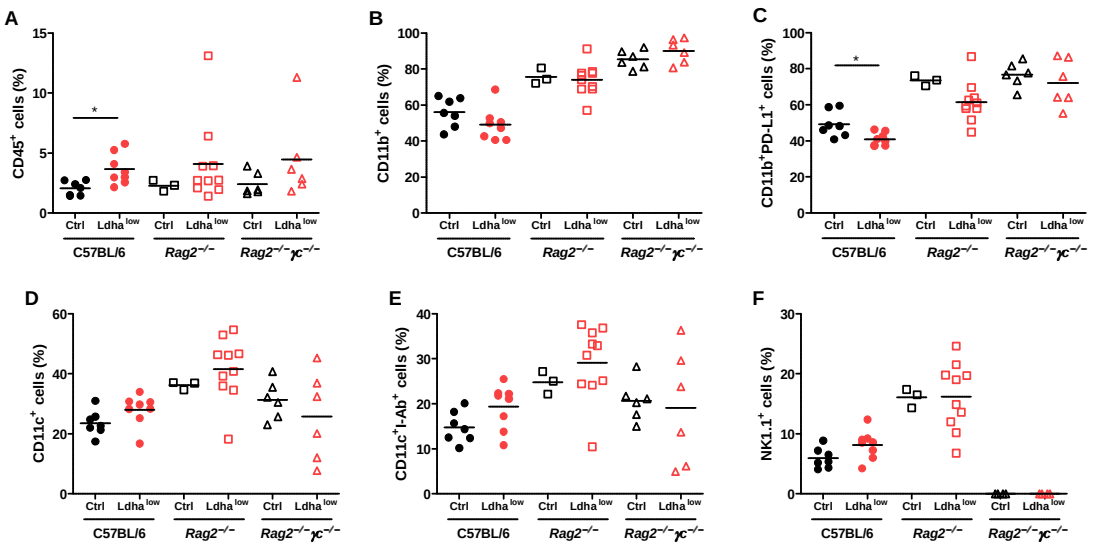

Figure 5-27. Differences in immune cell infiltration between control and Ldha^{low} tumors in immunodeficient and immunocompetent mice
(**A-F**) Percentage of CD45$^+$ leukocytes among all cells (**A**) derived from tumors grown after injection of 1 x 10^5 control (Ctrl) or Ldha^{low} cells in immunocompetent C57BL/6 mice and immunodeficient *Rag2*$^{-/-}$ and *Rag2*$^{-/-}$γc$^{-/-}$ mice, and percentage of immune cell populations among living CD45$^+$ leukocytes: myeloid cells (**B**), myeloid PD-L1$^+$ cells (**C**), CD11c$^+$ cells (**D**), MHC class II$^+$ CD11c$^+$ cells (**E**) and NK cells (**F**), determined by flow cytometry. Each symbol represents an individual mouse; small horizontal lines indicate the mean. * $P < 0.05$ (unpaired Student's *t*-test).

5.2.5 Analysis of Ldha^{low} tumors in immunodeficient *Pfp*$^{-/-}$ mice

Previous experiments indicated a link between the accumulation of cytotoxic T cells and NK cells in tumors with lower lactate levels and reduced tumor growth. To understand the underlying mechanism and to clarify whether T cells and NK cells control growth of Ldha^{low} tumors, 1 x 10^5 control and Ldha^{low} tumor cells were injected subcutaneously into perforin knockout mice (*Pfp*$^{-/-}$ mice). The pore-forming protein perforin is expressed by T cells and NK cells and essential to channel cytotoxic substances like granzymes into target cells. Surprisingly, in the absence of perforin, tumor growth control was still maintained in Ldha^{low} tumors (Figure 5-28) indicating that immunosurveillance is not linked to perforin.

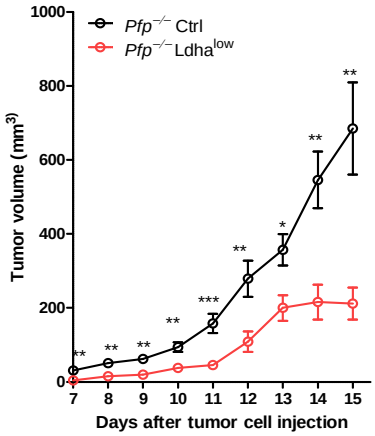

Figure 5-28. Perforin is irrelevant for tumor growth control in Ldha^{low} tumors
Tumor growth after subcutaneous injection of 1 x 10^5 control cells (Ctrl) and Ldha^{low} cells into *Pfp*$^{-/-}$ mice (n = 7-8). Data are presented as mean tumor volume and s.e.m. * $P < 0.05$, ** $P < 0.01$, and *** $P < 0.001$ (unpaired Student's t-test).

5.2.6 Analysis of Ldha^{low} tumors in mice lacking CD8$^+$ T cells

To clarify the impact of CD4$^+$ and CD8$^+$ T cells on tumor growth, α-CD4 and α-CD8 monoclonal antibodies were used to deplete CD4$^+$ and CD8$^+$ T cells in C57BL/6 mice, respectively. Therefore, 1 x 10^5 control and Ldha^{low} cells were injected subcutaneously into C57BL/6 mice after intraperitoneal injection of 250 µg of α-CD4, α-CD8 monoclonal antibodies and the respective isotypes as controls. In some experiments, treatment with the depleting antibodies was continued on day 3, 8, and 13 after tumor cell injection. Analyses of blood samples confirmed the successful depletion of CD4$^+$ and CD8$^+$ T cells, regardless of the treatment scheme (data not shown). However, similar to the results obtained during the depletion of CCR2$^+$ monocytes by an α-CCR2 monoclonal antibody (Figure 5-24), the isotype exerted inhibitory effects on tumor growth (data not shown).

As no reliable conclusions could be drawn from these experiments regarding the impact of CD4$^+$ and CD8$^+$ T cells on tumor growth, a different approach was undertaken to study the role of T cells. 1 x 10^5 control and Ldha^{low} cells were injected subcutaneously into immunocompetent C57BL/6 mice and immunodeficient *Cd8*$^{-/-}$ mice. Analyses revealed that tumor growth in *Cd8*$^{-/-}$ mice did not differ from tumor growth in C57BL/6 mice for both, control and Ldha^{low} tumors (Figure 5-29), suggesting that tumor growth control is not dependent on CD8$^+$ T cells.

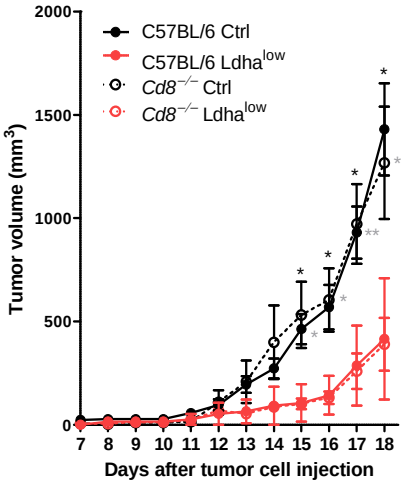

Figure 5-29. Tumor growth control of Ldha^{low} tumors is not impaired in *Cd8*$^{-/-}$ mice
Tumor growth after subcutaneous injection of 1 x 10^5 control cells (Ctrl) and Ldha^{low} cells into C57BL/6 and *Cd8*$^{-/-}$ mice (n = 5-6). In statistical analysis tumor growth of control and Ldha^{low} cells was compared in C57BL/6 mice (black asterisks) and in *Cd8*$^{-/-}$ mice (grey asterisks). Data are presented as mean tumor volume and s.e.m. * $P < 0.05$ and ** $P < 0.01$ (unpaired Student's t-test).

5.2.7 Analysis of Ldha^{low} tumors in immunodeficient *Ifng*$^{-/-}$ and *Ifngr1*$^{-/-}$ mice

Based on the results with immunocompetent C57BL/6 mice and immunodeficient *Rag2*$^{-/-}$ and *Rag2*$^{-/-}\gamma c^{-/-}$ mice, T cells and NK cells play an important role in the growth control of Ldha^{low} tumors (Figure 5-26 B), whereas results with *Pfp*$^{-/-}$ and *Cd8*$^{-/-}$ mice demonstrated that CD8$^+$ T cells and perforin, as effector molecule, seem to be negligible (Figure 5-28 and Figure 5-29). Therefore, the role of IFN-γ, which is a major cytokine in the regulation of innate and adaptive immunity, predominantly produced by T cells and NK cells and crucial for tumor control[192], was investigated.

5.2.7.1 Tumor growth

To elucidate the impact of IFN-γ on tumor growth, 1 x 10^5 control and Ldha^{low} cells were injected subcutaneously into the dorsal region of C57BL/6 mice and *Ifng*$^{-/-}$ mice. Measurements of tumor volumes confirmed that Ldha^{low} tumors showed a slower growth compared to control tumors in C57BL/6 mice (Figure 5-30 A). In contrast, Ldha^{low} tumors grown in *Ifng*$^{-/-}$ mice showed strikingly increased tumor volumes, comparable to those of control tumors. These results demonstrate a loss of tumor growth control in the absence of IFN-γ. To assess whether IFN-γ acts directly on tumor cells and thereby allows tumor immunosurveillance, subsequent experiments were performed in *Ifngr1*$^{-/-}$ mice, lacking IFN-γ receptors but with a normal IFN-γ production. After inoculation of 1 x 10^5 cells, control tumors showed similar tumor volumes in C57BL/6 mice and *Ifngr1*$^{-/-}$ mice at any time (Figure 5-30 B). Ldha^{low} tumors, though, grew slowly in C57BL/6 mice

but showed the same exponential growth in *Ifngr1*$^{-/-}$ mice as observed for control tumors. The pattern of tumor growth in *Ifngr1*$^{-/-}$ mice was identical to that of *Ifng*$^{-/-}$ mice (Figure 5-30 A,B), indicative of the importance of IFN-γ receptors on host immune cells for tumor growth control and concomitantly excluding a direct role of IFN-γ on tumor cells.

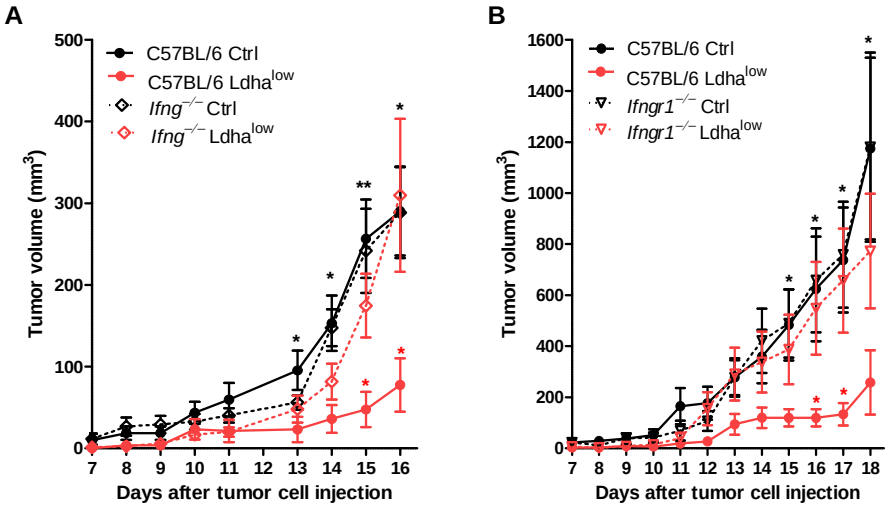

Figure 5-30. IFN-γ is responsible for tumor growth control of Ldha^{low} tumors
(**A**) Tumor growth after subcutaneous injection of 1 x 10^5 control cells (Ctrl) and Ldha^{low} cells into C57BL/6 mice and *Ifng*$^{-/-}$ mice (n = 5). In statistical analysis growth of control and Ldha^{low} tumors was compared in C57BL/6 mice (black asterisks) and growth of Ldha^{low} tumors in C57BL/6 mice was compared to growth of Ldha^{low} tumors in knockout mice (red asterisks). (**B**) Tumor growth in C57BL/6 mice and *Ifngr1*$^{-/-}$ mice as described in **A**. Data are presented as mean tumor volume and s.e.m. * P < 0.05 and ** P < 0.01 (unpaired Student's t-test).

5.2.7.2 Immune cell infiltration

As we observed that the lack of IFN-γ significantly increased growth in tumors with reduced lactate production, changes in the immune cell infiltration were investigated. To determine the immune cell infiltrate, tumors grown as described in Chapter 5.2.7.1 were dissected from the mice, single-cell suspensions were generated, antibody staining was performed and samples were subjected to flow cytometry. Regarding total immune cell numbers in the tumors, *Ifng*$^{-/-}$ and *Ifngr1*$^{-/-}$ mice exhibited a trend towards an increased infiltration of CD45$^+$ cells comparable to the effects in C57BL/6 mice (Figure 5-31 A). Myeloid cells, characterized by CD11b, were present in slightly reduced numbers in Ldha^{low} tumors compared to control tumors in all mice strains (Figure 5-31 B). The percentage of infiltrating B cells was significantly decreased in Ldha^{low} tumors compared to control tumors in C57BL/6 mice and a similar trend was observed in *Ifng*$^{-/-}$ and *Ifngr1*$^{-/-}$ mice (Figure 5-31 C). While in C57BL/6 mice the number of NK cells in Ldha^{low} tumors was significantly higher than in control tumors, this difference was completely lost in *Ifng*$^{-/-}$ and *Ifngr1*$^{-/-}$ mice (Figure 5-31 D). Surprisingly, the infiltration of cytotoxic T cells differed not only in C57BL/6 mice but by trend also in *Ifng*$^{-/-}$ and *Ifngr1*$^{-/-}$ mice (Figure 5-31 E). In addition, cytotoxic T cells were analyzed regarding their activity by means of CD25 staining. Results revealed that in C57BL/6 mice, cytotoxic T cells in Ldha^{low} tumors were more active than in control tumors, illustrated by an

increased number of CD25$^+$ cells in Ldha^{low} tumors (Figure 5-31 F). In contrast, this difference was abrogated in mice lacking IFN-γ or its receptor, where Ldha^{low} tumors contained the same low numbers of CD25$^+$ cytotoxic T cells as control tumors. These findings indicate that IFN-γ is not only responsible for the recruitment of NK cells into the tumor microenvironment but also for the activation of T cells, which in turn leads to tumor growth control.

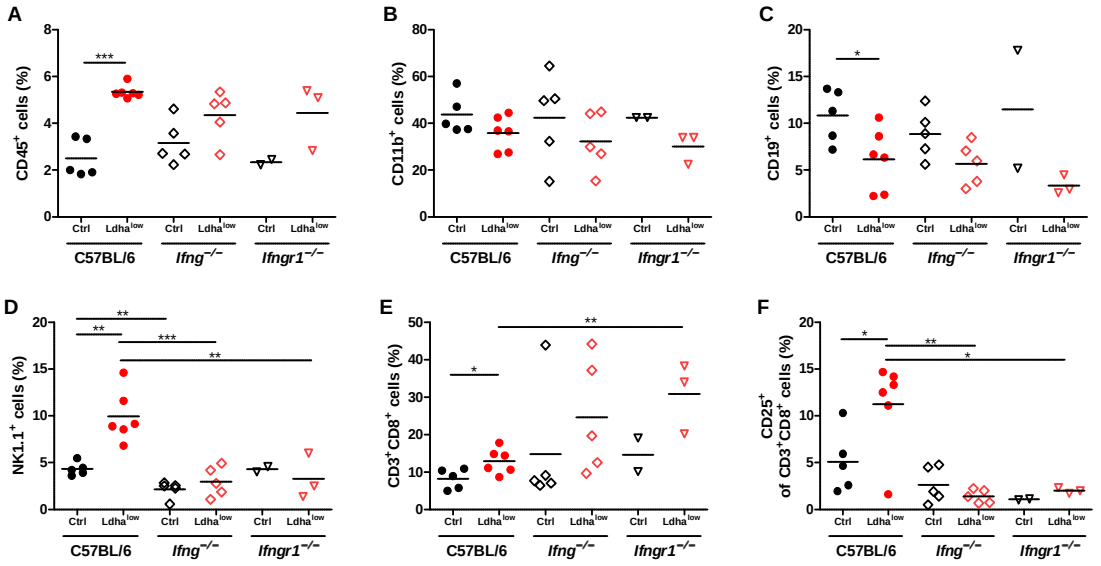

Figure 5-31. Ldha^{low} tumors in *Ifng*$^{-/-}$ mice lack NK cells and activated CD8$^+$ T cells
(**A-F**) Immune cell infiltration in tumors grown after injection of 1 x 10^5 control (Ctrl) or Ldha^{low} cells in immunocompetent C57BL/6 mice or immunodeficient *Ifng*$^{-/-}$ and *Ifngr1*$^{-/-}$ mice, determined by flow cytometry. Percentage of CD45$^+$ leukocytes among all cells of the tumor (**A**) and percentage of immune cell populations among living singular CD45$^+$ leukocytes: myeloid cells (**B**), B cells (**C**), NK cells (**D**) CD8$^+$ T cells (**E**) and percentage of CD25$^+$ cells among CD8$^+$ T cells (**F**). Each symbol represents an individual mouse; small horizontal lines indicate the mean. * $P < 0.05$, ** $P < 0.01$ and *** $P < 0.001$ (unpaired Student's *t*-test).

5.2.8 Molecular pathways involved in the immunomodulation by lactic acid

The above-mentioned results suggest that IFN-γ is a major immunologic player associated with the growth control of Ldha^{low} tumors *in vivo*. Furthermore, lactic acid suppressed the IFN-γ production of T cells and NK cells *in vitro* (Figure 5-1). Amongst others, the transcription factor NFAT is known to be involved in IFN-γ expression[193] and is upregulated on mRNA and protein levels during activation of T cells[194]. NFAT activation and translocation to the nucleus is calcineurin-dependent[193]. The activity of calcineurin, a Ca^{2+}-dependent phosphatase, was shown to be strongly associated with intracellular pH[195]. Hence, it was hypothesized that diminished amounts of IFN-γ in a high-lactate tumor microenvironment are due to intracellular acidification and subsequent downregulation of NFAT signaling. In order to test this hypothesis, the influence of lactic acid on intracellular pH and NFAT expression was determined.

5.2.8.1 Analysis of intracellular pH

Lactate is exported from the cell in co-transport with protons via MCTs[67], which leads to the subsequent acidification of the extracellular space[68]. To analyze the impact of extracellular acidification on the intracellular pH of T cells, the latter was quantified in $CD8^+$ T cells from spleens of *2C/Rag2*$^{-/-}$ mice after incubation with different concentrations of lactic acid (0, 10, 15 and 20 mM) for 30 minutes using a fluorescent pH-sensitive reagent. *In situ* calibration was performed with pH-controlled buffers. Flow cytometry measurements revealed that untreated cells exhibited an intracellular pH around pH 7.5, whereas T cells after treatment with lactic acid showed an intracellular acidification (Figure 5-32 A). Treatment with 15 mM lactic acid resulted in an intracellular pH shift to pH 5.5 and after incubation with 20 mM lactic acid the intracellular pH even dropped below pH 4.5. Comparative analyses of $CD8^+$ T cells incubated with 15 mM lactic acid or HCl corresponding to the pH of 15 mM lactic acid (~pH 6.4) for 7 hours showed that lactic acid leads to a stronger intracellular acidification (Figure 5-32 B).

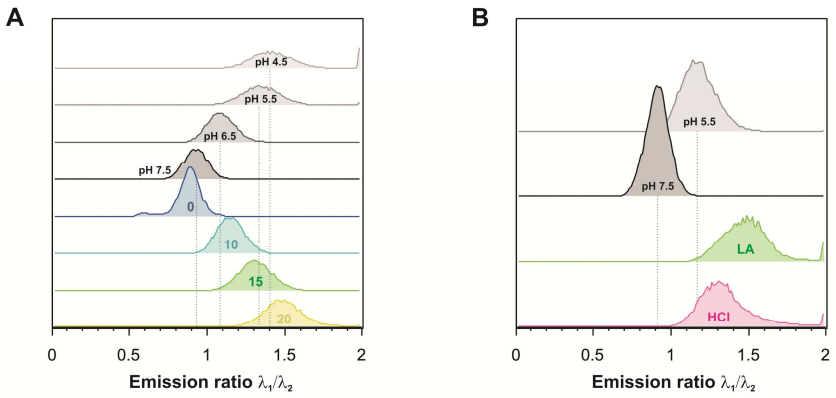

Figure 5-32. Lactic acid leads to intracellular acidification in $CD8^+$ T cells
(**A**,**B**) Quantification of the intracellular pH of activated $CD8^+$ T cells after incubation with different concentrations of lactic acid (0, 10, 15 and 20 mM) for 30 minutes (**A**) and after incubation with 15 mM lactic acid (LA) or HCl corresponding to the pH of 15 mM LA for 7 hours (**B**) by flow cytometry, using pH-controlled buffers for calibration (pH 4.5, pH 5.5, pH 6.5 and pH 7.5). One representative experiment out of three or two is shown.

5.2.8.2 Analysis of NFAT expression

The intracellular pH has been demonstrated to strongly regulate the activity of calcineurin[195], which in turn is responsible for nuclear translocation of NFAT[193]. As intracellular pH changes were observed upon incubation with lactic acid (Figure 5-32), NFAT expression was analyzed in the following. Therefore, $CD8^+$ T cells from spleens of *2C/Rag2*$^{-/-}$ mice and NK cells from spleens of C57BL/6 mice were cultured for 24 hours in the presence or absence of 15 mM lactic acid, HCl corresponding to the pH of 15 mM lactic acid (~pH 6.4) and 15 mM sodium lactate. 30 minutes before harvesting, cells were stimulated with PMA/ionomycin, subjected to intracellular staining and analyzed for NFAT expression using flow cytometry. NFAT expression was upregulated upon stimulation in $CD8^+$ T cells and NK cells but cultivation in the presence of lactic acid significantly decreased NFAT expression in both $CD8^+$ T cells and NK cells compared to untreated cells (Figure 5-33 A,B). Acidification corresponding to the pH of 15 mM lactic acid had the same strong

inhibitory effect, whereas the treatment with sodium lactate only caused a slight reduction in NFAT expression in $CD8^+$ T cells and NK cells. As total protein levels of NFAT were measured, these results indicate that lactic acid predominantly inhibits the activation-dependent upregulation of NFAT. Further experiments are necessary to clarify whether lactic acid also disturbs the translocation of NFAT to the nucleus.

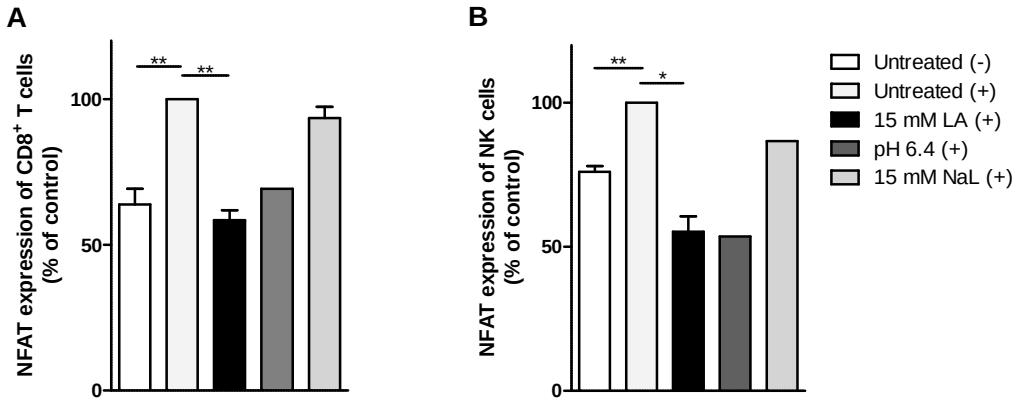

Figure 5-33. Lactic acid impairs NFAT expression in $CD8^+$ T cells and NK cells
(**A**,**B**) Quantification of NFAT expression in unstimulated (-) and stimulated (+) $CD8^+$ T cells (**A**) and NK cells (**B**) after incubation in the absence (untreated) or presence of 15 mM lactic acid (LA), HCl corresponding to the pH of 15 mM LA (~pH 6.4), and 15 mM sodium lactate (NaL) for 24 hours by flow cytometry (n = 2-4 per group, mean and s.e.m.). Data are shown as changes in % compared to control (untreated, +). * $P < 0.05$ and ** $P < 0.01$ (paired Student's t-test).

5.2.9 Characterization of *Ldha*$^{-/-}$clones generated with CRISPR/Cas9

To support the results obtained with the $Ldha^{low}$ clones, which were created using the shRNA technique to lower *Ldha* mRNA levels, additional B16 clones were generated by means of a CRISPR/Cas9 approach, which allowed gene editing. Cas9 was directed against two different loci in the *Ldha* gene of B16.SIY E12 cells (CRISPR1 and CRISPR2). These experiments were performed under the supervision of Jacques Pouysségur at the Institute of Research on Cancer and Ageing (IRCAN) of the University of Nice-Sophia Antipolis-CNRS-Inserm, Centre A. Lacassagne in Nice, France.

Western blot analyses of the clones revealed that the CRISPR/Cas9 approach was successful in several clones resulting from both the CRISPR1 and CRISPR2 approach. The absence of the LDHA protein was even confirmed under hypoxic conditions, where LDHA is upregulated, as seen in controls (Figure 5-34 A,B). Clones 7 and 9 of CRISPR1 and clone 10 of CRISPR2 were selected for further experiments.

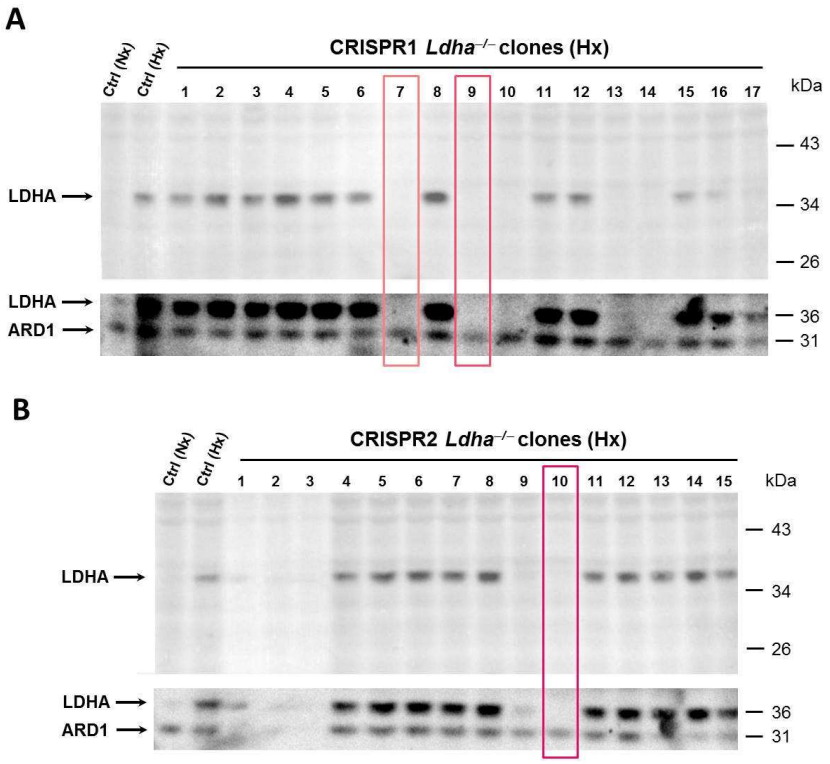

Figure 5-34. A CRISPR/Cas9 approach generates several *Ldha* knockout clones
(**A**,**B**) Western blot analysis of LDHA in whole-cell lysates of untreated B16.SIY E12 cells (Ctrl) cultured in normoxia (Nx) or 1% O_2 (hypoxia, Hx) and clones of B16.SIY E12 cells transfected with CRISPR/Cas9 plasmids against two different loci in the *Ldha* gene: CRISPR1 (**A**) and CRISPR2 (**B**), cultured in 1% O_2 (hypoxia, Hx). Arrest-defective-1 protein (ARD1) served as loading control. Clones in colored boxes were chosen for further analyses.

In order to examine the functionality of the *Ldha* knockout by CRISPR/Cas9, lactate levels were assessed in cell culture supernatants of 2.5 x 10^4 cells after 24 hours by an enzymatic assay. Experiments were carried out in cooperation with Lucia Wunderlich (Bachelor thesis). Analyses, performed by the Department of Clinical Chemistry (University Hospital Regensburg, Germany) revealed that despite the complete absence of the LDHA protein (Figure 5-34), lactate production in *Ldha*$^{-/-}$ cells was only reduced by ~30% compared to controls (Figure 5-35).

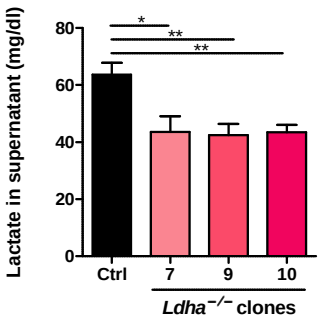

Figure 5-35. *Ldha*$^{-/-}$ clones produce lower amounts of lactate than controls
Lactate concentrations in the supernatant of 2.5 x 10^4 untransfected B16.SIY E12 cells (Ctrl) and B16.SIY E12 *Ldha* knockout cells, generated with CRISPR/Cas9 (*Ldha*$^{-/-}$ clones), cultured for 24 h (n = 4-8 per group, mean and s.e.m.). * $P < 0.05$, and ** $P < 0.01$ (unpaired Student's t-test).

To investigate the impact of the CRISPR/Cas9 approach on *Ldha* and *Ldhb* mRNA expression, qRT-PCR analyses of the *Ldha*$^{-/-}$ cells were performed. Experiments were carried out in cooperation with Lucia Wunderlich (Bachelor thesis). Results revealed that the mRNA expression of *Ldha* was about 100-fold reduced in *Ldha*$^{-/-}$ clones compared to control cells, with clone 7 showing the lowest amount of *Ldha* mRNA (Figure 5-36 A). However, levels of *Ldhb* mRNA remained unchanged in the in *Ldha*$^{-/-}$ clones compared to control cells (Figure 5-36 B). Thus, the abrogation of *Ldha* in *Ldha*$^{-/-}$ clones does not influence the expression of *Ldhb* mRNA.

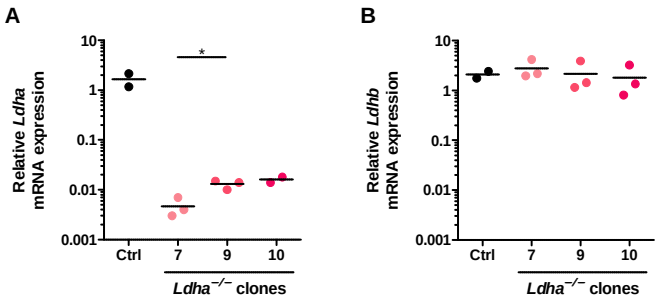

Figure 5-36. *Ldha* mRNA expression is drastically decreased in *Ldha*$^{-/-}$ cells but levels of *Ldhb* mRNA remain unchanged
(**A**,**B**) qRT-PCR analysis of *Ldha* (**A**) and *Ldhb* (**B**) in untransfected B16.SIY E12 cells (Ctrl) and B16.SIY E12 *Ldha* knockout cells, generated with CRISPR/Cas9 (*Ldha*$^{-/-}$ clones). The results are presented relative to the level of *18S* rRNA. Each dot represents an individual experiment and horizontal lines indicate the mean. * $P < 0.05$ (unpaired Student's *t*-test).

5.3 Immunomodulatory role of lactic acid in human melanoma?

In melanoma tumors of immunocompetent C57BL/6 mice, IFN-γ expression was impaired in the presence of high concentrations of tumor-derived lactate and this resulted in the loss of tumor growth control, which was maintained in the presence of lower lactate concentrations. For human melanoma, serum levels of LDH, the enzyme responsible for lactate generation, are used as a prognostic marker and elevated LDH serum levels indicate advanced disease and poor prognosis[196]. Results from immunohistochemical analyses demonstrated a low expression of LDH-5 in melanocytic nevi, whereas in melanoma and metastases, a higher expression of LDH-5 was observed. Consequently, high LDH-5 expression was related to a reduced disease-free and overall survival of melanoma patients[40]. Up to now, high LDH serum levels are often attributed to a high tumor load. However, in the light of our data, the link between high LDH-5 expression in tumor tissues and poor prognosis in human melanoma could also be attributed to an immunosuppression in the melanoma environment. Therefore, *LDHA* mRNA expression, lactate levels and the immune cell infiltrate were investigated in biopsies of melanoma in situ (the earliest stage of melanoma), primary melanoma, cutaneous metastases as well as healthy tissue of melanoma patients.

5.3.1 Analysis of *LDHA* expression and lactate levels

In order to assess *LDHA* expression, qRT-PCR analyses from total RNA of biopsies from melanoma in situ (Mis), melanoma lesions (M) and healthy tissue of melanoma patients (Ctrl M) were performed. Results revealed that melanoma lesions exhibited a wide distribution of *LDHA* expression but statistical analyses revealed a significantly elevated *LDHA* mRNA expression compared to melanoma in situ patients (Figure 5-37 A). As mere *LDHA* expression does not always correlate with the activity of the enzyme, lactate levels in tumor biopsies were determined. Therefore, biopsies of melanoma in situ, melanoma and healthy tissue of melanoma patients were snap-frozen after excision and intra-tissue lactate levels were analyzed using bioluminescence imaging by the group of Wolfgang Mueller-Klieser (Institute of Pathophysiology, University Medical Center of the Johannes Gutenberg University Mainz, Germany). These measurements revealed that lactate levels in lesions of melanoma in situ, melanoma and healthy tissue of melanoma patients were similar, with mean values of 6.5 µmol/g tissue (Figure 5-37 B). Hence, mRNA levels of *LDHA* and lactate levels were not corresponding. However, this may also be due to the fact that it was not possible to analyze the same biopsies in parallel for *LDHA* mRNA expression and lactate levels.

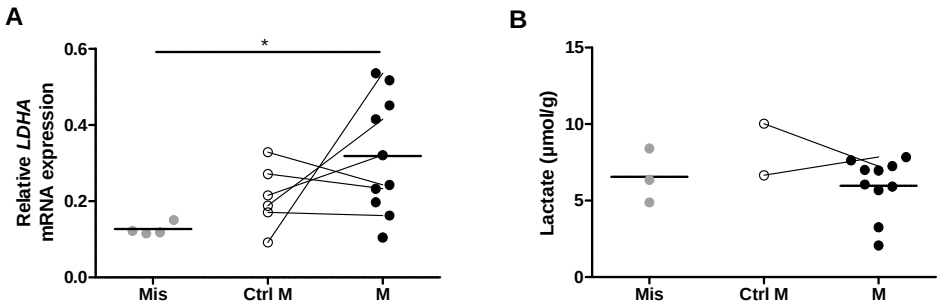

Figure 5-37. *LDHA* mRNA expression, but not lactate, is elevated in human melanoma biopsies compared to melanoma in situ
(**A**) qRT-PCR analysis of *LDHA* mRNA from human biopsies of melanoma in situ (Mis), melanoma lesions (M) and adjacent healthy tissue (Ctrl M). The results are presented relative to the level of *18S* rRNA. Each dot represents one individual patient and horizontal lines indicate the mean. Connections between dots link samples of the same donor. (**B**) Lactate levels from biopsies as described in **A** assessed by bioluminescence imaging. * $P < 0.05$ (unpaired Student's *t*-test).

In addition, lactate levels of cutaneous metastatic lesions of melanoma patients (M Met) and healthy skin of melanoma patients (Ctrl) with metastases were examined by bioluminescence imaging as described above. Strikingly, the results revealed that metastases exhibited mean lactate levels of 21 µmol/g (Figure 5-38), which represents a tremendous increase compared to melanoma lesions exhibiting 6.5 µmol/g (Figure 5-37 B).

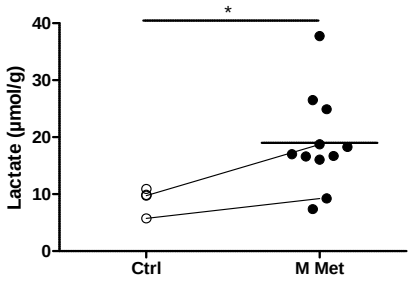

Figure 5-38. Cutaneous metastases of melanoma patients exhibit high lactate levels compared to healthy tissue
Lactate levels from cutaneous metastases (M Met) and healthy skin (Ctrl) of human melanoma patients, determined by bioluminescence imaging. Each dot represents one individual biopsy and horizontal lines indicate the mean (Ctrl: n = 4). Connections between dots link samples of the same donor. * $P < 0.05$ (unpaired Student's t-test).

5.3.2 Analysis of the immune cell infiltrate

Cutaneous melanoma metastases displayed significantly higher lactate levels than healthy tissue of the same donors. In order to analyze possible correlations between lactate levels and immune cell infiltration in metastases of melanoma patients, immune cells in biopsies were investigated by flow cytometry. Based on the results obtained in the mouse melanoma model, the activation status of cytotoxic T cells was investigated. Analyses revealed that higher numbers of infiltrating leukocytes were present in melanoma metastases than in adjacent tissue of the same donors (Figure 5-39 A). T cells represented the most abundant cell type among all leukocytes (65%), but levels of T cells did not differ in metastases and control tissue (Figure 5-39 B). $CD8^+$ T cells represented 35% of all T cells, in healthy tissue and a slightly increased amount of 45% was detected in metastatic lesions (Figure 5-39 C). Interestingly and in accordance with previous observations in the B16 mouse melanoma model, the numbers of $CD25^+$ cells among $CD8^+$ T cells were dramatically reduced in melanoma metastases compared to healthy control tissue of the same donor, ranging from 40% in healthy biopsies to values below 1% in metastatic lesions (Figure 5-39 D).

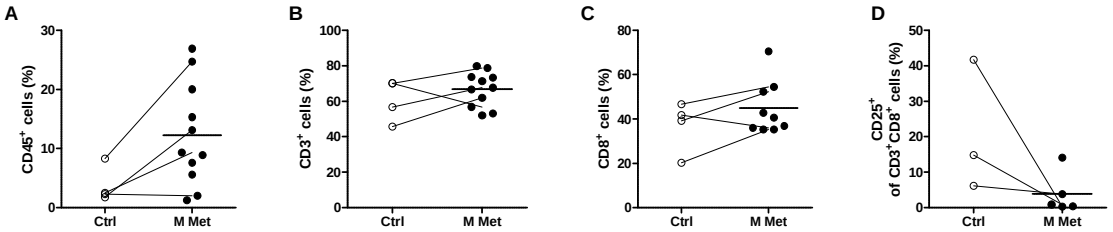

Figure 5-39. Cutaneous metastases of melanoma patients are highly infiltrated with inactive $CD8^+$ T cells
(**A-D**) Flow cytometry analyses of leukocytes among all cells of the tumor (**A**), T cells among all leukocytes (**B**), $CD8^+$ T cells among all T cells (**C**) and $CD25^+$ cells among $CD8^+$ T cells (**D**) in cutaneous metastases (M Met) and healthy skin (Ctrl) of human melanoma patients. Each dot represents one individual patient and horizontal lines indicate the mean. Connections between dots link samples of the same donor.

6 Discussion & Perspectives

6.1 Immunomodulatory role of lactic acid *in vitro*

Tumors are characterized by a rapid deregulated cell division and in order to maintain hyperproliferation, tumor cell metabolism is altered. The most prominent metabolic change is the switch from OXPHOS to aerobic glycolysis, termed Warburg effect. The Warburg phenotype exhibits excessive glycolysis and subsequent generation of high amounts of lactate. Lactate, which was previously regarded as a mere waste product of glycolysis, has recently emerged as a multifunctional player in tumorigenesis[197]. Its export from the cell in co-transport with protons via MCT1 and MCT4[67] leads to the extracellular accumulation of lactic acid and acidification of the tumor microenvironment. Tumor-derived lactic acid exerts direct tumor-promoting effects via the generation of tumor acidosis, which enhances the degradation of the ECM and thereby fosters tumor invasiveness[18]. Additionally, tumor-derived lactate functions as a promoter of angiogenesis[62,198,199].

Besides the direct effects of lactic acid on tumor progression, there is evidence that lactic acid modulates immune cell function. Only few papers investigated the effect of lactic acid on lymphoid cells *in vitro*. Fischer et al. revealed that lactic acid inhibited both the cytokine production and cytotoxic activity of human $CD8^+$ T cells[177]. The ablation of cytokine production was accompanied by an impaired lytic granule exocytosis of cytotoxic T cells upon lactic acid exposure[178]. Lactic acid production was further linked to a diminished ability of cytotoxic T cells to recognize tumor-associated antigens[188]. Besides lactic acid, lactate was shown to diminish the motility of T helper and cytotoxic T cells. Lactate polarized $CD4^+$ T cells into Th17 cells, producing IL-17, and lactic acid reduced the cytolytic capacity of $CD8^+$ T cells[189]. NK cells treated with lactic acid showed a diminished production of perforin and granzyme, and thereby blunted cytolytic activity[180].

The finding that lactic acid impaired the cytokine production in human T cells was confirmed for mouse T cells by the results obtained in this work. Starting from a concentration of 10 mM, which is in the lower range of pathophysiological concentrations measured in human tumor lesions[57], lactic acid provokes a striking decrease in IFN-γ production of $CD4^+$, $CD8^+$ T cells and NK cells. A similar effect was observed upon incubation in an acidic environment independent of lactate, whereas upon exposure of sodium lactate no impairment of IFN-γ production was observed. This dependence of lymphoid cells' cytokine production on the extracellular pH was also demonstrated by Mendler et al.[178]. On the other hand, granzyme B production by mouse $CD8^+$ T cells and NK cells was neither affected by lactic acid nor by acidosis or sodium lactate. As only intracellular granzyme B levels were assessed, it is conceivable that lactic acid interferes with the lytic granule exocytosis, as observed by Mendler et al.[178], and in this way impairs cytolytic functions of $CD8^+$ T cells[189]. Moreover, it is described that the production of IFN-γ facilitates the cytolytic function of NK cells via improving adhesion to target cells[200]. The impaired production of IFN-γ by lactic acid-

treated T or NK cells could, therefore, be another explanation for the compromised cytolytic activity observed by Haas et al.[189].

However, Fischer et al. and Husain et al. demonstrated the inhibition of perforin and granzyme production by lactic acid in human T cells[177,180]. The discrepancy between the observations regarding perforin and granzyme could be due to differences regarding the experimental settings. In this dissertation, mouse T cells were incubated with lactic acid only for a short time while in the cited publications long-time incubation was performed. To clarify the effects of lactic acid on cytolytic molecules, additional experiments will have to be performed.

The impact of lactic acid on myeloid cells has been investigated by several groups. Dietl et al. demonstrated an impeded production of both TNF and IL-6 in human monocytes upon lactic acid exposure[176]. Accordingly, DCs treated with lactic acid showed a tolerogenic phenotype, secreting diminished amounts of IL-12 and exhibiting an altered antigen expression profile[174]. Lactic acid also stimulated human monocytes to increase their production of IL-23[179], which is crucial for the generation of Th17 cells. A direct effect of lactate on Th17 generation was reported by Haas et al.[189]. Shime et al. reported an increase of the IL-6 production from human monocytes upon lactic acid exposure which contradicts the observations of Dietl et al.[176,179]. However, Shime et al. used a different experimental setting where monocytes were preincubated with lactic acid[179]. Yabu et al. demonstrated that lactic acid did not influence *Il6* mRNA expression in co-cultures of mouse $CD11b^+$ cells and $CD4^+$ T cells after incubation for 12 hours[201], which is consistent with the finding in this work that IL-6 production of myeloid cells was not affected by lactic acid or acidification. The discrepancy between the results could be due to a later onset of IL-6 regulation by lactic acid. Another plausible explanation would be differences in the immune regulation between mouse and human myeloid cells.

Furthermore, lactic acid was described to elevate ARG1 expression in mouse macrophages, which is known to impede T cell proliferation and activity. Interestingly, this feature was also attributed to the acidification caused by lactic acid[202].

Concluding, the impact of lactic acid on myeloid cells is not entirely clear. Controversial results could likely be related to the high plasticity of myeloid cells, depending on the cytokine profile in their environment and thereby on the stimulation and cultivation conditions during experiments.

Regarding lymphoid cells, increasing evidence suggests that lactic acid exerts immunoinhibitory effects on $CD4^+$ and $CD8^+$ T cells and NK cells.

6.2 Immunomodulatory role of lactic acid *in vivo*

In vitro analyses suggest an immunomodulatory role of lactic acid, yet, the investigation of single immune cell populations under cell culture conditions is not sufficient to mimic the complex situation in the tumor microenvironment. Tumors are composed of tumor cells themselves and stroma cells, including fibroblasts, endothelial cells, pericytes, mesenchymal cells and cells of the innate and adaptive immune system. The cross-talk between stroma cells and tumor cells

determines tumor growth. To elucidate the role of tumor-derived lactic acid in the tumor environment, its impact was studied in a mouse melanoma model.

6.2.1 Characterization of B16.SIY E12 Ldha^{low} cells for *in vivo* experiments

By means of shRNA technology, *Ldha*, coding for the lactate-producing enzyme LDH-5, was downregulated in B16.SIY E12 mouse melanoma cells in order to obtain tumor cells with a diminished lactate production (Ldha^{low} cells). *Ldha* expression as well as other (metabolic) properties of these model cell lines were examined. Results from qRT-PCR revealed a downregulation in *Ldha* mRNA expression of about 50% in Ldha^{low} clones accompanied by a decrease in LDHA protein expression compared to untransfected cells and control cells which were transfected with a scrambled shRNA sequence. Consequently, Ldha^{low} clones produced about 50% less lactate than untransfected cells and control cells. Thus, the *Ldha* shRNA approach created tumor cells with low lactate production. Additional analyses of the Ldha^{low} clones revealed that the decrease in *Ldha* mRNA expression was linked to increased mRNA levels of *Ldhb* which, though, did not result in a change of LDHB protein levels. We also investigated other marker genes of glycolysis. *Glut1* mRNA expression, coding for the main glucose transporter of tumor cells, was not impaired by the knockdown of *Ldha*. In contrast, *Hk1* mRNA expression was upregulated in Ldha^{low} clones compared to control cells, probably to compensate for the impaired lactic acid production. This hypothesis could be confirmed, as Ldha^{low} clones showed higher mitochondrial respiration due to increased mitochondrial content compared to control cells. Despite the metabolic differences in Ldha^{low} clones and control cells, proliferation and cell cycle properties were similar. The elevated mitochondrial respiration after *Ldha* attenuation was already observed in mouse mammary tumor cells by Fantin et al.[49], yet, associated with an impairment of proliferation under hypoxic conditions. In this work, for both Ldha^{low} and control cells, a similar proliferation even under hypoxic conditions was observed (data not shown). Consistent to the findings of Fantin et al.[49], an impaired proliferation even under normoxic conditions, decreased glycolysis along with increased OXPHOS and elevated levels of ROS were observed in mouse metastatic breast cancer *LDHA*-knockdown cells by Rizwan et al.[53], and Le et al. and Wang et al. who further observed increased apoptosis due to elevated ROS levels in *LDHA*-knockdown cells of human lymphoma and breast cancer[50,54]. A decreased proliferation and invasion, together with enhanced apoptosis after *LDHA* silencing, was additionally observed in prostate cancer cells and glioblastoma cells[203,204].

Thus, the metabolic switch towards OXPHOS seems to be a common feature of tumor cell lines with disrupted LDHA, while effects on proliferation and apoptosis are likely to be cell-type specific.

6.2.2 Analysis of Ldha^{low} tumors in immunocompetent C57BL/6 mice

In a next step, the Ldha^{low} clones were injected subcutaneously into immunocompetent C57BL/6 mice and tumors were analyzed regarding their metabolic profile and cytokine pattern. Most importantly, the *Ldha* mRNA expression was still downregulated in Ldha^{low} tumors, accompanied by an almost 50% diminished concentration of intratumoral lactate levels compared to control tumors. Moreover, after recultivation of cells from dissociated tumors, the difference in the lactate production between Ldha^{low} tumor cells and control tumor cells was still persistent. This clearly proved that the *Ldha* knockdown in the Ldha^{low} clones is not only stable *in vitro* but also *in vivo*. The expression of glycolysis-associated genes remained unchanged in Ldha^{low} tumors compared to the *in vitro* analyses, with the exception of *Ldhb* mRNA expression which was downregulated only in one Ldha^{low} clone *in vivo*. Besides LDHA, several other enzymes play roles in immunomodulation, among them IDO1 and IDO2, ARG1 and ARG2, COX1 and COX2 as well as iNOS. Their mRNA expression was assessed in Ldha^{low} tumors and no differences were found compared to control tumors, ensuring that the observed immunoregulatory effects were caused by lactate.

Since tumors are known to create an immunosuppressive microenvironment, not only by changes in their metabolism, but also by the production of pro- and anti-inflammatory cytokines, gene expression of crucial tumor-promoting factors was analyzed by qRT-PCR. Analyses of Ldha^{low} tumors in comparison with control tumors did not show alterations in mRNA levels of pro-tumoral *Vegfa*, *Csf2*, *Il6*, *Il10*, *Tnf* and *Il17a*. Therefore, the described lactic acid-induced production of VEGF by endothelial cells[62] seems to play no role in the analyzed *Ldha* shRNA tumor model. *Csf2* mRNA expression, which is linked to MDSC function and expansion of the highly immunosuppressive monocytic MDSC subset[127,128] was also not affected by lactic acid. The induction of IL-17 by lactic acid, which was described by Shime et al.[179], was not observed on mRNA levels in B16.SIY E12 control tumors, most likely due to the limited number of Th17 cells in tumors. As the main fraction of cells within tumor samples are tumor cells, and stroma cells represent only a minor fraction, it is conceivable that possible differences in the expression of cytokines, which are produced by immune cells, are concealed and not detected by qRT-PCR. However, the results revealed significant differences in *Tgfb1* and *Ifng* mRNA expression, the former being significantly downregulated in Ldha^{low} tumors, while the latter was found to be increased. Lactic acid was shown to increase *TGFB1* mRNA and protein levels in co-cultures of fibroblasts and endothelial cells in a pH-dependent manner[205]. Knockdown of *LDHA* by means of siRNA was shown to decrease *TGFB2* mRNA and protein levels in glioma cells[206]. In the light of these findings and the results obtained in this work, it is likely that both *TGFB1* and *TGFB2* expression are induced by lactic acid. However, only little amounts of TGF-β protein were detectable in supernatants of control and Ldha^{low} tumors, with no significant differences between the two groups.

The heightened *Ifng* mRNA expression observed in Ldha^{low} tumors is a hint for a less immunosuppressive tumor microenvironment in the absence of high lactate levels. Analysis of

T cell markers by means of qRT-PCR measurements did not show differences regarding *Cd4*, *Foxp3* and *Cd8a* mRNA expression in Ldha^{low} tumors compared to controls, which is in contrast to the actual protein levels analyzed by flow cytometry, as discussed below.

To get an impression of the actual immune cell infiltration in tumors derived from Ldha^{low} cells and control cells, intratumoral immune cells were stained with antibodies against surface and cytokine markers. To exclude effects linked to tumor size, only tumors with a maximum volume of 1,000 mm^3 were included in the analyses. The size distribution of tumors derived from Ldha^{low} and control cells was similar. Analyses revealed that tumors contained about 5% of immune cells. Ldha^{low} tumors were infiltrated with increased numbers of leukocytes compared to control tumors. Among the infiltrating leukocytes, myeloid cells were the most abundant cells in both Ldha^{low} tumors and control tumors. The majority of myeloid cells represented MDSCs, which were present in similar amounts in Ldha^{low} tumors and control tumors. MDSCs share many characteristics with M2 macrophages, whose development can be promoted by lactic acid[181]. As MDSC numbers did not differ between Ldha^{low} and control tumors in C57BL/6 mice and the expression of the M2 marker gene *Arg1* was similar, there is no hint that lactic acid promotes M2 or MDSC development in this model. Further analyses of the immune cell infiltration demonstrated that about 10% of all leukocytes in control tumors were B cells, whereas their infiltration in Ldha^{low} tumors was significantly reduced. In contrast, the number of T cells among all immune cells was increased in Ldha^{low} tumors compared to control tumors. T helper cell numbers were not altered significantly in Ldha^{low} tumors compared to controls whereas significantly more cytotoxic T cells were found in Ldha^{low} tumors compared to control tumors. The most striking difference between Ldha^{low} tumors and control tumors was the amount of infiltrating NK cells. Ldha^{low} tumors contained about twofold more NK cells among all leukocytes. Thus, local immunomodulation by tumor-derived lactic acid could be confirmed.

To gain inside into possible systemic effects of tumor-derived lactic acid, blood and spleens of tumor-bearing mice were analyzed. The results revealed that tumor burden in mice increased the levels of circulating myeloid cells, MDSCs and NK cells accompanied by decreased levels of T cells in comparison to healthy mice. In spleens, the increase of NK cells and the decrease of T cells were observed. However, no differences of immune cell numbers between mice bearing Ldha^{low} tumors and control tumors were detectable in the blood or the spleens, suggestive of a locally restricted immunomodulation by tumor-derived lactic acid. In contradiction with this hypothesis is the finding of Husain and colleagues that MDSCs occurred less frequently in spleens of mice bearing *LDHA*-silenced tumors[180]. As T cells and NK cells play major roles in tumor suppression, their effector functions were assessed by means of cytokine analyses. The activity of T helper cells remained unaffected by lactic acid, as IFN-γ and IL-17 production of CD4$^+$ T cells from Ldha^{low} tumors and control tumors did not differ. In contrast, IFN-γ production of cytotoxic T cells and NK cells from Ldha^{low} tumors was significantly increased, along with elevated granzyme B production. Decreased expression of perforin, granzyme B and IFN-γ by T cells and NK cells was observed in malignant tissue of lung cancer patients compared to non-cancer tissue and could partially be attributed to alterations in the COX2 pathway[207]. Recent observations from Zelenay et al. unfold that COX2 seems to be responsible for tumor-promoting inflammation and

immunosuppression in mouse melanoma tumors, and that its ablation leads to a decreased expression of IL-6, along with an increased expression of IFN-γ and immune-dependent tumor eradication[208]. In contrast, the results obtained in this dissertation attribute the impaired release of IFN-γ and granzyme B from tumor-infiltrating T and NK cells to tumor-derived lactic acid, while no differences in *Cox* mRNA expression between control and Ldha^{low} tumors were observed. The negative impact of lactic acid on IFN-γ production in CD8$^+$ T cells and NK cells was further supported by *in vitro* experiments. Moreover, enhanced cytolytic properties of NK cells in *LDHA*-silenced tumors were confirmed by Husain et al.[180]. In line with this finding is the observation that soluble LDH-5 impairs NK cell activity via induction of ligands for the activating receptor NKG2D on myeloid cells, and thereby subsequent downregulation of NKG2D on NK cells[209].

Conflicting results between *in vitro* and *in vivo* experiments were obtained regarding IFN-γ, IL-6 and granzyme B production. Lactic acid exposure suppressed IFN-γ in CD4$^+$ T cells *in vitro*, but not *in vivo*, indicating a decreased sensitivity of CD4$^+$ T cells towards lactic acid *in vivo*, compared to CD8$^+$ T cells. The opposite holds true for granzyme B production, which was impaired in tumors with higher lactate levels, but lactic acid did not inhibit granzyme B expression under cell culture conditions, suggesting that other factors besides lactic acid are involved in granzyme B downregulation *in vivo*. Furthermore, IL-6 production by myeloid cells was diminished in Ldha^{low} tumors but lactic acid did not promote IL-6 secretion by myeloid cells *in vitro*, indicating that other factors besides lactic acid are necessary to upregulate IL-6 expression *in vivo*. These results highlight that *in vitro* experiments, especially in the field of tumor immunology, where a multitude of different cell types interact with one another, often do not portray the actual (patho-) physiological situation.

Here, it could be shown that tumor-derived lactate impedes infiltration of CD8$^+$ T cells and NK cells into tumor sites, along with an inhibition of effector functions by circumventing the production of cytokines and other effector molecules. Cytotoxic lymphocytes are major players involved in tumor suppression. Besides their direct cytolytic effects on tumor cells via secretion of perforin and granzyme[135,148], their release of IFN-γ leads to the activation of Th1 cells and macrophages[134]. IFN-γ further inhibits the production of TGF-β[164], which could be observed in Ldha^{low} tumors on mRNA level, displaying elevated *Ifng* and decreased *Tgfb1* expression.

IL-6 has been shown to exert a dual role in tumorigenesis, counteracting tumor growth in early stages of melanoma, while possessing stimulatory capacities in later stages of melanoma[210-212]. Yet, in a model of spontaneous melanoma, IL-6 deficient mice formed less and smaller tumors compared to immunocompetent mice, indicative of IL-6 being implicated in both the development of precursor lesions and subsequent growth of melanomas[213]. Accordingly, Ldha^{low} tumors containing diminished amounts of IL-6 showed a restricted tumor growth compared to faster proliferating control tumors in which higher amounts of IL-6 were present.

The increased abundance and higher activity of cytotoxic lymphocytes should limit tumor growth in a low-lactate tumor microenvironment. And in fact, Ldha^{low} cells, which proliferate similarly as control cells *in vitro*, showed a significantly decreased tumor growth compared to control tumors after injection into immunocompetent C57BL/6 mice. However, this result was dependent on the

number of injected tumor cells. When 1 x 10^4 cells were injected, tumor formation from Ldha^{low} cells was completely prevented until day 17. Injection of 1 x 10^5 tumor cells still allowed tumor growth control in Ldha^{low} tumors. In contrast, upon injection of 1 x 10^6 tumor cells, the growth difference between Ldha^{low} tumors and control tumors was lost. The unphysiologically high tumor load seems to have overcome any possible anti-tumor immunity. Flow cytometry analyses of the immune cell infiltrate in those tumors revealed that differences between Ldha^{low} tumors and control tumors regarding myeloid cells, B cells and T cells were lost.

B cells have been shown to contribute to tumor growth[110,214,215], which is in accord with the finding of elevated levels of B cells in rapidly proliferating control tumors after injection of 1 x 10^5 cells. The observed increase in the number of infiltrating B cells in control tumors suggests an insensitivity of B cells towards lactic acid, but further experiments have to be performed to confirm this hypothesis.

Numbers of infiltrating cytotoxic T cells and NK cells were increased in Ldha^{low} tumors, which was associated with a decreased tumor growth after injection of low numbers of tumor cells. Surprisingly, after injection of high numbers of tumor cells, the majority of infiltrating immune cells represented T cells. These findings seem to be contradictory to the observations that infiltration with cytotoxic T cells is associated with favorable prognosis in several kinds of cancer, including colon carcinoma[216] and melanoma[217]. Regarding NK cells, despite high infiltration, a similar proliferation was found in Ldha^{low} tumors compared to control tumors after the injection of high numbers of tumor cells. NK cell infiltration, besides T cell infiltration, is also associated with improved outcome in various human tumors[138,139]. However, tumor-promoting NK cell phenotypes with compromised cytolytic functions and pro-angiogenic properties were observed in a range of tumors[135]. Therefore, not the abundance but the activity of immune cells in the tumor microenvironment is decisive.

6.2.3 Analysis of Ldha^{low} tumors in CCR2-deficient mice

Monocytic, as well as granulocytic MDSCs have been described as potent inhibitors of T cells, and their amount correlates to a poor outcome in various types of cancer[127]. Furthermore, myeloid cells can be influenced by lactic acid[174-176,179,181] and thereby could contribute to tumor immune escape. Lesokhin et al. demonstrated that the monocytic subset of MDSCs, expressing CCR2, regulates the infiltration of CD8$^+$ T cells into the tumor microenvironment[128]. Therefore, we tried to elucidate a possible link between monocytic MDSCs, regulation by lactic acid and tumor growth. For this purpose, we used an α-CCR2 antibody and the respective isotype control. However, the administration of the isotype antibody already resulted in a reduction of tumor growth compared to control tumors. Powerful anti-tumor effects of IgG administration have been described in cancer[218] and high-dose infusion of IgG serves as an anti-inflammatory therapeutic agent in several autoimmune and inflammatory diseases[219].

To circumvent any unspecific effects of immunoglobulins, further experiments were conducted using CCR2-deficient mice in order to examine the role of monocytic MDSCs in tumor growth.

Results showed that the absence of monocytes led to diminished tumor growth compared to that of wild type mice. These findings suggest that monocytes play a role in tumor-promotion in the B16 mouse melanoma model, which needs to be further investigated.

6.2.4 Analysis of Ldha^{low} tumors in immunodeficient *Rag2*$^{-/-}$ and *Rag2*$^{-/-}\gamma c^{-/-}$ mice

The presence of monocytic MDSCs seems to promote tumor growth, indicating that tumor immunosurveillance is based on the balance between pro-tumor and anti-tumor effector cells. To further prove the (lactate-dependent) role of T and NK cells in tumor immunosurveillance, Ldha^{low} and control tumor cells were injected in T and B cell-deficient *Rag2*$^{-/-}$ mice, and lymphocyte-deficient *Rag2*$^{-/-}\gamma c^{-/-}$ mice. As previously observed, tumor growth of Ldha^{low} tumors in immunocompetent C57BL/6 mice was slow. In *Rag2*$^{-/-}$ mice, the lack of T and B lymphocytes led to accelerated growth of Ldha^{low} tumors. Tumor growth in *Rag2*$^{-/-}\gamma c^{-/-}$ mice, in the absence of both T, B and NK cells, outpaced growth of Ldha^{low} tumors in C57BL/6 and *Rag2*$^{-/-}$ mice. In contrast, similar growth was observed for control tumors, irrespective of the presence or absence of lymphocytes in C57BL/6 mice, *Rag2*$^{-/-}$ mice and *Rag2*$^{-/-}\gamma c^{-/-}$ mice. These findings confirm that tumor immunosurveillance in our model is dependent on tumor-derived lactate and that it involves both T and NK cells. In a tumor environment containing low amounts of lactate, T and NK cells together are able to attenuate tumor growth. This is impossible in a tumor environment containing high amounts of lactate. Likewise, the absence of T and NK cells obviates tumor growth control, even in a low-lactate environment.

Analyses of immune cell infiltrates in the tumor specimen revealed that in *Rag2*$^{-/-}$ mice, the difference of NK cell numbers between Ldha^{low} tumors and control tumors, which was observed in C57BL/6 mice, was lost. In addition, higher levels of myeloid cells were detected in *Rag2*$^{-/-}$ mice and *Rag2*$^{-/-}\gamma c^{-/-}$ mice, as the fraction of lymphoid cells is missing. Immune cell infiltration was representative for tumor growth, as in *Rag2*$^{-/-}\gamma c^{-/-}$ mice, in the absence of lymphocytes, Ldha^{low} and control tumors grew similarly, along with no observed differences regarding infiltrating immune cells. In *Rag2*$^{-/-}$ mice, pro-tumoral expression of PD-L1 on myeloid cells was decreased in Ldha^{low} tumors, a higher abundance of DCs was found, and growth of Ldha^{low} tumors was diminished in comparison to controls. This suggests that PD-L1 expression on myeloid cells may be regulated by NK cell activity. NK cells might additionally be responsible for elevated levels of DCs in Ldha^{low} tumors in *Rag2*$^{-/-}$ mice. In fact, there is evidence that NK cells are able to induce and enhance DC maturation[220,221]. As previous observations demonstrated higher IFN-γ production of NK cells in tumors with impaired lactate production, it is conceivable that this leads to the increased infiltration of DCs in Ldha^{low} tumors of *Rag2*$^{-/-}$ mice and C57BL/6 mice, and likely contributes to dampened tumor growth. Activated DCs, in turn possess the capability to activate NK cells or exert direct cytotoxic effects against tumor cells and in this way can contribute to tumor immunosurveillance[133].

6.2.5 Analysis of Ldha^{low} tumors in immunodeficient *Pfp*$^{-/-}$ mice

Previous experiments proved that activated cytotoxic T cells and NK cells together are capable to control tumor growth in a low-lactate tumor microenvironment. To understand the mechanism of tumor growth control by T and NK cells, one major effector molecule, the pore-forming protein perforin, which is necessary to channel cytotoxic substances like granzymes into target cells, was further investigated. Results from tumor cell inoculation experiments into perforin knockout mice (*Pfp*$^{-/-}$ mice) revealed that despite the ablation of perforin production, tumor growth in Ldha^{low} tumors was significantly compromised compared to controls. This shows that in our model, perforin is not implicated in tumor suppression, even though perforin-dependent tumor control was described for several tumors and metastases[222-225]. However, there is evidence that tumor regression by cytotoxic T cells can occur also independently of perforin[226].

6.2.6 Analysis of Ldha^{low} tumors in mice lacking CD8$^+$ T cells

As the cytotoxic effector molecule perforin secreted from both cytotoxic T cells and NK cells was not involved in tumor inhibition, the question arose whether another T cell-derived factor leads to the suppression of tumor growth. Therefore, an attempt was made to deplete CD4$^+$ or CD8$^+$ T cells by administering monoclonal antibodies prior to injection of tumor cells into C57BL/6 mice. Blood analyses proved that the depletion of T cells was successful. However, similar to the results obtained during the depletion of CCR2$^+$ monocytic myeloid cells with an α-CCR2 monoclonal antibody, the control antibody itself exerted suppressive effects on tumor cell proliferation and excluded interpretations regarding the role of CD4$^+$ or CD8$^+$ T cells in tumor growth. In further experiments, tumor growth was analyzed in *Cd8*$^{-/-}$ mice lacking CD8$^+$ effector T cells, but surprisingly, the difference in tumor growth between Ldha^{low} and control tumors was comparable to that in immunocompetent C57BL/6 mice. Thus, tumor growth control of Ldha^{low} tumors was still possible in the absence of cytotoxic T cells. These data are concordant with a study which describes that NK cells and CD4$^+$ Th1 cells together with IFN-γ are essential for tumor rejection in mice lacking CD8$^+$ T cells[227]. CD4$^+$ T cell numbers and activity were similar in Ldha^{low} tumors and control tumors from C57BL/6 mice, which suggests that lactate-dependent tumor growth control is independent of CD4$^+$ T cells. Yet, in the absence of CD8$^+$ T cells, CD4$^+$ T cells seem to take over CD8$^+$ T cell effector functions and contribute to tumor growth suppression in a low-lactate tumor microenvironment, alongside with cytotoxic NK cells.

6.2.7 Analysis of Ldha^{low} tumors in immunodeficient *Ifng*$^{-/-}$ and *Ifngr1*$^{-/-}$ mice

Since both the results obtained in this dissertation and data from the literature suggest that IFN-γ plays a crucial role in tumor immunosurveillance, its role was investigated by using mice that lack IFN-γ. As expected, control tumors showed similar growth in C57BL/6 and *Ifng*$^{-/-}$ mice, indicating that in a high-lactate tumor microenvironment IFN-γ is dispensable, as tumor-promoting factors seem to overrule anti-tumor effector mechanisms. Strikingly, tumor control in a low-lactate tumor microenvironment, i.e. reduced proliferation of Ldha^{low} tumors, was completely abolished in the absence of IFN-γ. Ldha^{low} tumors in *Ifng*$^{-/-}$ mice showed similar growth as control tumors in C57BL/6 and *Ifng*$^{-/-}$ mice. Hence, IFN-γ is a crucial mediator of tumor control by immune cells and modulated by tumor-derived lactate. The contribution of IFN-γ to tumor immunosurveillance is well described[228] and impaired IFN-γ signaling caused by the loss of function of the tumor suppressor interferon regulatory factor 1 (IRF-1) is linked to human leukemia and gastric cancer[229,230]. IFN-γ has also been shown to limit tumor growth by inhibiting tumor-induced angiogenesis[231], by promoting anti-tumor host responses or by directly impeding tumor cell proliferation[232,233]. The question whether tumor immunosurveillance of Ldha^{low} tumors in C57BL/6 mice is due to direct effects of IFN-γ on tumor proliferation was clarified using *Ifngr1*$^{-/-}$ mice. In these mice, IFN-γ receptors are absent on host cells, but injected tumor cells still express IFN-γ receptors. Analyses of these experiments demonstrated a similar growth pattern as observed in *Ifng*$^{-/-}$ mice, with Ldha^{low} tumor proliferation being accelerated in the absence of host IFN-γ receptors. This result excludes the possibility that IFN-γ controls tumor growth via direct effects on tumor cells, as the presence of IFN-γ receptors on tumor cells would allow tumor suppression in Ldha^{low} tumors. IFN-γ dependent tumor growth inhibition, therefore, rather seems to be related to the activation of anti-tumor responses by immune effector cells. In order to confirm this hypothesis, the immune cell infiltrate in C57BL/6 mice, *Ifng*$^{-/-}$ and *Ifngr1*$^{-/-}$ mice was investigated. Total leukocyte numbers were consistently higher in Ldha^{low} tumors compared to controls, irrespective of the mouse strain, but a statistically significant difference was only detected in C57BL/6 mice. Among infiltrating leukocytes, myeloid cells showed slightly decreased numbers in Ldha^{low} tumors of all mouse strains in comparison to control tumors. B cells were also slightly diminished in Ldha^{low} tumors in *Ifng*$^{-/-}$ and *Ifngr1*$^{-/-}$ mice, whereas a significant reduction was observed in C57BL/6 mice. As this immune cell pattern of diminished amounts of infiltrating myeloid cells and B cells in Ldha^{low} tumors compared to controls was present in all mice strains but tumor growth was only delayed in Ldha^{low} tumors in C57BL/6 mice, these immune cell populations seem to play no role in tumor suppression. Interestingly, exponential tumor growth in control tumors and Ldha^{low} tumors of both *Ifng*$^{-/-}$ and *Ifngr1*$^{-/-}$ mice was accompanied by diminished NK cell infiltration. Consistently, limited growth of Ldha^{low} tumors in C57BL/6 mice was associated with higher numbers of infiltrating NK cells. Not only were the levels of NK cells significantly elevated in slowly growing Ldha^{low} tumors, but also the percentage of activated CD8^{+} T cells was markedly increased. In contrast, tumors

with excessive proliferation derived from Ldha^{low} and control cells in *Ifng*$^{-/-}$ and *Ifngr1*$^{-/-}$ mice as well as control tumors from C57BL/6, only contained marginal amounts of activated T cells. Surprisingly, Ldha^{low} tumors from *Ifng*$^{-/-}$ and *Ifngr1*$^{-/-}$ mice exhibited higher numbers of infiltrating CD8^{+} T cells compared to C57BL/6 mice but the majority of these T cells were inactive as they showed no expression of CD25. Expansion of CD8^{+} T cells could have served as a mechanism to compensate for their decreased activity.

In summary, IFN-γ was necessary for both NK cell recruitment into the tumor microenvironment and activation of CD8^{+} T cells, and thereby seems to represent the central factor for tumor growth suppression in this model. The IFN-γ-mediated tumor immunosurveillance was compromised by the excessive production of lactate from tumor cells. Thus, these findings demonstrate that lactate is a potent immunomodulatory factor in highly glycolytic tumors which promotes tumor growth via the suppression of IFN-γ production by T and NK cells (Figure 6-1).

However, in none of the performed tumor inoculation experiments, the growth of Ldha^{low} tumors could be prevented completely. Even in the absence of excessive lactate production by tumor cells, where recruitment of NK and CD8^{+} T cells into the tumor microenvironment and activation via IFN-γ was feasible, residual tumor proliferation was observed. Results from *Ccr2*$^{-/-}$ mice, displaying diminished tumor growth compared to controls, suggest that monocytic myeloid cells exhibit tumor promoting effects and thereby are responsible for residual Ldha^{low} tumor proliferation in C57BL/6 mice. This notion is corroborated by the finding that IFN-γ fosters immunosuppression driven by monocytic MDSCs[234]. Results obtained in this dissertation also indicate that the function and activity of MDSCs seem not to be directly regulated by lactate but rather develop in dependence of cytotoxic effector cells which are sensitive to the lactate abundance in the tumor microenvironment.

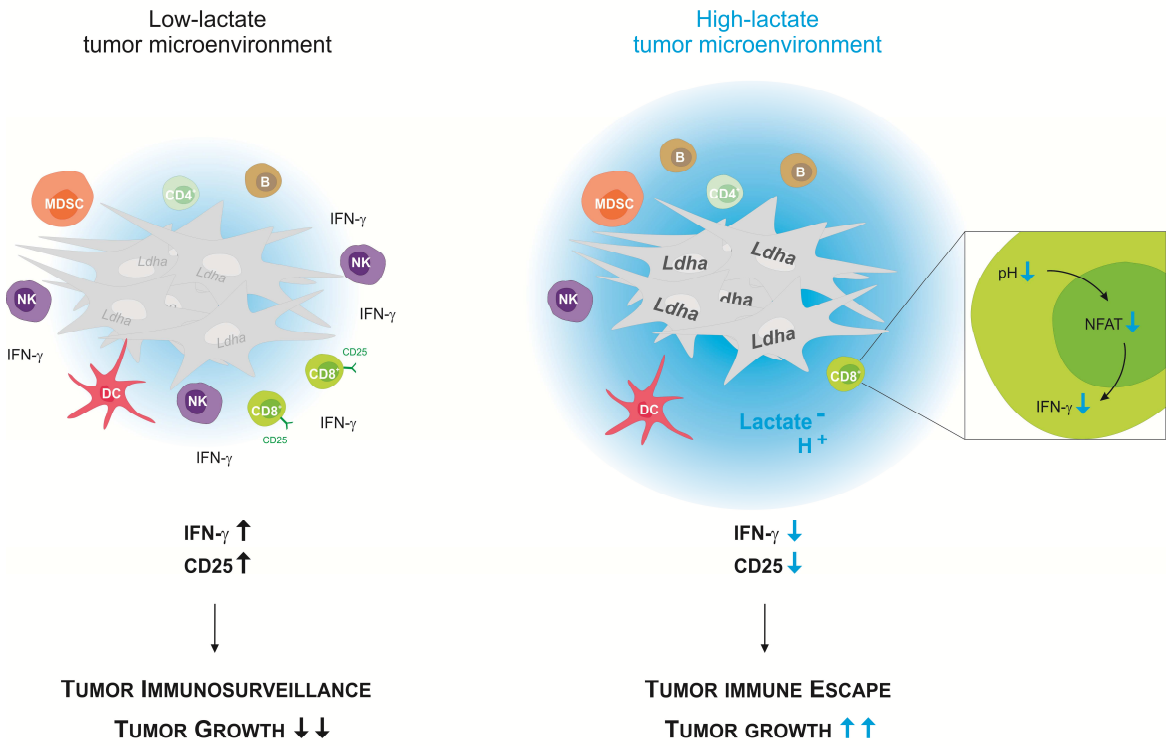

Figure 6-1. Tumor-derived lactic acid leads to tumor immune escape
In a low-lactate tumor microenvironment, the abundance of $CD8^+$ T cells and NK cells and the subsequent production of IFN-γ and activation of $CD8^+$ T cells (CD25) leads to tumor immunosurveillance and tumor growth control. In contrast, high amounts of lactate in the tumor microenvironment compromise IFN-γ production of NK cells and $CD8^+$ T cells via intracellular acidification and downregulation of NFAT and thereby inhibit $CD8^+$ T cell activation and NK cell infiltration. This further leads to tumor immune escape and tumor progression. MDSC, myeloid-derived suppressor cell; B, B cell; DC, dendritic cell; $CD4^+$, T helper cell.

6.2.8 Molecular pathways involved in the immunomodulation by lactic acid

Tumor-derived lactate has been shown to drive tumor growth via compromising tumor immunosurveillance by impairing the IFN-γ production of $CD8^+$ T cells and NK cells. Analyses on the mechanism of the IFN-γ inhibition by lactate or its protonated form lactic acid revealed that lactic acid led to a concentration-dependent intracellular acidification in $CD8^+$ T cells. The intracellular pH of pH 7.5 in untreated cells decreased to pH 5.5 upon exposure with 15 mM lactic acid within 30 minutes after treatment. The effect was lactate-dependent, as the sole incubation with HCl led to a decrease in the intracellular pH but did not reach the same low pH values observed upon lactic acid exposure. This is likely based on the fact that in the presence of lactate, proton transport is not only possible via sodium-proton exchangers and bicarbonate transporters, but also through the activity of MCTs, which maximizes proton transport into the cell. Consistent with these findings, Fischer et al. observed a decrease in intracellular pH upon lactic acid incubation in human $CD8^+$ T cells[177]. In pmel mouse T cells, however, exposure to low extracellular pH levels did not change the intracellular pH[73]. This discrepancy to the aforementioned findings could possibly be due to a significantly longer incubation time of pmel

mouse T cells compared to experiments with mouse and human $CD8^+$ T cells. It is possible that after long-term incubation, T cells find ways to block proton influx and/or buffer their intracellular pH.

The activity of enzymes depends on an optimal pH and it has been shown that lowering the pH strongly decreased the activity of calcineurin[195]. Calcineurin is responsible for the activation and nuclear translocation of NFAT, which is involved in IFN-γ expression[193]. NFAT is upregulated on mRNA and protein levels during activation of T cells[194]. Flow cytometry analysis revealed that NFAT upregulation in $CD8^+$ T and NK cells during activation was inhibited upon lactic acid exposure. Acidification by HCl revealed similar results, whereas incubation with sodium lactate only resulted in slightly reduced NFAT levels. This indicates that generation of lactate during excessive glycolysis in tumors and subsequent accumulation of lactic acid in the tumor microenvironment leads to intracellular acidification of T cells and NK cells. Thereby, the upregulation of NFAT is disturbed. Furthermore, inhibition of the calcineurin activity prevents translocation of NFAT into the nucleus[195], resulting in impaired IFN-γ production by $CD8^+$ T and NK cells (Figure 6-1).

Yet, NFAT is not only involved in IFN-γ regulation but also in the regulation of genes from the granule exocytosis pathway, including perforin and granzyme[193]. This may explain that granzyme B expression was diminished in tumor-infiltrating lymphocytes in a high-lactate tumor microenvironment. Besides the granule exocytosis pathway, lymphocyte-mediated cytotoxicity is executed by a “death-ligand” mechanism. Here, binding of FASL on NK or T cells to FAS receptor on target cells induces apoptosis of tumor cells. Since FASL expression has also been shown to be regulated by NFAT[235] and lactic acid was demonstrated to influence NFAT expression, a possible role of FAS/FASL interactions in the B16 $Ldha^{low}$ setting cannot be excluded.

6.2.9 Characterization of *Ldha*$^{-/-}$ clones generated with CRISPR/Cas9

In order to support the findings on the immunomodulatory role of lactic acid, additional B16 clones were generated by means of *Ldha*-gene editing using CRISPR/Cas9. In the respective clones, a total absence of the LDHA protein was observed under hypoxic conditions, which cause *Ldha* upregulation. Strikingly, despite the complete absence of LDHA, the lactate production of these *Ldha*$^{-/-}$ clones was only reduced by 30% compared to the control cells. Analyses by qRT-PCR further revealed a 100-fold lower *Ldha* mRNA expression in *Ldha*$^{-/-}$ clones compared to control cells, whereas no differences were observed regarding *Ldhb* expression. These results suggest that the LDH-1 enzyme, formed by the LDHB tetramer, is capable to replace LDH-5 enzyme activity. Accordingly, attempts with zinc-finger nuclease-mediated targeting of *Ldha* in Chinese hamster ovary cells failed to create cells without lactate production. However, the authors exclude the possibility of compensation by other LDH isoforms and attributed the lactate production to the recovery of heterozygous mutants and the lethality of cells with complete *Ldha* deficiency[236].

Although further characterization of the *Ldha*$^{-/-}$ clones will be necessary to clarify the source of lactate production, these cells will serve as an additional system to confirm the immunomodulatory role of tumor-derived lactate in future experiments.

6.3 Immunomodulatory role of lactic acid in human melanoma?

Results from metabolic flux analyses revealed that human melanoma cell lines, unlike melanocytes, exhibit the Warburg phenotype[237]. *BRAF*, an oncogene mutated in about 50% of melanomas[238], and more specifically, the mutation of ^{V600E}*BRAF*, which accounts for the broad majority of *BRAF* mutations detected in melanoma[239], has been demonstrated to upregulate glycolysis-related genes. Consistently, knockdown of ^{V600E}*BRAF* in melanoma cells reversed the Warburg phenotype and reduced glycolysis[240], and treatment with the ^{V600E}BRAF inhibitor vemurafenib resulted in improved survival of patients with ^{V600E}*BRAF*-positive metastatic melanoma[241].

Moreover, serum LDH levels have long been used as a prognostic marker in human melanoma, with elevated levels being indicative of an advanced disease and poor prognosis[196]. Additionally, higher LDH-5 expression was observed in melanoma and metastasis compared to melanocytic nevi and was associated with reduced survival of melanoma patients[40].

High numbers of $CD8^+$ T cells, on the contrary, are considered as a positive prognostic marker[150]. Furthermore, adoptive immunotherapy with tumor-infiltrating lymphocytes seems to be a promising therapeutic approach in metastatic melanoma[242], whereas immunotherapy of other tumors seems to be difficult. Due to challenges in T cell isolation, attempts have been made to genetically engineer TCRs of isolated T cells or to generate chimeric antigen receptors (CARs), in order to boost T cell anti-tumor functions[243-247]. The tremendous potential of immunotherapy was demonstrated using CAR T cells against CD19 for acute lymphoblastic leukemia patients, leading to a remission rate of 90% and durable remission up to 2 years[248].

Despite the widely recognized negative association of LDH serum levels with the outcome of human melanoma and the observation of high numbers of infiltrating $CD8^+$ T cells, the possible connection between human LDH levels and immune cell infiltrate has not been investigated up to now. Therefore, experiments were carried out to establish a link between *LDHA* expression, lactate levels and immune cell infiltrate in human melanoma. Analyses revealed that in lesions of primary melanoma, *LDHA* was overexpressed compared to early melanoma stages, i.e. melanoma in situ, though *LDHA* expression was not different compared to adjacent healthy tissue. This was not consistent with the intra-tissue lactate concentrations detected, which showed similar levels in melanoma in situ, melanoma lesions and adjacent healthy tissue. Thus, lactate levels do not always correlate with *LDHA* expression and as lactate levels are similar in healthy tissue and primary melanoma, lactate seems to play no role in immunoregulation in primary melanoma.

However, with regard to metastases, lactate levels were significantly higher. Cutaneous metastatic lesions of melanoma patients revealed lactate concentrations ranging from 16 µmol/g to 38 µmol/g, whereas healthy tissue of the respective patients exhibited lactate levels around 10 µmol/g. Subsequent analyses of the immune cell infiltrate demonstrated similar high numbers of infiltrating T cells, representing about 65% of all leukocytes, in both control and metastatic tissue. The numbers of cytotoxic T cells were slightly elevated in melanoma metastases compared to controls. Therefore, T cell migration into the tumor microenvironment does not seem to be influenced by extracellular lactate levels. Numbers of activated $CD8^+$ T cells, however, were drastically diminished in melanoma metastases compared to adjacent healthy tissue. This is in line with the finding of reduced amounts of activated $CD8^+$ T cells in high-lactate mouse melanoma tumors.

In conclusion, the attenuation of $CD8^+$ T cell activation by tumor-derived lactate observed in the mouse melanoma model partially mirrors the situation in cutaneous metastases of human melanoma patients. Results from the mouse melanoma model suggest the intracellular acidification, subsequent downregulation of NFAT and the reduction of IFN-γ in cytotoxic lymphocytes as a possible underlying mechanism. Further analyses are needed to clarify the importance of these findings for other tumor entities.

6.4 Perspectives

It has been known for many years that the excessive generation of lactate by highly glycolytic tumors and the subsequent accumulation of lactic acid in the tumor microenvironment exert direct pro-tumoral effects. This dissertation demonstrates a link between lactic acid accumulation and suppression of cytotoxic effector functions of immune cells, which allows evasion from immunosurveillance and thereby promotes tumor progression.

Thus, it seems likely that lactate, which plays a critical role in tumorigenesis, can be relevant as a prognostic marker[249]. Walenta et al. established a link between lactate metabolism and aggressiveness of cancer by demonstrating that lactate accumulation correlates with decreased survival of cervical cancer patients[57]. The negative outcome of high lactate levels in tumors with regard to patient survival was likewise described for head and neck squamous cell carcinoma and glioblastoma multiforme[185,250,251]. Furthermore, intratumoral lactate content was shown to be associated with the incidence of metastasis[185].

Besides lactate, LDHA, which as a tetramer forms LDH-5, a crucial enzyme of the glucose metabolism responsible for the generation of lactate from pyruvate, also represents a potential prognostic marker in cancer[38,39]. In renal cell carcinoma, gastric cancer, pancreatic cancer and melanoma, overexpression of LDHA is associated with poor prognosis[38-40,252]. In pancreatic cancer, LDHA expression also correlated inversely with $CD8^+$ T cell infiltration[252]. Immunohistochemistry analyses demonstrated the correlation of LDH-5 overexpression with unfavorable outcome in non-small cell lung cancer and colorectal cancer[253,254].

These results underline the importance of glycolysis and subsequent lactate production for tumor progression and metastasis. Hence, increasing attempts are being undertaken to therapeutically target tumor glycolysis and lactate accumulation in order to dampen tumor progression and metastasis. The application of the small-molecule LDHA inhibitor FX11, a gossypol derivative, succeeded to obstruct tumor growth of human cancer xenografts[50]. Moreover, the combination of novel LDHA inhibitors and the chemotherapeutic agent gemcitabine in hypoxic pancreatic cancer cells, which are characterized by increased chemoresistance, led to synergistic cytotoxic effects with increased apoptosis and impaired cell migration[255]. Since LDH-5 inhibition appears to selectively affect highly glycolytic tumor cells, drugs targeting LDH-5 are likely safe agents counteracting tumor growth and invasiveness. Accordingly, research on potent and selective LDH-5 inhibitors is conducted by several groups across academia and industry. However, the high polarity and small size of its natural substrate, and the rather large and open active site of LDH-5 make it a difficult target. Thus, the commonly poor pharmacokinetic profile of novel LDH-5-inhibiting molecules and low penetration into cells are the reasons why only a small number of LDH-5 inhibitors have progressed to preclinical and clinical trials. The development of more potent and selective LDH-5 inhibitors with a high bioavailability will, therefore, be a major future challenge[36].

Importantly, besides glycolysis and lactate production, lactate uptake and subsequent OXPHOS have been described as a feature of some tumor cell populations in heterogeneous tumors[58]. Consequently, the efficacy of LDHA inhibitors could be further increased by the treatment with anti-diabetic drugs such as pioglitazone or metformin, which drive tumor cells towards glycolysis[256].

Diclofenac, a non-steroidal anti-rheumatic drug, has been shown to inhibit *Ldha* expression and lactate production in mouse glioma cells *in vitro*. *In vivo*, diclofenac treatment resulted in decreased intratumoral lactate levels and repressed glioma growth, accompanied by a recovered IL-12 production of DCs. Although diclofenac impaired mouse T cell activation and proliferation, it likely represents a promising anti-glycolytic cancer drug[257].

Targeting MCTs represents another promising tool in anti-cancer treatment as lactate is exported from the cell via MCT1 and MCT4[67] and elevated levels of MCT1 and/or MCT4 are typical features of several human malignancies[197,258]. A second-generation MCT1 inhibitor, AZD3965, is currently undergoing phase I clinical trials for patients with solid tumors, prostate and gastric cancer and diffuse large B cell lymphoma[259]. Results from Marchiq et al. revealed that the treatment with the OXPHOS inhibitor phenformin induced cell death of MCT4 knockout cells due to a rapid drop in intracellular ATP and a subsequent metabolic catastrophe. Similar effects were observed for cells depleted of the MCT chaperone basigin[187]. These data suggest that combined targeting of glycolysis via MCT inhibitors or LDHA inhibitors, and OXPHOS via phenformin provides a powerful anti-cancer strategy.

However, it has to be considered that targeting glucose metabolism may also inhibit the proliferation and activation of T cells, as upregulation of glycolysis is a common feature of activated T cells[260]. Impaired activation of tumor-infiltrating T cells was recently attributed to the glucose-deprivation by tumor cells leading to dampened T cell effector functions[171,172].

Anti-glycolytic strategies for cancer therapy have, therefore, to be carefully evaluated, as they might act not only on tumor cells but as well on T cell metabolism and function[260]. Furthermore, off-target effects of anti-glycolytic drugs on other benign cells are possible. Thus, drug-delivery strategies like bi-specific antibodies, which redirect immune effector cells to the tumor microenvironment[261], transporter-mediated drug uptake, e.g., a glucose-conjugated LDHA inhibitor[262] and nanoparticle-based delivery systems to increase permeability and retention in the tumor[263] are being investigated.

The export of lactate from the cell via MCT1 and MCT4 is executed in co-transport with protons[67] and the accumulation of lactic acid in the tumor microenvironment leads to a subsequent acidification of the extracellular space[68]. Tumor acidosis is associated with increased invasiveness of tumors[18]. Neutralization of tumor acidity with bicarbonate monotherapy was previously shown to diminish tumor growth and to improve the anti-tumor responses to immunotherapy[73]. Regulators of pH, like the proton pump, sodium-proton exchangers and bicarbonate transporters could thereby also serve as potential targets for anti-tumor therapy[71,72,264].

In the light of the findings obtained in this dissertation, the strategies described above could lead to the reduction of immunosuppression by tumor-derived lactate and lactic acid, and thereby improve immunotherapeutic approaches in cancer treatment. In line with this hypothesis is the observation that serum LDH levels of patients with metastatic melanoma represent a selection criterion for immunotherapy with ipilimumab, a monoclonal antibody blocking CTLA-4. CTLA-4 represents an immune checkpoint, as this receptor downregulates immune cell function. In case of baseline serum LDH concentrations exceeding twice the upper limit of normal values, ipilimumab treatment was unlikely to cause long-term benefits[265]. Another inhibitory checkpoint receptor is PD-1, which is predominantly expressed on activated T cells[266]. Metastatic melanoma has been linked to extensive infiltration with cytotoxic T cells which are hyporesponsive and cannot inhibit tumor progression. Tumor immune evasion was attributed, amongst others, to PD-L1 expression[267]. PD-L1 is expressed on tumor cells and represents the ligand for PD-1[266]. Concordantly, preclinical studies have demonstrated that interfering with PD-1/PD-L1 interactions improved effector functions of tumor-specific cytotoxic T cells in the tumor microenvironment and thereby supported tumor rejection[268,269]. Hence, two anti-PD-1 antibodies, nivolumab and pembrolizumab, have been approved for the treatment of advanced melanoma and therapy-refractory metastatic non-small cell lung cancer, and various other PD-1 or PD-L1 inhibitors are currently undergoing clinical trials[266]. Treatment with nivolumab and pembrolizumab has led to increased response rates and improved progression-free and overall patient survival in comparison to chemotherapy and ipilimumab treatment[270-275]. However, the data obtained from clinical trials for solid tumors revealed low response rates of PD-1 inhibitors[266]. Tang et al. demonstrated that induction of immune checkpoint blockade responses requires sufficient T cell infiltration[276].

Strikingly, serum LDH levels in patients with metastatic melanoma can predict clinical outcome early after anti-PD-1 therapy, with elevated LDH concentrations being linked to poor survival[277]. These observations, together with the data from this work on the immunomodulatory role of lactic acid, might serve as an explanation not only for the low response rates of PD-1 inhibitors in

advanced malignancies, but also for limitations of cancer immunotherapies in general. Consequently, combination therapies of promising immunotherapeutic agents and anti-metabolic drugs have to be developed in order to overcome immune tolerance and improve the anti-tumor immune response for the successful treatment of human cancer.

7 Summary

Tumors show alterations in their metabolism to fulfill the requirements of excessive proliferation. The most prominent metabolic change is the switch from OXPHOS to aerobic glycolysis, termed Warburg effect. The increased uptake of glucose, subsequent conversion of pyruvate to lactate and the export of lactate in co-transport with protons lead to the extracellular accumulation of lactic acid and occur in the majority of malignant neoplasia. Extracellular lactic acid has been shown to exert a range of direct tumor-promoting effects and there is evidence that various immune cells are impaired by lactic acid. The aim of this dissertation was to clarify the immunomodulatory role of tumor-derived lactic acid.

Ldha expression, coding for the lactate-generating enzyme LDH-5, was downregulated by means of shRNA technology in B16.SIY E12 mouse melanoma cells, resulting in low-lactate producing clones ($Ldha^{low}$). Cells transfected with scrambled shRNA were used as a control. $Ldha^{low}$ clones showed higher OXPHOS than control cells due to increased mitochondrial content. Despite the metabolic differences in $Ldha^{low}$ clones and control cells, proliferation and cell cycle properties were similar *in vitro*. In immunocompetent C57BL/6 mice, however, tumor growth of $Ldha^{low}$ clones was significantly decreased compared to that of control cells. Bioluminescence analyses revealed 50% lower intratumoral lactate concentrations, along with reduced *Ldha* mRNA expression in $Ldha^{low}$ tumors compared to control tumors. As other enzymes involved in tumorigenesis and immunosuppression, including IDO, ARG, COX and iNOS, did not show any differences in mRNA expression in $Ldha^{low}$ tumors and control tumors, reduced tumor growth of $Ldha^{low}$ clones could be attributed to their diminished lactate production.

$Ldha^{low}$ tumors contained more leukocytes and among them lower numbers of myeloid cells and B cells, which are said to be pro-tumorigenic, whereas the amount of infiltrating anti-tumoral cytotoxic T cells and NK cells was increased compared to control tumors. Moreover, cytotoxic T cells and NK cells from $Ldha^{low}$ tumors produced significantly greater amounts of IFN-γ, thereby showing a higher activity than T cells and NK cells from control tumors. Consistently, IFN-γ production of T cells and NK cells was inhibited by lactic acid *in vitro*. This suggests that tumor immunosurveillance by activated T and NK cells is possible in a low-lactate tumor microenvironment but compromised in the presence of high amounts of lactate.

Accordingly, in the absence of T cells and/or NK cells, tumor growth of $Ldha^{low}$ clones was accelerated and became similar to that of control cells. Growth control of $Ldha^{low}$ tumors was also lost in the absence of IFN-γ. This was accompanied by a diminished infiltration of NK cells and activated cytotoxic T cells, indicating a lactate-dependent regulation of IFN-γ production.

In vitro analyses of cytotoxic T cells revealed a lactic-acid induced drop of intracellular pH, and subsequent compromised NFAT expression resulting in a diminished IFN-γ production.

In summary, this dissertation highlights tumor-derived lactic acid as a potent immunomodulatory metabolite which limits effector cell recruitment into the tumor and impairs IFN-γ production of

cytotoxic T and NK cells in highly glycolytic tumors. Thereby, tumor immunosurveillance is lost and tumor progression is facilitated.

Interestingly, analyses of cutaneous metastases from melanoma patients displayed high lactate levels along with a reduced infiltration of activated cytotoxic T cells. These findings suggest that lactic acid has immunomodulatory relevance, not only in the mouse model but also for human malignancies.

8 Zusammenfassung

Tumoren weisen verschiedene Veränderungen in ihrem Stoffwechsel auf. Der Warburg-Effekt, die wohl bedeutendste metabolische Veränderung, ist durch gesteigerte aerobe glykolytische Aktivität charakterisiert. Hierbei wird vermehrt Glukose in die Zelle aufgenommen und zu Laktat umgewandelt. Dieses wird im Co-Transport mit Protonen aus der Zelle ausgeschleust, was zu einer Anreicherung von Laktat und Protonen (Milchsäure) im Tumormikromilieu führt. Neben einer Reihe direkter tumorfördernder Effekte gibt es Hinweise auf eine Immunregulation durch Milchsäure. Ziel dieser Arbeit war die Untersuchung der immunmodulatorischen Rolle tumorassoziierter Milchsäure.

Dafür wurde die Expression von *Ldha*, welche für das laktatproduzierende Enzym LDH-5 kodiert, in B16.SIY E12 Mausmelanom-Zellen mittels shRNA-Technologie herunterreguliert. Auf diese Weise generierte Klone (Ldha^{low}) zeigten eine verminderte Laktatproduktion im Vergleich zu Kontrollzellen, die mit einer “scrambled”-shRNA transfiziert wurden. Ldha^{low}-Klone wiesen eine erhöhte oxidative Phosphorylierung auf, die der höheren Anzahl an Mitochondrien zuzuschreiben war. Trotz metabolischer Unterschiede der Ldha^{low}-Klone und der Kontrollzellen differierten diese nicht in Proliferation und Zellzyklus. Jedoch war das Tumorwachstum der Ldha^{low}-Klone in immunkompetenten C57BL/6-Mäusen deutlich vermindert. Biolumineszenz-Messungen von Ldha^{low}-Tumoren zeigten eine um 50 % verringerte intratumorale Laktatkonzentration im Vergleich zu Kontrolltumoren. Eine erniedrigte *Ldha* mRNA-Expression in Ldha^{low}-Klonen wurde sowohl *in vitro* als auch *in vivo* beobachtet. Dies bestätigte die stabile Herrunterregulation der *Ldha* in den Ldha^{low}-Klonen. Da sich die mRNA-Expression von anderen in Karzinogenese und Immunsuppression involvierten Enzymen wie IDO, ARG, COX und iNOS, zwischen beiden Gruppen nicht unterschied, wurde das verminderte Tumorwachstum der Ldha^{low}-Klone der verringerten Laktatproduktion zugeschrieben.

In durchflusszytometrischen Analysen der Ldha^{low}-Tumoren wurde, im Vergleich zu den Kontrolltumoren, eine erhöhte Infiltration mit Leukozyten gefunden, darunter eine geringere Anzahl an myeloiden Zellen und B-Zellen, welche als protumoral gelten. Antitumorale Immunzellen, wie zytotoxische T-Zellen und NK-Zellen, waren jedoch vermehrt vorhanden. Zudem produzierten zytotoxische T-Zellen und NK-Zellen aus Ldha^{low}-Tumoren signifikant höhere Mengen an IFN-γ, was ein Zeichen erhöhter Aktivität darstellt. In Übereinstimmung damit ergaben *in vitro*-Experimente, dass die IFN-γ-Produktion von T- und NK-Zellen durch Milchsäure gehemmt wird. Dies legte nahe, dass eine Tumorimmunkontrolle durch aktivierte T- und NK-Zellen in einer Tumorumgebung mit niedrigen Laktatmengen möglich ist, ein hoher Laktatspiegel dies jedoch verhindert. In Abwesenheit von T- und/oder NK-Zellen wiesen Ldha^{low}-Tumoren ein vergleichbar schnelles Tumorwachstum auf wie Kontrolltumoren. Die immunologische Wachstumskontrolle von Ldha^{low}-Tumoren war in Abwesenheit von IFN-γ ebenfalls nicht mehr möglich. Entsprechend waren in diesen Tumoren eine geringere Anzahl infiltrierender NK-Zellen und aktivierter

zytotoxischer T-Zellen nachweisbar, was auf eine laktatabhängige Regulation der IFN-γ-Produktion sowie der Rekrutierung von NK-Zellen und aktivierten T-Zellen hindeutet. *In vitro*-Experimente zeigten, dass Milchsäure eine intrazelluläre Ansäuerung in T-Zellen bewirkt, was die NFAT-Expression beeinträchtigt und so zu verminderter IFN-γ-Produktion führt.

Zusammenfassend zeigt diese Arbeit, dass die LDHA-assoziierte Anreicherung von Milchsäure im Tumormilieu die Rekrutierung und Aktivierung von zytotoxischen Effektorzellen limitiert. Insbesondere scheint die IFN-γ-Produktion zytotoxischer T-Zellen und NK-Zellen in hochglykolytischen Tumoren beeinträchtigt zu sein. Auf diese Weise kommt es zum Verlust der Tumorimmunkontrolle und zu gesteigertem Tumorwachstum.

Interessanterweise zeigten erste Analysen von Biopsien kutaner Metastasen des humanen Melanoms ebenfalls einen Zusammenhang zwischen hohen Laktatspiegeln und einer geringen Infiltration mit aktivierten zytotoxischen T-Zellen. Diese Erkenntnisse deuten darauf hin, dass Milchsäure nicht nur im Mausmodel sondern auch in humanen Tumoren immunmodulatorische Effekte hat.

9 References

1. Torre, L.A., Bray, F., Siegel, R.L., Ferlay, J., Lortet-Tieulent, J. and Jemal, A. (2015). Global cancer statistics, 2012. *CA Cancer J Clin* 65(2)**:** 87-108.

2. Hanahan, D. and Weinberg, R.A. (2011). Hallmarks of cancer: the next generation. *Cell* 144(5)**:** 646-674.

3. Vogelstein, B., Papadopoulos, N., Velculescu, V.E., Zhou, S., Diaz, L.A., Jr. and Kinzler, K.W. (2013). Cancer genome landscapes. *Science* 339(6127)**:** 1546-1558.

4. Kandoth, C., McLellan, M.D., Vandin, F., Ye, K., Niu, B., Lu, C., Xie, M., Zhang, Q., McMichael, J.F., Wyczalkowski, M.A., Leiserson, M.D., Miller, C.A., Welch, J.S., Walter, M.J., Wendl, M.C., Ley, T.J., Wilson, R.K., Raphael, B.J. and Ding, L. (2013). Mutational landscape and significance across 12 major cancer types. *Nature* 502(7471)**:** 333-339.

5. Davies, M.A. and Samuels, Y. (2010). Analysis of the genome to personalize therapy for melanoma. *Oncogene* 29(41)**:** 5545-5555.

6. Jiang, B.H. and Liu, L.Z. (2009). PI3K/PTEN signaling in angiogenesis and tumorigenesis. *Adv Cancer Res* 102**:** 19-65.

7. Yuan, T.L. and Cantley, L.C. (2008). PI3K pathway alterations in cancer: variations on a theme. *Oncogene* 27(41)**:** 5497-5510.

8. Dvorak, H.F. (1986). Tumors: wounds that do not heal. Similarities between tumor stroma generation and wound healing. *N Engl J Med* 315(26)**:** 1650-1659.

9. Vander Heiden, M.G., Cantley, L.C. and Thompson, C.B. (2009). Understanding the Warburg effect: the metabolic requirements of cell proliferation. *Science* 324(5930)**:** 1029-1033.

10. Warburg, O. (1961). [On the facultative anaerobiosis of cancer cells and its use in chemotherapy]. *Munch Med Wochenschr* 103**:** 2504-2506.

11. Jones, R.G. and Thompson, C.B. (2009). Tumor suppressors and cell metabolism: a recipe for cancer growth. *Genes Dev* 23(5)**:** 537-548.

12. DeBerardinis, R.J., Lum, J.J., Hatzivassiliou, G. and Thompson, C.B. (2008). The biology of cancer: metabolic reprogramming fuels cell growth and proliferation. *Cell Metab* 7(1)**:** 11-20.

13. Hsu, P.P. and Sabatini, D.M. (2008). Cancer cell metabolism: Warburg and beyond. *Cell* 134(5)**:** 703-707.

14. Lewis, D.Y., Soloviev, D. and Brindle, K.M. (2015). Imaging tumor metabolism using positron emission tomography. *Cancer J* 21(2)**:** 129-136.

15. Christofk, H.R., Vander Heiden, M.G., Wu, N., Asara, J.M. and Cantley, L.C. (2008). Pyruvate kinase M2 is a phosphotyrosine-binding protein. *Nature* 452(7184)**:** 181-186.

16. Moreno-Sanchez, R., Rodriguez-Enriquez, S., Marin-Hernandez, A. and Saavedra, E. (2007). Energy metabolism in tumor cells. *Febs j* 274(6)**:** 1393-1418.

17. Viale, A., Pettazzoni, P., Lyssiotis, C.A., Ying, H., Sanchez, N., Marchesini, M., Carugo, A., Green, T., Seth, S., Giuliani, V., Kost-Alimova, M., Muller, F., Colla, S., Nezi, L., Genovese, G., Deem, A.K., Kapoor, A., Yao, W., Brunetto, E., Kang, Y., Yuan, M., Asara, J.M., Wang, Y.A., Heffernan, T.P., Kimmelman, A.C., Wang, H., Fleming, J.B., Cantley, L.C., DePinho, R.A. and Draetta, G.F. (2014). Oncogene ablation-resistant pancreatic cancer cells depend on mitochondrial function. *Nature* 514(7524)**:** 628-632.

18. Gatenby, R.A. and Gillies, R.J. (2004). Why do cancers have high aerobic glycolysis? *Nat Rev Cancer* 4(11)**:** 891-899.

19. Altenberg, B. and Greulich, K.O. (2004). Genes of glycolysis are ubiquitously overexpressed in 24 cancer classes. *Genomics* 84(6)**:** 1014-1020.

20. Levine, A.J. and Puzio-Kuter, A.M. (2010). The control of the metabolic switch in cancers by oncogenes and tumor suppressor genes. *Science* 330(6009)**:** 1340-1344.

21. Vaupel, P. (2004). The role of hypoxia-induced factors in tumor progression. *Oncologist* 9 Suppl 5**:** 10-17.

22. Gordan, J.D. and Simon, M.C. (2007). Hypoxia-inducible factors: central regulators of the tumor phenotype. *Curr Opin Genet Dev* 17(1)**:** 71-77.

23. Pouyssegur, J., Dayan, F. and Mazure, N.M. (2006). Hypoxia signalling in cancer and approaches to enforce tumour regression. *Nature* 441(7092)**:** 437-443.

24. Kroemer, G. and Pouyssegur, J. (2008). Tumor cell metabolism: cancer's Achilles' heel. *Cancer Cell* 13(6)**:** 472-482.

25. Kim, J.W., Tchernyshyov, I., Semenza, G.L. and Dang, C.V. (2006). HIF-1-mediated expression of pyruvate dehydrogenase kinase: a metabolic switch required for cellular adaptation to hypoxia. *Cell Metab* 3(3)**:** 177-185.

26. Gottlieb, E. and Tomlinson, I.P. (2005). Mitochondrial tumour suppressors: a genetic and biochemical update. *Nat Rev Cancer* 5(11)**:** 857-866.

27. Rohwer, N., Lobitz, S., Daskalow, K., Jons, T., Vieth, M., Schlag, P.M., Kemmner, W., Wiedenmann, B., Cramer, T. and Hocker, M. (2009). HIF-1alpha determines the metastatic potential of gastric cancer cells. *Br J Cancer* 100(5)**:** 772-781.

28. Dewhirst, M.W. (2007). Intermittent hypoxia furthers the rationale for hypoxia-inducible factor-1 targeting. *Cancer Res* 67(3)**:** 854-855.

29. Corzo, C.A., Condamine, T., Lu, L., Cotter, M.J., Youn, J.I., Cheng, P., Cho, H.I., Celis, E., Quiceno, D.G., Padhya, T., McCaffrey, T.V., McCaffrey, J.C. and Gabrilovich, D.I. (2010). HIF-1alpha regulates function and differentiation of myeloid-derived suppressor cells in the tumor microenvironment. *J Exp Med* 207(11)**:** 2439-2453.

30. Dang, C.V., Kim, J.W., Gao, P. and Yustein, J. (2008). The interplay between MYC and HIF in cancer. *Nat Rev Cancer* 8(1)**:** 51-56.

31. Shim, H., Dolde, C., Lewis, B.C., Wu, C.S., Dang, G., Jungmann, R.A., Dalla-Favera, R. and Dang, C.V. (1997). c-Myc transactivation of LDH-A: implications for tumor metabolism and growth. *Proc Natl Acad Sci U S A* 94(13)**:** 6658-6663.

32. Matoba, S., Kang, J.G., Patino, W.D., Wragg, A., Boehm, M., Gavrilova, O., Hurley, P.J., Bunz, F. and Hwang, P.M. (2006). p53 regulates mitochondrial respiration. *Science* 312(5780)**:** 1650-1653.

33. Bensaad, K., Tsuruta, A., Selak, M.A., Vidal, M.N., Nakano, K., Bartrons, R., Gottlieb, E. and Vousden, K.H. (2006). TIGAR, a p53-inducible regulator of glycolysis and apoptosis. *Cell* 126(1)**:** 107-120.

34. Feng, Z., Hu, W., de Stanchina, E., Teresky, A.K., Jin, S., Lowe, S. and Levine, A.J. (2007). The regulation of AMPK beta1, TSC2, and PTEN expression by p53: stress, cell and tissue specificity, and the role of these gene products in modulating the IGF-1-AKT-mTOR pathways. *Cancer Res* 67(7)**:** 3043-3053.

35. Feng, Z., Zhang, H., Levine, A.J. and Jin, S. (2005). The coordinate regulation of the p53 and mTOR pathways in cells. *Proc Natl Acad Sci U S A* 102(23)**:** 8204-8209.

36. Rani, R. and Kumar, V. (2016). Recent Update on Human Lactate Dehydrogenase Enzyme 5 (hLDH5) Inhibitors: A Promising Approach for Cancer Chemotherapy. *J Med Chem* 59(2)**:** 487-496.

37. Goldman, R.D., Kaplan, N.O. and Hall, T.C. (1964). LACTIC DEHYDROGENASE IN HUMAN NEOPLASTIC TISSUES. *Cancer Res* 24**:** 389-399.

38. Girgis, H., Masui, O., White, N.M., Scorilas, A., Rotondo, F., Seivwright, A., Gabril, M., Filter, E.R., Girgis, A.H., Bjarnason, G.A., Jewett, M.A., Evans, A., Al-Haddad, S., Siu, K.M. and Yousef, G.M. (2014). Lactate dehydrogenase A is a potential prognostic marker in clear cell renal cell carcinoma. *Mol Cancer* 13**:** 101.

39. Sun, X., Sun, Z., Zhu, Z., Guan, H., Zhang, J., Zhang, Y., Xu, H. and Sun, M. (2014). Clinicopathological significance and prognostic value of lactate dehydrogenase A expression in gastric cancer patients. *PLoS One* 9(3)**:** e91068.

40. Zhuang, L., Scolyer, R.A., Murali, R., McCarthy, S.W., Zhang, X.D., Thompson, J.F. and Hersey, P. (2010). Lactate dehydrogenase 5 expression in melanoma increases with disease progression and is associated with expression of Bcl-XL and Mcl-1, but not Bcl-2 proteins. *Mod Pathol* 23(1)**:** 45-53.

41. Koukourakis, M.I., Giatromanolaki, A., Simopoulos, C., Polychronidis, A. and Sivridis, E. (2005). Lactate dehydrogenase 5 (LDH5) relates to up-regulated hypoxia inducible factor pathway and metastasis in colorectal cancer. *Clin Exp Metastasis* 22(1)**:** 25-30.

42. Semenza, G.L. (2007). Oxygen-dependent regulation of mitochondrial respiration by hypoxia-inducible factor 1. *Biochem J* 405(1)**:** 1-9.

43. Cui, J., Shi, M., Xie, D., Wei, D., Jia, Z., Zheng, S., Gao, Y., Huang, S. and Xie, K. (2014). FOXM1 promotes the warburg effect and pancreatic cancer progression via transactivation of LDHA expression. *Clin Cancer Res* 20(10)**:** 2595-2606.

44. Kaller, M., Liffers, S.T., Oeljeklaus, S., Kuhlmann, K., Roh, S., Hoffmann, R., Warscheid, B. and Hermeking, H. (2011). Genome-wide characterization of miR-34a induced changes in protein and mRNA expression by a combined pulsed SILAC and microarray analysis. *Mol Cell Proteomics* 10(8)**:** M111.010462.

45. Davis-Dusenbery, B.N. and Hata, A. (2010). MicroRNA in Cancer: The Involvement of Aberrant MicroRNA Biogenesis Regulatory Pathways. *Genes Cancer* 1(11)**:** 1100-1114.

46. Fan, J., Hitosugi, T., Chung, T.W., Xie, J., Ge, Q., Gu, T.L., Polakiewicz, R.D., Chen, G.Z., Boggon, T.J., Lonial, S., Khuri, F.R., Kang, S. and Chen, J. (2011). Tyrosine phosphorylation of lactate dehydrogenase A is important for NADH/NAD(+) redox homeostasis in cancer cells. *Mol Cell Biol* 31(24)**:** 4938-4950.

47. Zhao, D., Xiong, Y., Lei, Q.Y. and Guan, K.L. (2013). LDH-A acetylation: implication in cancer. *Oncotarget* 4(6)**:** 802-803.

48. Zhao, D., Zou, S.W., Liu, Y., Zhou, X., Mo, Y., Wang, P., Xu, Y.H., Dong, B., Xiong, Y., Lei, Q.Y. and Guan, K.L. (2013). Lysine-5 acetylation negatively regulates lactate dehydrogenase A and is decreased in pancreatic cancer. *Cancer Cell* 23(4)**:** 464-476.

49. Fantin, V.R., St-Pierre, J. and Leder, P. (2006). Attenuation of LDH-A expression uncovers a link between glycolysis, mitochondrial physiology, and tumor maintenance. *Cancer Cell* 9(6)**:** 425-434.

50. Le, A., Cooper, C.R., Gouw, A.M., Dinavahi, R., Maitra, A., Deck, L.M., Royer, R.E., Vander Jagt, D.L., Semenza, G.L. and Dang, C.V. (2010). Inhibition of lactate dehydrogenase A induces oxidative stress and inhibits tumor progression. *Proc Natl Acad Sci U S A* 107(5)**:** 2037-2042.

51. Xie, H., Valera, V.A., Merino, M.J., Amato, A.M., Signoretti, S., Linehan, W.M., Sukhatme, V.P. and Seth, P. (2009). LDH-A inhibition, a therapeutic strategy for treatment of hereditary leiomyomatosis and renal cell cancer. *Mol Cancer Ther* 8(3)**:** 626-635.

52. Xie, H., Hanai, J., Ren, J.G., Kats, L., Burgess, K., Bhargava, P., Signoretti, S., Billiard, J., Duffy, K.J., Grant, A., Wang, X., Lorkiewicz, P.K., Schatzman, S., Bousamra, M., 2nd, Lane, A.N., Higashi, R.M., Fan, T.W., Pandolfi, P.P., Sukhatme, V.P. and Seth, P. (2014). Targeting lactate dehydrogenase--a inhibits tumorigenesis and tumor progression in mouse models of lung cancer and impacts tumor-initiating cells. *Cell Metab* 19(5)**:** 795-809.

53. Rizwan, A., Serganova, I., Khanin, R., Karabeber, H., Ni, X., Thakur, S., Zakian, K.L., Blasberg, R. and Koutcher, J.A. (2013). Relationships between LDH-A, lactate, and metastases in 4T1 breast tumors. *Clin Cancer Res* 19(18)**:** 5158-5169.

54. Wang, Z.Y., Loo, T.Y., Shen, J.G., Wang, N., Wang, D.M., Yang, D.P., Mo, S.L., Guan, X.Y. and Chen, J.P. (2012). LDH-A silencing suppresses breast cancer tumorigenicity through induction of oxidative stress mediated mitochondrial pathway apoptosis. *Breast Cancer Res Treat* 131(3)**:** 791-800.

55. Augoff, K., Hryniewicz-Jankowska, A. and Tabola, R. (2015). Lactate dehydrogenase 5: an old friend and a new hope in the war on cancer. *Cancer Lett* 358(1)**:** 1-7.

56. Walenta, S., Salameh, A., Lyng, H., Evensen, J.F., Mitze, M., Rofstad, E.K. and Mueller-Klieser, W. (1997). Correlation of high lactate levels in head and neck tumors with incidence of metastasis. *Am J Pathol* 150(2)**:** 409-415.

57. Walenta, S., Wetterling, M., Lehrke, M., Schwickert, G., Sundfor, K., Rofstad, E.K. and Mueller-Klieser, W. (2000). High lactate levels predict likelihood of metastases, tumor recurrence, and restricted patient survival in human cervical cancers. *Cancer Res* 60(4)**:** 916-921.

58. Sonveaux, P., Vegran, F., Schroeder, T., Wergin, M.C., Verrax, J., Rabbani, Z.N., De Saedeleer, C.J., Kennedy, K.M., Diepart, C., Jordan, B.F., Kelley, M.J., Gallez, B., Wahl, M.L., Feron, O. and Dewhirst, M.W. (2008). Targeting lactate-fueled respiration selectively kills hypoxic tumor cells in mice. *J Clin Invest* 118(12)**:** 3930-3942.

59. Martinez-Outschoorn, U.E., Prisco, M., Ertel, A., Tsirigos, A., Lin, Z., Pavlides, S., Wang, C., Flomenberg, N., Knudsen, E.S., Howell, A., Pestell, R.G., Sotgia, F. and Lisanti, M.P. (2011). Ketones and lactate increase cancer cell "stemness," driving recurrence, metastasis and poor clinical outcome in breast cancer: achieving personalized medicine via Metabolo-Genomics. *Cell Cycle* 10(8)**:** 1271-1286.

60. Goetze, K., Walenta, S., Ksiazkiewicz, M., Kunz-Schughart, L.A. and Mueller-Klieser, W. (2011). Lactate enhances motility of tumor cells and inhibits monocyte migration and cytokine release. *Int J Oncol* 39(2)**:** 453-463.

61. Baumann, F., Leukel, P., Doerfelt, A., Beier, C.P., Dettmer, K., Oefner, P.J., Kastenberger, M., Kreutz, M., Nickl-Jockschat, T., Bogdahn, U., Bosserhoff, A.K. and Hau, P. (2009). Lactate promotes glioma migration by TGF-beta2-dependent regulation of matrix metalloproteinase-2. *Neuro Oncol* 11(4)**:** 368-380.

62. Beckert, S., Farrahi, F., Aslam, R.S., Scheuenstuhl, H., Konigsrainer, A., Hussain, M.Z. and Hunt, T.K. (2006). Lactate stimulates endothelial cell migration. *Wound Repair Regen* 14(3)**:** 321-324.

63. Rudrabhatla, S.R., Mahaffey, C.L. and Mummert, M.E. (2006). Tumor microenvironment modulates hyaluronan expression: the lactate effect. *J Invest Dermatol* 126(6)**:** 1378-1387.

64. Stern, R., Shuster, S., Neudecker, B.A. and Formby, B. (2002). Lactate stimulates fibroblast expression of hyaluronan and CD44: the Warburg effect revisited. *Exp Cell Res* 276(1)**:** 24-31.

65. Koukourakis, M.I., Giatromanolaki, A., Harris, A.L. and Sivridis, E. (2006). Comparison of metabolic pathways between cancer cells and stromal cells in colorectal carcinomas: a metabolic survival role for tumor-associated stroma. *Cancer Res* 66(2)**:** 632-637.

66. Sattler, U.G., Meyer, S.S., Quennet, V., Hoerner, C., Knoerzer, H., Fabian, C., Yaromina, A., Zips, D., Walenta, S., Baumann, M. and Mueller-Klieser, W. (2010). Glycolytic metabolism and tumour response to fractionated irradiation. *Radiother Oncol* 94(1)**:** 102-109.

67. Halestrap, A.P. (2013). Monocarboxylic acid transport. *Compr Physiol* 3(4)**:** 1611-1643.

68. Poole, R.C. and Halestrap, A.P. (1993). Transport of lactate and other monocarboxylates across mammalian plasma membranes. *Am J Physiol* 264(4 Pt 1)**:** C761-782.

69. Webb, B.A., Chimenti, M., Jacobson, M.P. and Barber, D.L. (2011). Dysregulated pH: a perfect storm for cancer progression. *Nat Rev Cancer* 11(9)**:** 671-677.

70. Calcinotto, A., Filipazzi, P., Grioni, M., Iero, M., De Milito, A., Ricupito, A., Cova, A., Canese, R., Jachetti, E., Rossetti, M., Huber, V., Parmiani, G., Generoso, L., Santinami, M., Borghi, M., Fais, S., Bellone, M. and Rivoltini, L. (2012). Modulation of microenvironment acidity reverses anergy in human and murine tumor-infiltrating T lymphocytes. *Cancer Res* 72(11)**:** 2746-2756.

71. De Milito, A., Canese, R., Marino, M.L., Borghi, M., Iero, M., Villa, A., Venturi, G., Lozupone, F., Iessi, E., Logozzi, M., Della Mina, P., Santinami, M., Rodolfo, M., Podo, F., Rivoltini, L. and Fais, S. (2010). pH-dependent antitumor activity of proton pump inhibitors against human melanoma is mediated by inhibition of tumor acidity. *Int J Cancer* 127(1)**:** 207-219.

72. Robey, I.F., Baggett, B.K., Kirkpatrick, N.D., Roe, D.J., Dosescu, J., Sloane, B.F., Hashim, A.I., Morse, D.L., Raghunand, N., Gatenby, R.A. and Gillies, R.J. (2009). Bicarbonate increases tumor pH and inhibits spontaneous metastases. *Cancer Res* 69(6)**:** 2260-2268.

73. Pilon-Thomas, S., Kodumudi, K.N., El-Kenawi, A.E., Russell, S., Weber, A.M., Luddy, K., Damaghi, M., Wojtkowiak, J.W., Mule, J.J., Ibrahim-Hashim, A. and Gillies, R.J. (2016). Neutralization of Tumor Acidity Improves Antitumor Responses to Immunotherapy. *Cancer Res* 76(6)**:** 1381-1390.

74. Fukumura, D., Xu, L., Chen, Y., Gohongi, T., Seed, B. and Jain, R.K. (2001). Hypoxia and acidosis independently up-regulate vascular endothelial growth factor transcription in brain tumors in vivo. *Cancer Res* 61(16)**:** 6020-6024.

75. Mazurek, S., Eigenbrodt, E., Failing, K. and Steinberg, P. (1999). Alterations in the glycolytic and glutaminolytic pathways after malignant transformation of rat liver oval cells. *J Cell Physiol* 181(1)**:** 136-146.

76. Wise, D.R., DeBerardinis, R.J., Mancuso, A., Sayed, N., Zhang, X.Y., Pfeiffer, H.K., Nissim, I., Daikhin, E., Yudkoff, M., McMahon, S.B. and Thompson, C.B. (2008). Myc regulates a transcriptional program that stimulates mitochondrial glutaminolysis and leads to glutamine addiction. *Proc Natl Acad Sci U S A* 105(48)**:** 18782-18787.

77. Aledo, J.C., Segura, J.A., Medina, M.A., Alonso, F.J., Nunez de Castro, I. and Marquez, J. (1994). Phosphate-activated glutaminase expression during tumor development. *FEBS Lett* 341(1)**:** 39-42.

78. Droge, W., Eck, H.P., Betzler, M. and Naher, H. (1987). Elevated plasma glutamate levels in colorectal carcinoma patients and in patients with acquired immunodeficiency syndrome (AIDS). *Immunobiology* 174(4-5)**:** 473-479.

79. Prendergast, G.C. (2011). Cancer: Why tumours eat tryptophan. *Nature* 478(7368)**:** 192-194.

80. Uyttenhove, C., Pilotte, L., Theate, I., Stroobant, V., Colau, D., Parmentier, N., Boon, T. and Van den Eynde, B.J. (2003). Evidence for a tumoral immune resistance mechanism based on tryptophan degradation by indoleamine 2,3-dioxygenase. *Nat Med* 9(10)**:** 1269-1274.

81. Lob, S., Konigsrainer, A., Zieker, D., Brucher, B.L., Rammensee, H.G., Opelz, G. and Terness, P. (2009). IDO1 and IDO2 are expressed in human tumors: levo- but not dextro-1-methyl tryptophan inhibits tryptophan catabolism. *Cancer Immunol Immunother* 58(1)**:** 153-157.

82. Weinlich, G., Murr, C., Richardsen, L., Winkler, C. and Fuchs, D. (2007). Decreased serum tryptophan concentration predicts poor prognosis in malignant melanoma patients. *Dermatology* 214(1)**:** 8-14.

83. Brandacher, G., Perathoner, A., Ladurner, R., Schneeberger, S., Obrist, P., Winkler, C., Werner, E.R., Werner-Felmayer, G., Weiss, H.G., Gobel, G., Margreiter, R., Konigsrainer, A., Fuchs, D. and Amberger, A. (2006). Prognostic value of indoleamine 2,3-dioxygenase expression in colorectal cancer: effect on tumor-infiltrating T cells. *Clin Cancer Res* 12(4)**:** 1144-1151.

84. Grohmann, U., Fallarino, F. and Puccetti, P. (2003). Tolerance, DCs and tryptophan: much ado about IDO. *Trends Immunol* 24(5)**:** 242-248.

85. Opitz, C.A., Litzenburger, U.M., Sahm, F., Ott, M., Tritschler, I., Trump, S., Schumacher, T., Jestaedt, L., Schrenk, D., Weller, M., Jugold, M., Guillemin, G.J., Miller, C.L., Lutz, C., Radlwimmer, B., Lehmann, I., von Deimling, A., Wick, W. and Platten, M. (2011). An endogenous tumour-promoting ligand of the human aryl hydrocarbon receptor. *Nature* 478(7368)**:** 197-203.

86. Qian, F., Villella, J., Wallace, P.K., Mhawech-Fauceglia, P., Tario, J.D., Jr., Andrews, C., Matsuzaki, J., Valmori, D., Ayyoub, M., Frederick, P.J., Beck, A., Liao, J., Cheney, R., Moysich, K., Lele, S., Shrikant, P., Old, L.J. and Odunsi, K. (2009). Efficacy of levo-1-methyl tryptophan and dextro-1-methyl tryptophan in reversing indoleamine-2,3-dioxygenase-mediated arrest of T-cell proliferation in human epithelial ovarian cancer. *Cancer Res* 69(13)**:** 5498-5504.

87. Zheng, X., Koropatnick, J., Li, M., Zhang, X., Ling, F., Ren, X., Hao, X., Sun, H., Vladau, C., Franek, J.A., Feng, B., Urquhart, B.L., Zhong, R., Freeman, D.J., Garcia, B. and Min, W.P. (2006). Reinstalling antitumor immunity by inhibiting tumor-derived immunosuppressive molecule IDO through RNA interference. *J Immunol* 177(8)**:** 5639-5646.

88. Yen, M.C., Lin, C.C., Chen, Y.L., Huang, S.S., Yang, H.J., Chang, C.P., Lei, H.Y. and Lai, M.D. (2009). A novel cancer therapy by skin delivery of indoleamine 2,3-dioxygenase siRNA. *Clin Cancer Res* 15(2)**:** 641-649.

89. Muller, A.J., DuHadaway, J.B., Donover, P.S., Sutanto-Ward, E. and Prendergast, G.C. (2005). Inhibition of indoleamine 2,3-dioxygenase, an immunoregulatory target of the cancer suppression gene Bin1, potentiates cancer chemotherapy. *Nat Med* 11(3)**:** 312-319.

90. Wu, G. and Morris, S.M., Jr. (1998). Arginine metabolism: nitric oxide and beyond. *Biochem J* 336 (Pt 1)**:** 1-17.

91. Munder, M., Mollinedo, F., Calafat, J., Canchado, J., Gil-Lamaignere, C., Fuentes, J.M., Luckner, C., Doschko, G., Soler, G., Eichmann, K., Muller, F.M., Ho, A.D., Goerner, M. and Modolell, M. (2005). Arginase I is constitutively expressed in human granulocytes and participates in fungicidal activity. *Blood* 105(6)**:** 2549-2556.

92. Cederbaum, S.D., Yu, H., Grody, W.W., Kern, R.M., Yoo, P. and Iyer, R.K. (2004). Arginases I and II: do their functions overlap? *Mol Genet Metab* 81 Suppl 1**:** S38-44.

93. Bronte, V. and Zanovello, P. (2005). Regulation of immune responses by L-arginine metabolism. *Nat Rev Immunol* 5(8)**:** 641-654.

94. Nathan, C. (1992). Nitric oxide as a secretory product of mammalian cells. *Faseb j* 6(12)**:** 3051-3064.

95. Bogdan, C. (2001). Nitric oxide and the immune response. *Nat Immunol* 2(10)**:** 907-916.

96. Xu, W., Liu, L., Smith, G.C. and Charles l, G. (2000). Nitric oxide upregulates expression of DNA-PKcs to protect cells from DNA-damaging anti-tumour agents. *Nat Cell Biol* 2(6)**:** 339-345.

97. Warner, T.D. and Mitchell, J.A. (2004). Cyclooxygenases: new forms, new inhibitors, and lessons from the clinic. *Faseb j* 18(7)**:** 790-804.

98. Denkert, C., Weichert, W., Winzer, K.J., Muller, B.M., Noske, A., Niesporek, S., Kristiansen, G., Guski, H., Dietel, M. and Hauptmann, S. (2004). Expression of the ELAV-like protein HuR is associated with higher tumor grade and increased cyclooxygenase-2 expression in human breast carcinoma. *Clin Cancer Res* 10(16)**:** 5580-5586.

99. Kaidi, A., Qualtrough, D., Williams, A.C. and Paraskeva, C. (2006). Direct transcriptional up-regulation of cyclooxygenase-2 by hypoxia-inducible factor (HIF)-1 promotes colorectal tumor cell survival and enhances HIF-1 transcriptional activity during hypoxia. *Cancer Res* 66(13)**:** 6683-6691.

100. Masferrer, J.L., Leahy, K.M., Koki, A.T., Zweifel, B.S., Settle, S.L., Woerner, B.M., Edwards, D.A., Flickinger, A.G., Moore, R.J. and Seibert, K. (2000). Antiangiogenic and antitumor activities of cyclooxygenase-2 inhibitors. *Cancer Res* 60(5)**:** 1306-1311.

101. Kundu, N. and Fulton, A.M. (2002). Selective cyclooxygenase (COX)-1 or COX-2 inhibitors control metastatic disease in a murine model of breast cancer. *Cancer Res* 62(8)**:** 2343-2346.

102. Rodriguez, P.C., Hernandez, C.P., Quiceno, D., Dubinett, S.M., Zabaleta, J., Ochoa, J.B., Gilbert, J. and Ochoa, A.C. (2005). Arginase I in myeloid suppressor cells is induced by COX-2 in lung carcinoma. *J Exp Med* 202(7)**:** 931-939.

103. Fujita, M., Kohanbash, G., Fellows-Mayle, W., Hamilton, R.L., Komohara, Y., Decker, S.A., Ohlfest, J.R. and Okada, H. (2011). COX-2 blockade suppresses gliomagenesis by inhibiting myeloid-derived suppressor cells. *Cancer Res* 71(7)**:** 2664-2674.

104. Veltman, J.D., Lambers, M.E., van Nimwegen, M., Hendriks, R.W., Hoogsteden, H.C., Aerts, J.G. and Hegmans, J.P. (2010). COX-2 inhibition improves immunotherapy and is associated with decreased numbers of myeloid-derived suppressor cells in mesothelioma. Celecoxib influences MDSC function. *BMC Cancer* 10**:** 464.

105. Virchow, R. *Cellular pathology as based upon physiological and pathological histology*. Philadelphia: J. B. Lippincott, 1863.

106. Karin, M. (2006). Nuclear factor-kappaB in cancer development and progression. *Nature* 441(7092)**:** 431-436.

107. Aggarwal, B.B., Vijayalekshmi, R.V. and Sung, B. (2009). Targeting inflammatory pathways for prevention and therapy of cancer: short-term friend, long-term foe. *Clin Cancer Res* 15(2)**:** 425-430.

108. Nickoloff, B.J., Ben-Neriah, Y. and Pikarsky, E. (2005). Inflammation and cancer: is the link as simple as we think? *J Invest Dermatol* 124(6)**:** x-xiv.

109. Mantovani, A., Allavena, P., Sica, A. and Balkwill, F. (2008). Cancer-related inflammation. *Nature* 454(7203)**:** 436-444.

110. de Visser, K.E., Eichten, A. and Coussens, L.M. (2006). Paradoxical roles of the immune system during cancer development. *Nat Rev Cancer* 6(1)**:** 24-37.

111. Lin, W.W. and Karin, M. (2007). A cytokine-mediated link between innate immunity, inflammation, and cancer. *J Clin Invest* 117(5)**:** 1175-1183.

112. Muenst, S., Laubli, H., Soysal, S.D., Zippelius, A., Tzankov, A. and Hoeller, S. (2016). The immune system and cancer evasion strategies: therapeutic concepts. *J Intern Med*.

113. Mapara, M.Y. and Sykes, M. (2004). Tolerance and cancer: mechanisms of tumor evasion and strategies for breaking tolerance. *J Clin Oncol* 22(6)**:** 1136-1151.

114. Koebel, C.M., Vermi, W., Swann, J.B., Zerafa, N., Rodig, S.J., Old, L.J., Smyth, M.J. and Schreiber, R.D. (2007). Adaptive immunity maintains occult cancer in an equilibrium state. *Nature* 450(7171)**:** 903-907.

115. Teng, M.W., Galon, J., Fridman, W.H. and Smyth, M.J. (2015). From mice to humans: developments in cancer immunoediting. *J Clin Invest* 125(9)**:** 3338-3346.

116. Schreiber, R.D., Old, L.J. and Smyth, M.J. (2011). Cancer immunoediting: integrating immunity's roles in cancer suppression and promotion. *Science* 331(6024)**:** 1565-1570.

117. Qian, B.Z., Li, J., Zhang, H., Kitamura, T., Zhang, J., Campion, L.R., Kaiser, E.A., Snyder, L.A. and Pollard, J.W. (2011). CCL2 recruits inflammatory monocytes to facilitate breast-tumour metastasis. *Nature* 475(7355)**:** 222-225.

118. Murdoch, C., Giannoudis, A. and Lewis, C.E. (2004). Mechanisms regulating the recruitment of macrophages into hypoxic areas of tumors and other ischemic tissues. *Blood* 104(8)**:** 2224-2234.

119. Condeelis, J. and Pollard, J.W. (2006). Macrophages: obligate partners for tumor cell migration, invasion, and metastasis. *Cell* 124(2)**:** 263-266.

120. Murdoch, C., Muthana, M., Coffelt, S.B. and Lewis, C.E. (2008). The role of myeloid cells in the promotion of tumour angiogenesis. *Nat Rev Cancer* 8(8)**:** 618-631.

121. Sica, A., Allavena, P. and Mantovani, A. (2008). Cancer related inflammation: the macrophage connection. *Cancer Lett* 267(2)**:** 204-215.

122. Biswas, S.K. and Mantovani, A. (2010). Macrophage plasticity and interaction with lymphocyte subsets: cancer as a paradigm. *Nat Immunol* 11(10)**:** 889-896.

123. Bronte, V., Serafini, P., Mazzoni, A., Segal, D.M. and Zanovello, P. (2003). L-arginine metabolism in myeloid cells controls T-lymphocyte functions. *Trends Immunol* 24(6)**:** 302-306.

124. Sica, A. and Bronte, V. (2007). Altered macrophage differentiation and immune dysfunction in tumor development. *J Clin Invest* 117(5)**:** 1155-1166.

125. Rodriguez, P.C., Zea, A.H., DeSalvo, J., Culotta, K.S., Zabaleta, J., Quiceno, D.G., Ochoa, J.B. and Ochoa, A.C. (2003). L-arginine consumption by macrophages modulates the expression of CD3 zeta chain in T lymphocytes. *J Immunol* 171(3)**:** 1232-1239.

126. Nagaraj, S., Gupta, K., Pisarev, V., Kinarsky, L., Sherman, S., Kang, L., Herber, D.L., Schneck, J. and Gabrilovich, D.I. (2007). Altered recognition of antigen is a mechanism of CD8+ T cell tolerance in cancer. *Nat Med* 13(7)**:** 828-835.

127. Gabrilovich, D.I., Ostrand-Rosenberg, S. and Bronte, V. (2012). Coordinated regulation of myeloid cells by tumours. *Nat Rev Immunol* 12(4)**:** 253-268.

128. Lesokhin, A.M., Hohl, T.M., Kitano, S., Cortez, C., Hirschhorn-Cymerman, D., Avogadri, F., Rizzuto, G.A., Lazarus, J.J., Pamer, E.G., Houghton, A.N., Merghoub, T. and Wolchok, J.D. (2012). Monocytic CCR2(+) myeloid-derived suppressor cells promote immune escape by limiting activated CD8 T-cell infiltration into the tumor microenvironment. *Cancer Res* 72(4)**:** 876-886.

129. da Cunha, A., Michelin, M.A. and Murta, E.F. (2014). Pattern response of dendritic cells in the tumor microenvironment and breast cancer. *World J Clin Oncol* 5(3)**:** 495-502.

130. Vitale, M., Cantoni, C., Pietra, G., Mingari, M.C. and Moretta, L. (2014). Effect of tumor cells and tumor microenvironment on NK-cell function. *Eur J Immunol* 44(6)**:** 1582-1592.

131. Fainaru, O., Almog, N., Yung, C.W., Nakai, K., Montoya-Zavala, M., Abdollahi, A., D'Amato, R. and Ingber, D.E. (2010). Tumor growth and angiogenesis are dependent on the presence of immature dendritic cells. *Faseb j* 24(5)**:** 1411-1418.

132. Benencia, F., Muccioli, M. and Alnaeeli, M. (2014). Perspectives on reprograming cancer-associated dendritic cells for anti-tumor therapies. *Front Oncol* 4**:** 72.

133. Tel, J., Anguille, S., Waterborg, C.E., Smits, E.L., Figdor, C.G. and de Vries, I.J. (2014). Tumoricidal activity of human dendritic cells. *Trends Immunol* 35(1)**:** 38-46.

134. Gross, E., Sunwoo, J.B. and Bui, J.D. (2013). Cancer immunosurveillance and immunoediting by natural killer cells. *Cancer J* 19(6)**:** 483-489.

135. Bruno, A., Ferlazzo, G., Albini, A. and Noonan, D.M. (2014). A think tank of TINK/TANKs: tumor-infiltrating/tumor-associated natural killer cells in tumor progression and angiogenesis. *J Natl Cancer Inst* 106(8)**:** dju200.

136. Matta, J., Baratin, M., Chiche, L., Forel, J.M., Cognet, C., Thomas, G., Farnarier, C., Piperoglou, C., Papazian, L., Chaussabel, D., Ugolini, S., Vely, F. and Vivier, E. (2013). Induction of B7-H6, a ligand for the natural killer cell-activating receptor NKp30, in inflammatory conditions. *Blood* 122(3)**:** 394-404.

137. Moretta, L., Montaldo, E., Vacca, P., Del Zotto, G., Moretta, F., Merli, P., Locatelli, F. and Mingari, M.C. (2014). Human natural killer cells: origin, receptors, function, and clinical applications. *Int Arch Allergy Immunol* 164(4)**:** 253-264.

138. Burke, S., Lakshmikanth, T., Colucci, F. and Carbone, E. (2010). New views on natural killer cell-based immunotherapy for melanoma treatment. *Trends Immunol* 31(9)**:** 339-345.

139. Larsen, S.K., Gao, Y. and Basse, P.H. (2014). NK cells in the tumor microenvironment. *Crit Rev Oncog* 19(1-2)**:** 91-105.

140. Sconocchia, G., Spagnoli, G.C., Del Principe, D., Ferrone, S., Anselmi, M., Wongsena, W., Cervelli, V., Schultz-Thater, E., Wyler, S., Carafa, V., Moch, H., Terracciano, L. and Tornillo, L. (2009). Defective infiltration of natural killer cells in MICA/B-positive renal cell carcinoma involves beta(2)-integrin-mediated interaction. *Neoplasia* 11(7)**:** 662-671.

141. Mamessier, E., Sylvain, A., Thibult, M.L., Houvenaeghel, G., Jacquemier, J., Castellano, R., Goncalves, A., Andre, P., Romagne, F., Thibault, G., Viens, P., Birnbaum, D., Bertucci, F., Moretta, A. and Olive, D. (2011). Human breast cancer cells enhance self tolerance by promoting evasion from NK cell antitumor immunity. *J Clin Invest* 121(9)**:** 3609-3622.

142. Balsamo, M., Vermi, W., Parodi, M., Pietra, G., Manzini, C., Queirolo, P., Lonardi, S., Augugliaro, R., Moretta, A., Facchetti, F., Moretta, L., Mingari, M.C. and Vitale, M. (2012). Melanoma cells become resistant to NK-cell-mediated killing when exposed to NK-cell numbers compatible with NK-cell infiltration in the tumor. *Eur J Immunol* 42(7)**:** 1833-1842.

143. Sconocchia, G., Arriga, R., Tornillo, L., Terracciano, L., Ferrone, S. and Spagnoli, G.C. (2012). Melanoma cells inhibit NK cell functions. *Cancer Res* 72(20)**:** 5428-5429; author reply 5430.

144. Balsamo, M., Manzini, C., Pietra, G., Raggi, F., Blengio, F., Mingari, M.C., Varesio, L., Moretta, L., Bosco, M.C. and Vitale, M. (2013). Hypoxia downregulates the expression of activating receptors involved in NK-cell-mediated target cell killing without affecting ADCC. *Eur J Immunol* 43(10)**:** 2756-2764.

145. Sungur, C.M. and Murphy, W.J. (2014). Positive and negative regulation by NK cells in cancer. *Crit Rev Oncog* 19(1-2)**:** 57-66.

146. Dong, H.P., Elstrand, M.B., Holth, A., Silins, I., Berner, A., Trope, C.G., Davidson, B. and Risberg, B. (2006). NK- and B-cell infiltration correlates with worse outcome in metastatic ovarian carcinoma. *Am J Clin Pathol* 125(3)**:** 451-458.

147. Rathore, A.S., Goel, M.M., Makker, A., Kumar, S. and Srivastava, A.N. (2014). Is the tumor infiltrating natural killer cell (NK-TILs) count in infiltrating ductal carcinoma of breast prognostically significant? *Asian Pac J Cancer Prev* 15(8)**:** 3757-3761.

148. Chavez-Galan, L., Arenas-Del Angel, M.C., Zenteno, E., Chavez, R. and Lascurain, R. (2009). Cell death mechanisms induced by cytotoxic lymphocytes. *Cell Mol Immunol* 6(1)**:** 15-25.

149. Bachmayr-Heyda, A., Aust, S., Heinze, G., Polterauer, S., Grimm, C., Braicu, E.I., Sehouli, J., Lambrechts, S., Vergote, I., Mahner, S., Pils, D., Schuster, E., Thalhammer, T., Horvat, R., Denkert, C., Zeillinger, R. and Castillo-Tong, D.C. (2013). Prognostic impact of tumor infiltrating CD8+ T cells in association with cell proliferation in ovarian cancer patients--a study of the OVCAD consortium. *BMC Cancer* 13**:** 422.

150. Clemente, C.G., Mihm, M.C., Jr., Bufalino, R., Zurrida, S., Collini, P. and Cascinelli, N. (1996). Prognostic value of tumor infiltrating lymphocytes in the vertical growth phase of primary cutaneous melanoma. *Cancer* 77(7)**:** 1303-1310.

151. Prall, F., Duhrkop, T., Weirich, V., Ostwald, C., Lenz, P., Nizze, H. and Barten, M. (2004). Prognostic role of CD8+ tumor-infiltrating lymphocytes in stage III colorectal cancer with and without microsatellite instability. *Hum Pathol* 35(7)**:** 808-816.

152. Mahmoud, S.M., Paish, E.C., Powe, D.G., Macmillan, R.D., Grainge, M.J., Lee, A.H., Ellis, I.O. and Green, A.R. (2011). Tumor-infiltrating CD8+ lymphocytes predict clinical outcome in breast cancer. *J Clin Oncol* 29(15)**:** 1949-1955.

153. Manzo, T., Heslop, H.E. and Rooney, C.M. (2015). Antigen-specific T cell therapies for cancer. *Hum Mol Genet* 24(R1)**:** R67-73.

154. Brown, S.D., Warren, R.L., Gibb, E.A., Martin, S.D., Spinelli, J.J., Nelson, B.H. and Holt, R.A. (2014). Neo-antigens predicted by tumor genome meta-analysis correlate with increased patient survival. *Genome Res* 24(5)**:** 743-750.

155. Rosenberg, S.A. and Restifo, N.P. (2015). Adoptive cell transfer as personalized immunotherapy for human cancer. *Science* 348(6230)**:** 62-68.

156. Savage, P.A., Leventhal, D.S. and Malchow, S. (2014). Shaping the repertoire of tumor-infiltrating effector and regulatory T cells. *Immunol Rev* 259(1)**:** 245-258.

157. Vesely, M.D., Kershaw, M.H., Schreiber, R.D. and Smyth, M.J. (2011). Natural innate and adaptive immunity to cancer. *Annu Rev Immunol* 29**:** 235-271.

158. Ruffell, B., DeNardo, D.G., Affara, N.I. and Coussens, L.M. (2010). Lymphocytes in cancer development: polarization towards pro-tumor immunity. *Cytokine Growth Factor Rev* 21(1)**:** 3-10.

159. Grivennikov, S.I., Greten, F.R. and Karin, M. (2010). Immunity, inflammation, and cancer. *Cell* 140(6)**:** 883-899.

160. Lippitz, B.E. (2013). Cytokine patterns in patients with cancer: a systematic review. *Lancet Oncol* 14(6)**:** e218-228.

161. Nelson, B.H. (2004). IL-2, regulatory T cells, and tolerance. *J Immunol* 172(7)**:** 3983-3988.

162. Fehniger, T.A., Cooper, M.A., Nuovo, G.J., Cella, M., Facchetti, F., Colonna, M. and Caligiuri, M.A. (2003). CD56bright natural killer cells are present in human lymph nodes and are activated by T cell-derived IL-2: a potential new link between adaptive and innate immunity. *Blood* 101(8)**:** 3052-3057.

163. Trinchieri, G. (1995). Interleukin-12: a proinflammatory cytokine with immunoregulatory functions that bridge innate resistance and antigen-specific adaptive immunity. *Annu Rev Immunol* 13**:** 251-276.

164. Beatty, G.L. and Paterson, Y. (2001). Regulation of tumor growth by IFN-gamma in cancer immunotherapy. *Immunol Res* 24(2)**:** 201-210.

165. Schuett, H., Luchtefeld, M., Grothusen, C., Grote, K. and Schieffer, B. (2009). How much is too much? Interleukin-6 and its signalling in atherosclerosis. *Thromb Haemost* 102(2)**:** 215-222.

166. Romano, M., Sironi, M., Toniatti, C., Polentarutti, N., Fruscella, P., Ghezzi, P., Faggioni, R., Luini, W., van Hinsbergh, V., Sozzani, S., Bussolino, F., Poli, V., Ciliberto, G. and Mantovani, A. (1997). Role of IL-6 and its soluble receptor in induction of chemokines and leukocyte recruitment. *Immunity* 6(3)**:** 315-325.

167. Bettelli, E., Carrier, Y., Gao, W., Korn, T., Strom, T.B., Oukka, M., Weiner, H.L. and Kuchroo, V.K. (2006). Reciprocal developmental pathways for the generation of pathogenic effector TH17 and regulatory T cells. *Nature* 441(7090)**:** 235-238.

168. Mocellin, S., Marincola, F.M. and Young, H.A. (2005). Interleukin-10 and the immune response against cancer: a counterpoint. *J Leukoc Biol* 78(5)**:** 1043-1051.

169. Mosser, D.M. and Zhang, X. (2008). Interleukin-10: new perspectives on an old cytokine. *Immunol Rev* 226**:** 205-218.

170. Singer, K., Kastenberger, M., Gottfried, E., Hammerschmied, C.G., Buttner, M., Aigner, M., Seliger, B., Walter, B., Schlosser, H., Hartmann, A., Andreesen, R., Mackensen, A. and Kreutz, M. (2011). Warburg phenotype in renal cell carcinoma: high expression of glucose-transporter 1 (GLUT-1) correlates with low CD8(+) T-cell infiltration in the tumor. *Int J Cancer* 128(9)**:** 2085-2095.

171. Ho, P.C., Bihuniak, J.D., Macintyre, A.N., Staron, M., Liu, X., Amezquita, R., Tsui, Y.C., Cui, G., Micevic, G., Perales, J.C., Kleinstein, S.H., Abel, E.D., Insogna, K.L., Feske, S., Locasale, J.W., Bosenberg, M.W., Rathmell, J.C. and Kaech, S.M. (2015). Phosphoenolpyruvate Is a Metabolic Checkpoint of Anti-tumor T Cell Responses. *Cell* 162(6)**:** 1217-1228.

172. Chang, C.H., Qiu, J., O'Sullivan, D., Buck, M.D., Noguchi, T., Curtis, J.D., Chen, Q., Gindin, M., Gubin, M.M., van der Windt, G.J., Tonc, E., Schreiber, R.D., Pearce, E.J. and Pearce, E.L. (2015). Metabolic Competition in the Tumor Microenvironment Is a Driver of Cancer Progression. *Cell* 162(6)**:** 1229-1241.

173. Gottfried, E., Kreutz, M. and Mackensen, A. (2012). Tumor metabolism as modulator of immune response and tumor progression. *Semin Cancer Biol* 22(4)**:** 335-341.

174. Gottfried, E., Kunz-Schughart, L.A., Ebner, S., Mueller-Klieser, W., Hoves, S., Andreesen, R., Mackensen, A. and Kreutz, M. (2006). Tumor-derived lactic acid modulates dendritic cell activation and antigen expression. *Blood* 107(5)**:** 2013-2021.

175. Puig-Kroger, A., Pello, O.M., Selgas, R., Criado, G., Bajo, M.A., Sanchez-Tomero, J.A., Alvarez, V., del Peso, G., Sanchez-Mateos, P., Holmes, C., Faict, D., Lopez-Cabrera, M., Madrenas, J. and Corbi, A.L. (2003). Peritoneal dialysis solutions inhibit the differentiation and maturation of human monocyte-derived dendritic cells: effect of lactate and glucose-degradation products. *J Leukoc Biol* 73(4)**:** 482-492.

176. Dietl, K., Renner, K., Dettmer, K., Timischl, B., Eberhart, K., Dorn, C., Hellerbrand, C., Kastenberger, M., Kunz-Schughart, L.A., Oefner, P.J., Andreesen, R., Gottfried, E. and Kreutz, M.P. (2010). Lactic acid and acidification inhibit TNF secretion and glycolysis of human monocytes. *J Immunol* 184(3)**:** 1200-1209.

177. Fischer, K., Hoffmann, P., Voelkl, S., Meidenbauer, N., Ammer, J., Edinger, M., Gottfried, E., Schwarz, S., Rothe, G., Hoves, S., Renner, K., Timischl, B., Mackensen, A., Kunz-Schughart, L., Andreesen, R., Krause, S.W. and Kreutz, M. (2007). Inhibitory effect of tumor cell-derived lactic acid on human T cells. *Blood* 109(9)**:** 3812-3819.

178. Mendler, A.N., Hu, B., Prinz, P.U., Kreutz, M., Gottfried, E. and Noessner, E. (2012). Tumor lactic acidosis suppresses CTL function by inhibition of p38 and JNK/c-Jun activation. *Int J Cancer* 131(3)**:** 633-640.

179. Shime, H., Yabu, M., Akazawa, T., Kodama, K., Matsumoto, M., Seya, T. and Inoue, N. (2008). Tumor-secreted lactic acid promotes IL-23/IL-17 proinflammatory pathway. *J Immunol* 180(11)**:** 7175-7183.

180. Husain, Z., Huang, Y., Seth, P. and Sukhatme, V.P. (2013). Tumor-derived lactate modifies antitumor immune response: effect on myeloid-derived suppressor cells and NK cells. *J Immunol* 191(3)**:** 1486-1495.

181. Colegio, O.R., Chu, N.Q., Szabo, A.L., Chu, T., Rhebergen, A.M., Jairam, V., Cyrus, N., Brokowski, C.E., Eisenbarth, S.C., Phillips, G.M., Cline, G.W., Phillips, A.J. and Medzhitov, R. (2014). Functional polarization of tumour-associated macrophages by tumour-derived lactic acid. *Nature* 513(7519)**:** 559-563.

182. Spiotto, M.T., Yu, P., Rowley, D.A., Nishimura, M.I., Meredith, S.C., Gajewski, T.F., Fu, Y.X. and Schreiber, H. (2002). Increasing tumor antigen expression overcomes "ignorance" to solid tumors via crosspresentation by bone marrow-derived stromal cells. *Immunity* 17(6)**:** 737-747.

183. Kastenberger, M. (2012). Analyse und Modulation des Tumormetabolismus in humanen Tumorzelllinien und Tumorgeweben. Universität Regensburg.

184. Walenta, S., Schroeder, T. and Mueller-Klieser, W. (2002). Metabolic mapping with bioluminescence: basic and clinical relevance. *Biomol Eng* 18(6)**:** 249-262.

185. Walenta, S. and Mueller-Klieser, W.F. (2004). Lactate: mirror and motor of tumor malignancy. *Semin Radiat Oncol* 14(3)**:** 267-274.

186. Gaj, T., Gersbach, C.A. and Barbas, C.F., 3rd. (2013). ZFN, TALEN, and CRISPR/Cas-based methods for genome engineering. *Trends Biotechnol* 31(7)**:** 397-405.

187. Marchiq, I., Le Floch, R., Roux, D., Simon, M.P. and Pouyssegur, J. (2015). Genetic disruption of lactate/H+ symporters (MCTs) and their subunit CD147/BASIGIN sensitizes glycolytic tumor cells to phenformin. *Cancer Res* 75(1)**:** 171-180.

188. Feder-Mengus, C., Ghosh, S., Weber, W.P., Wyler, S., Zajac, P., Terracciano, L., Oertli, D., Heberer, M., Martin, I., Spagnoli, G.C. and Reschner, A. (2007). Multiple mechanisms underlie defective recognition of melanoma cells cultured in three-dimensional architectures by antigen-specific cytotoxic T lymphocytes. *Br J Cancer* 96(7)**:** 1072-1082.

189. Haas, R., Smith, J., Rocher-Ros, V., Nadkarni, S., Montero-Melendez, T., D'Acquisto, F., Bland, E.J., Bombardieri, M., Pitzalis, C., Perretti, M., Marelli-Berg, F.M. and Mauro, C. (2015). Lactate Regulates Metabolic and Pro-inflammatory Circuits in Control of T Cell Migration and Effector Functions. *PLoS Biol* 13(7)**:** e1002202.

190. Kaplon, J., van Dam, L. and Peeper, D. (2015). Two-way communication between the metabolic and cell cycle machineries: the molecular basis. *Cell Cycle* 14(13)**:** 2022-2032.

191. Wang, D. and Dubois, R.N. (2010). Eicosanoids and cancer. *Nat Rev Cancer* 10(3)**:** 181-193.

192. Schoenborn, J.R. and Wilson, C.B. (2007). Regulation of interferon-gamma during innate and adaptive immune responses. *Adv Immunol* 96**:** 41-101.

193. Glimcher, L.H., Townsend, M.J., Sullivan, B.M. and Lord, G.M. (2004). Recent developments in the transcriptional regulation of cytolytic effector cells. *Nat Rev Immunol* 4(11)**:** 900-911.

194. Yan, J., Su, H., Xu, L. and Wang, C. (2013). OX40-OX40L interaction promotes proliferation and activation of lymphocytes via NFATc1 in ApoE-deficient mice. *PLoS One* 8(4)**:** e60854.

195. Hisamitsu, T., Nakamura, T.Y. and Wakabayashi, S. (2012). Na(+)/H(+) exchanger 1 directly binds to calcineurin A and activates downstream NFAT signaling, leading to cardiomyocyte hypertrophy. *Mol Cell Biol* 32(16)**:** 3265-3280.

196. Deichmann, M., Benner, A., Bock, M., Jackel, A., Uhl, K., Waldmann, V. and Naher, H. (1999). S100-Beta, melanoma-inhibiting activity, and lactate dehydrogenase discriminate progressive from nonprogressive American Joint Committee on Cancer stage IV melanoma. *J Clin Oncol* 17(6)**:** 1891-1896.

197. Doherty, J.R. and Cleveland, J.L. (2013). Targeting lactate metabolism for cancer therapeutics. *J Clin Invest* 123(9)**:** 3685-3692.

198. Vegran, F., Boidot, R., Michiels, C., Sonveaux, P. and Feron, O. (2011). Lactate influx through the endothelial cell monocarboxylate transporter MCT1 supports an NF-kappaB/IL-8 pathway that drives tumor angiogenesis. *Cancer Res* 71(7)**:** 2550-2560.

199. Lee, D.C., Sohn, H.A., Park, Z.Y., Oh, S., Kang, Y.K., Lee, K.M., Kang, M., Jang, Y.J., Yang, S.J., Hong, Y.K., Noh, H., Kim, J.A., Kim, D.J., Bae, K.H., Kim, D.M., Chung, S.J., Yoo, H.S., Yu, D.Y., Park, K.C. and Yeom, Y.I. (2015). A lactate-induced response to hypoxia. *Cell* 161(3)**:** 595-609.

200. Wang, R., Jaw, J.J., Stutzman, N.C., Zou, Z. and Sun, P.D. (2012). Natural killer cell-produced IFN-gamma and TNF-alpha induce target cell cytolysis through up-regulation of ICAM-1. *J Leukoc Biol* 91(2)**:** 299-309.

201. Yabu, M., Shime, H., Hara, H., Saito, T., Matsumoto, M., Seya, T., Akazawa, T. and Inoue, N. (2011). IL-23-dependent and -independent enhancement pathways of IL-17A production by lactic acid. *Int Immunol* 23(1)**:** 29-41.

202. Ohashi, T., Akazawa, T., Aoki, M., Kuze, B., Mizuta, K., Ito, Y. and Inoue, N. (2013). Dichloroacetate improves immune dysfunction caused by tumor-secreted lactic acid and increases antitumor immunoreactivity. *Int J Cancer* 133(5)**:** 1107-1118.

203. Xian, Z.Y., Liu, J.M., Chen, Q.K., Chen, H.Z., Ye, C.J., Xue, J., Yang, H.Q., Li, J.L., Liu, X.F. and Kuang, S.J. (2015). Inhibition of LDHA suppresses tumor progression in prostate cancer. *Tumour Biol*.

204. Li, J., Zhu, S., Tong, J., Hao, H., Yang, J., Liu, Z. and Wang, Y. (2016). Suppression of lactate dehydrogenase A compromises tumor progression by downregulation of the Warburg effect in glioblastoma. *Neuroreport* 27(2)**:** 110-115.

205. Schmid, S.A., Gaumann, A., Wondrak, M., Eckermann, C., Schulte, S., Mueller-Klieser, W., Wheatley, D.N. and Kunz-Schughart, L.A. (2007). Lactate adversely affects the in vitro formation of endothelial cell tubular structures through the action of TGF-beta1. *Exp Cell Res* 313(12)**:** 2531-2549.

206. Seliger, C., Leukel, P., Moeckel, S., Jachnik, B., Lottaz, C., Kreutz, M., Brawanski, A., Proescholdt, M., Bogdahn, U., Bosserhoff, A.K., Vollmann-Zwerenz, A. and Hau, P. (2013). Lactate-modulated induction of THBS-1 activates transforming growth factor (TGF)-beta2 and migration of glioma cells in vitro. *PLoS One* 8(11)**:** e78935.

207. Hodge, G., Barnawi, J., Jurisevic, C., Moffat, D., Holmes, M., Reynolds, P.N., Jersmann, H. and Hodge, S. (2014). Lung cancer is associated with decreased expression of perforin, granzyme B and interferon (IFN)-gamma by infiltrating lung tissue T cells, natural killer (NK) T-like and NK cells. *Clin Exp Immunol* 178(1)**:** 79-85.

208. Zelenay, S., van der Veen, A.G., Bottcher, J.P., Snelgrove, K.J., Rogers, N., Acton, S.E., Chakravarty, P., Girotti, M.R., Marais, R., Quezada, S.A., Sahai, E. and Reis e Sousa, C. (2015). Cyclooxygenase-Dependent Tumor Growth through Evasion of Immunity. *Cell* 162(6)**:** 1257-1270.

209. Crane, C.A., Austgen, K., Haberthur, K., Hofmann, C., Moyes, K.W., Avanesyan, L., Fong, L., Campbell, M.J., Cooper, S., Oakes, S.A., Parsa, A.T. and Lanier, L.L. (2014). Immune evasion mediated by tumor-derived lactate dehydrogenase induction of NKG2D ligands on myeloid cells in glioblastoma patients. *Proc Natl Acad Sci U S A* 111(35)**:** 12823-12828.

210. Lu, C., Vickers, M.F. and Kerbel, R.S. (1992). Interleukin 6: a fibroblast-derived growth inhibitor of human melanoma cells from early but not advanced stages of tumor progression. *Proc Natl Acad Sci U S A* 89(19)**:** 9215-9219.

211. Lu, C. and Kerbel, R.S. (1993). Interleukin-6 undergoes transition from paracrine growth inhibitor to autocrine stimulator during human melanoma progression. *J Cell Biol* 120(5)**:** 1281-1288.

212. Silvani, A., Ferrari, G., Paonessa, G., Toniatti, C., Parmiani, G. and Colombo, M.P. (1995). Down-regulation of interleukin 6 receptor alpha chain in interleukin 6 transduced melanoma cells causes selective resistance to interleukin 6 but not to oncostatin M. *Cancer Res* 55(10)**:** 2200-2205.

213. von Felbert, V., Cordoba, F., Weissenberger, J., Vallan, C., Kato, M., Nakashima, I., Braathen, L.R. and Weis, J. (2005). Interleukin-6 gene ablation in a transgenic mouse model of malignant skin melanoma. *Am J Pathol* 166(3)**:** 831-841.

214. Ammirante, M., Luo, J.L., Grivennikov, S., Nedospasov, S. and Karin, M. (2010). B-cell-derived lymphotoxin promotes castration-resistant prostate cancer. *Nature* 464(7286)**:** 302-305.

215. Andreu, P., Johansson, M., Affara, N.I., Pucci, F., Tan, T., Junankar, S., Korets, L., Lam, J., Tawfik, D., DeNardo, D.G., Naldini, L., de Visser, K.E., De Palma, M. and Coussens, L.M. (2010). FcRgamma activation regulates inflammation-associated squamous carcinogenesis. *Cancer Cell* 17(2)**:** 121-134.

216. Galon, J., Costes, A., Sanchez-Cabo, F., Kirilovsky, A., Mlecnik, B., Lagorce-Pages, C., Tosolini, M., Camus, M., Berger, A., Wind, P., Zinzindohoue, F., Bruneval, P., Cugnenc, P.H., Trajanoski, Z., Fridman, W.H. and Pages, F. (2006). Type, density, and location of immune cells within human colorectal tumors predict clinical outcome. *Science* 313(5795)**:** 1960-1964.

217. Haanen, J.B., Baars, A., Gomez, R., Weder, P., Smits, M., de Gruijl, T.D., von Blomberg, B.M., Bloemena, E., Scheper, R.J., van Ham, S.M., Pinedo, H.M. and van den Eertwegh, A.J. (2006). Melanoma-specific tumor-infiltrating lymphocytes but not circulating melanoma-specific T cells may predict survival in resected advanced-stage melanoma patients. *Cancer Immunol Immunother* 55(4)**:** 451-458.

218. Carmi, Y., Spitzer, M.H., Linde, I.L., Burt, B.M., Prestwood, T.R., Perlman, N., Davidson, M.G., Kenkel, J.A., Segal, E., Pusapati, G.V., Bhattacharya, N. and Engleman, E.G. (2015). Allogeneic IgG combined with dendritic cell stimuli induce antitumour T-cell immunity. *Nature* 521(7550)**:** 99-104.

219. Matsuda, A., Morita, H., Unno, H., Saito, H., Matsumoto, K., Hirao, Y., Munechika, K. and Abe, J. (2012). Anti-inflammatory effects of high-dose IgG on TNF-alpha-activated human coronary artery endothelial cells. *Eur J Immunol* 42(8)**:** 2121-2131.

220. Piccioli, D., Sbrana, S., Melandri, E. and Valiante, N.M. (2002). Contact-dependent stimulation and inhibition of dendritic cells by natural killer cells. *J Exp Med* 195(3)**:** 335-341.

221. Gerosa, F., Baldani-Guerra, B., Nisii, C., Marchesini, V., Carra, G. and Trinchieri, G. (2002). Reciprocal activating interaction between natural killer cells and dendritic cells. *J Exp Med* 195(3)**:** 327-333.

222. van den Broek, M.F., Kagi, D., Zinkernagel, R.M. and Hengartner, H. (1995). Perforin dependence of natural killer cell-mediated tumor control in vivo. *Eur J Immunol* 25(12)**:** 3514-3516.

223. van den Broek, M.E., Kagi, D., Ossendorp, F., Toes, R., Vamvakas, S., Lutz, W.K., Melief, C.J., Zinkernagel, R.M. and Hengartner, H. (1996). Decreased tumor surveillance in perforin-deficient mice. *J Exp Med* 184(5)**:** 1781-1790.

224. Smyth, M.J., Kelly, J.M., Baxter, A.G., Korner, H. and Sedgwick, J.D. (1998). An essential role for tumor necrosis factor in natural killer cell-mediated tumor rejection in the peritoneum. *J Exp Med* 188(9)**:** 1611-1619.

225. Smyth, M.J., Thia, K.Y., Cretney, E., Kelly, J.M., Snook, M.B., Forbes, C.A. and Scalzo, A.A. (1999). Perforin is a major contributor to NK cell control of tumor metastasis. *J Immunol* 162(11)**:** 6658-6662.

226. Seki, N., Brooks, A.D., Carter, C.R., Back, T.C., Parsoneault, E.M., Smyth, M.J., Wiltrout, R.H. and Sayers, T.J. (2002). Tumor-specific CTL kill murine renal cancer cells using both perforin and Fas ligand-mediated lysis in vitro, but cause tumor regression in vivo in the absence of perforin. *J Immunol* 168(7)**:** 3484-3492.

227. Hong, C., Lee, H., Oh, M., Kang, C.Y., Hong, S. and Park, S.H. (2006). CD4+ T cells in the absence of the CD8+ cytotoxic T cells are critical and sufficient for NKT cell-dependent tumor rejection. *J Immunol* 177(10)**:** 6747-6757.

228. Dunn, G.P., Koebel, C.M. and Schreiber, R.D. (2006). Interferons, immunity and cancer immunoediting. *Nat Rev Immunol* 6(11)**:** 836-848.

229. Taniguchi, T. (1997). Transcription factors IRF-1 and IRF-2: linking the immune responses and tumor suppression. *J Cell Physiol* 173(2)**:** 128-130.

230. Nozawa, H., Oda, E., Ueda, S., Tamura, G., Maesawa, C., Muto, T., Taniguchi, T. and Tanaka, N. (1998). Functionally inactivating point mutation in the tumor-suppressor IRF-1 gene identified in human gastric cancer. *Int J Cancer* 77(4)**:** 522-527.

231. Qin, Z., Schwartzkopff, J., Pradera, F., Kammertoens, T., Seliger, B., Pircher, H. and Blankenstein, T. (2003). A critical requirement of interferon gamma-mediated angiostasis for tumor rejection by CD8+ T cells. *Cancer Res* 63(14)**:** 4095-4100.

232. Kakuta, S., Tagawa, Y., Shibata, S., Nanno, M. and Iwakura, Y. (2002). Inhibition of B16 melanoma experimental metastasis by interferon-gamma through direct inhibition of cell proliferation and activation of antitumour host mechanisms. *Immunology* 105(1)**:** 92-100.

233. Wang, L., Wang, Y., Song, Z., Chu, J. and Qu, X. (2015). Deficiency of interferon-gamma or its receptor promotes colorectal cancer development. *J Interferon Cytokine Res* 35(4)**:** 273-280.

234. Medina-Echeverz, J., Haile, L.A., Zhao, F., Gamrekelashvili, J., Ma, C., Metais, J.Y., Dunbar, C.E., Kapoor, V., Manns, M.P., Korangy, F. and Greten, T.F. (2014). IFN-gamma regulates survival and function of tumor-induced CD11b+ Gr-1high myeloid derived suppressor cells by modulating the anti-apoptotic molecule Bcl2a1. *Eur J Immunol* 44(8)**:** 2457-2467.

235. Furuke, K., Shiraishi, M., Mostowski, H.S. and Bloom, E.T. (1999). Fas ligand induction in human NK cells is regulated by redox through a calcineurin-nuclear factors of activated T cell-dependent pathway. *J Immunol* 162(4)**:** 1988-1993.

236. Yip, S.S., Zhou, M., Joly, J., Snedecor, B., Shen, A. and Crawford, Y. (2014). Complete knockout of the lactate dehydrogenase A gene is lethal in pyruvate dehydrogenase kinase 1, 2, 3 down-regulated CHO cells. *Mol Biotechnol* 56(9)**:** 833-838.

237. Scott, D.A., Richardson, A.D., Filipp, F.V., Knutzen, C.A., Chiang, G.G., Ronai, Z.A., Osterman, A.L. and Smith, J.W. (2011). Comparative metabolic flux profiling of melanoma cell lines: beyond the Warburg effect. *J Biol Chem* 286(49)**:** 42626-42634.

238. Michaloglou, C., Vredeveld, L.C., Mooi, W.J. and Peeper, D.S. (2008). BRAF(E600) in benign and malignant human tumours. *Oncogene* 27(7)**:** 877-895.

239. Davies, H., Bignell, G.R., Cox, C., Stephens, P., Edkins, S., Clegg, S., Teague, J., Woffendin, H., Garnett, M.J., Bottomley, W., Davis, N., Dicks, E., Ewing, R., Floyd, Y., Gray, K., Hall, S., Hawes, R., Hughes, J., Kosmidou, V., Menzies, A., Mould, C., Parker, A., Stevens, C., Watt, S., Hooper, S., Wilson, R., Jayatilake, H., Gusterson, B.A., Cooper, C., Shipley, J., Hargrave, D., Pritchard-Jones, K., Maitland, N., Chenevix-Trench, G., Riggins, G.J., Bigner, D.D., Palmieri, G., Cossu, A., Flanagan, A., Nicholson, A., Ho, J.W., Leung, S.Y., Yuen, S.T., Weber, B.L., Seigler, H.F., Darrow, T.L., Paterson, H., Marais, R., Marshall, C.J., Wooster, R., Stratton, M.R. and Futreal, P.A. (2002). Mutations of the BRAF gene in human cancer. *Nature* 417(6892)**:** 949-954.

240. Hall, A., Meyle, K.D., Lange, M.K., Klima, M., Sanderhoff, M., Dahl, C., Abildgaard, C., Thorup, K., Moghimi, S.M., Jensen, P.B., Bartek, J., Guldberg, P. and Christensen, C. (2013). Dysfunctional oxidative phosphorylation makes malignant melanoma cells addicted to glycolysis driven by the (V600E)BRAF oncogene. *Oncotarget* 4(4)**:** 584-599.

241. Chapman, P.B., Hauschild, A., Robert, C., Haanen, J.B., Ascierto, P., Larkin, J., Dummer, R., Garbe, C., Testori, A., Maio, M., Hogg, D., Lorigan, P., Lebbe, C., Jouary, T., Schadendorf, D., Ribas, A., O'Day, S.J., Sosman, J.A., Kirkwood, J.M., Eggermont, A.M., Dreno, B., Nolop, K., Li, J., Nelson, B., Hou, J., Lee, R.J., Flaherty, K.T. and McArthur, G.A. (2011). Improved survival with vemurafenib in melanoma with BRAF V600E mutation. *N Engl J Med* 364(26)**:** 2507-2516.

242. Dudley, M.E., Wunderlich, J.R., Yang, J.C., Sherry, R.M., Topalian, S.L., Restifo, N.P., Royal, R.E., Kammula, U., White, D.E., Mavroukakis, S.A., Rogers, L.J., Gracia, G.J., Jones, S.A., Mangiameli, D.P., Pelletier, M.M., Gea-Banacloche, J., Robinson, M.R., Berman, D.M., Filie, A.C., Abati, A. and Rosenberg, S.A. (2005). Adoptive cell transfer therapy following non-myeloablative but lymphodepleting chemotherapy for the treatment of patients with refractory metastatic melanoma. *J Clin Oncol* 23(10)**:** 2346-2357.

243. Parkhurst, M.R., Joo, J., Riley, J.P., Yu, Z., Li, Y., Robbins, P.F. and Rosenberg, S.A. (2009). Characterization of genetically modified T-cell receptors that recognize the CEA:691-699 peptide in the context of HLA-A2.1 on human colorectal cancer cells. *Clin Cancer Res* 15(1)**:** 169-180.

244. Parkhurst, M.R., Yang, J.C., Langan, R.C., Dudley, M.E., Nathan, D.A., Feldman, S.A., Davis, J.L., Morgan, R.A., Merino, M.J., Sherry, R.M., Hughes, M.S., Kammula, U.S., Phan, G.Q., Lim, R.M., Wank, S.A., Restifo, N.P., Robbins, P.F., Laurencot, C.M. and Rosenberg, S.A. (2011). T cells targeting carcinoembryonic antigen can mediate regression of metastatic colorectal cancer but induce severe transient colitis. *Mol Ther* 19(3)**:** 620-626.

245. Chinnasamy, N., Wargo, J.A., Yu, Z., Rao, M., Frankel, T.L., Riley, J.P., Hong, J.J., Parkhurst, M.R., Feldman, S.A., Schrump, D.S., Restifo, N.P., Robbins, P.F., Rosenberg, S.A. and Morgan, R.A. (2011). A TCR targeting the HLA-A*0201-restricted epitope of MAGE-A3 recognizes multiple epitopes of the MAGE-A antigen superfamily in several types of cancer. *J Immunol* 186(2)**:** 685-696.

246. Grupp, S.A., Kalos, M., Barrett, D., Aplenc, R., Porter, D.L., Rheingold, S.R., Teachey, D.T., Chew, A., Hauck, B., Wright, J.F., Milone, M.C., Levine, B.L. and June, C.H. (2013). Chimeric antigen receptor-modified T cells for acute lymphoid leukemia. *N Engl J Med* 368(16)**:** 1509-1518.

247. Park, J.R., Digiusto, D.L., Slovak, M., Wright, C., Naranjo, A., Wagner, J., Meechoovet, H.B., Bautista, C., Chang, W.C., Ostberg, J.R. and Jensen, M.C. (2007). Adoptive transfer of chimeric antigen receptor re-directed cytolytic T lymphocyte clones in patients with neuroblastoma. *Mol Ther* 15(4)**:** 825-833.

248. Maude, S.L., Frey, N., Shaw, P.A., Aplenc, R., Barrett, D.M., Bunin, N.J., Chew, A., Gonzalez, V.E., Zheng, Z., Lacey, S.F., Mahnke, Y.D., Melenhorst, J.J., Rheingold, S.R., Shen, A., Teachey, D.T., Levine, B.L., June, C.H., Porter, D.L. and Grupp, S.A. (2014). Chimeric antigen receptor T cells for sustained remissions in leukemia. *N Engl J Med* 371(16)**:** 1507-1517.

249. Hirschhaeuser, F., Sattler, U.G. and Mueller-Klieser, W. (2011). Lactate: a metabolic key player in cancer. *Cancer Res* 71(22)**:** 6921-6925.

250. Ziebart, T., Walenta, S., Kunkel, M., Reichert, T.E., Wagner, W. and Mueller-Klieser, W. (2011). Metabolic and proteomic differentials in head and neck squamous cell carcinomas and normal gingival tissue. *J Cancer Res Clin Oncol* 137(2)**:** 193-199.

251. Saraswathy, S., Crawford, F.W., Lamborn, K.R., Pirzkall, A., Chang, S., Cha, S. and Nelson, S.J. (2009). Evaluation of MR markers that predict survival in patients with newly diagnosed GBM prior to adjuvant therapy. *J Neurooncol* 91(1)**:** 69-81.

252. Mohammad, G.H., Olde Damink, S.W., Malago, M., Dhar, D.K. and Pereira, S.P. (2016). Pyruvate Kinase M2 and Lactate Dehydrogenase A Are Overexpressed in Pancreatic Cancer and Correlate with Poor Outcome. *PLoS One* 11(3)**:** e0151635.

253. Koukourakis, M.I., Giatromanolaki, A., Sivridis, E., Bougioukas, G., Didilis, V., Gatter, K.C. and Harris, A.L. (2003). Lactate dehydrogenase-5 (LDH-5) overexpression in non-small-cell lung cancer tissues is linked to tumour hypoxia, angiogenic factor production and poor prognosis. *Br J Cancer* 89(5)**:** 877-885.

254. Koukourakis, M.I., Giatromanolaki, A., Sivridis, E., Gatter, K.C. and Harris, A.L. (2006). Lactate dehydrogenase 5 expression in operable colorectal cancer: strong association with survival and activated vascular endothelial growth factor pathway--a report of the Tumour Angiogenesis Research Group. *J Clin Oncol* 24(26)**:** 4301-4308.

255. Maftouh, M., Avan, A., Sciarrillo, R., Granchi, C., Leon, L.G., Rani, R., Funel, N., Smid, K., Honeywell, R., Boggi, U., Minutolo, F., Peters, G.J. and Giovannetti, E. (2014). Synergistic interaction of novel lactate dehydrogenase inhibitors with gemcitabine against pancreatic cancer cells in hypoxia. *Br J Cancer* 110(1)**:** 172-182.

256. Gottfried, E., Rogenhofer, S., Waibel, H., Kunz-Schughart, L.A., Reichle, A., Wehrstein, M., Peuker, A., Peter, K., Hartmannsgruber, G., Andreesen, R. and Kreutz, M. (2011). Pioglitazone modulates tumor cell metabolism and proliferation in multicellular tumor spheroids. *Cancer Chemother Pharmacol* 67(1)**:** 117-126.

257. Chirasani, S.R., Leukel, P., Gottfried, E., Hochrein, J., Stadler, K., Neumann, B., Oefner, P.J., Gronwald, W., Bogdahn, U., Hau, P., Kreutz, M. and Grauer, O.M. (2013). Diclofenac inhibits lactate formation and efficiently counteracts local immune suppression in a murine glioma model. *Int J Cancer* 132(4)**:** 843-853.

258. Parks, S.K., Chiche, J. and Pouyssegur, J. (2013). Disrupting proton dynamics and energy metabolism for cancer therapy. *Nat Rev Cancer* 13(9)**:** 611-623.

259. ClinicalTrials.gov, https://clinicaltrials.gov/ct2/show/NCT01791595 (as at 16-04-2016)

260. Chang, C.H. and Pearce, E.L. (2016). Emerging concepts of T cell metabolism as a target of immunotherapy. *Nat Immunol* 17(4)**:** 364-368.

261. Lameris, R., de Bruin, R.C., Schneiders, F.L., van Bergen en Henegouwen, P.M., Verheul, H.M., de Gruijl, T.D. and van der Vliet, H.J. (2014). Bispecific antibody platforms for cancer immunotherapy. *Crit Rev Oncol Hematol* 92(3)**:** 153-165.

262. Calvaresi, E.C., Granchi, C., Tuccinardi, T., Di Bussolo, V., Huigens, R.W., 3rd, Lee, H.Y., Palchaudhuri, R., Macchia, M., Martinelli, A., Minutolo, F. and Hergenrother, P.J. (2013). Dual targeting of the Warburg effect with a glucose-conjugated lactate dehydrogenase inhibitor. *Chembiochem* 14(17)**:** 2263-2267.

263. Mundra, V., Li, W. and Mahato, R.I. (2015). Nanoparticle-mediated drug delivery for treating melanoma. *Nanomedicine (Lond)* 10(16)**:** 2613-2633.

264. Izumi, H., Torigoe, T., Ishiguchi, H., Uramoto, H., Yoshida, Y., Tanabe, M., Ise, T., Murakami, T., Yoshida, T., Nomoto, M. and Kohno, K. (2003). Cellular pH regulators: potentially promising molecular targets for cancer chemotherapy. *Cancer Treat Rev* 29(6)**:** 541-549.

265. Kelderman, S., Heemskerk, B., van Tinteren, H., van den Brom, R.R., Hospers, G.A., van den Eertwegh, A.J., Kapiteijn, E.W., de Groot, J.W., Soetekouw, P., Jansen, R.L., Fiets, E., Furness, A.J., Renn, A., Krzystanek, M., Szallasi, Z., Lorigan, P., Gore, M.E., Schumacher, T.N., Haanen, J.B., Larkin, J.M. and Blank, C.U. (2014). Lactate dehydrogenase as a selection criterion for ipilimumab treatment in metastatic melanoma. *Cancer Immunol Immunother* 63(5)**:** 449-458.

266. Hamanishi, J., Mandai, M., Matsumura, N., Abiko, K., Baba, T. and Konishi, I. (2016). PD-1/PD-L1 blockade in cancer treatment: perspectives and issues. *Int J Clin Oncol*.

267. Harlin, H., Kuna, T.V., Peterson, A.C., Meng, Y. and Gajewski, T.F. (2006). Tumor progression despite massive influx of activated CD8(+) T cells in a patient with malignant melanoma ascites. *Cancer Immunol Immunother* 55(10)**:** 1185-1197.

268. He, Y.F., Zhang, G.M., Wang, X.H., Zhang, H., Yuan, Y., Li, D. and Feng, Z.H. (2004). Blocking programmed death-1 ligand-PD-1 interactions by local gene therapy results in enhancement of antitumor effect of secondary lymphoid tissue chemokine. *J Immunol* 173(8)**:** 4919-4928.

269. Blank, C., Brown, I., Peterson, A.C., Spiotto, M., Iwai, Y., Honjo, T. and Gajewski, T.F. (2004). PD-L1/B7H-1 inhibits the effector phase of tumor rejection by T cell receptor (TCR) transgenic CD8+ T cells. *Cancer Res* 64(3)**:** 1140-1145.

270. Robert, C., Long, G.V., Brady, B., Dutriaux, C., Maio, M., Mortier, L., Hassel, J.C., Rutkowski, P., McNeil, C., Kalinka-Warzocha, E., Savage, K.J., Hernberg, M.M., Lebbe, C., Charles, J., Mihalcioiu, C., Chiarion-Sileni, V., Mauch, C., Cognetti, F., Arance, A., Schmidt, H., Schadendorf, D., Gogas, H., Lundgren-Eriksson, L., Horak, C., Sharkey, B., Waxman, I.M., Atkinson, V. and Ascierto, P.A. (2015). Nivolumab in previously untreated melanoma without BRAF mutation. *N Engl J Med* 372(4)**:** 320-330.

271. Robert, C., Schachter, J., Long, G.V., Arance, A., Grob, J.J., Mortier, L., Daud, A., Carlino, M.S., McNeil, C., Lotem, M., Larkin, J., Lorigan, P., Neyns, B., Blank, C.U., Hamid, O., Mateus, C., Shapira-Frommer, R., Kosh, M., Zhou, H., Ibrahim, N., Ebbinghaus, S. and Ribas, A. (2015). Pembrolizumab versus Ipilimumab in Advanced Melanoma. *N Engl J Med* 372(26)**:** 2521-2532.

272. Robert, C., Ribas, A., Wolchok, J.D., Hodi, F.S., Hamid, O., Kefford, R., Weber, J.S., Joshua, A.M., Hwu, W.J., Gangadhar, T.C., Patnaik, A., Dronca, R., Zarour, H., Joseph, R.W., Boasberg, P., Chmielowski, B., Mateus, C., Postow, M.A., Gergich, K., Elassaiss-Schaap, J., Li, X.N., Iannone, R., Ebbinghaus, S.W., Kang, S.P. and Daud, A. (2014). Anti-programmed-death-receptor-1 treatment with pembrolizumab in ipilimumab-refractory advanced melanoma: a randomised dose-comparison cohort of a phase 1 trial. *Lancet* 384(9948)**:** 1109-1117.

273. Larkin, J., Chiarion-Sileni, V., Gonzalez, R., Grob, J.J., Cowey, C.L., Lao, C.D., Schadendorf, D., Dummer, R., Smylie, M., Rutkowski, P., Ferrucci, P.F., Hill, A., Wagstaff, J., Carlino, M.S., Haanen, J.B., Maio, M., Marquez-Rodas, I., McArthur, G.A., Ascierto, P.A., Long, G.V., Callahan, M.K., Postow, M.A., Grossmann, K., Sznol, M., Dreno, B., Bastholt, L., Yang, A., Rollin, L.M., Horak, C., Hodi, F.S. and Wolchok, J.D. (2015). Combined Nivolumab and Ipilimumab or Monotherapy in Untreated Melanoma. *N Engl J Med* 373(1)**:** 23-34.

274. Ribas, A., Puzanov, I., Dummer, R., Schadendorf, D., Hamid, O., Robert, C., Hodi, F.S., Schachter, J., Pavlick, A.C., Lewis, K.D., Cranmer, L.D., Blank, C.U., O'Day, S.J., Ascierto, P.A., Salama, A.K., Margolin, K.A., Loquai, C., Eigentler, T.K., Gangadhar, T.C., Carlino, M.S., Agarwala, S.S., Moschos, S.J., Sosman, J.A., Goldinger, S.M., Shapira-Frommer, R., Gonzalez, R., Kirkwood, J.M., Wolchok, J.D., Eggermont, A., Li, X.N., Zhou, W., Zernhelt, A.M., Lis, J., Ebbinghaus, S., Kang, S.P. and Daud, A. (2015). Pembrolizumab versus investigator-choice chemotherapy for ipilimumab-refractory melanoma (KEYNOTE-002): a randomised, controlled, phase 2 trial. *Lancet Oncol* 16(8)**:** 908-918.

275. Weber, J.S., D'Angelo, S.P., Minor, D., Hodi, F.S., Gutzmer, R., Neyns, B., Hoeller, C., Khushalani, N.I., Miller, W.H., Jr., Lao, C.D., Linette, G.P., Thomas, L., Lorigan, P., Grossmann, K.F., Hassel, J.C., Maio, M., Sznol, M., Ascierto, P.A., Mohr, P., Chmielowski, B., Bryce, A., Svane, I.M., Grob, J.J., Krackhardt, A.M., Horak, C., Lambert, A., Yang, A.S. and Larkin, J. (2015). Nivolumab versus chemotherapy in patients with advanced melanoma who progressed after anti-CTLA-4 treatment (CheckMate 037): a randomised, controlled, open-label, phase 3 trial. *Lancet Oncol* 16(4)**:** 375-384.

276. Tang, H., Wang, Y., Chlewicki, L.K., Zhang, Y., Guo, J., Liang, W., Wang, J., Wang, X. and Fu, Y.X. (2016). Facilitating T Cell Infiltration in Tumor Microenvironment Overcomes Resistance to PD-L1 Blockade. *Cancer Cell* 29(3)**:** 285-296.

277. Diem, S., Kasenda, B., Spain, L., Martin-Liberal, J., Marconcini, R., Gore, M. and Larkin, J. (2016). Serum lactate dehydrogenase as an early marker for outcome in patients treated with anti-PD-1 therapy in metastatic melanoma. *Br J Cancer* 114(3)**:** 256-261.

10 Appendix

Plasmid used for the generation of *Ldha*$^{-/-}$ clones with CRISPR/Cas9

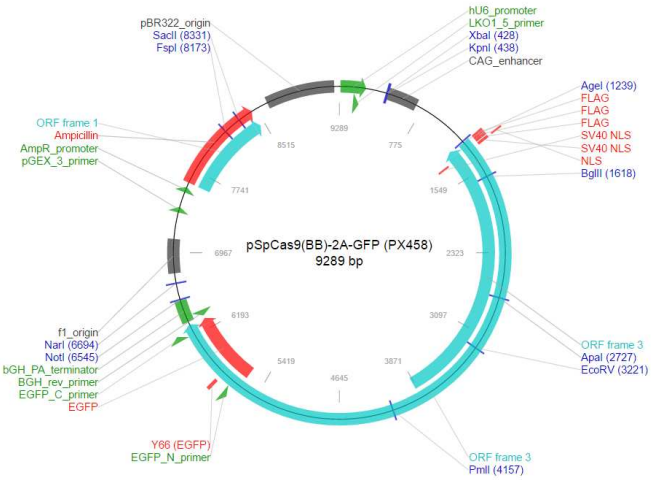

Figure 10-1. Plamid map of pSpCas9(BB)-2A-GFP (PX458)
Plasmid used for the knockdown of *Ldha* in B16.SIY E12 mouse melanoma cells with CRISPR/Cas9 (CRISPR *Ldha*$^{-/-}$ clones). Two guide RNAs (gRNAs) targeting different loci on exon 4 of the *Ldha* gene were included in the vector to obtain CRISPR1 plasmid and CRISPR2 plasmid. pSpCas9(BB)-2A-GFP (PX458) was purchased from Addgene, Cambridge, MA, USA.

Publications

Soomro, S., Langenberg, T., Mahringer, A., Konkimalla, V.B., Horwedel, C., Holenya, P., **Brand, A**., Cetin, C., Fricker, G., Dewerchin, M., Carmeliet, P., Conway, E.M., Jansen, H., and Efferth, T. (2011). Design of novel artemisinin-like derivatives with cytotoxic and anti-angiogenic properties. *J Cell Mol Med* 15(5):1122-35

Brand, A., Singer, K., Koehl, G.E., Kolitzus, M., Schoenhammer, G., Thiel, A., Matos, C., Bruss, C., Klobuch, S., Peter, K., Kastenberger, M., Bogdan, C., Schleicher, U., Mackensen, A., Ullrich, E., Fichtner-Feigl, S., Kesselring, R., Mack, M., Ritter, U., Schmid, M., Blank, C., Dettmer, K., Oefner, P.J., Hoffmann, P., Walenta, S., Geissler, E.K., Pouyssegur, J., Villunger, A., Steven, A., Seliger, B., Schreml, S., Haferkamp, S., Kohl, E., Karrer, S., Berneburg, M., Herr, W., Mueller-Klieser, W., Renner, K., and Kreutz, M. (2016). LDHA-Associated Lactic Acid Production Blunts Tumor Immunosurveillance by T and NK Cells. *Cell Metab*, http://dx.doi.org/10.1016/j.cmet.2016.08.011

Acknowledgment

Ich möchte mich zu allererst und ausdrücklich bei **Prof. Dr. Marina Kreutz** bedanken. Dass ich die Möglichkeit hatte an diesem sehr interessanten und vielversprechenden Thema arbeiten zu können, aber vor allem Deine große Offenheit, Dein Verständnis und Dein Vertrauen haben meine Promotionszeit zu einem sehr angenehmen Erlebnis gemacht. Danke für Deine engagierte Betreuung, für alle anregenden und lehrreichen Diskussionen, die mich jedes Mal wieder ein Stück nach vorne gebracht haben, und die stetige Förderung meiner Weiterbildung. Nicht nur in Nizza und Tel Aviv konnte ich enorm viel lernen.

Herrn **Prof. Dr. Richard Warth** und **Prof. Dr. Andreas Mackensen** danke ich für die gewissenhafte Betreuung der Doktorarbeit und die konstruktiven Vorschläge im Rahmen der 'research reports' bzw. der Forschungsretreats in Hirschberg.

Vielen Dank an Herrn **Prof. Dr. Wolfgang Müller-Klieser** für die super Kooperation, die Durchführung von Express-Biolumineszenz-Messungen und die sofortige Bereitschaft meine Doktorarbeit zu begutachten.

Mein Dank gilt **Prof. Dr. Reinhard Andreesen** und seinem Nachfolger **Prof. Dr. Wolfgang Herr** für die Ermöglichung dieser Arbeit sowie schöne Forschungsretreats, Weihnachtsfeiern und Betriebsausflüge.

Ein riesengroßes Dankeschön geht an **KP** und **KS**. Ihr habt es geschafft, dass ich mich von Anfang an in unserer Arbeitsgruppe so wohl gefühlt habe. Danke für all die beantworteten Fragen, experimentellen Hilfen, das Korrekturlesen und die schönen Diskussionen. Eure Hilfsbereitschaft sucht ihresgleichen.

Danke, liebe **Julia** und liebe **Sandra**, für die geteilten guten und schlechten Zeiten. Es war toll mit Euch!

Herzlichen Dank an alle Mitglieder der AG Kreutz: **Alice** für ihre Geduld mit den 'Kraut und Rüben-' Zellen, **Annette** für spontane Einsätze in chaotischen Zeiten, **Kathrin** für die Respirometrie-Expertise, ihre Hilfe bei Problemen und das Korrekturlesen, **Carina** and **Tina** for being unselfish, helping out and sympathizing with me, **Sakhila** for her gorgeous smell and lifting my spirits with lab-singing in the evenings, and **Eli** for the Mexican flair. Die gute Stimmung, das Miteinander und der Zusammenhalt haben die Arbeit auch in anstrengenden Zeiten immer angenehm erscheinen lassen. **Moni**, **Gabi** und **Steffi**, ohne Eurer Engagement, Eure professionelle Arbeitsweise und Euren Fleiß wäre dieses Projekt niemals so schnell so weit gekommen. Danke dafür!

Bedanken möchte ich mich außerdem bei allen unseren Kooperationspartnern, insbesondere bei **PD Dr. Petra Hoffmann, Prof. Dr. Uwe Ritter, Prof. Dr. Christian Blank, Prof. Dr. Christian Bogdan, PD Dr. Ulrike Schleicher, Prof. Dr. Evelyn Ullrich** und **Prof. Dr. Matthias Mack**, nicht nur für Mäuse oder Antikörper sondern auch für hilfreichen Input.
Danke an **Dr. Rebecca Kesselring** für die anfängliche Unterstützung bei den Intrazellulär-Färbungen.
Ich danke außerdem **Dr. Elisabeth Kohl** und **PD Dr. Sebastian Haferkamp** für die Probensammlung humaner Biopsien zur metabolischen und immunologischen Analyse.
Für 'metabolomics' und 'proteomics' geht mein Dank an **Dr. Katja Dettmer-Wilde**, **Dr. Jörg Reinders** und **Prof. Dr. Wolfram Gronwald**.

Danke an **Prof. Dr. Michael Rehli** für die konstruktiven Vorschläge in den Laborseminaren und an die gesamte **AG Rehli** für die freundschaftliche Zusammenarbeit. Das gilt ebenso für die **AG Edi/Hoff**. Auf Euch war in allen FACS-Angelegenheiten immer Verlass und Ihr habt uns so manches Experiment gerettet.

Dr. Gudrun Köhl und **Anna Höhn** danke ich für all die mühsamen Mausversuche und die treue Hilfe bei den Aufarbeitungen.

I would like to thank **Dr. Jacques Pouysségur** for giving me the opportunity to realize my EMBO fellowship in his lab and learn genome editing by CRISPR/Cas9. His incredible knowledge, his passion for science and his perpetual willingness for scientific discussions were a great benefit during my dissertation.

A big thanks to the lab members of J. Pouysségur and G. Pagès, who welcomed me very warmly and fully integrated me into the group. Thanks **Roser**, **Philippe**, **Marie-Pierre** and **Nirvana** for your kindness and the good times in the lab. Thanks **Masa** for our great discussions and beautiful trips. Thanks **Ibti** for all the fun we had in the lab and for taking care of me so well. You are incredible.

Martalein, Du hast mir damals bei meinen ersten Gehversuchen mit dem 'FlowJo' geholfen und bist heute nicht nur meine Lieblingsärztin. Danke für Deine wunderbar erfrischend ehrliche Art.

Und natürlich, danke, meine **Sibylle**, für die mega Studienzeit die wir hatten, dafür, dass es Dich gibt und es immer ist wie früher wenn wir uns sehen.

Merci infiniment, **Pape**, de m'avoir réconforté encore, encore et encore. Sans toi, tout cela n'aurait pas été possible.

Mein größter Dank aber gilt **meiner Familie**, ohne die ich niemals da wäre wo ich jetzt bin. Die bedingungslose Unterstützung zu jeder Zeit hat es mir ermöglicht Erfahrungen zu machen, auf die ich nicht mehr verzichten wollen würde. Danke!